Open Research Online

The Open University's repository of research publications
and other research outputs

Insights into the biological role of ovothiol in sea urchins and diatoms

Thesis

oro.open.ac.uk

Alfonsina Milito (M.Sc)

Insights into the biological role of ovothiol in sea urchins and diatoms

Doctor of Philosophy

The Open University, UK

School of Life, Health and Chemical Sciences

Stazione Zoologica Anton Dohrn, IT

Department of Biology and Evolution of Marine Organisms

September 2018

Director of studies:

Anna Palumbo

Department of Biology and Evolution of Marine Organisms,

Stazione Zoologica Anton Dohrn, Naples, Italy

Internal Supervisor:

Christophe Brunet

Department of Integrative Marine Ecology,

Stazione Zoologica Anton Dohrn, Naples, Italy

External Supervisor:

Gary Stephen Caldwell

School of Marine Science and Technology,

Newcastle University, Newcastle upon Tyne, UK

Abstract

Ovothiols are π-methyl-5-thiohistidines, first isolated and characterised from ovary, eggs and biological fluids of marine invertebrates (Palumbo *et al.,* 2018). They are produced in large amounts by sea urchin eggs as a protection from the oxidative burst at fertilisation and from environmental cues during embryonic development (Castellano *et al.,* 2016).

The position of the thiol group on the imidazole ring confers to these molecules unique chemical properties allowing them to play numerous biological roles in nature, as well as they are receiving an increasing interest as pharmacological compounds for a potential therapeutic use in humans (Castellano and Seebeck, 2018).

The key enzymes responsible for ovothiol biosynthesis, OvoA and OvoB, have been characterised revealing that its biosynthesis is much more widespread than previously thought (Braunshausen and Seebeck, 2011; Naowarojna *et al.,* 2018).

In this thesis, the physiological roles of ovothiol have been investigated in two marine organisms inhabiting coastal areas, sea urchins and diatoms, with the aim to highlight new biological functions and possible applications for human health.

Through molecular and functional analyses of OvoA transcript and protein carried out during development of the Mediterranean sea urchin *Paracentrotus lividus,* this study has revealed that ovothiol biosynthesis is fundamental for the progression of a correct developmental program. In particular, the role of this metabolite is likely related to fundamental processes like cell cycle during early development, skeletogenesis and gut functionality in larval stages.

On the other hand, molecular experiments performed in the centric diatom *Skeletonema marinoi* have revealed that *OvoA* transcription is modulated by light and is associated with

reactive oxygen and nitrogen species variations, thus suggesting that ovothiol can be involved in the antioxidant response triggered by light in diatoms. These studies are relevant considering the possibility to use diatoms to produce high amounts of the compound necessary for applied research.

Table of contents

Figures index

List of abbreviations

A = anterior

Ab = abanal

ABC = ATP binding cassette transporter

ACT = actin

AHR = aryl hydrocarbon receptor

AKR = aldo-keto reductase

Ala = anterolateral arms

An = anal

anti DIG-POD = anti-digoxigenin antibodies conjugated to horseradish peroxidase

AP = alkaline phosphatase

AV = animal-vegetal

AX = antheraxanthin

B = blue

BCIP = 5-bromo-4-chloro-3'-indoly phosphate p-toluidine

BF = bright field

BH_4 = tetrahydrobiopterin

BSA = bovine serum albumin

C = chloroplast

CaM = calmodulin

CAs = carbonic anhydrases

CAT = catalase

CC = Calvin Cycle

CCMs = carbon-concentrating mechanisms

cdk = cyclin dependent kinases

Chl = chlorophyll

CISH = chromogenic *in situ* hybridization

CRE = cAMP-Responsive Element

CtrlMO = control morpholino

CYP = cytochrome P450 enzyme

DAPI = 4′,6-Diamidine-2′-phenylindole dihydrochloride

DD = diadinoxanthin

DDE = diadinoxanthin de-epoxidase

DEPC = dietilpirocarbonato

dopa = 3,4-dihydroxyphenylalanine

DT = diatoxanthin

e = invaginating ectoderm

EB = early blastula

EF1α = elongation factor 1α

EgtB = gamma-glutamyl hercynylcysteine sulfoxide synthase

eNOS = endothelial nitric oxide synthase

EPHX = epoxide hydrolase

epn = egg pronucleus

ER = endoplasmic reticulum

FAD = flavin adenine dinucleotide

FCP = fucoxanthin-Chl proteins

FE = fertilised eggs

FGE-sulfatase = formylglycine-generating sulfatase

FISH = fluorescent *in situ* hybridisation

FMN = flavin mononucleotide

FMO = flavoprotein monooxygenase enzyme

FX = fucoxantin

G = green

GABA = acido γ-amminobutirrico

GAPDH = glyceraldehyde-3-phosphate dehydrogenase

GPX = glutathione peroxidase

GSH = glutathione in reduced form

GSSG = glutathione in disulphide form

GST = glutathione-S-transferase

h = hydrocoel

H_2DCF = 2',7'-dichlorofluorescein

H_2DCFDA = 2',7'-dichlorofluorescein diacetate

H4 = histone 4

HPLC-MS = high performance liquid chromatography-mass spectrometry

HSL600 = high sinusoidal light 600

HSWL300 = high square-wave light 300

HSWL600 = high square-wave light 600

IHC = immunohistochemistry

iNOS = inducible nitric oxide synthase

L = Left larval side

LC3 = 1A/1B-light chain 3

LCPAs = long chain polyamines

LHC = light harvesting complex

LSL600 = low sinusoidal light 150

M = Mouth

MALDI-TOF = Matrix Assisted Laser Desorption Ionization-Time of Flight

MFP-4MI = 1-methyl-2-[3-trifluoromethylphenyl]-4-mercapto-imidazole

MGDG =monogalactosyldiacylglycerol

MO = morpholino oligonucleotide

MOPS = 3-(N-morpholino)propanesulfonic acid

MRE = Metal Responsive Elements

MT = metallothionein

N = Nucleus

NADPH = nicotinamide adenine dinucleotide phosphate reduced

NAT = *N*-acetyl transferase

nfdmilk = non fat dried milk

nNOS = neuronal nitric oxide synthase

NO = nitric oxide

NOS = nitric oxide synthase

NPQ = non-photochemical quenching

NR = nuclear receptor

OA = oral-aboral

OSH = ovothiol in reduced form

OSSO = ovothiol in disulphide form

OvoA = 5-histidylcysteine sulfoxide synthase

OvoAMO = OvoA morpholino

OvoB = Pyridoxal 5'-phosphate-dependent sulfoxide lyase

P = posterior

PABA = para-aminobenzoic acid

PBS = phosphate buffer saline

PBST = phosphate buffer saline 0.1% Tween-20

PD = postdorsal arms

PE = Perkin-Elmer

PFD = photon flux density

Pl = pluteus

PMCs = primary mesenchyme cells

PMSF = phenylmethylsulfonyl fluoride

PO = postoral arms

Pr = prism

preI = pre-immune IgGs

PrO = preoral arms

Prx = peroxiredoxin

PSI = photosystem I

PSII = photosystem II

R = red

R = Right larval side

RC = Reaction Center

RNS = reactive nitrogen species

ROS = reactive oxygen species

RT-qPCR = reverse transcription-quantitative PCR

SAM-transferase = S-adenosylmethionine-methyltransferase

SB = swimming blastula

SD = standard deviation

SDS-PAGE = Sodium Dodecyl Sulphate - PolyAcrylamide Gel Electrophoresis

SDVs = silica deposition vesicle

SITs = silicic acid transporters

SLC = solute carrier

SM = Storage Molecules

SOD = superoxide dismutase

spn = sperm pronucleus

SQDG = sulfoquinovosyldiacylglycerol

SRE = Stress Responsive Elements

St = stomach

SULT = sulfotransferase

TBS = tris-buffered saline

TBST = tris-buffered saline 0.1 % tween-20

TUB A = α- tubulin

TUNEL = terminal dUTP nick end labeling

TXN = thioredoxin

Udx1 = urchin dual oxidase

UE = unfertilised eggs

UGT = UDP-glucorunosyl transferase

UVR = ultraviolet radiation

VE = virgin eggs

VLSL10 = very low sinusoidal light 10

VLSWL10 = very low square-wave light 10

VX = violaxanthin

W = white

WB = western blot

WT = wild type

WVS = water vascular system

XC = xanthophyll cycle

zn = zygote nucleus

ZX = zeaxanthin

CHAPTER 1

General Introduction

1.1. Ovothiols: from chemistry to biochemistry

Thiols play a critical role in living organisms to maintain the cellular redox potentials and the protein thiol-disulphide ratios, as well as to protect cells from reactive oxygen (ROS) and nitrogen species (RNS). The identification and characterisation of various intracellular thiols (fig. 1A), present at millimolar concentrations in various cell types, have contributed in expanding our biochemical knowledge on complex life processes, with implications in several areas such as parasitology and drug design (Hand and Honek, 2005).

The best characterised thiol is the tripeptide glutathione (GSH), which is the thiol mostly found in eukaryotes, as well as in some bacteria including *Escherichia coli*. GSH is a cysteine-based thiol (Glu-Cys-Gly), whose class includes also trypanothione and mycothiol. Trypanothione (bis-GSH-spermidine) is an unusual form of glutathione containing two molecules of glutathione joined by a spermidine linker found in the genera *Trypanosoma* and *Leishmania* (Fairlamb *et al.,* 1985). Mycothiol (AcCys-GlcN-Ins) is a thiol compound composed of a cysteine residue with an acetylated amino group linked to glucosamine, which is then linked to inositol, found in the Actinomycetales bacteria (Newton *et al.,* 1996).

A second class of intracellular thiols, based on histidine, includes ergothioneine and ovothiols. Ovothiols (OSHs) are 3-*N*-methyl-5-thiohistidines (referred also as 1-*N*-methyl-4-mercaptohistidines or $\pi-N-$methyl-5-tiohistidines depending on the adopted nomenclature system, Palumbo *et al.*, 2018), occurring in nature in three forms: ovothiol A (OSH$_A$), ovothiol B (OSH$_B$) and ovothiol C (OSH$_C$) which differ in the degree of methylation on the α-amino group (fig. 1B).

Thiol groups are highly reactive to electrophiles and oxidants and have a high affinity for metals (Winterbourn *et al.,* 2008; Higdon *et al.,* 2012; Nagy *et al.,* 2013).
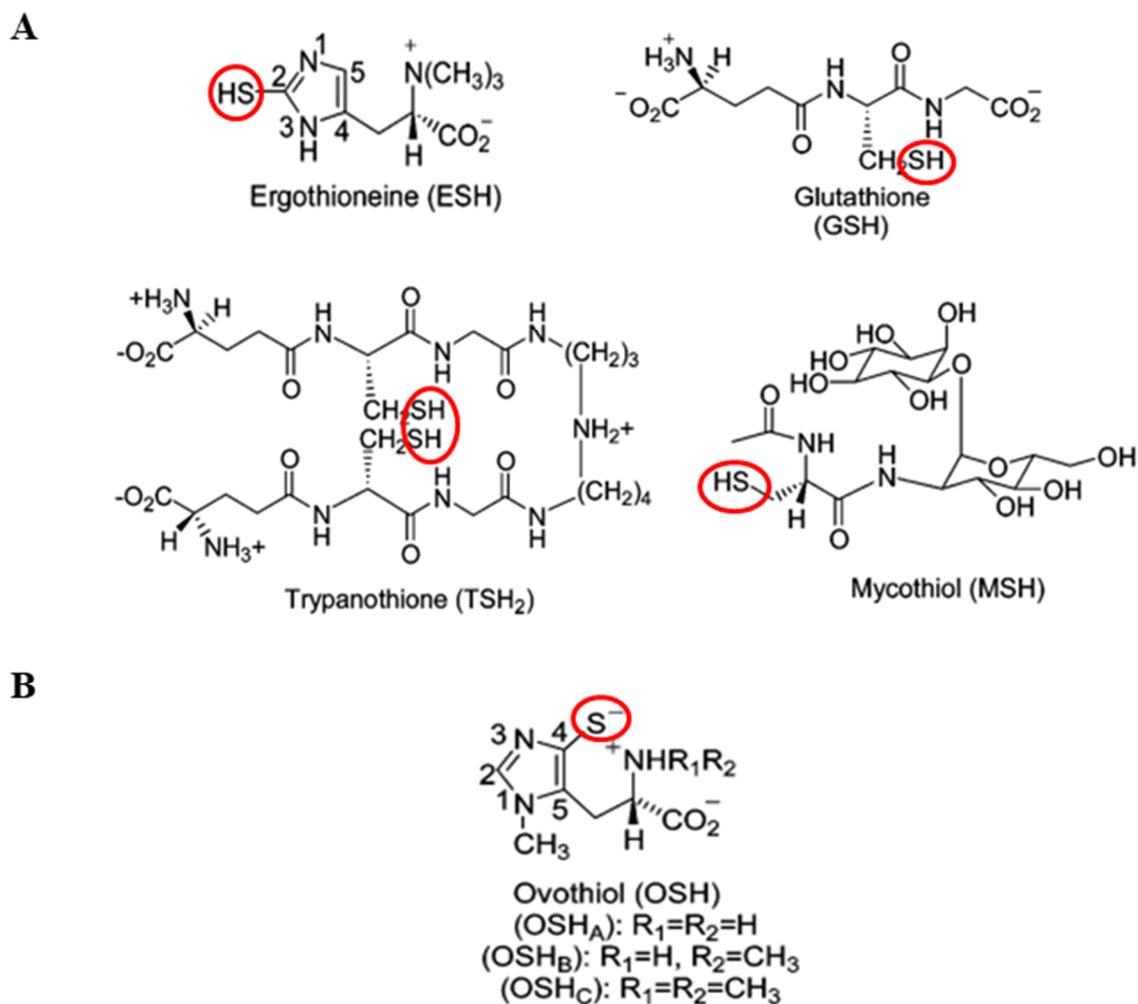
Figure 1 Chemical structure of naturally occurring thiols.
A. On top: ergothioneine and glutathione; on bottom: trypanothione and mycothiol; **B.** Ovothiols.

Thiol compounds are typically referred to the R-SH form, which can be deprotonated to form the thiolate anion (R-S⁻). Unlike the protonated form of the thiol group, which is not particularly reactive, the thiolate anion is nucleophilic thanks to the availability of electrons (LoPachin *et al.,* 2007). The tendency of a thiol group to be deprotonated is defined by the acid dissociation constant (pK_a), i.e. the pH at which that molecule is at 50% in thiol form and 50% in thiolate form. This parameter is characteristic for each thiol group and at physiological pH (7.4) thiols having a relatively low pK_a are more reactive compared to those with a higher pK_a (fig. 2, Wall *et al.,* 2012).
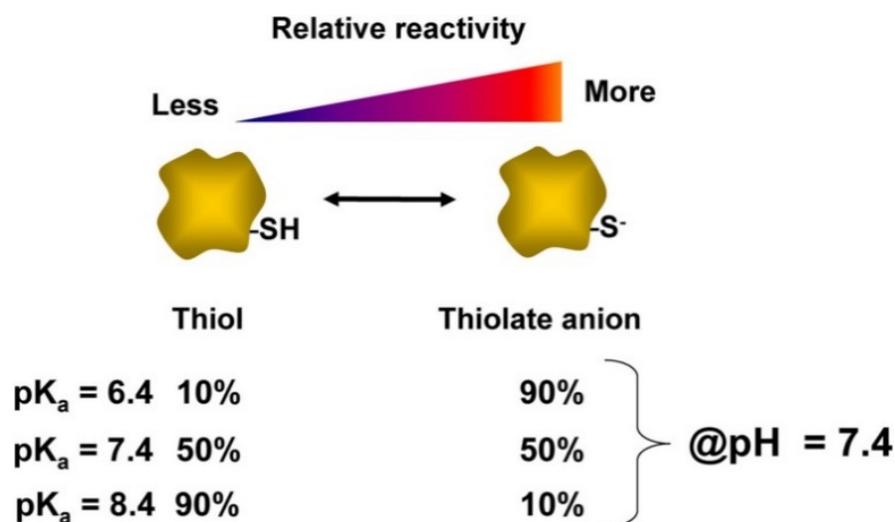
Figure 2 Relationship of thiol pKa and reactivity (Wall *et al.,* 2012).

The position of the thiol group on the imidazole ring confers an extremely low basicity to the thiolate group of the OSHs compared to histidine (Holler *et al.,* 1988; Weaver and Rabenstein, 1995). These chemical features result in a very low pKa value (1.4) and a much more positive redox potential (-0.09 V) compared to other intracellular thiols (for glutathione pKa = 8.75 and redox potential = -0.26 V) (Marjanovic *et al.,* 1995; Weaver and Rabenstein, 1995; Ariyanayagam *et al.,* 2001). Therefore, this site tends to be anionic not only at basic, but also at neutral and even acidic pHs, making this molecule particularly susceptible to oxidation. Therefore, OSHs are extremely reactive, they react with H_2O_2 five times faster compared to glutathione, forming water and the ovothiol disulphide (OSSO), which, in turn, is reduced non-enzymatically via thiol-disulphide exchange with GSH (Turner *et al*, 1988, reactions reported below) or by TSH (Fairlamb and Cerami, 1992).

$$2OSH + H_2O_2 \longrightarrow OSSO + 2H_2O$$

$$OSSO + 2GSH \longrightarrow 2OSH + GSSG$$
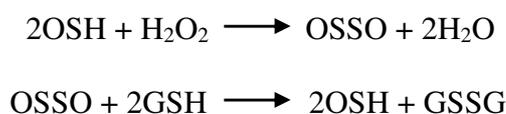
The vulnerability to oxidation renders OSHs very efficient scavengers of radicals and peroxides (Turner *et al.,* 1987; Holler *et al.,* 1990; Bailly *et al.,* 2000). This feature has stimulated interest in the synthesis of various ovothiol derivatives with the aim to enhance their activity for drug development (Zoete *et al.,* 1997; Bailly *et al.,* 2003).

In biological systems, ovothiol is produced thanks to different enzymatic activities, first identified in crude extracts of the protist *Crithidia fasciculata,* following the incubation of cells with radiolabelled precursors (^{35}S cysteine, ^{35}S methionine) (Steenkamp *et al.,* 1996; Vogt *et al.,* 2001).

Recently the two enzymes responsible for ovothiol biosynthesis have been characterised. The first ovothiol biosynthetic enzyme (OvoA) is a 5-histidylcysteine sulfoxide synthase, which catalyses the insertion of the sulfur atom of cysteine into the C5 position of the imidazole ring of histidine leading to the formation of the sulfoxide intermediate (fig. 3). It is an iron-dependent enzyme, identified and characterised from *Erwinia tasmaniensis* and *Trypanosoma cruzi,* which requires O_2 as four electron acceptor for the formation of the C-S bond and the sulfoxidation of the thioether bond (Braunshausen and Seebeck, 2011, Seebeck, 2013). The second enzyme (OvoB) is a Pyridoxal 5'-phosphate-dependent sulfoxide lyase which catalyses the formation of mercaptohistidine (fig. 3) (Naowarojna *et al.,* 2018), which is then methylated by OvoA itself, thanks to the presence of a methyl transferase domain, to give ovothiol A (Naowarojna *et al.,* 2018).

The peculiar formation of C-S bond by the action of OvoA has received a good deal of attention for the similarity of the reaction catalysed by EgtB, a gamma-glutamyl hercynylcysteine sulfoxide synthase, and leading to the synthesis of ergothioneine. EgtB catalyses the insertion of the gamma-glutamyl cysteine sulfur into the C2 position of N-alpha-trimethyl histidine with the formation of the corresponding sulfoxide, which gives rise to ergothioneine by a five-gene cluster (fig. 4) (Seebeck, 2010; Goncharenko *et al.,* 2015).

OvoA homologous enzymes are encoded in several genomes ranging from proteobacteria to animalia, revealing that ovothiol biosynthesis is much more widespread in nature than initially thought (Castellano and Seebeck, 2018).
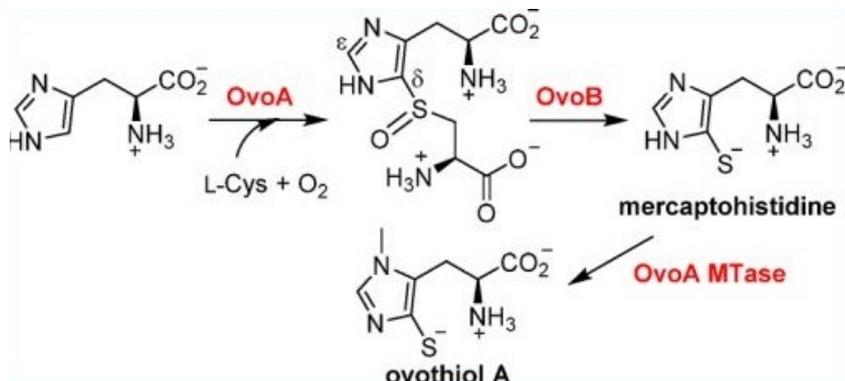
Figure 3 Ovothiol A biosynthesis (Naowarojna *et al.,* 2018).
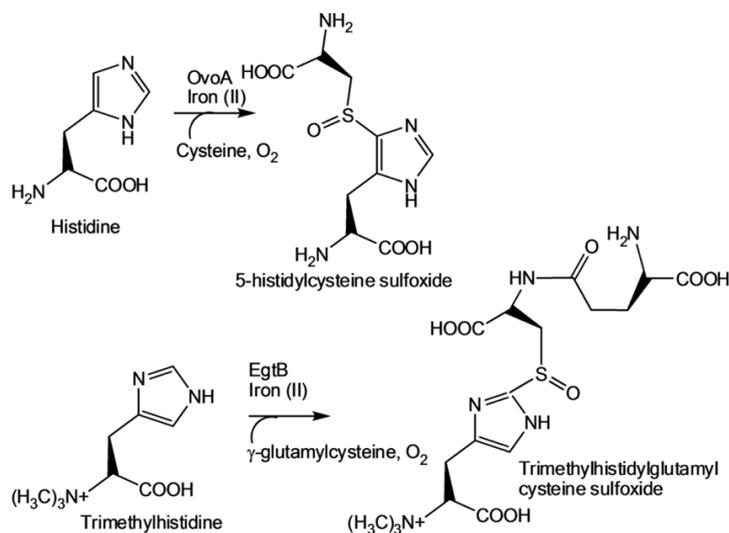
Figure 4 Comparison between OvoA and EgtB enzymatic reactions (Palumbo *et al.,* 2018).

The kinetics and substrate specificity of OvoA have been deeply investigated on the recombinant proteins of the bacteria *Erwinia tasmaniensis and Trypanosoma cruzi.* (Braunshausen and Seebeck, 2011; Mashabela and Seebeck, 2013). It has been shown that

OvoA is much more flexible in substrate specificity compared to EgtB (Song *et al.,* 2013; Song *et al.,* 2014). Indeed, OvoA can accept also the substrates of EgtB, gamma-glutamyl cysteine and trimethyl histidine, leading to the formation of the intermediate precursor of ergothioneine. Interestingly, modulation of the histidine methylation state (from histidine to trimethyl histidine) leads to a change in the OvoA catalysis, from an OvoA to an EgtB type chemistry, i.e. insertion of the sulfur atom of cysteine into the C5 or C2 position of the imidazole ring, respectively (Song *et al.,* 2013).

OvoA gene loci structure has recently been characterised in sea urchin (Castellano *et al.,* 2016) revealing the multi-intron-exon composition and the presence of Metal Responsive Elements (MRE) and Stress Responsive Elements (SRE) in the promoter regions of *OvoA*s from the purple sea urchin, *Strongylocentrotus purpuratus*, and the mediterranean one, *Paracentrotus lividus*. This latter species showed two additional regulatory elements: one AP-1 Element and one cAMP-Responsive Element (CRE) (Fig. 5).
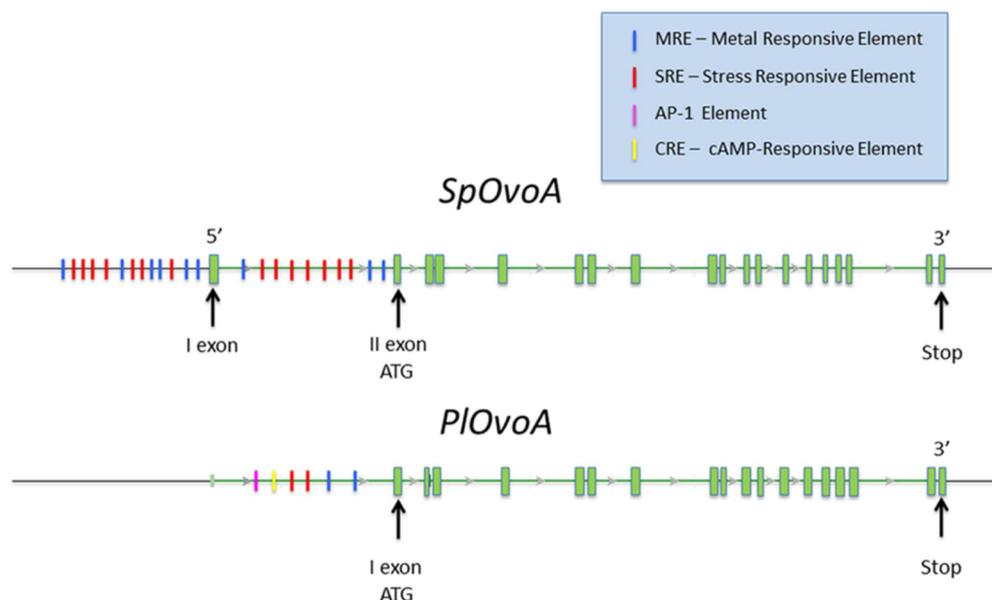
Figure 5 Gene structure of *OvoA* from sea urchin (Castellano *et al.,* 2016).
Abbreviations: *SpOvoA* = *OvoA* from *Strongylocentrotus purpuratus*; *PlOvoA* = OvoA from *Paracentrotus lividus.*

Protein domain analysis has revealed that OvoA from sea urchin is characterised by all three characteristic domains of such enzyme: the DinB superfamily domain, containing the conserved HX3HXE putative iron-binding motif, the formylglycine-generating sulfatase (FGE-sulfatase), both in the N-terminal region, and the S-adenosylmethionine-methyltransferase (SAM-transferase) domain in the C-terminal region (fig. 6) (Castellano *et al.,* 2016). This latter domain is absent in EgtB and represents a useful criterion to distinguish between OvoA and EgtB.

The evolutionary history of OvoA has also been investigated in metazoans (Castellano *et al.* 2016). Protein domains are highly conserved from porifera, placozoa, cnidaria (anthozoa) to protostomes (annelida and mollusca) and deuterostomes. The authors reported two gene losses: one, among protostomes, in nematoda (*Caenorhabditis elegans*) and arthropoda (*Drosophila melanogaster*), and a second independent one, among deuterostomes, in Osteichthyes, the ancestors of bony vertebrates. These results suggested that *OvoA* could have been lost during the transition from water to land, due to the emergence of other regulatory mechanisms, more suitable to an air-based environment.
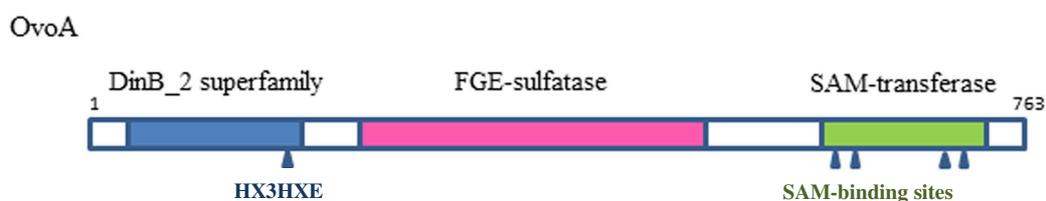
Figure 6 Protein characterisation of OvoA from *P. lividus* (modified from Castellano *et al.,* 2016).

OvoA and EgtB-like catalytic activities are considered evolutionarily distant, due to their different regioselectivity (insertion of sulfur atom into the C5 or C2 position of the imidazole ring), the low sequence similarity and the presence in OvoA of the additional methyltransferase domain. Nevertheless, a much shorter evolutionary path between the two

enzymatic activities has been recently suggested (Liao and Seebeck, 2017). In their work, the authors demonstrated that a class of ancient ovothiol producing cyanobacteria acquired, through few genetic changes, the ability to synthetise ergothioneine by an OvoA-like sulfoxide synthase. This adaptaption took presumably place following some changes in the environment, by which ergothioneine production resulted more useful in the new conditions compared to that of ovothiol.

1.1.1. Occurrence and biological role of ovothiols in nature

In the eighties, ovothiol A was isolated in millimolar concentrations from unfertilised eggs of the sea urchin *P. lividus* (Palumbo *et al.,* 1982; 1984) (fig. 7).

Ovothiol A was also found in the eggs or ovary of other echinoderms, such as the holothuroid *Holothuria tubulosa* and several species of sea stars (Palumbo *et al.,* 1984; Turner *et al.,* 1987), in the eggs and urine of the European squid *Loligo vulgaris* and in urine of *Octopus vulgaris* (Rossi *et al.,* 1985). Later, it was found in the coelomic fluid of sexually mature males of marine worms, where it seems to act as a pheromone by triggering the eggs release in mature females (Rohl *et al.,* 1999; Breithaupt and Hardege, 2012).

The other forms of ovothiol, B and C, were found in other marine organisms. Ovothiol B was found in the ovaries of clams (Turner *et al.,* 1987) and ovothiol C in the eggs of the sea urchins *Sphaerechinus granularis* (Palumbo *et al.,* 1984) and *S. purpuratus* (Turner *et al.,* 1986) (fig. 7). Several studies have highlighted a key role of ovothiol in sea urchins during fertilisation and development. Ovothiol protects sea urchin eggs from the deleterious effects of H_2O_2, which is produced during the high oxidative burst at fertilisation (Shapiro *et al.,* 1990). In its reduced form (OSH), it reacts very fast with H_2O_2 leading to the formation of the disulphide form (OSSO). This is, in turn, reduced by the intracellular glutathione (GSH), which is then oxidized (GSSG). Glutathione is finally maintained in the reduced form by the action of the glutathione reductase (fig 8).

Recently, the expression of *OvoA* (*PlOvoA*) was followed during *P. lividus* development by quantitative PCR (Castellano *et al*., 2016). *PlOvoA* expression strongly decreases at early and swimming blastula stages compared to the highest value in the unfertilised eggs (indicated as virgin eggs in fig. 9). Thereafter, the expression significantly increases at the pluteus stage (fig. 9).

During development, ovothiol protects sea urchin embryos from oxidative stress produced by environmental cues (Castellano *et al.,* 2016). Indeed, treatment of *P. lividus* fertilised eggs with cadmium concentrations miming polluted sea-water resulted in increased expression of *PlOvoA* mRNA and higher levels of ovothiol.
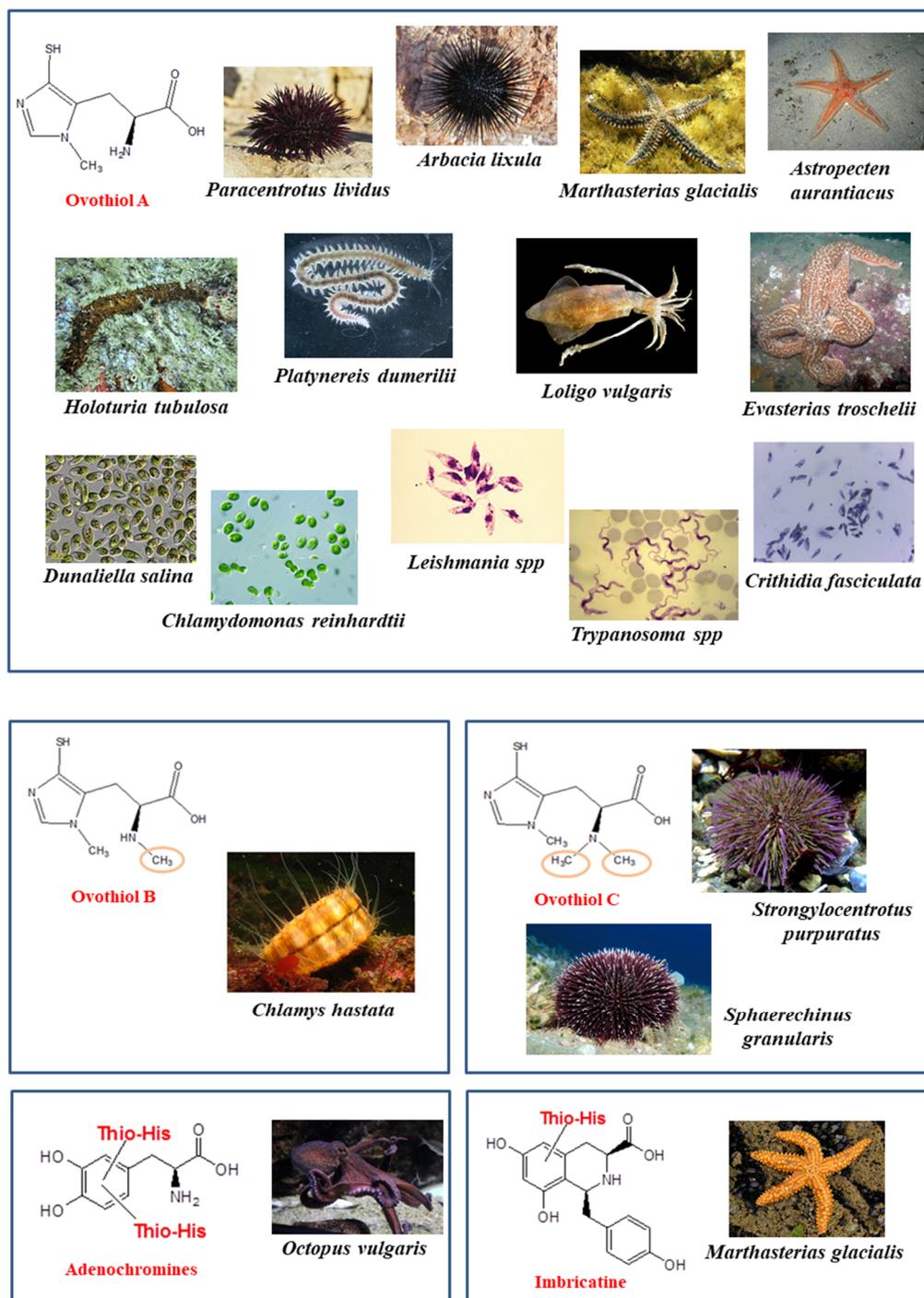
Figure 7 Occurrence of ovothiols in nature (modified from table 1, Palumbo *et al.,* 2018).

Also other environmental factors, such as toxic blooms, regulate *OvoA* expression. Indeed, blastula stages of sea urchins offspring cyclically exposed to the natural toxic bloom of the dinoflagellate *Ostreopsis* cf. *ovata* exhibited significant increase of *PlOvoA* mRNA compared to embryos from control females collected at control site with negligible concentrations of *O*. cf. *ovata* (Castellano *et al.,* 2016).
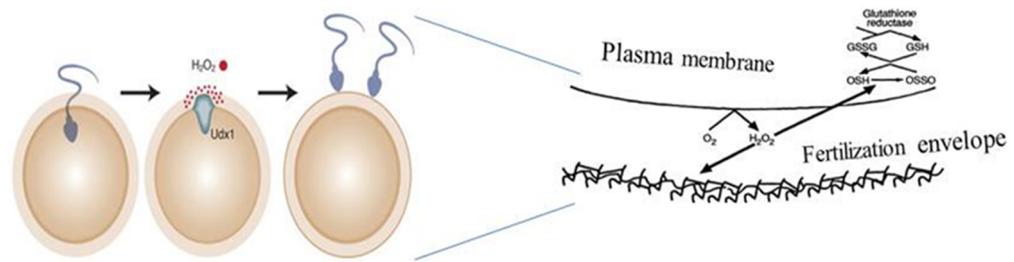
Figure 8 Proposed model for the biological role of ovothiol during sea urchin fertilisation (Palumbo *et al.,* 2018).

Ovothiol protects sea urchin eggs from the deleterious effects of H_2O_2, produced during fertilisation by the action of the Udx1 (urchin dual oxidase 1) enzyme, acting as a non-enzymatic glutathione peroxidase.
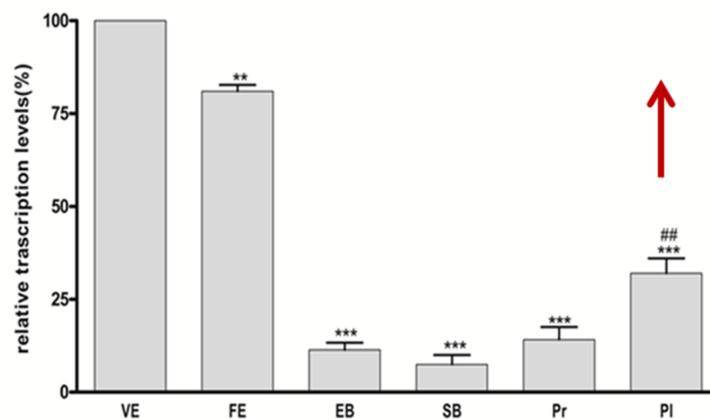
Figure 9 *OvoA* gene expression during *P. lividus* development (Castellano *et al.,* 2016).

OvoA gene expression levels from unfertilised eggs to plutei larvae. Abbreviations: VE = virgin eggs, FE = fertilised eggs, EB = early blastula, SB = swimming blastula, Pr = prism, Pl = pluteus.

On the basis of these results, a mechanism for ovothiol biosynthesis has been suggested, according to which when sea urchins release gametes in the seawater column, developing embryos are exposed to stress agents, such as natural toxins or heavy metals, which induce the production of ROS and activate redox-sensitive transcription factors to bind MRE and/or SRE, promoting *OvoA* transcription and finally ovothiol synthesis (fig. 10).
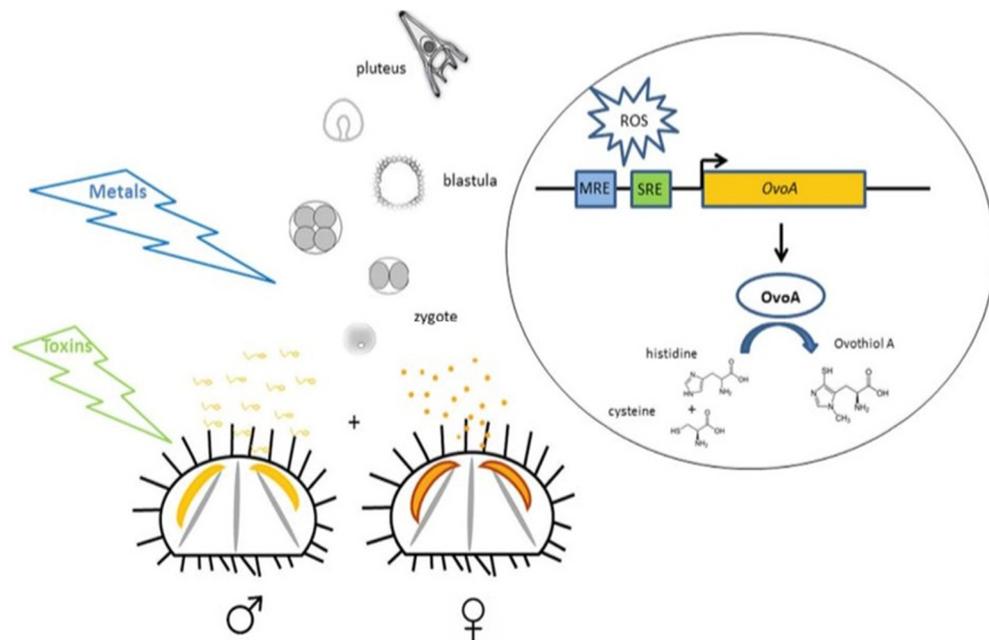
Figure 10 Proposed model for the biological role of ovothiol in sea urchins (Castellano *et al.,* 2016). Developing embryos are exposed, in the water column, to stress agents like heavy metals and natural toxins. These induce an overproduction of reactive oxygen species (ROS) and the consequence activation of transcription factors, leading to the *OvoA* overexpression. Thus, the OvoA enzyme catalyses ovothiol biosynthesis, which contributes to the protection of developing sea urchin embryos from environmental cues. Abbreviations: MRE = metals responsive element; SRE = stress responsive element.

The occurrence of *OvoA* in most broadcast spawners suggested that this thiohistidine may protect the eggs and the embryos of many marine invertebrates, from damaging environmental cues, when they are released in seawater (Castellano *et al.,* 2016). However,

the presence of *OvoA* also in marine organisms with internal fertilisation, such as cartilaginous fishes, indicated a broader role of OvoA, probably related to fundamental processes linked to the embryonic development (Castellano *et al.,* 2016).

Besides marine invertebrates, ovothiol A is also widespread in the microbial world (fig. 7). In particular, it is present in different species of protozoa of the Trypanosomatidae family, like the pathogenic parasites *Leishmania* spp., *Trypanosoma cruzi* and *T. brucei*, where it has been supposed to play a key role to protect them from the oxidative stress during infection (Spies and Steenkamp, 1994; Ariyanayagam and Fairlamb, 2001), providing the parasites with an efficient system to decompose the S-nitroso groups of nitrosoglutathione and dinitrotrypanothione, formed from the high levels of nitric oxide released by macrophages (Murray and Nathan, 1999; Vogt and Steenkamp, 2003; Krauth-Siegel and Leroux, 2012).

Several photosynthesic microrganisms have also been reported to produce ovothiol A, such as the green microalga *Dunaliella salina*, in which it has been reported to be a redox regulator in chloroplasts (Selmar-Reimer *et al.,* 1991) and the microalga *Euglena gracilis*, where the presence of different OvoA transcripts in light and dark conditions has allowed to hypothesise a light-dependent biosynthesis (O'Neill *et al.,* 2015).

The thiohistidine unit is also present as component in larger structures of some marine natural products, like adenochrome and imbricatine (fig. 7).

Adenochrome, the red iron-binding pigment present in the branchial hearts of *Octopus vulgaris*, is a mixture of peptides formed by glycine and three isomeric adenochromines. These are aminoacids derived from the conjugation of 5-thiohistidine with 3,4-dihydroxyphenylalanine (dopa) quinone enzymatically generated from dopa (Ito *et al.,* 1979a, b). The presence of the 5-thiohistidine in the iron chelating agent, adenochrome, has suggested its possible involvement in the detoxification of the animal from metal ions.

Imbricatine is a cytotoxic alkaloid formed by 5-thiohistidine linked to an isoquinoline nucleus, identified in the starfish *Dermasterias imbricata*. This compound induces escape

response in the starfish prey *Stamphia coccinea*, causing its detachment and swimming response (Pathirana and Andersen, 1986; Burgoyne *et al.,* 1991).

Up to now, the best source for ovothiols is represented by sea urchin eggs. Indeed, ovothiol A can be isolated as disulphide from *P. lividus* eggs by purification of the lipid-free aqueous extract by sequential ion exchange chromatographies (Palumbo *et al.,* 2018). From 10 g of sea urchin eggs 2.5 mg of ovothiol A can be obtained.

Regarding the chemical synthesis, in the ninethies a synthetic procedure involving many steps was developed to synthesise enantiopure ovothiols A, B and C (Holler *et al.,* 1989). Recently, a straightforward cost-effective synthetic route was reported to afford in only five steps enantiopure ovothiol A from L-histidine, as starting compound (Mirzahosseini *et al.,* 2014). Also a synthesis has been developed for 5-thiohistidine, the precursor of ovothiols, unmethylated at the imidazole ring (Daunay *et al.,* 2016). Although these studies, the synthesis of ovothiols still remains cumbersome.

1.1.2. Bioactivities in human systems and potentialities as pharmacological natural products

Sulfur plays a key role in biology and it is found in many natural compounds produced by plants, bacteria, fungi and animals, which, thanks to their unique chemical and biochemical properties, possess promising antibiotic and anticancer activities (Jacob *et al.,* 2006). Indeed, they can undergo a plenty of reactions due to the ability of sulfur to occupy different oxidation states *in vivo,* each one able to form different chemotypes with various chemical properties, including, in addition to redox-activity, metal binding and nucleophilic substitution, which are often used by cells against oxidative stressors, metal ions and toxins. Among thiols, ergothioneine and OSHs have unique antioxidant, metal-binding and catalytic properties making them very interesting from a pharmacological perspective. In particular, as mentioned in the previous chapter, OSHs are able to catalyse the peroxidase-like reduction of H_2O_2, unlike ergothioneine, which reduces various oxidants but apparently not H_2O_2.

In humans, the catalytic removal of peroxides to give water and alcohols is afforded by the enzymes GPx (glutathione peroxidase) and Prx (peroxiredoxin) (Rhee *et al.,* 2005). GPx mimetics is a highly interesting topic in artificial enzyme research for potential pharmacological application (Wang *et al.,* 2017). However, most GPx-mimics are unsuitable for therapeutic use for the content of selenium or tellurium. In this context, OSHs and derivatives of chemical synthesis can be a less toxic alternative (Bailly *et al.,* 2000; Zoete *et al.,* 2000). In particular, the synthetic derivative of OSHs, 1-methyl-2-[3-trifluoromethylphenyl]-4-mercapto-imidazole (MFP-4MI, fig. 11) revealed to be a promising neuroprotective agent in both immature and mature mouse brain (Vamecq *et al.,* 2003). Classical approaches for neuroprotection in adult brain involve GABA receptor activation and inhibition of N-methyl-D-aspartate receptor and sodium voltage-gated

channel (Ikonomidou *et al.,* 2001; Olney, 2002). However, the action on these targets may be dangerous for immature or developing brain.
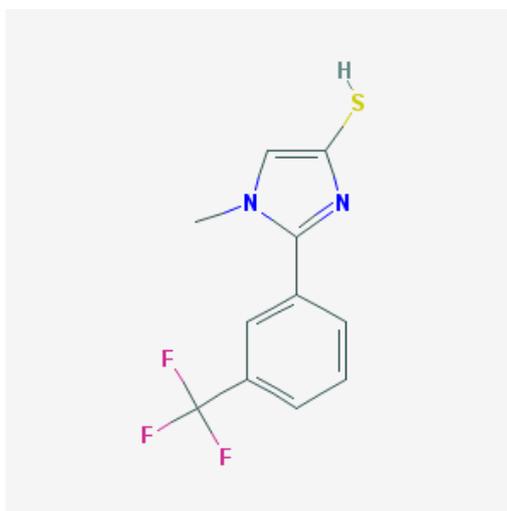
Figure 11 MFP-4MI 2D structure (pubchem.ncbi.nlm.nih.gov; PubChem CID: 10308114).

Therefore, MFP-4MI is an attractive pharmacological option for neuroprotection considering that antioxidants have, in general, low toxicity since their mechanism of action does not involve the binding to these receptors.

Ovothiol A purified from *P. lividus* unfertilised eggs has been found to affect the proliferative activity of a human epatocarcinoma cell line (Russo *et al.,* 2014). Indeed, it has been demonstrated that it is able to induce cell death in Hep-G2 cell line. A similar effect has also been found after treatment with ovothiol C, suggesting that methylation on the aminoacidic side chain does not affect the bioactivity of these molecules. The treatment with chloroquine, a largely accepted autophagy inhibitor, showed that the anti-proliferative effect was consequence of the activation of an autophagic mechanism, assessed through fluorescent labeling of autolysosomes and protein over-expression of specific autophagic markers, i.e. the microtubule-associated protein 1A/1B-light chain 3 (LC3) II and Beclin-1.

The ability of OSHs to induce autophagy in cancer cell lines is revelant considering the correlation between this process and cancer metabolism (Lozy and Karantza, 2012).

In addition, ovothiol A has also shown to have anti-inflammatory activities in a human umbilical vein endothelial cell line (HUVECs) from women affected by gestational diabetes (Castellano *et al.,* 2018). Indeed, ovothiol A represents a promising anti-inflammatory agent to be used as dietary supplement and/or as a drug for prevention/treatment of chronic inflammation related to atherosclerotic processes and cardiovascular diseases, especially linked to diabetes. Interestingly, ovothiol A is effective at lower concentrations compared to other compounds used for the treatment of diabetes.

Despite the peculiar chemical properties of OSHs and the great pharmacological potential of these molecules, further studies will be required to assess their activities on other biological systems.

1.2. Model systems

1.2.1. The Mediterranean sea urchin *Paracentrotus lividus*

Paracentrotus lividus (Lamarck 1816, fig. 12) is a common sea urchin species inhabiting rocky sea-beds and meadow of *Posidonia oceanica* in the Mediterranean sea. It can be found up to 40 m of depth and, at high densities, can influence the phytobenthos community hampering the growth of erect algae and seagrasses and the formation of coralline barrens (Sala *et al.,* 1998; Boudouresque & Verlaque, 2001; Guidetti *et al.,* 2003). *P. lividus* is harvested for the commercial exploitation of its gonads, from both male and female individuals, referred as "roe" in fishery market (Lawrence, 2001).
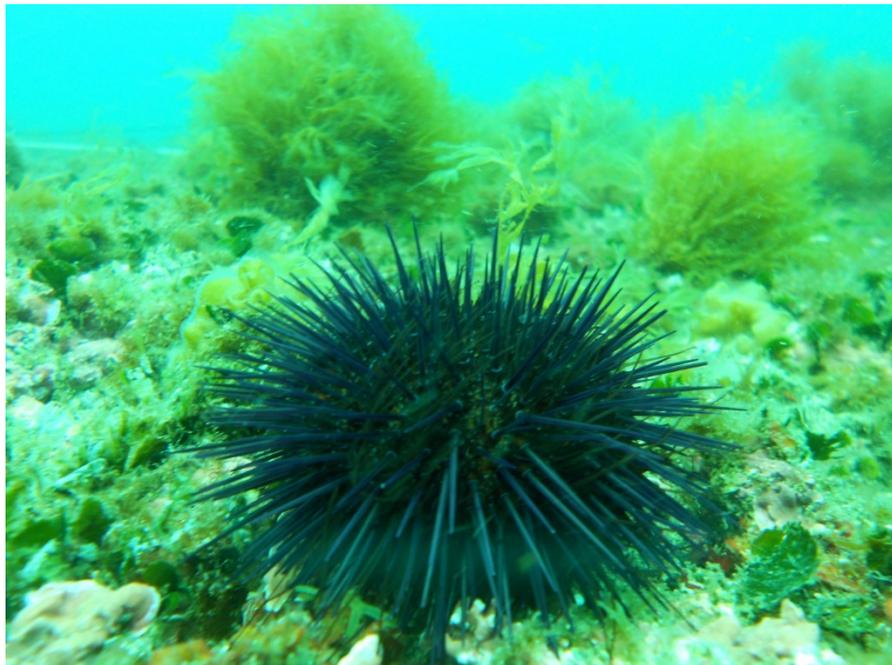
Figure 12 *P. lividus* sea urchins from the gulf of Naples, Italy (photo: Gianluca Zazo and Marco Cannavacciuolo, SZN).

The animals belonging to this species are highly variable as regarding the colour of their spines, ranging from different tones of purple and brown to olive green (Boudouresque & Verlaque, 2001). The body colour seems to be affected by the habitat, being prevalently brown in rocky bottom animals. By contrast, colour distribution is more homogeneous in individuals inhabiting on *Posidonia oceanica* meadows (Addis *et al.,* 2015).

Sea urchins are ancient benthic invertebrates, belonging to the *phylum* of Echinoderms (fig. 13), appeared before the Cambrian explosion, 520 million years ago (Bottjer *et al.,* 2006).
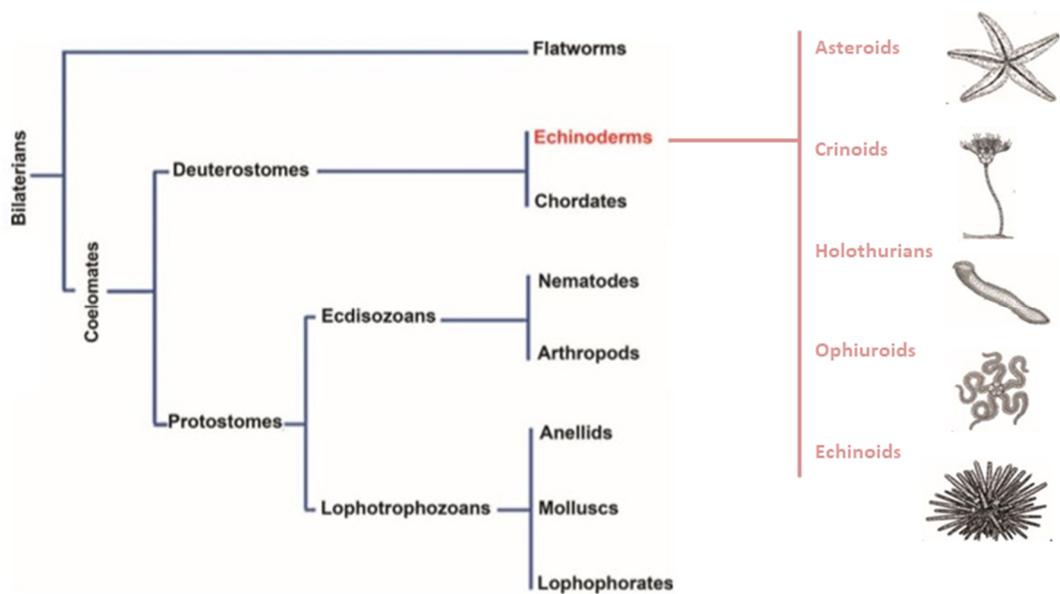
Figure 13 Phylogeny of echinoderms (modified from Agnello, 2017).

From an evolutionary point of view, echinoderms occupy a strategic phylogenetic position, representing a link between invertebrates and vertebrates. The sequencing of the genome of the "California purple sea urchin", *Strongylocentrotus purpuratus,* strongly supported this evidence, estimating the occurrence of representative genes of almost all vertebrate gene families (Davidson, 2006; Sodergren *et al.,* 2006). This revealed that sea urchins are more closely related to humans than to other invertebrate groups.

The Echinoderms *phylum* is divided in 5 different classes: asteroids, crinoids, holothurians, ophiuroids and echinoids. Although the class phylogeny in Echinoderms is quite clear, the position of the ophiuroids relative to asteroids, echinoids and holothurians is still controversial. The cryptosyringid hypothesis considers ophiuroids as sister group of holothurians and echinoids, while, according to the Asterozoan hypothesis, supported by most molecular phylogenetic studies, ophiuroids and asteroids constitute a distinct clade (Telford *et al.,* 2014). All classes belonging to this *phylum* share some particular features, such as the adult radial symmetry, a water vascular system, a calcite endoskeleton and they all have a benthic lifestyle (Agnello, 2017). Echinoids represent the most various group of echinoderms, including, besides sea urchins, also heart urchins and sand dollars (fig. 14).
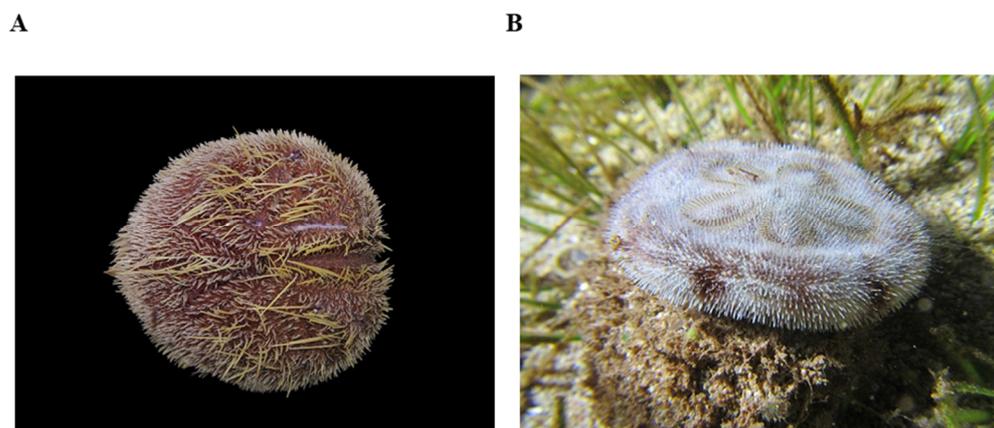
Figure 14 Heart urchins and sand dollars.
A. The heart sea urchin *Spatangus purpureus* from the Belgian continental shelf; **B.** The sand dollar *Clypeaster reticulatus* from Mayotte island.

Echinoids have an internal skeleton consisting of many calcium carbonate plates, that collectively form five ambulacra. Regular echinoids, like sea urchins, are characterised by a spherical body, a pentaradial symmetry and the anus location at the centre of the animal, above the mouth. They are easily distinguished by irregular echinoids who have an elongated

shape in the adult stage and the anus in posterior position (Rupper *et al.,* 2004; Smith and Kroh, 2013).

A graphical representation of the anatomy of sea urchin is showed in figure 15. The body of sea urchins is covered by spines and tube feet. The spines are used for locomotion, as defence against predators and to trap food particles, while tube feet are utilised to attach to substrates and to capture food. Small jaws, called pedicellariae, are also used to protect themselves and to catch food. The mouth is formed by a five-pointed jaw, called Aristotle's lantern, and is located on the underside of the animal (Ruppert *et al.,* 2004). A five-part gut, in which the food is digested, extends from the mouth to the anus on the top of the animal. Echinoderms possess a nervous system consisting of a circumoral nerve ring connected to five radial nerve cords that extend into the tube feet (Sly *et al.,* 2002). Recent studies have revealed that neurogenesis in echinoderms shares typical metazoan features of asymmetric division of neural progenitors, giving rise to central and peripheral components in both larvae and adults, similarly to other bilaterian nervous systems (Hinman and Burke, 2018). Also the gene regulatory networks and signalling pathways, which regulate neural patterning and differentiation have been characterised in *S. purpuratus* larvae, revealing the complexity of the sea urchin larval nervous system at neurochemical level, which is necessary to control various aspects of embryonic and larval behaviour (Wood *et al.,* 2018).

Sea urchins, as all echinoderms, have an open water vascular system (WVS), which connects with the external environment through a single opening next to the anus, called madreporite. From the madreporite, the seawater enters into a short canal, connected to the ring canal at the level of oesophagus. This is, in turn, linked to the radial canals, which bring the water to the ampullae and, then, to the tube feet (fig. 15).
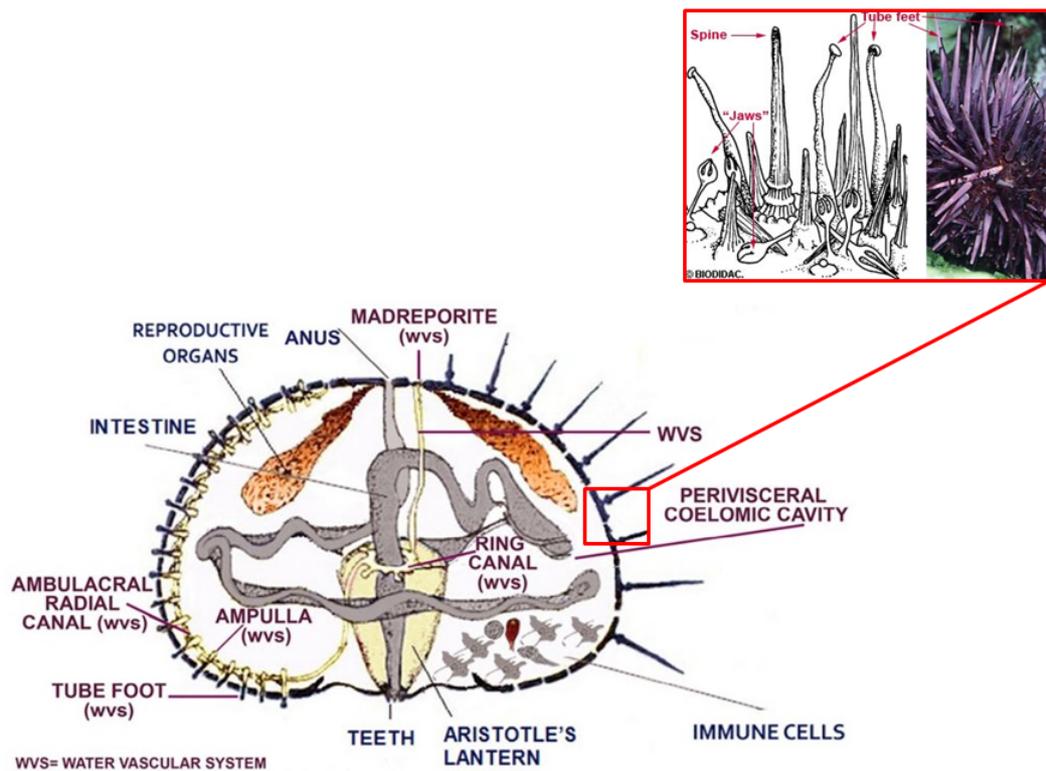
Figure 15 Sea urchin anatomy (modified from Pinsino and Matranga, 2015).

Besides playing the functions typical of the vertebrate vascular system, the WVS is also involved in generating and controlling the hydrostatic pressure, needed for several physiological functions related to locomotion, respiration, feeding, reproduction and excretion (Nichols, 1972; Smith, 1981). Moreover, echinoderms possess a very efficient stress-sensing and immune defence system, able to counteract both biotic and abiotic stressors, through the production of a vast repertoire of recognition molecules (Pinsino and Matranga, 2015 and bibliography therein). The immune system of echinoderms is able to protect them against both external stressors and internal pathological threats conferring to this group of invertebrates a great resistance to cancer, immune and age-related diseases (Bodnar, 2009).

Due to these features, sea urchin can offer a promising model system to investigate processes related to cell damage, senescence and longevity (Du *et al.,* 2013; Bodnar and Coffman, 2016).

1.2.1.1. Sea urchin fertilisation and development

Most of the sea urchin species have separate sexes and undergo an indirect development producing a free-swimming larva, from which the penta-radial juvenile emerges at metamorphosis and grows into the adult (McClay, 2011). About one-fifth of sea urchin species reachs the juvenile stage directly after the gastrulation and, generally, they are able to bypass the larval feeding stage by producing larger eggs (~300 µm in diameter) (Parks *et al*., 1988; Wray and Raff, 1989). Eggs and sperm are spawned into the seawater and fertilisation occurs externally.

Sea urchin eggs are released into the sea water after the completion of meiosis, thus they are fully mature and more stable compared to other echinoderm eggs, i.e. starfish. Indeed, starfish eggs are normally fertilised before the completion of the first meiotic division and, therefore, represent a good model system to study the fast events of sperm-egg interaction (Santella *et al.,* 2015).

When the sperm-egg interaction occurs, the acrosome of the spermatozoon releases enzymes to digest the jelly coat surrounding the egg (fig. 16). Then, actin filaments bind to receptors in the vitelline layer and the sperm and egg plasma membranes fuse, leading to the opening of ion channels and the consequent depolarization of the membrane, often called "fast block to polyspermy" (Reece *et al.,* 2013), as suggested by electrophysiological data. However, this theory has been recently questioned because it has been pointed out that laboratory experiments performed with sea urchin oocytes deprived of their extracellular coats and inseminated at high densities are artifactual and can lead to wrong assumptions. It has been, instead, suggested that a key factor in determing monospermy is the ability of the fertilising spermatozoon, intrinsically different from the others, to locate at the preferential entry site in the egg, regardless to the membrane potential (Dale, 2016 and bibliography therein). Upon interaction with the sperm, a wave of Ca^{2+} spreads through the egg from the sperm

interaction site to the opposite pole, leading to the exocytosis of the cortical granules beneath the plasma membrane and the consequent release of their contents into the perivitelline space with the elevation of a "soft" external fertilisation envelope. Cortical granules release a cocktail of enzymes and macromolecules, including a peroxidase which is responsible for the hardening of the elevated fertilisation membrane by cross-linking the tyrosine residues of the vitelline coat aided by hydrogen peroxide. This hardened protective layer protects the developing embryo during the early stages of development and provides a microclimate for the early division cycles and morphometric movements (Dale, 2016). Fertilisation triggers a rapid activation of protein synthesis in sea urchin eggs in absence of ongoing transcription, inducing, in parallel, cell cycle entry of the eggs formerly blocked in the G1-phase (Epel, 1990), allowing them to launch the embryonic developmental program. Cell cycle progression is triggered by transient increases of intracellular free calcium, which regulates control proteins (pp34 and cyclin), both at translational and post-translational levels. In particular, the cell cycle entry is triggered by the phosphorylation of pp34 and cyclin synthesis, while the mitosis entry is induced by cyclin phosphorylation. Cyclin degradation, instead, represents the signal for mitosis exit (Crosby, 2007; Wolf *et al.,* 2007).

The early embryonic cell cycle of many acquatic organisms differs from the somatic cell cycle for the following features:

- It is controlled by an autonomous biochemical oscillator, without any influence by developmental signals/checkpoints;

- It is extremely rapid, lacking the G1 and G2 phases between the S-phase and mitosis;

- The egg cytoplasm does not grow but it is progressively divided in smaller cells;

- It is exclusively controlled by maternal RNAs and proteins.

In sea urchin, only in the first cell cycle there is a lengthy G1 phase, while during the next cell cycles S-phase begins immediately after mitotic telophase, until mid-blastula stage (12 hours post fertilisation), when gap phases are regained and zygotic genes are first transcribed (Davidson *et al.,* 1982; Whitaker and Patel, 1990; Siefert *et al.,* 2015).
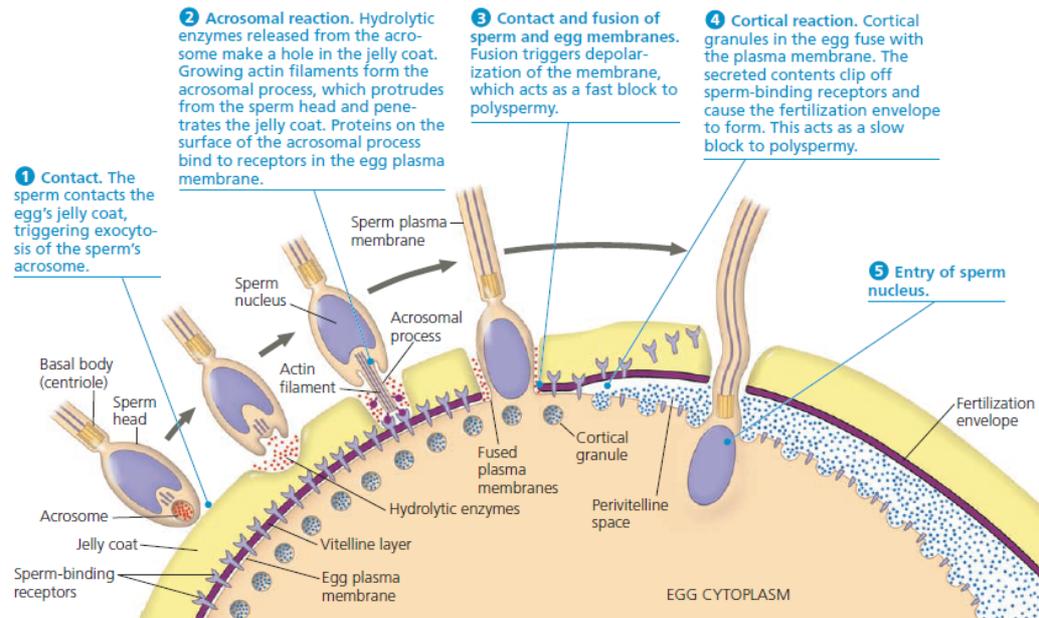
Figure 16 Acrosomal reaction during fertilisation in sea urchin (Reece *et al.,* 2013).

The zygote begins a stereotypic radial pattern of cleavage (fig. 17) giving rise, by the fourth unequal cleavage, to different sized blastomeres with specific fates: eight mesomeres at the animal hemisphere (future aboral and oral ectoderm and neural ectoderm), four macromeres (future endoderm and non skeletogenic mesoderm, NSM, including pigment cells, blastocoelar cells, muscle cells and coelomic pouch cells), and four micromeres at the vegetal pole, which, in turn, will divide, by the fifth cleavage, in four small micromeres (thought to migrate and reside in the coelomic pouches of the larva; Yajima and Wessel, 2011) and four large micromeres (future skeletogenic cells, often called primary mesenchyme cells, PMCs) (fig. 17).
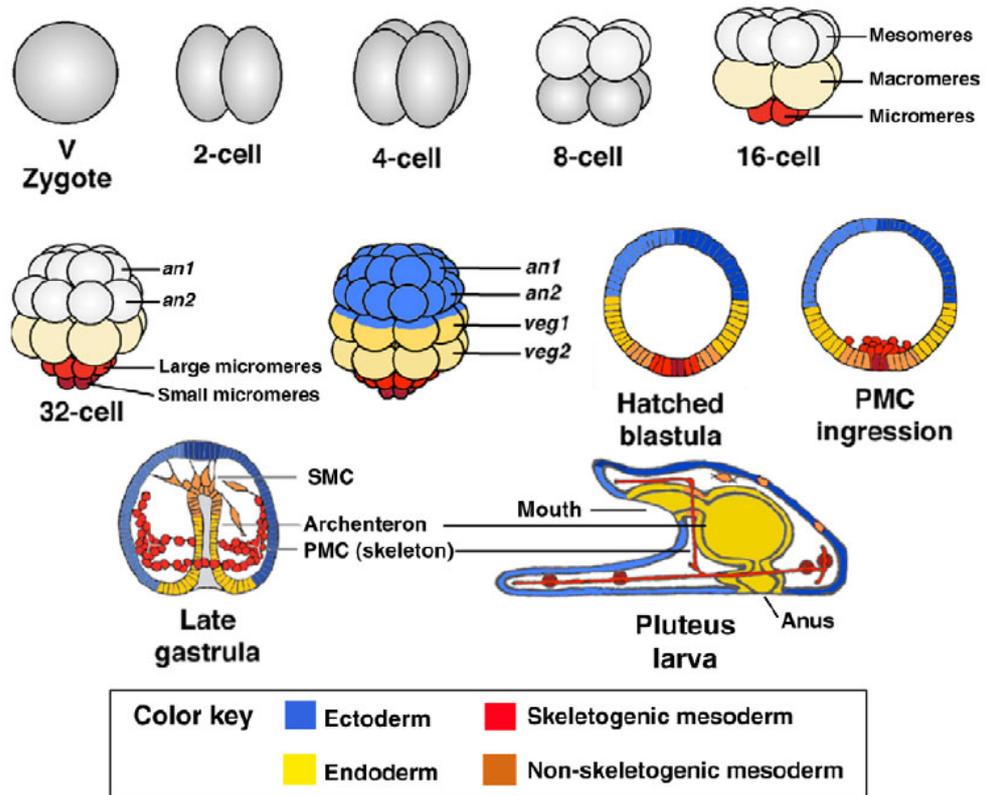
Figure 17 Sea urchin development from zygote to pluteus larva (modified from McClay, 2011).

By the sixth cleavage, the embryo, now called blastula, forms an internal cavity called blastocoel. At mid-blastula stage, the embryo produces cilia, hatches from its fertilisation envelope and enters the plankton community. During early gastrulation the PMCs enter the blastocoel and, after extending highly dynamic filopodia, they migrate below the equator of the embryo forming a ring of cells, where spicule rudiments are formed (Okazaki, 1975). As PMCs complete the ingression, the vegetal plate bends and the archenteron (future gut) begins to invaginate (often called primary invagination). A secondary invagination occurs with the elongation of the archenteron, surrounded by the ring structure formed by PMCs (Kominami and Takata, 2004).

The archenteron reaches a target site at the animal pole, where the ectoderm invaginates to form the stomodeum (future mouth and oral cavity), which then fuses with the foregut epithelium. The embryo develops into the pluteus larva by changing shape in the ectoderm,

partially due to the growth of the skeletal rods, whereas the gut compartmentalisation into the foregut (esophagus), midgut (stomach) and hindgut (intestine) occurs (McClay, 2011). In particular, the foregut consists of two regions: the one proximal to the mouth, that is narrow, densely ciliated and provided with circumferential muscle fibers; and the distal one, bulbous, characterised by few cilia and muscle fibers parallel to the central axis (Burke and Alvarez, 1988). The cardiac sphincter separates the foregut from the midgut, which is constituted by al least two columnar epithelial cell types: type I cells, distributed in all stomach epithelium and characterised by the presence of a single cilium and several kinds of vesicles in the cytoplasm; type II cells, restricted to the anterior part, which do not have cilia and, generally, contain partially digested algal cells. Thus, the function of these two cell types is thought to be secretory for type I cells, and phagocytic/digestive for type II cells (Burke, 1981). The hindgut, separated by the midgut through the pyloric sphincter, is composed by squamous epithelial cells, containing a single cilium and numerous cytoplasmatic vesicles. The food (algal cells) enters from the mouth and is transported, thanks to the action of the cilia and peristaltic contrations, through the foregut, where it is aggregated as "bolus". This is transported to the midgut, through the cardiac sphincter, and the undigested material is first collected at the level of the pyloric sphincter, passed to the hindgut and finally defecated through the anal sphincter (Pearse and Cameron, 1991).

Complex gene regulatory networks regulate the gut morphogenesis from the early specification of the endoderm in the embryo to the final compartimentalisation of the larval gut, with ParaHox genes playing a central role (Annunziata *et al.,* 2014 and bibliography therein).

Coelomic pouches bulge at the sides of the foregut and the differentiation of the larva leads to the formation of cells needed for skeleton, neural transmission and feeding.

Different from the adults, sea urchin larvae, being bilaterally symmetric, have a body plan developing along two orthogonal axes: the animal-vegetal (AV) axis, maternally determined and specifying ectoderm, endoderm and mesoderm; and the oral-aboral (OA) axis, along

which oral ectoderm, ciliated band ectoderm and aboral ectoderm differentiate (Coffman *et al.,* 2009). In particular, the OA axis is mediated by specific signals, i.e. Nodal signalling, expressed to the oral side of the embryo, which contains a higher concentration of mitochondria, asymmetrically distributed already in the unfertilised eggs. The higher density and/or activity of mitochondria on the prospective oral side respect to the aboral side generates a redox gradient which is responsible for the OA axis specification (Coffman *et al.,* 2014). Indeed, experiments performed immobilising sea urchin embryos in tight clusters of four "rosettes", thus experimentally inducing a respiratory asymmetry from the inside of the rosette to the outside, demonstrated that the most oxidising side of the embryos (faced to the outside of the rosette) tends to develop into the oral side of the embryo (Coffman and Davidson, 2001).

As the larva grows, from the left coelomic pouch the rudiment develops and, at metamorphosis, the bilateral larva settles and transforms into the pentameral juvenile sea urchin (fig. 18).

Compared to other organisms (insects and frogs), little is known about the metamorphic process in echinoderms. A detailed staging scheme of rudiment development in the purple sea urchin has been described by Heyland and Hodin in 2014, focused on soft tissues and primordia of skeletal elements. On the left side of the larva, the ectoderm (vestibule) starts to invaginate until it reachs and flattens against the hydrocoel (fig. 19C-F). At this point, the first signs of pentameral symmetry appear with the formation of five bumps in the left hydrocoel, which penetrate the vestibule (fig. 19G), which also reveals a pentameral pattern (fig 19H). Following, the five bumps (primary podia) start to elongate and finally they curve towards the oral field of the rudiment and touch each other (fig. 19I-K).
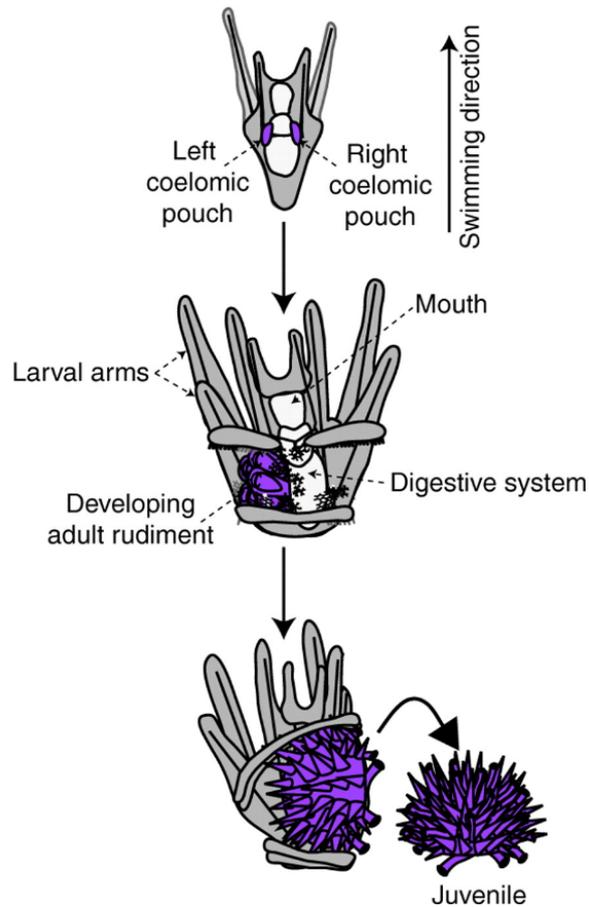
Figure 18 Scheme of the indirect development in sea urchin leading to the formation of the juvenile (modified from Juliano *et al.,* 2010).

At soft tissue stage vi or vii (fig. 19I,J), the first skeletal elements appear as small spicule dots (fig. 20C), which will develop first in triradiate spicules and then in multi-branched spicules (fig. 20D-E).

The first spicules to be formed are the ocular plate and interambulacral plate primordia. At this stage, skeletal spicule dots are formed in correspondence of the primary podia and, after becoming triradiate spicules, they elongate to form the first ring of the tube foot and plates (fig. 20F-G).

At skeletogenic stage 5 (fig. 20G,H), primordia of the adult spines are formed as 6-sided spicules, which then elongate to form the base of the adult spine (fig. 20H-I). At stage 7, six parallell fronds are formed from the elongation of the spine primordia and the second tube

foot skeletal ring begins to form (fig. 20J). Then, the spine fronds are connected through the first cross hatch and, finally, the second concentric ring is completed to form the tube foot skeleton (fig. 20K-M) (Heyland and Hodin, 2014 and bibliography therein).
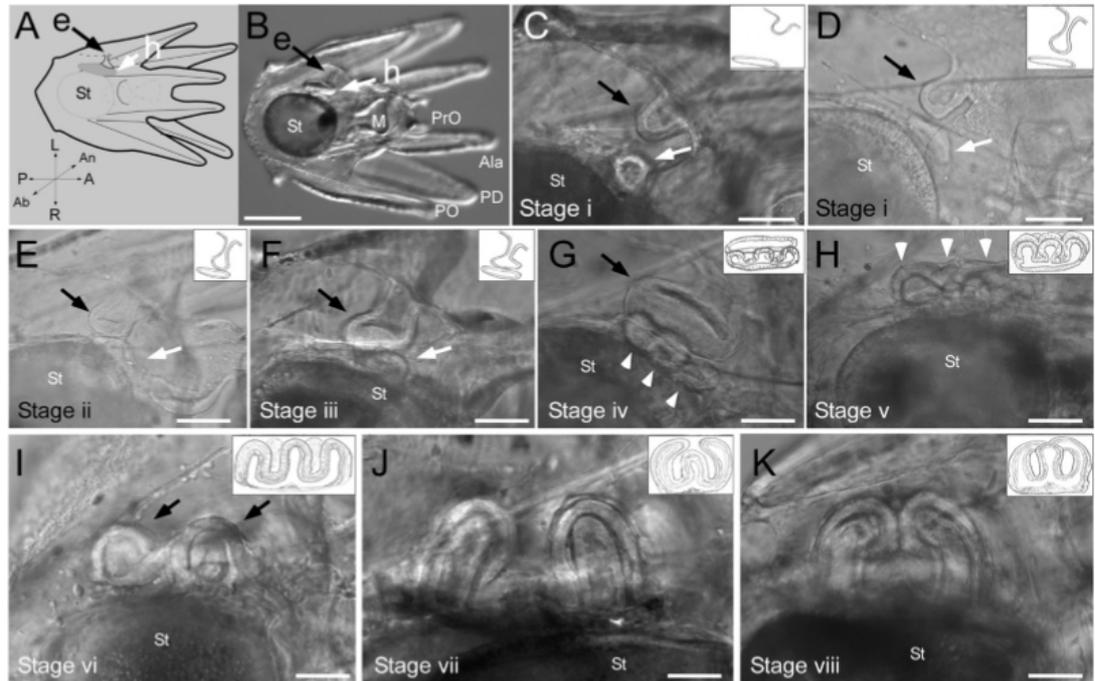
Figure 19 Development of soft tissues in rudiment formation in *S. purpuratus* (Heyland and Hodin, 2014).

A. Scheme of the abanal view of the larva (all images are in this orientation, except where indicated); **B.** DIC image of the larva (anal view); **C-F.** Invagination of the ectoderm, black arrows, towards the hydrocoel, white arrows (C = stage i, 60% invagination; D = stage i, 90% invagination, anal view; E = stage ii, ectoderm contacts the hydrocoel, anal view; F = stage iii, ectoderm flattens against the hydrocoel (anal view); **G.** at stage iv, 5-fold mesoderm appears (3 of the 5 primary podia are visible and indicated by white arrowheads), black arrow indicates the invaginating ectoderm; **H.** 5-fold ectoderm appears (stage v) indicated by white arrowheads; **I-J.** formation of the primary podia (black arrows); **K.** primary podia bend at the tip and touch each other (anal view).

Abbreviations: e = invaginating ectoderm; h = hydrocoel; Ala = anterolateral arms; M = Mouth; St = stomach; PD = postdorsal arms; PO = postoral arms; PrO = preoral arms; L = Left larval side; R = Right larval side; A = anterior; P = posterior; An = anal; Ab = abanal. Scale bars: B - 200μm; C, D, E - 35 μm; F - 25μm; G, H, I - 40μm; J - 30μm; K - 40μm.
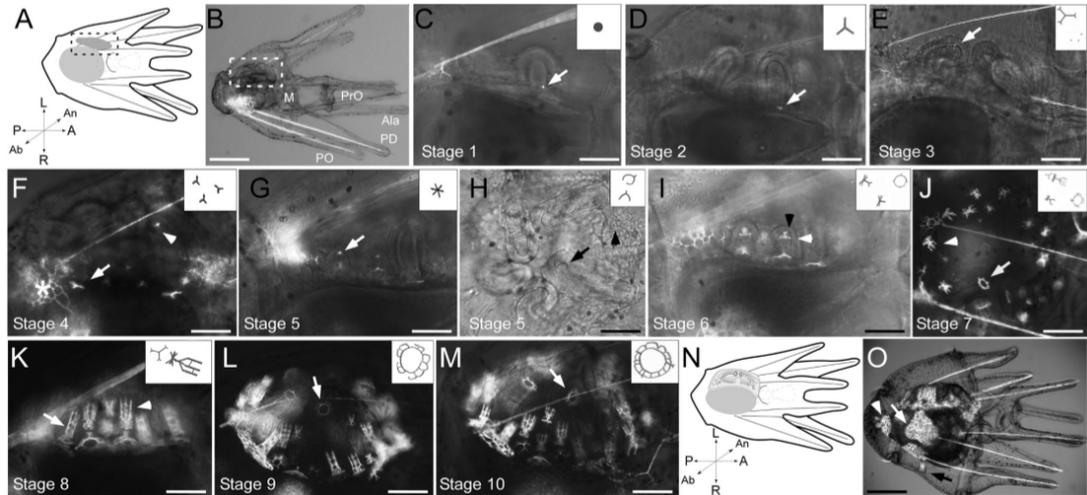
Figure 20 Development of skeletal elements in rudiment formation in *S. purpuratus* (Heyland and Hodin, 2014).

A. scheme of an early stage of the larva (abanal view). All images are in this orientation except where indicated; **B.** live image of an early stage; **C.** the first spicule dot is formed, stage 1 (white arrow); **D.** spicule formation, stage 2 (white arrow); **E.** a tube foot spicule dot is visible (white arrow), anal view; **F.** triradiate tube foot spicule (white arroheads) and multi-branched spicule (white arrow) which will form the ocular plate 1, anal view; **G.** formation of a 6-sided star, anal view (spine primordium, white arrow); **H.** an incomplete tube foot ring is visible (black arrow) and multi-branched spicule is indicated (black arrowhead), which will form the interambulacral skeleton at the base of the adult spine; **I.** spine primordium (white arrowhead) with an extending base of spine (black arrowhead); **J.** pre-spine (white arrowhead) and tube foot ring with second ring completed less than 50% (white arrow); **K.** adult spine (white arrowhead) and juvenile spine, indicated for comparison (white arrow), anal view; **L.** tube foot ring with second ring completed more than 50%, white arrow; **M.** completion of the second ring, anal view, white arrow; **N.** scheme of a later stage, abanal view; **O.** developed larva, white arrow indicates the genital plate 5, white arrowhead indicates the posterior juvenile spine which articulates with genital plate 4, black arrow indicates the right side posterior juvenile spine.

Abbreviations: Ala = anterolateral arms; M = Mouth; St = stomach; PD = postdorsal arms; PO = postoral arms; PrO = preoral arms. Scale bars B - 300 μm; C-D - 70μm; E - 80μm; F-M - 70 μm; O - 200μm.

1.2.1.2. Sea urchin embryos in marine environment: challenges and defences

Marine organisms are constantly exposed to several environmental factors and they continuously face the impact of a variety of increasing pressures, acting individually or simultaneously in coastal environments, and adopt strategies in order to maintain homeostasis, growth and reproduction.

Oxidative stress in marine environments can result from intrinsic factors or from extrinsic/anthropogenic factors. Among the intrinsic factors of environmental stress, are the photochemical production of reactive oxygen species resulting from the absorption of solar radiation, especially UVR wavelenghs, by the dissolved organic matter in seawater (Moper and Kieber, 2000) and hydrothermal vents, that leads to the oxidation of hydrogen sulfide (H_2S). Indeed, the abundance of H_2S and O_2 near the vents, results in the production of oxygen- and sulfur-centered radicals (Tapley *et al.,* 1999). Sea urchin embryos may be susceptible to the dangerous effects of UVR as indicated by elevated concentrations of SOD, DNA damage, and apoptosis in embryos exposed in laboratory to the UVR irradiances found in shallow temperate coastal environments (Lesser *et al.,* 2003). On the other hand, metal contamination is one of the major sources of anthropogenic pollution at the sea, and sea urchins are shown to be affected in reproduction and progeny fitness following cadmium and manganese exposure (Filosto *et al.,* 2008; Pinsino *et al.,* 2010; Migliaccio *et al.,* 2014, 2015).

However, organisms are able, to some extent, to maintain homeostasis in an adverse environment, through the evolution of gene families and pathways, involved in the protection and repairing from damage. The "chemical defensome" is defined as an integrated network of genes and pathways allowing the organism to sense and defend itself from toxic chemicals, including products of microbial origin, heavy metals, phytotoxins or

anthropogenic compounds like polycyclic aromatic hydrocarbons and halogenated organic compounds. Many of these toxicants are hydrophobic and, therefore, can easily pass through the plasma membrane and lead to cellular damage. The chemical defensome (fig. 21) is principally formed by i) soluble receptors and transcription factors activated by ligand binding, which allow the cell to sense toxic molecules or any damage; ii) enzymes able to convert toxic compounds to less toxic or more easily excreted molecules through oxidative, reductive or conjugating biotransformation reactions; iii) efflux proteins, which excrete, in an active way, chemicals from the cell; and iv) antioxidant enzymes, involved in the protection from ROS and other radicals (Goldstone *et al.*, 2006 and bibliography therein).
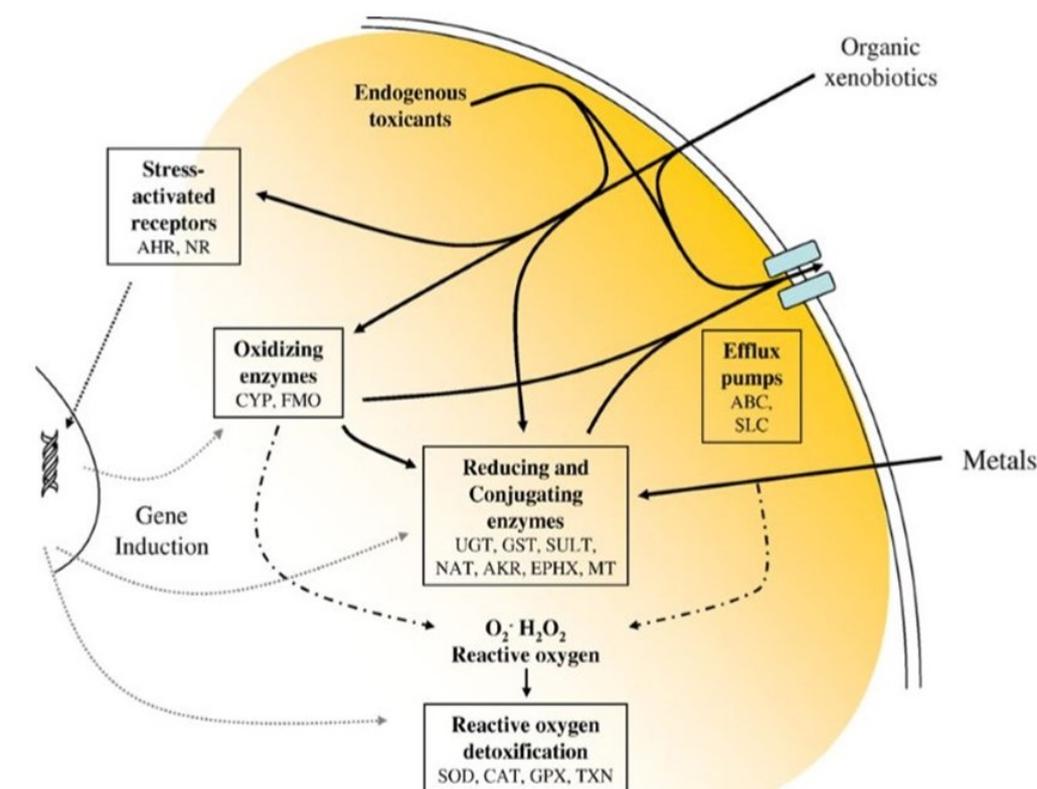
Figure 21 Graphical representation of the chemical defensome (Goldstone *et al.,* 2006).
Toxic molecules are sensed inside the cells through stress-activated receptors, actively exported by efflux pumps, or eventually biotransformed by oxidixing, reducing and conjugating enzymes. ROS are eliminated through antioxidant genes. Abbreviations: AHR = aryl hydrocarbon receptor; NR = nuclear receptor; CYP = cytochrome P450 enzyme; FMO = flavoprotein monooxygenase enzyme;

ABC = ATP binding cassette transporter; SLC = solute carrier ; UGT = UDP-glucorunosyl transferase; GST = glutathione-S-transferase; SULT = sulfotransferase; NAT = *N*-acetyl transferase; AKR = aldo-keto reductase; EPHX = epoxide hydrolase; MT = metallothionein; SOD = superoxide dismutase; CAT = catalase; GPX = glutathione peroxidase; TXN = thioredoxin; continue arrows = possible pathway for exogenous toxicants; dotted arrows = possible gene induction by stress-activated receptors; dot-dashed arrows = possible toxicant-triggered endogenous source for ROS production.

Analysis of the *S. purpuratus* genome has revealed the presence of almost all the gene families and superfamilies used as chemical defence in vertebrates, but in a higher number of genes compared to those found in humans, zebrafish and tunicates (fig. 22). At the moment, it's unclear if the greater number of genes in some gene families in sea urchin is due to gene loss in other (e.g., chordates) lineages or to specific expansion in echinoderms (Goldstone *et al.,* 2006).
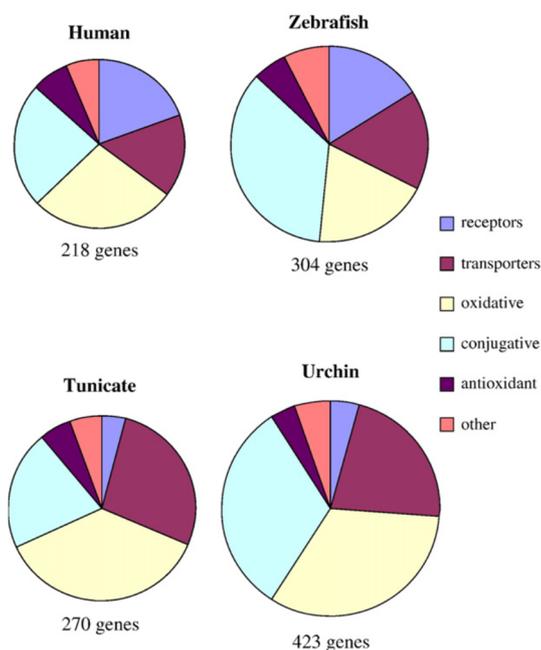
Figure 22 Comparison of the presence of various classes of defensome genes among humans, zebrafish, tunicates and sea urchin (Goldstone *et al.,* 2006).
The area of every pie portion is proportional to the number of genes present in the class indicated in the legend.

The presence of an integrated defence network in sea urchin is relevant considering that embryos are constantly exposed to damaging factors in an extremely sensitive period for their differentiation and development and they lack specific tissues and organs for defence. All cells in the embryos have to possess defence and antioxidant genes to ensure a protection against environmental factors. Eggs accumulate, during oogenesis, some defence gene products, to provide early developmental stages with a protective system, when rapid divisions occur and nucleus/cytoplasm ratio is low (Epel, 2003; Giudice *et al.,* 1999; Hamdoun *et al.,* 2004).

In addition to ovothiol (Palumbo *et al.,* 1982, 1984; Turner *et al.,* 1986, 1988; Shapiro and Hopkins, 1991) (see chapter 1.1.1. Occurrence and biological role of ovothiols in nature) sea urchins synthetise other antioxidants, like tocopherols, ascorbic acid (Backstrom, 1957), carotenoids (Griffiths, 1966; Griffiths and Perrott, 1976) and glutathione (Sakai and Dan, 1959). These antioxidant molecules are present at high concentrations in the eggs and during development (Turner *et al.,* 1986, 1988; Nardi and Cipollaro, 1988; Schomer and Epel, 1998; Castellano *et al.,* 2016), thus, confirming the vital necessity for the embryos to defence themselves from oxidative stress because a disregulation of the defence system can alter development, causing teratogenesis and lethality. The action of the antioxidants is integrated with the regulation of genes involved in neutralising the deleterious effects of ROS which are important stressors for sea urchins. Indeed, three different SOD genes (Goldstone et al., 2006) and an uncommon peroxidase, ovoperoxidase, having a SOD-like activity (Heinecke and Shapiro, 1990) have been identified in *S. purpuratus* genome (Goldstone *et al.,* 2006).

Recently, a series of studies have been performed on the possible involvement of nitric oxide (NO) in the sea urchins' defence system. This important physiological messenger, discovered in the eighties in the human body, has been reported to be also produced in many invertebrates where it is involved in many processes, ranging from neurotransmission and feeding to defence and development (Colasanti and Venturini, 1998; Palumbo, 2005; Rivero, 2006). Particular attention has been focused on the structure, function and evolution of nitric

oxide synthase (NOS), the enzyme responsible for the oxidation of L-arginine to L-citrulline with production of NO, which can be subsequently oxidised to nitrite and nitrate (Andreakis *et al.,* 2010). NOS enzymes have two domains: oxygenase and reductase. The oxygenase domain binds heme, the substrate (L-Arginine), and the cofactor tetrahydrobiopterin (BH_4). The reductase domain provides electrons to the oxygenase domain and binds the cofactors flavin mononucleotide (FMN), flavin adenine dinucleotide (FAD), and nicotinamide adenine dinucleotide phosphate reduced (NADPH). The two domains are linked by a calmodulin (CaM)-binding site (Griffith and Stuehr, 1995; Ghosh and Salerno, 2003). In addition, a Zn binding region participates in binding the BH_4 side chain through an N-terminal hook (Crane *et al.,* 1998; Li and Poulos, 2005). In mammals there are three different NOS enzymes, referred as neuronal (nNOS), endothelial (eNOS) and inducible NOS (iNOS), depending on the cell type in which they were isolated (Griffith and Stuehr, 1995; Alderton *et al.,* 2001). The characterisation of the different NOSs is generally based on the presence/absence of some structural features specific for each mammalian enzyme:

1) the inhibitory loop, present in the reductase domain of the constitutive nNOS and eNOS, controlling the Ca^{2+}/CaM-dependent electron transfer, and whose absence in the inducible iNOS is considered an index of a Ca^{2+} independent isoform (Salerno *et al.,* 1997; Daff *et al.,* 1999);

2) the myristoylation and palmitoylation motifs, required for the efficient localisation of eNOS to the caveolae of endothelial cells (Liu *et al.,* 1995, 1997; Lamas *et al.,* 1992; Sessa *et al.,* 1992);

3) the PDZ domain, responsible for targeting nNOS to synapses in brain and skeletal muscle (Cho *et al.,* 1992; Brenman *et al.,* 1995).

Most invertebrates possess only one constitutive NOS which, through a series of duplication events and gain and losses of protein motifs, gave rise to the three NOSs in mammals (Andreakis *et al.,* 2010).

A series of experiments involving NOS inhibition in developing sea urchin embryos reared in the presence of different stress agents have revealed the protective role of NO. Indeed, production of NO increases in *P. lividus* sea urchin embryos after treatment of fertilised eggs with various stress agents, including the polyunsaturated aldehyde decadienal (Romano *et al.,* 2011) and the metal ions, cadmium and manganese (Migliaccio *et al.,* 2014). NO regulates directly or indirectly the transcriptional expression of some genes involved in stress response, skeletogenesis, detoxification and multi-drug efflux (Romano *et al.,* 2011; Migliaccio *et al.,* 2014, 2015). Recently, the health of a *P. lividus* population living in a marine protected area affected by toxic algal blooms was investigated analysing the animals and their progeny before, during, and after the bloom, along the reproductive season (Migliaccio *et al.,* 2016). A compromised reproductive ability, resulting in abnormal development of the progeny, has been reported, which persists several months after the bloom and is partially recovered towards the end of the reproductive period. Monitoring of NO levels in the gonads and in different developmental stages, together with the analysis of gene expression under conditions of low or high endogenous NO levels (using a NOS inhibitor or a NO donor, respectively), allowed to demonstrate the key role of NO in the transmission of the toxic effect across generations. Indeed, NO initially modifies the functionality of the major protein in the gonads, toposome, and subsequently acts in the defence mechanisms and in the recovery of the offspring (Migliaccio *et al.,* 2016; Castellano *et al.,* 2018).

1.2.2. The coastal diatom *Skeletonema marinoi*

1.2.2.1. Biology of diatoms

Diatoms are unicellular photosynthetic eukaryotes widely distributed in the plankton and benthos of all acquatic environments, contributing to one-fifth of the photosynthesis carried out on earth (Nelson *et al.,* 1995) and responsible for about 20-25 % of global primary production, linking the marine carbon and silicon cycles (Falkowski and Raven, 2007).

They are characterised by a cell size ranging between 10 and 200 µm, although some species can reach up to 1.9 mm in length (Villareal, 1992).

Diatoms have a different and more complex evolutionary history compared to land plants (Parker *et al.,* 2008). Indeed, they evolved from two endosymbiotic events: the first one occurred about 1.5 billion years ago between a eukaryotic heterotroph host and a cyanobacterium, giving rise to the group of Plantae, including land plants, red and green algae; then, about 500 million years later, a secondary endosymbiosis occurred when a different eukaryotic heterotroph engulfed a red alga, which became the plastids of the Stramenopiles group, including diatoms, brown macroalgae and plant parasites (fig. 23). Moreover, gene transfer from bacteria and viruses contributed to the unique combination of genes and pathways in diatoms, presumably allowing them to adapt to new ecological niches (Montsant *et al.,* 2007; Bowler *et al.,* 2008).

Like Plantae, diatoms have the ability to synthetise fatty acids, isoprenoids and amino acids in their plastids, but, due to the second endosymbiotic event, they have, unlike plants, a complete ornithine-urea cycle, essential for diatom growth and contribution to primary productivity (Armbrust *et al.,* 2004; Allen *et al.,* 2011).

Other biochemical peculiarities distinguish diatoms from green algae and land plants. The storage of carbohydrates for instance is different: diatoms store β-glucan chrysolaminarin,

whose structure is based on a β-1,3-linked glucan backbone branched with mostly β-1,6-linkages (Schreiber *et al.,* 2017), in cytosolic vacuoles, different from green algae and land plants, which accumulate α-glucan starch in plastids.
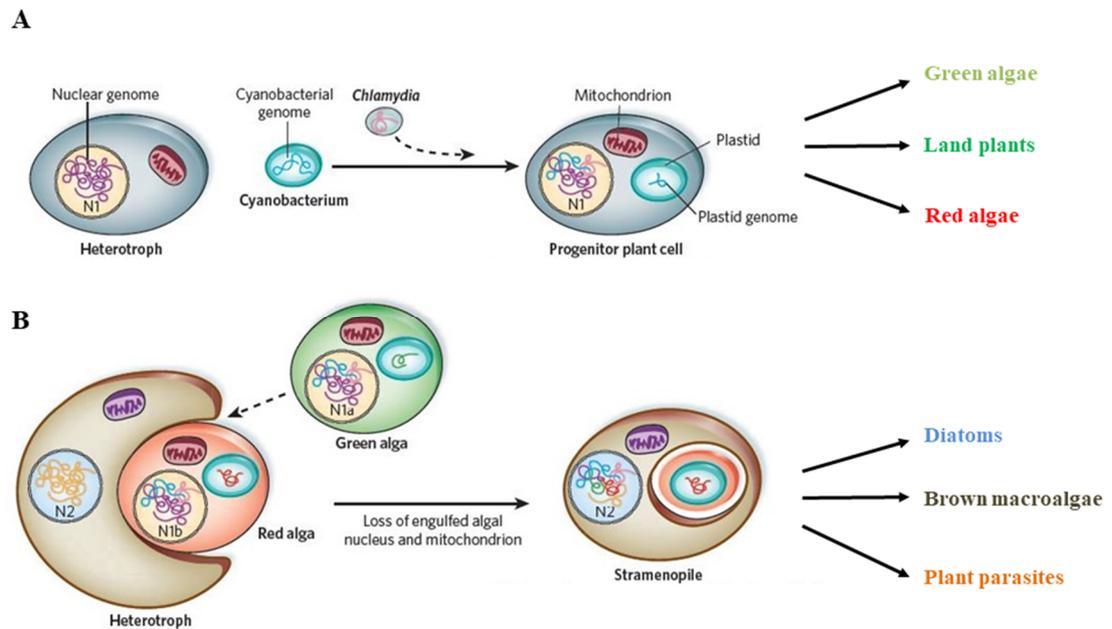
Figure 23 Endosymbiotic origin of diatoms (modified from Armbrust, 2009).
A. During the primary endosymbiosis, the majority of the cyanobacterial genome was transferred to the heterotrophic host nucleus (N1), retaining only few genes in the plastic genome. During these early stages, an invasion of the host from a chlamydial parasite was also suggested (dashed black arrow). From the progenitor plant cell, red and green algae and land plants evolved. **B.** A secondary endosymbiosis occurred between a different heterotroph and a red alga (or green alga as indicated by a dashed arrow). Algal nuclear and plastid genes were transferred to the host nucleus (N2) giving rise to the progenitor of diatoms, brown microalgae and plant parasites.

Diatoms differ from the "green lineage" also for the intracellular localisation of some key metabolic pathways. While green algae and land plants contain two Calvin cycle pathways, one occurring in plastids and the other one in cytosol, diatoms lack the plastidial pathway, and, moreover, they carry out the second half of the glycolysis reaction chain into the mitochondria (Gruber and Kroth, 2017 and bibliography therein). Yet, diatoms have evolved

inorganic carbon-concentrating mechanisms (CCMs) in support of the photosynthetic carbon fixation at the lower concentration of CO_2 present in the acquatic environment, compared to the terrestrial one (Reinfelder, 2011), having the ability to concentrate the CO_2 levels at the site of fixation by RuBisCO, through the action of bicarbonate transporters and carbonic anhydrases (CAs) (Matsuda *et al.,* 2011).

Probably, one of the most relevant peculiarities of diatoms concerns their morphology. Indeed, they possess a silica cell wall, called frustule, whose architecture is extremely various (Compton, 2011) and so highly ornamental (fig. 24A) that it has always been a fascinating object of study inspiring Charles Darwin to write:

"Few objects are more beautiful than the minute siliceous cases of diatoms: were they only created to be admired under the microscope?" in its "On the Origin of Species by Mean of Natural Selection" (Darwin, 1959).

The frustule resembles a petri-dish in which an "hypotheca" is inserted inside an "epitheca", viewed as two valves connected by lateral girdle bands, conferring flexibility to the structure (Friedrichs *et al.,* 2012). This external structure implies that the average size of the cells inside a population progressively decreases during mitotic divisions of the frustule. The cell size is restored in most diatoms through sexual reproduction (Godhe *et al.,* 2014 and bibliography therein). The vertical rim of the epitheca is called epicingulum, which overlaps the hypocingulum of the hypotheca (fig. 24B). The architecture of each valve is constituted by several layers with an ordered pattern of pores (areolae), increasing in diameter from external to internal layers (called cribellum, cribrum and foramen, from the outside layer to the inside one) (fig. 24C).

The valves are formed internally through a complex biomineralisation process occurring in specialised silica deposition vesicle (SDVs). Orthosilicic acid $Si(OH)_4$, abundant in almost every water habitat, is uptaken by diatoms by specific transmembrane silicic acid transporters (SITs). Inside the SDVs, a silica network is formed from $Si(OH)_4$, long chain

polyamines (LCPAs), specific proteins called silaffins and polyanionic peptides (silacidins) (fig. 25).
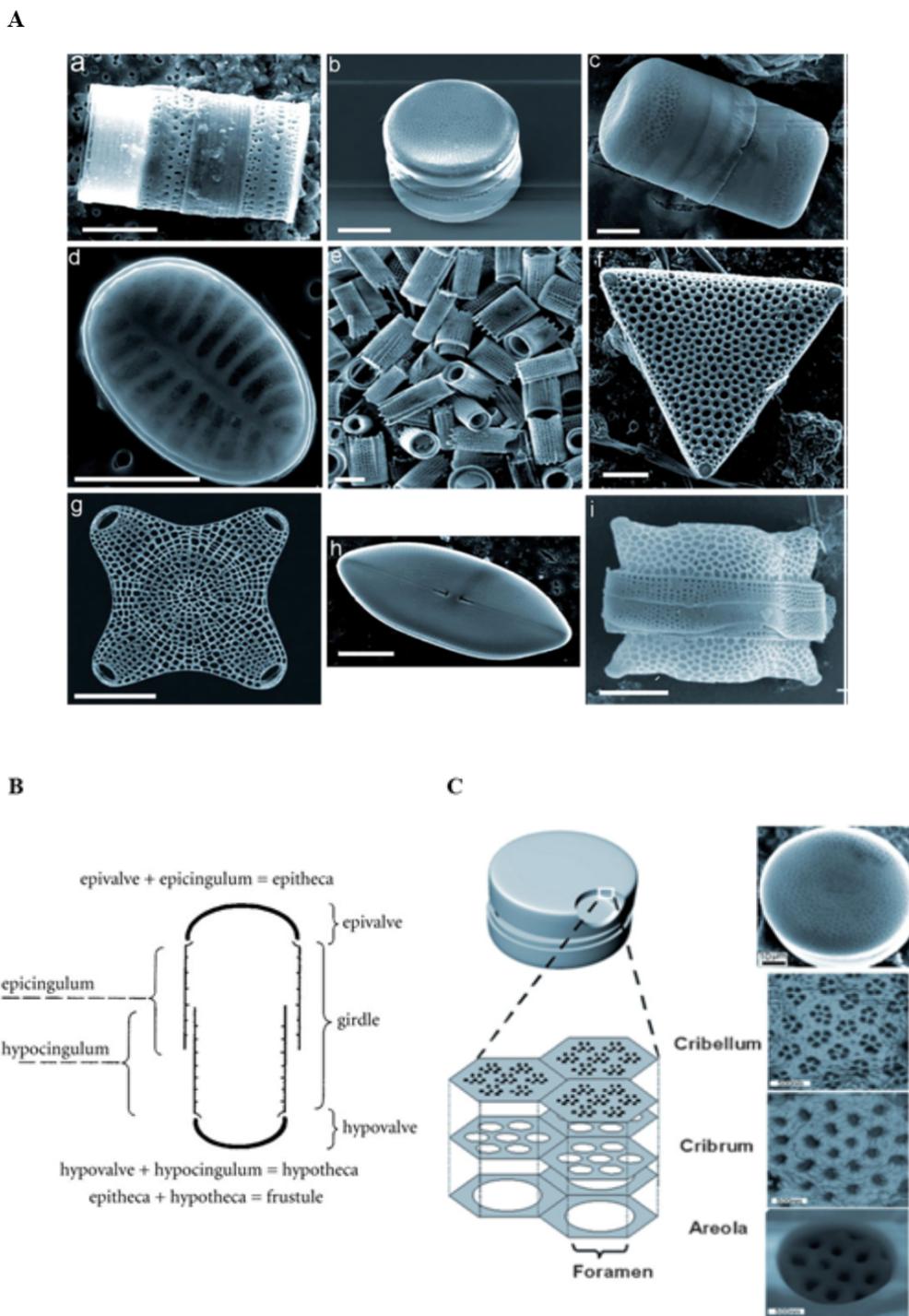
Figure 24 Diatom diversity and frustule ultrastructure (Benton and Harper, 2009; Losic *et al.,* 2009)
A. Shape diversity; **B.** schematic representation of frustule; **C.** architecture of valves.

Due to their features, including biocompatibility, high surface area, possibility to modulate pore size and versatile surface chemistry, these structures are attractive materials, for several purposes, like drug delivery, optics and photonics applications (Ragni *et al.,* 2016 and bibliography therein).
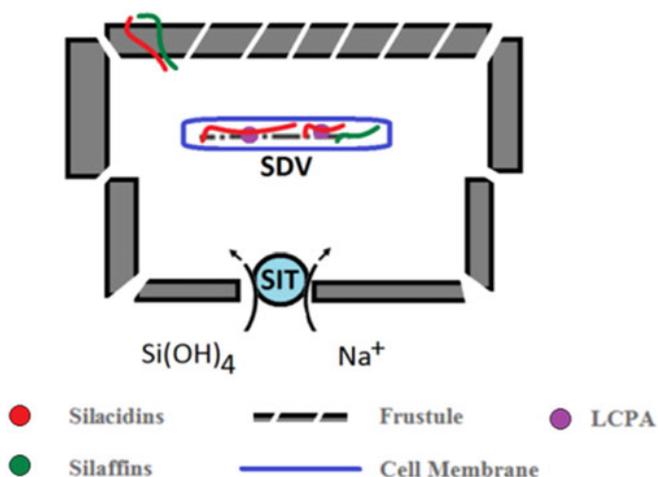
Figure 25 Formation of valves in diatoms (Ragni *et al.,* 2016).
$Si(OH)_4$ is uptaken inside the cells by SITs proteins, which bind it through glutamine residues. Silica network is assembled in specific SDVs from $Si(OH)_4$ in the presence of organic components, like silaffins, silacidins and LCPA.
Abbreviations: SITs = silicic acid transporter proteins; SDVs = silica deposition vesicles; LCPA = long chain polyamines.

Diatoms can be dinstinguished on the basis of the symmetry of their frustules in centric diatoms, typically planktonic, characterised by a radial symmetry, and pennates diatoms, mostly benthic having a bilateral symmetry (Round *et al.,* 1990).

Centric diatoms include radial centrics, which constitute the most ancient group, and multipolar centrics, slightly younger. Pennate group is relatively young, and, within it, the raphid pennates, having a slit called raphe, represent the most recently diversified and richest

group in terms of species (Kooistra *et al.,* 2007; Kooistra, 2008 and bibliography therein; fig. 26).
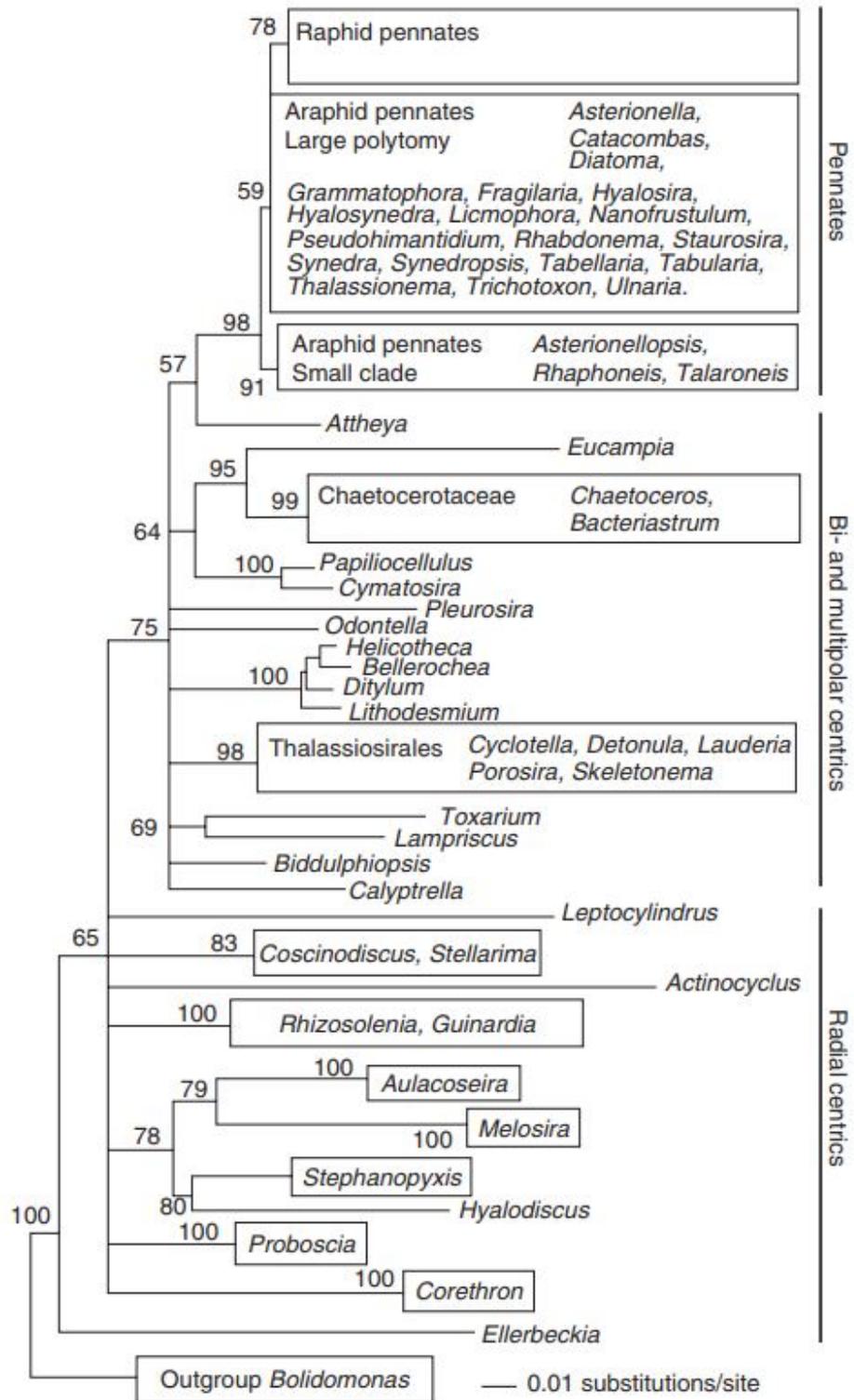
Figure 26 Neighbor joining phylogeny of various diatom species (Kooistra *et al.,* 2007).

1.2.2.2. The model species: *Skeletonema marinoi* Sarno & Zingone

Skeletonema marinoi is a centric diatom species (fig. 27) dominating phytoplankton assemblages in temperate coastal regions and worldwide distributed, except in the polar regions (Kooistra *et al.,* 2008). Where present, *S. marinoi* dominates the plankton community during the spring bloom (Sarno *et al.,* 2005), reaching densities of 10^4 cells per ml (Saravanan and Godhe, 2010).

The strain (CCMP 2092) used in my work was collected from the surface waters of the northern Adriatic Sea, where this diatom provides the major contributor to the late winter blooms (Miralto *et al.,* 1999) and can be found in very shallow waters (Brunet, Personal Communication).

It forms chains and, although reproduces mainly through vegetative division, sexual reproduction and formation of auxospores have also been reported (Godhe *et al.,* 2014). It can form benthic resting stages, which can survive in anoxic sediments for long time, representing seed banks for future blooms (McQuoid *et al.,* 2002).
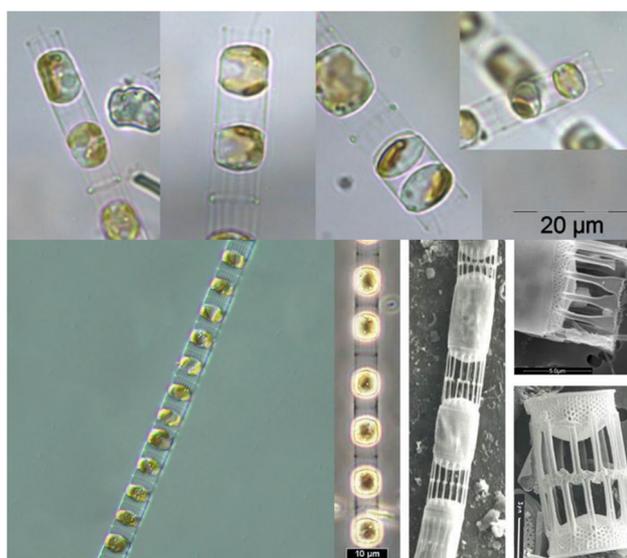
Figure 27 *Skeletonema marinoi* Sarno & Zingone, 2005 (photographers/artists: Susanne Busch, Bengt Karlson, Regina Hansen).

This species is particularly suitable for the study of phenotypic responses, compared to other diatom species, due to its short mitotic generation time, approximately one division per day, and the fact that it is easy to collect, isolate and maintain in culture. Moreover, its transcriptome is available, while genome is under study (Godhe, 2017). Yet, a lot of information is already available on the biology and photophysiology of this species (Orefice *et al.,* 2016, 2019).

S. marinoi was selected as model in my study since its high growth rate (Chandrasekaran *et al*., 2014; Kourtchenko *et al.,* 2018), its use as feed in acquaculture (Liao *et al.*, 1983; Su *et al*., 1990; Coutteau and Sorgeloos, 1992; Brown *et al*., 1997) and its potential other biotechnological applications (Smerilli *et al.,* 2017).

Finally, the fact that this species was already present at SZN and whose culturing was set up in the laboratory of Christophe Brunet (EMI department, SZN) constituted a great advantage for its use in this study. In addition, preliminary experiments showing that *OvoA* gene was modulated by light in *S. marinoi* (data not showed) provided the basis for this work and stimulated the interest in investigating the ovothiol formation in this species.

1.2.2.3. Photosynthesis in diatoms

Oxygenic photosynthesis is a unique process able to use sunlight energy to produce oxygen, from water, and reducing power in form of NADPH, allowing the fixation of CO_2 into organic matter, thus fueling the food chain. In eukaryotes, photosynthesis occurs in plastids. In plants, plastids are surrounded by a two-membrane envelope and contain thylakoid domains, segregating the different photosystems. Indeed, they present stacked regions (grana), which are rich of photosystem II (PSII) and unstacked regions (stroma lamellae), rich of photosystem I (PSI) (Anderson, 1986) (fig. 28, top).

Differently, diatoms contain complex plastids, due to their origin from the eukaryote-eukaryote endosymbiosis (Gould *et al.,* 2008; Archibald, 2015). Unlike primary plastids present in the green lineage (derived from the primary endosymbiosis with cyanobacterial ancestors), diatoms' plastids are surrounded by four membranes, whose outermost membrane is continuous with the endoplasmic reticulum (ER). This implies that nuclear-encoded plastid proteins are previously imported into the ER and then targeted to the plastid stroma or the associated compartments, i.e. periplastidial compartment (lacking in plants and representing the former cytosol of the secondary endosymbiont) and thylakoid lumen due to the presence of different signal peptides (Kroth, 2002; Patron and Waller, 2007) (fig. 28, bottom). Thylakoid architecture is also peculiar in diatom plastids, where they are not stacked like in higher plants or in green algae but they are organised into loosely appressed bands of three lamellae (fig. 28, top) (Larkum and Vesk, 2003). By consequence, there is not a specific segregation of photosystems even if it has been reported that PSI seems to have the tendency to concentrate on the unappressed regions exposed to the stroma (Pyszniak and Gibbs, 1992). Finally, algal plastids also contain a specific compartment, called pyrenoid, in which CO_2 is concentrated and fixed by the action of RuBisCO (fig. 28, top).
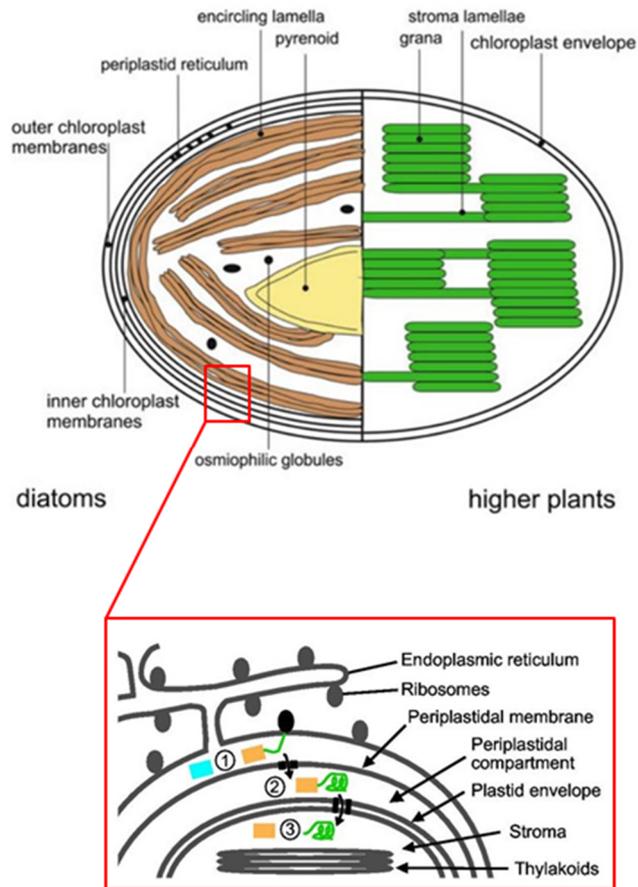
Figure 28 Plastid architecture in diatoms (modified from Grouneva *et al.,* 2013; Huesgen *et al.,* 2013).

On top. Scheme of the chloroplast architecture in diatoms (on left) compared with higher plants (on right) in which differences are highlighted like the organization of thylakoids, loosely appressed in bands of three lamellae in diatoms, different from grana and stroma lamellae in higher plants, and the presence of pyrenoid. The stroma can also contain osmiophilic globules as indicated in figure; **on bottom.** Nuclear encoded protein import in diatom plastids is carried out thanks to the presence of different signal peptides: the first for the ER lumen (light blue), then removed through a signal peptidase (1); a second transit peptide for the periplastidial compartment (orange, 2), then cleaved once it has entered into the stroma, through the translocons of the plastid, by a stromal peptidase (3).

The first step in photosynthesis is the light harvesting through the light harvesting complex (LHC), able to bind pigments, which in diatoms (like in brown algae) are chlorophyll α and c (Raven, 1970) and carotenoids, mainly fucoxanthin and β-carotene derivatives, such as the xanthophyll cycling pigments. The xanthophyll cycle (XC) has a key photoprotection role

(Müller *et al.,* 2001), since it is responsible for most of the non-photochemical quenching of chlorophyll α fluorescence (NPQ), the process in which the excess of the absorbed light energy is dissipated as heat, leading to a decrease of the excitation pressure on PSII (Lavaud, 2007). NPQ is essential for photosynthetic organisms because an over-excitation of the photosystems can lead to the formation of Chlα triplet (^{3}Chl*), which can react with oxygen, leading to the production of singlet oxygen ($^1O_2$), or induce an over-reduction of NADP and the reduction of O_2 to form singlet superoxide (O_2^-), hydrogen peroxide (H_2O_2), and hydroxyl radical (OH$^•$), all reactive species causing oxidative stress (Foyer and Shigeoka, 2011) (fig. 29).
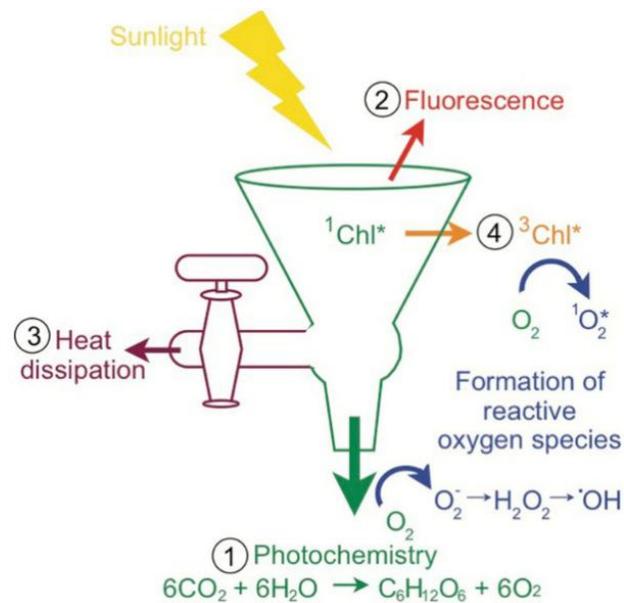
Figure 29 Graphical schematisation of oxidative stress produced during photosynthesis and the possible fates of absorbed light (Roth, 2014).
When chlorophyll absorbs sunlight, it is converted to singlet Chl (^{1}Chl*) whose excitation energy can be used for (1) photochemistry, with production of ROS as side products, (2) released as fluorescence, (3) be dissipated as heat during NPQ, or (4) be converted to triplet Chl (^{3}Chl*), which can lead to the formation of the highly reactive singlet oxygen ($^1O_2^*$).

The dominant carotenoids in diatoms are fucoxantin (FX), conferring them the typical gold-brown color, and the two pigments forming the XC, diadinoxanthin (DD) and diatoxanthin

(DT) (Stransky and Hager, 1970; Kirk, 1977). By contrast, zeaxanthin (ZX), antheraxanthin (AX) and violaxanthin (VX), which in higher plants and brown algae are involved in the photoprotection under high light exposure, in diatoms are only indermediate products in the formaton of DD and FX (Lohr and Wilhelm, 1999).

Based on data of lipid, protein and pigment composition, a model of the thylakoid membrane in diatom plastids has been proposed (Lepetit *et al.,* 2007; Wilhelm *et al.,* 2014). According to this model, the inner parts of the three thylakoid membranes are rich of PSII and fucoxanthin-Chl proteins (FCP), which are surrounded by a large amount of the monogalactosyldiacylglycerol (MGDG) present in the thylakoids. Since MGDG represents the docking site for the diadinoxanthin de-epoxidase (DDE, the enzyme responsible for the conversion of DD to DT), the inner part of the thylakoid membranes is the region where most of the photoprotective XC occurs. In fact, most of the ROS produced during photosynthesis are formed in PSII, where free DT acts as an antioxidant defence. Binding the FCP, DT can also participate in NPQ through a direct quenching of excited Chl and the detachment and aggregation of FCPs.

On the contrary, the outer regions are enriched in PSI and ATP synthases, surrounded by sulfoquinovosyldiacylglycerol (SQDG), which inhibits the de-epoxidation of DD and the aggregation of FCP complexes (Wilhelm *et al.,* 2014 and bibliography therein).

Although this separation of domains is already present in low light acclimated species, high light rienforces the heterogeneity of thylakoid membranes (Lepetit *et al.,* 2012). Indeed, in high light conditions, it is observed an enrichment in SQDG in the outer regions, an increase in the synthesis of Lhcx proteins involved in the photoprotection, a higher incorporation of XC pigments close to the FCPs in the inner regions and an increase in the detachment and aggregation of FCPs (fig. 30).
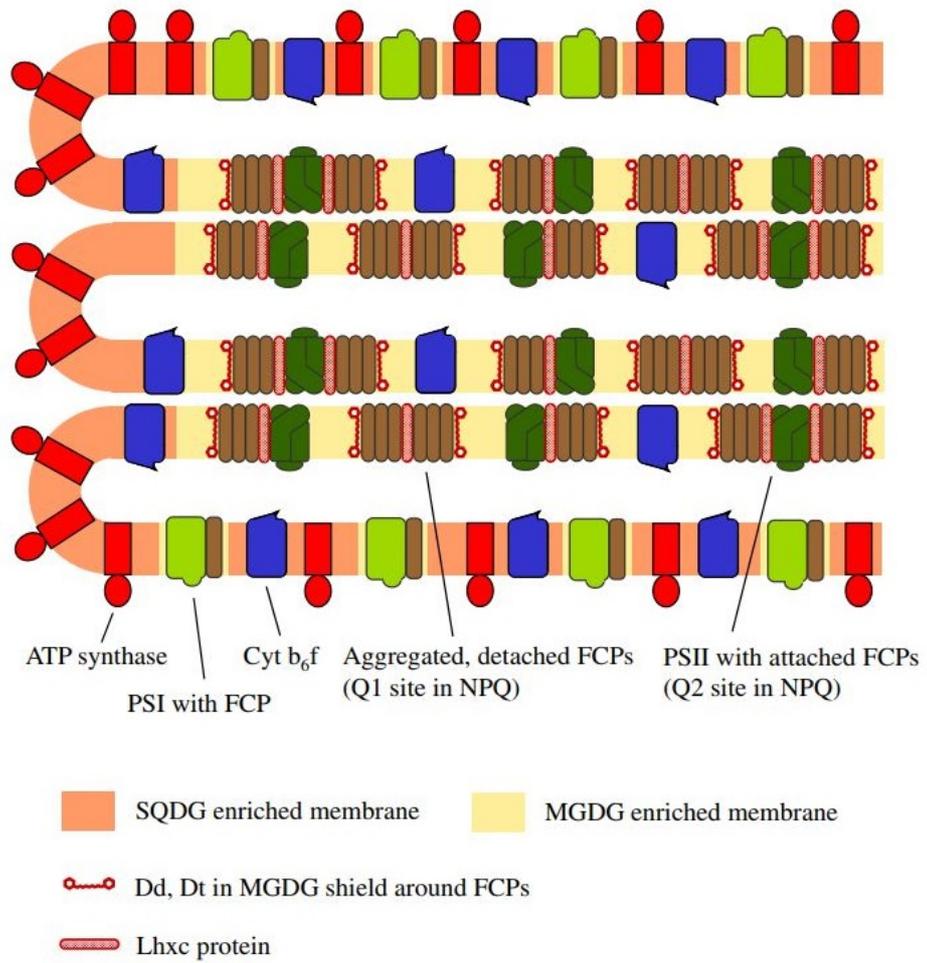
Figure 30 Model of diatom thylakoid membranes in high light acclimated cells (Wilhelm *et al.,* 2014).

1.2.2.4. Biotechnological potential of diatoms

It is known that microalgae represent a relevant resource for biotechnological purposes, due to their huge biodiversity and the possibility to modulate their growth, physiology and biochemistry. In this context, diatoms are particularly suitable to this aim, due to their ability to efficiently adapt to environmental changes (Dubinsky and Stambler, 2009). Indeed, they are highly responsive to external forcing, not only light but also hydrology (temperature, salinity) and chemistry (pH, macro- and micronutrients) (Barra *et al.,* 2014 and bibliography therein).

In marine waters, phytoplankton is exposed to a high variable light availability because it continuously moves among different depths through vertical mixing. Since high light can be dangerous especially for PSII, due to the photoinhibition process (Murata *et al.,* 2007), phytoplankton evolved an extremely high resilience to short term changes of light intensity. Diatoms, in particular, have demonstrated high ability to cope with high light, thus providing a partial explanation for their ecological success in the ocean (Brunet and Lavaud, 2010).

Light manipulation can be used to modify diatom (and microalgal in general) productive yield in the context of the Photosynthetic Regulation Biotechnology (Barra *et al,* 2014; Brunet *et al.,* 2014). In particular, light can be modulated in terms of different variables, like the instantaneous photon flux density (PFD, the instantaneous intensity of the light), the daily light dose intensity, the photoperiod (length of the day/night phases), light distribution (velocity of light increase/decrease over the day), frequency of PFD variability and spectral composition (Barra *et al.,* 2014).

In this way, light conditions can be optimised in order to reduce energy loss and enhance biomass production and primary metabolites biosynthesis (fig. 31).
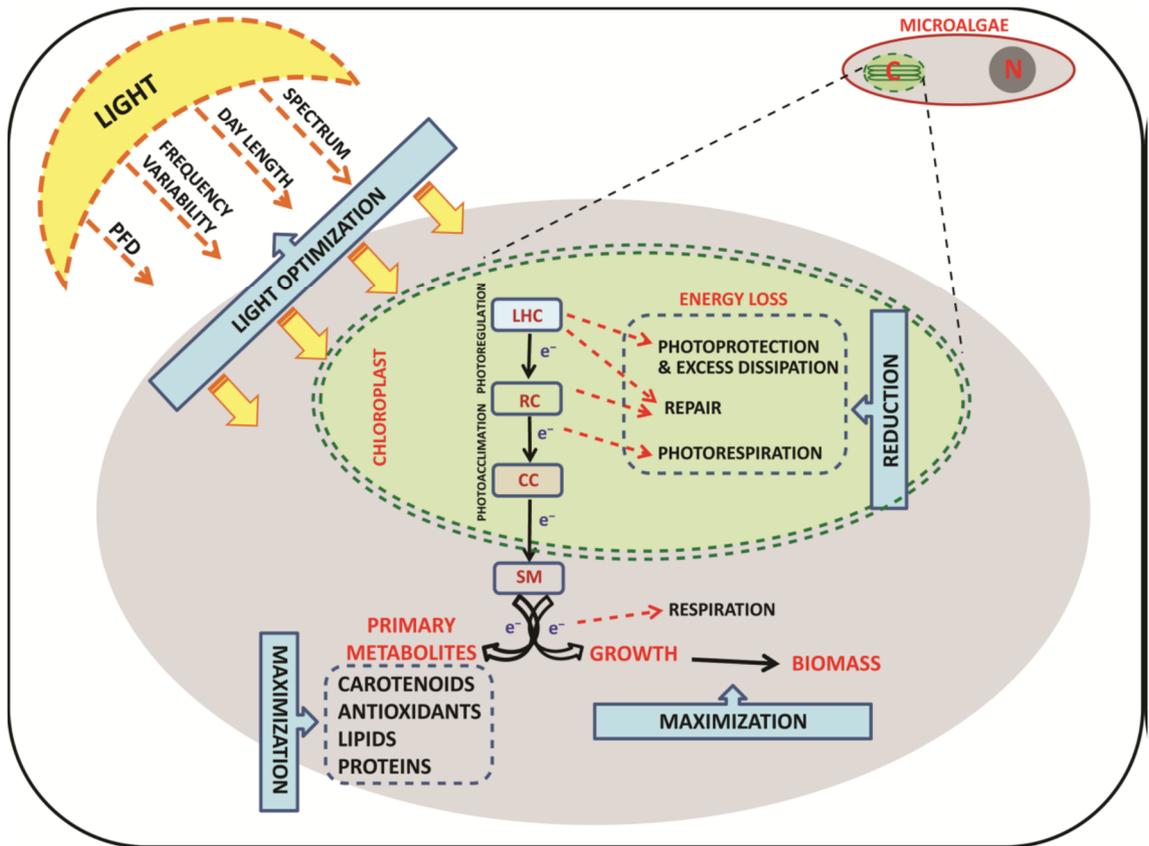
Figure 31 Maximisation of photosynthesis for biotechnological purposes (Barra *et al.,* 2014).
Light manipulation allows to modulate microalgal growth and physiology acting on photoregulation
and photoacclimation processes. The reduction of energy losses leads to the enhancement of growth
and biosynthesis of primary metabolites. Abbreviations: PFD = Photon Flux Density; LHC = light
harvesting complex; RC = Reaction Center; CC = Calvin Cycle; SM = Storage Molecules; C =
chloroplast; N = Nucleus.

CHAPTER 2

Investigating the function of ovothiol during

P. lividus development

2.1. Aims of the study

Thanks to their chemical features, ovothiols are receiving an increasing interest as promising pharmacological compounds for a potential therapeutic use in humans. Indeed, an ovothiol analogue, 1-methyl-2-(3-trifluoromethylphenyl)-4-mercaptoimidazole, has shown to have a potent action in mammalian cerebral protection (Vamecq *et al.*, 2003) and ovothiol A itself has anti-proliferative activity on the human hepatocellular carcinoma cell line (Russo *et al.*, 2014) and an anti-inflammatory activity in an *in vitro* cellular model of hyperglycemia-induced endothelial dysfunction (Castellano *et al.*, 2018).

With this in mind, the comprehension of the physiological roles of these molecules in organisms in which they are naturally produced would allow to exploit all the possible applications of ovothiols, especially related to human health and wellness.

Although ovothiols were initially isolated and characterised from sea urchins, there is still an incomplete knowledge about their biological role in these animals.

In *S. purputatus* ovothiol C was proposed as the low molecular weight heat stable factor of the NADPH oxidase activity of ovoperoxidase (Turner *et al.*, 1986), an enzyme exocytosed at fertilisation, responsible for the hardening of the external membrane (Deits *et al.*, 1984; Foerder and Shapiro, 1977). However, the involvement of ovothiol in the H_2O_2 production following fertilisation was then questioned and a role in the control of H_2O_2 toxicity was suggested (Turner *et al.*, 1987; Shapiro *et al.*, 1990). Based on its properties, ovothiol could be also involved in the maintenance of the redox gradient which has been reported in *S. purpuratus* to play a role in oral-aboral axis specification (Coffman and Denegre, 2007; Coffman *et al.*, 2009). However, further studies are necessary to better clarify the role of ovothiol in theses processes.

Taking advantage of the recent characterisation of OvoA from bacteria (Braunshausen and Seebeck, 2011), the *OvoA* gene homologue was identified in the Mediterranean sea urchin

P. lividus transcriptome (*PlOvoA*) and its expression was reported to be up-regulated by stressful agents, such as cadmium and toxic blooms, leading to ovothiol biosynthesis. These studies allowed to identify a key role of ovothiol in protecting embryos from environmental cues (Castellano *et al.,* 2016), triggering new interest in investigating the function of this compound during embryonic development of sea urchin.

On this background, this work is aimed to investigate the temporal and spatial expression of OvoA during *P. lividus* development in order to shed light on the role of ovothiol. The expression of *OvoA* mRNA was followed by *in situ* hydridisation. For the protein, a polyclonal antibody specific for OvoA from *P. lividus* was produced by a company and the expression and the localisation of the enzyme was assessed at different developmental stages through Western Blot analyses and immunohistochemistry experiments respectively. Finally, perturbation experiments through morpholino microinjection were performed to assess the functional significance of ovothiol biosynthesis in sea urchin embryos.

2.2. Material and methods

2.2.1. Ethics statement

P. lividus (Lamarck) sea urchins were collected from a location not privately-owned nor protected in any way, according to the authorisation of Marina Mercantile (DPR 1639/68,09/19/1980 confirmed on 01/10/2000). All animal procedures were in compliance with the guidelines of the European Union (directive 609/86).

2.2.2. Gamete collection, fertilisation and embryo culture

Sea urchins were collected in the Gulf of Naples during the breeding season by SCUBA divers, transported in an insulated box to the laboratory within 1 h after collection, kept in tanks with circulating sea water at a density of 1 animal/5 L and fed every 3 days with fresh macroalgae (*Ulva* sp.). The animals were acclimated for a minimum of 10 days before the experiments and kept in a controlled temperature chamber ($18 \pm 2°C$) at a 12:12 light:dark cycle. Very rare spontaneous spawning or mortalities were observed during the acclimation period. The gametes spawning was induced by the injection of a 0.5 M KCl solution through the peribuccal membrane of the animals. Concentrated sperm was collected dry, deriving from at least three different males, and kept undiluted at +4°C until use. Eggs from individual females were washed three times with 0.22 µm filtered sea water (FSW) and fertilised at a density of 150 eggs/mL with few drops of diluted sperm (1:1000). The fertilisation success was approximately 90 %.

For *in situ* hybridisation and immunohistochemistry experiments on pre-hatching developmental stages, eggs were fertilised in the presence of para-aminobenzoic acid

(PABA) (1 mmol/L) to prevent the hardening of the fertilisation membrane, then removed by passing the fertilised eggs through a 70 µm mesh filter.

Embryos were allowed to develop at $18 \pm 2^{\circ}C$ in a controlled temperature chamber at a 12:12 light:dark cycle. All the experiments were performed in triplicate.

2.2.3. Preparation of sense and antisense probes anti-*OvoA* RNA

Total RNA was extracted from about 1500 embryos (5 hours post fertilisation) using RNAqueous-Microkit (Ambion), and 600 ng was retrotranscribed with iScript™ cDNA Synthesis kit (Biorad), following the manufacturer's instructions.

1 µl of total cDNA was used to obtain OvoA cDNA by PCR using the following primers:

OvoA-F: 5'-CATCCGTCCTCATCCGTCAG-3';

OvoA-R: 5'-CCTAACTGGCACGTCTTGGT-3'

and then cloned into the pGEM®-T Easy Vector (PROMEGA).

Plasmid fraction was purified by GenElute™ HP Plasmid Miniprep Kit (NA0160, Sigma) and then linearised by PCR. The PCR product (fig. 32A) was purified by QIAquick PCR Purification Kit (Qiagen) and used as template for RNA labeling with digoxigenin-UTP by *in vitro* transcription with SP6 and T7 polymerases, to obtain antisense and sense probes respectively (probe size: 974 bp, fig. 32B). Probes were finally purified by gel filtration chromatography on Sephadex G-50 columns and quantified by assessing the absorbance at 260 nm (ND-1000 Spectrophotometer; NanoDrop Technologies, Wilmington, DE, USA).
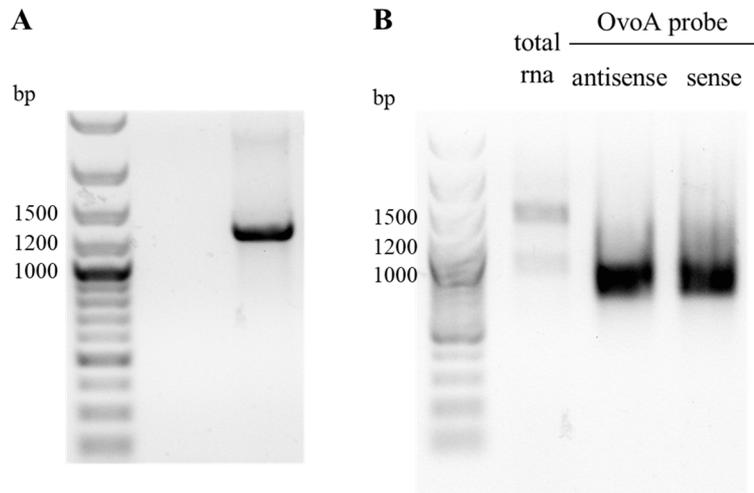
Figure 32 OvoA probe preparation.

Agarose gel electrophoresis: **A.** PCR fragment obtained by the amplification of OvoA-plasmid miniprep; **B.** antisense and sense probes.

2.2.4. *OvoA* **RNA** *in situ* **hybridisation**

In situ hybridisation experiments were performed according to the protocol described in Andrikou *et al.* 2013.

Briefly, embryos were fixed in fixative solution (4% paraformaldehyde, 0.1M MOPS pH 7, 0.5M NaCl, DEPC water) for 1h at room temperature, washed three times in MOPS buffer (0.1M MOPS pH 7, 0.5M NaCl, 0.1% tween-20, DEPC water) and stored at -20 °C in 70% ethanol in DEPC water until use. After three washes in MOPS buffer, the embryos were incubated in hybridisation buffer (MOPS buffer supplemented with 70% formamide, 1mg/ml BSA and tRNA) for 3h at 50°C and treated with antisense probe (0.1 ng/µl) for 1 week at the same temperature. Then, samples were rinsed in post-hybridisation buffer (same recipe of hybridisation buffer, without tRNA) for 3h at 50°C and washed 5 times in MOPS buffer.

For fluorescent *in situ* hybridisation (FISH) embryos were blocked with Perkin-Elmer (PE) blocking reagent for 30' at room temperature and then incubated with anti-digoxigenin antibodies conjugated to horseradish peroxidase (anti DIG-POD) (Roche) 1:1000 in PE

reagent overnight at 4°C. Following 5 washes in MOPS buffer, samples were incubated in amplification diluent (AD, 1.6 µl 30% H_2O_2 in 10 ml TBS 1x, 50 mM Tris-HCl, pH 7.6, 150 mM NaCl) for 30' at room temperature and then treated with Cyanin 5 (Cy5, FP1171, Perkin Elmer) 1:400 in AD for 30' at room temperature in dark. DAPI was added to the samples and embryos were visualised at the confocal microscope (Zeiss LSM 700).

For chromogenic *in situ* hybridization (CISH), samples were washed 4 times in alkaline phosphatase (AP) buffer (0.1M Tris-HCl, pH 7.6, 2.5mM $MgCl_2$, 0.1M NaCl) and then 2 times in AP buffer supplemented with 0.2% tween-20 and 1mM levamisole. Incubation was carried out in dye solution composed by 10% dimethylformamide, 100mM Tris-HCl pH 9.5, 50mM $MgCl_2$, 0.1M NaCl, 1mM levamisole, and the two substrates for alkaline phosphatase: 0.3 mg/ml nitro-blue tetrazolium chloride (NBT) and 0.2 mg/ml 5-bromo-4-chloro-3'-indoly phosphate p-toluidine (BCIP). Coloration was carried out over night at room temperature, checking under microscope the desired intensity. The reaction was stopped with 50mM EDTA in TBS 0.1 % tween-20 (TBST). Samples were washed 2 times in TBST, rinsed in glycerol 30% in MOPS buffer and finally visualised on glass slides under the microscope (Zeiss Axio Imager M1).

Negative controls were performed on the same batch of animals and in the same conditions using sense probe.

For FISH and CISH experiments, about 50 embryos/larvae were visualised under the microscope for each developmental stage.

2.2.5. Preparation of the antibody anti-OvoA and the IgGs from pre-immune serum

P. lividus OvoA protein sequence (ID: AMM72581.1）was downloaded from the NCBI protein database. Based on the aminoacidic sequence of OvoA protein from *P. lividus*, a

prediction of the antigenic determinants and eventual signal peptides and transmembrane domains was performed by Primm company (www.primm.it). They selected 5 antigenic peptides on the basis of the antigenic determinants and the hydropathy value, deriving from the sum of the hydropathy values for each residue divided for the length of the sequence (GRAVY result ≤ 0; Kyte and Doolittle, 1982), being the hydrophilic peptides preferable for peptide synthesis, conjugation and solubilisation: P1 (KTEDAIYKAPDRLRLC; 52- 67 aa); P2 (PDQNQNSSQYRYRSC; 313 - 327 aa); P3 (EAKAYAAWKGPGYRC; 346 - 359 aa); P4 (KSAEELLSKKQKVFYC; 609 - 624 aa); P5 (CLDRVPNKRAWLIR; 681 - 694 aa).

Using the structure similarity with EgtB, the enzyme responsible for the biosynthesis of the 2-thio analogue of ovothiol, ergothioneine, a model of OvoA, based on the DinB superfamily and FGE-sulfatase domains shared by the two enzymes, was done by Dr. Immacolata Castellano (Stazione Zoologica Anton Dohrn, Naples) in collaboration with Prof. Antonello Merlino (Università degli studi di Napoli "Federico II", Naples). This model has allowed to identify the epitopes exposed on the tertiary structure of the protein with the aim to prepare an antibody able to recognise the protein both in denatured and in native form. Three peptides were selected: P1, 52-67 aa and P2, 313-327 aa, exposed on the surface of the protein and P4, 609-624 aa, present in the C-terminal region.

Based on these information, a polyclonal antibody was produced by Primm in two rabbits, using the mix of the three synthetic antigenic peptides conjugated with OVA (Ovoalbumin) as carrier protein, and was provided as IgGs purified from the immune sera.

Primm provided also the preimmune sera from the two rabbits and IgGs were purified through affinity chromatography using protein A agarose (Sigma-Aldrich srl, Milano, Italy) according to standard procedures. Briefly, the serum was diluted with 3 volumes of loading buffer (1M potassium phosphate, pH 9) and loaded onto a 1 mL column of protein A agarose, equilibrated with loading buffer. The unbound fractions have been discarded and the column was then eluted with 0.1 M citric acid, pH 3. The elution of the fractions was followed by measuring the absorbance at 280 nm. The fractions containing the IgGs were neutralised to

pH 6-8 with 1.5 M Tris-base, pooled and dialysed against phosphate-buffered saline (PBS), pH 7 at 4 °C. After dialysis, protein concentration was measured by Bradford assay (Bradford, 1976).

Company tested the sera from both rabbits at different dilutions for reactivity against the antigenic peptides conjugated to a carrier protein different from that one used for immunisation, i.e. KLH (Keyhole Limpet Haemocyanin), through ELISA assay, using pre-immune sera as negative controls. The results showed that both sera developed a higher immunoreactivity against P1, compared to the other peptides. Moreover, serum from rabbit 1 developed a similar immunoreactivity against P4, while that one of serum from rabbit 2 was lower. A decrease of immunoreactivity of both sera was detected against P2 (see supplementary fig. 1S). Primm Company subjected the reactive sera to epitope-specific antibody purification on CNBr-sepharose-column evaluating the presence of IgGs in the eluted fractions through Maldi-TOF Mass Spectrometry. The reactivity of the purified anti-OvoA IgGs against the synthetic peptides conjugated to KLH was determined through ELISA assay. The results showed that anti-OvoA IgGs from rabbit 2 had a higher immunoreactivity against all the peptides, compared to IgGs from rabbit 1 (see supplementary fig. 2S).

Anti-OvoA IgGs from both rabbits were tested in WB and IHC experiments, using pre-immune IgGs at the same protein concentration. A representative WB, showing the immunoreactivity of pre-immune IgGs from both rabbits, is reported in supplementary fig. 3S. Pre-immune IgGs from rabbit 1 showed absence of any immunopositive band compared to the one from rabbit 2, thus it was used for all the experiments.

2.2.6. Western Blot analyses

For every developmental stage (from unfertilised eggs to larval stages), 200 mL of culture (30000 embryos) were centrifuged at 1500 rpm for 10 min at 4°C in a swing-out rotor centrifuge. The collected pellets were combined, washed in PBS, centrifuged again in the same conditions, weighed, rapidly freezed in liquid N_2 and kept at -80°C until use.

For western blot analyses (WB), pellets collected as above, were dounce-homogenised on ice in PBS with 0.5% Triton X-100, pH 7.4 (Amaroli *et al.,* 2013), supplemented with proteases and phosphatases inhibitors (1mM $NaVO_4$, 1mM NaF, 1mM PMSF, cocktail of phosphatases and proteases inhibitors). A protein amount corresponding to 20 µg was separated by electrophoresis on 12% SDS/PAGE gels and transferred to PVDF membranes. Membranes were incubated with 5% non fat dried milk (nfdmilk) blocking solution for 1 hour and then with anti-OvoA IgGs (dilution 1:500, final concentration 1 µg/mL) or anti-α actin (1:5000) overnight at 4°C. After multiple washes in PBST, membranes were incubated with horseradish peroxidase-conjugated goat anti-rabbit IgGs (Santa Cruz Biotechnology, Inc., Texas, USA) (dilution 1:5000) in 5% nfdmilk for 1 hour at RT. Protein bands were visualised on Hyperfilm-ECL films using the ECL Western blotting Detection Reagents (GE Healthcare, Buckinghamshire, UK).

2.2.7. Mass spectrometry analyses

Immunopositive bands were analysed through MALDI-TOF technology. A protein amount corresponding to 20 µg in quadruplicate was separated by electrophoresis on 12% SDS/PAGE gels. The gel was incubated in a fixative solution (40% methanol, 7% acetic acid) for 1 hour at RT and stained with a Colloidal Coomassie solution (20% methanol, 16% Brilliant Blue G colloidal concentrate, Sigma–Aldrich, St. Louis, MO) over night at 4°C.

The gel was incubated in a destaining solution (25% methanol, 10% acetic acid) until the desired destaining and bands of interest were cut and kept in 5% acetic acid. MALDI-TOF analyses were performed by Prof. Gabriella Tedeschi, Università degli studi di Milano, Milan.

2.2.8. Immunohistochemistry analyses

For immunohistochemistry experiments (IHC), different *P. lividus* developmental stages, from unfertilised eggs to larval stages, were fixed in 2% PFA in FSW for 10 min at room temperature (RT), and then treated with ice-cold methanol for 1 min to optimise the entrance of the antibody inside the embryos. After multiple washes in PBS with 0.1% Tween-20 (PBST), embryos were blocked in 4% sheep serum in PBST for 1 hour at RT and incubated overnight at 4°C with the anti-OvoA IgGs (dilution 1:100, final concentration 5 µg/mL) in 4% sheep serum in PBST. Pre-immune IgGs were used at the same protein concentration (5 µg/mL) as negative control. After multiple washes in PBST, embryos were incubated with CF555 Goat Anti-Rabbit IgGs (H+L) (Cat. 20033, Biotium, Inc., CA, USA) for 2 hours at RT in dark (dilution 1:1000) in 4% sheep serum, then rinsed in PBST, added with 4′,6-Diamidine-2′-phenylindole dihydrochloride (DAPI) (1:5000; final concentration 0.2 µg/mL) to stain the nuclei and finally visualised under a confocal microscope (Zeiss LSM 700).

For IHC experiments, about 50 embryos/larvae were visualised under the microscope for each developmental stage.

2.2.9. Morpholino microinjection

Morpholino oligonucleotide (MO) against OvoA was newly designed and acquired from Gene Tools (Corvallis) (5'-TTCGAGGCTCAGTTCCGTTGCCATG-3').

For each experiment around 400 embryos were injected with approximately 2-4 pl of 0.3 mM oligonucleotide solution and each experiment was repeated three times. As negative control, for each experiment embryos were injected with 0.3 mM of the standard control morpholino (GeneTools) and compared with uninjected and OvoA perturbated embryos. The injection of the standard control morpholino did not have any effect on the development of embryos.

This part was done in collaboration with Dr. Maria Ina Arnone, Department of Biology and Evolution of Marine Organisms, SZN.

2.3. Results

2.3.1. *OvoA* mRNA localisation during *P. lividus* development

Previous studies reported high levels of OvoA transcript in *P. lividus* unfertilised eggs, followed by a strong decrease after fertilisation and a *de-novo* synthesis at pluteus stage (Castellano *et al.,* 2016, see fig. 9). In order to investigate the OvoA mRNA spatial expression in the embryos, *in situ* hybridisation (ISH) experiments were performed on *P. lividus* developmental stages.

Both fluorescent (FISH) and chromogenic (CISH) detection were performed following the incubation of fixed embryos with antisense and sense (negative controls) *OvoA* probes.

FISH results showed that in 32-cell stage *OvoA* mRNA is expressed in all blastomeres without a restricted pattern (fig. 33A). The experiments performed in gastrula and prism stages showed an *OvoA* diffuse expression in all cells, although the signal appeared stronger in the archenteron region (fig. 33B,C).

In plutei larvae *OvoA* mRNA is expressed in all the larva, although a stronger signal was detected in the digestive trait and primary mesenchyme cells (fig. 33D).

Chromogenic detection (CISH) confirmed the results obtained by FISH. Indeed, CISH results confirmed the diffuse *OvoA* expression in all blastomeres at 32-cell stage (fig. 34A). In gastrula and prism stages the expression is restricted to the blastopore and oral ectoderm (fig. 34B-F), although it can not be excluded a diffuse *OvoA* mRNA expression also in all other cells, due to the presence of a faint color. In plutei larvae there is a strong signal in digestive trait region (fig. 34G-I), although a faint color is also present in primary mesenchyme cells, which appeared more intense by FISH.

Developmental stages hybridised with sense probe, as negative controls, showed absence of signal both in FISH and CISH esperiments (fig. 35).
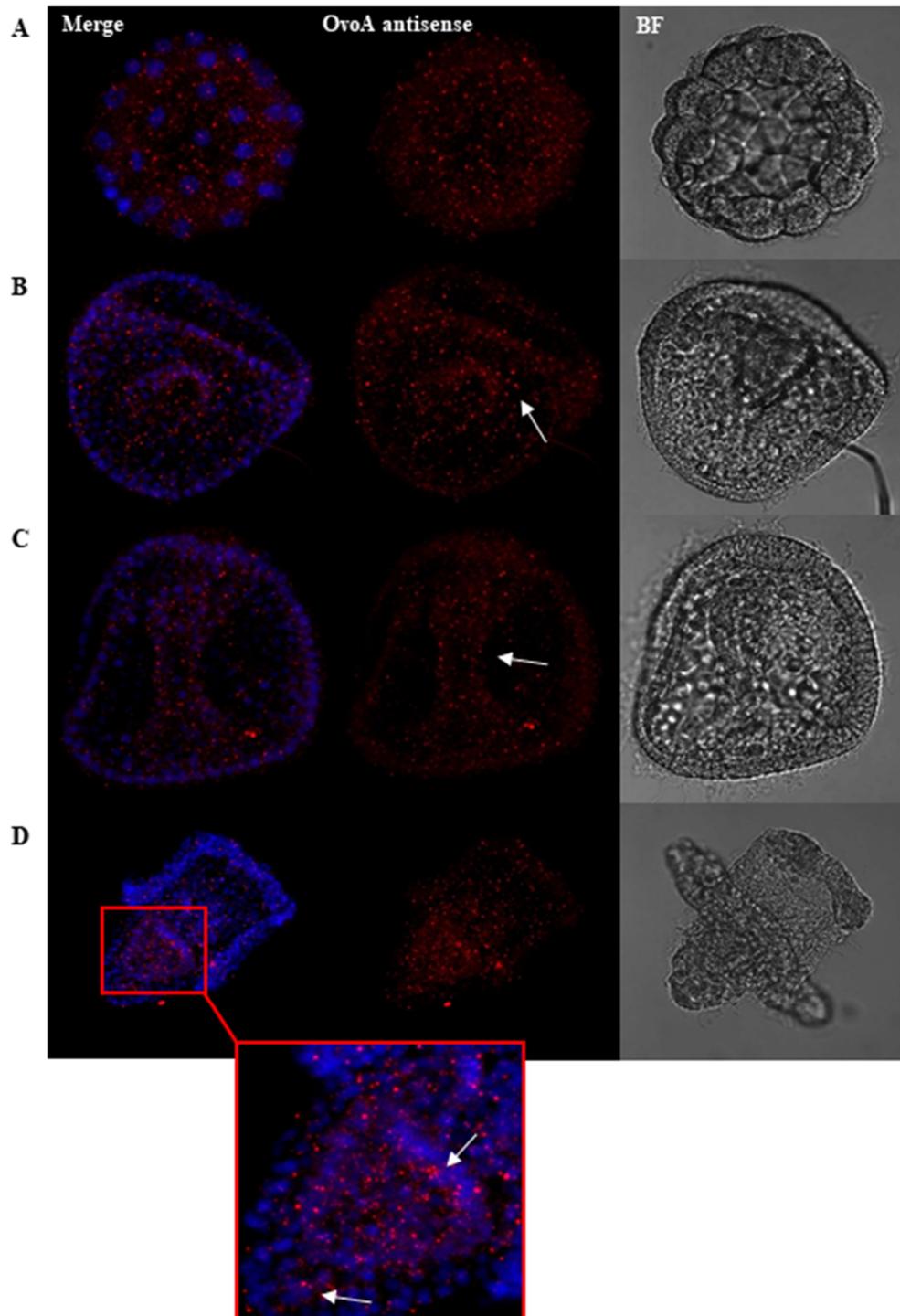
Figure 33 *OvoA* fluorescent *in situ* hybridisation (FISH) experiments: fixed *P. lividus* developmental stages hybridised with *OvoA* antisense probe.

OvoA antisense/DAPI merge (on left), *OvoA* antisense signal (middle) and images in bright field (BF, on right) are shown for some representative *P. lividus* developmental stages: **A.** 32-cell stage; **B.** Gastrula; **C.** Prism stage; **D.** Pluteus larva. White arrows indicate the antisense probe localisation

(for details refer to the text). Pictures were taken at confocal microscope (Zeiss LSM 700) at 20x magnification and partial maximum intensity Z-projections were obtained through ImageJ software.
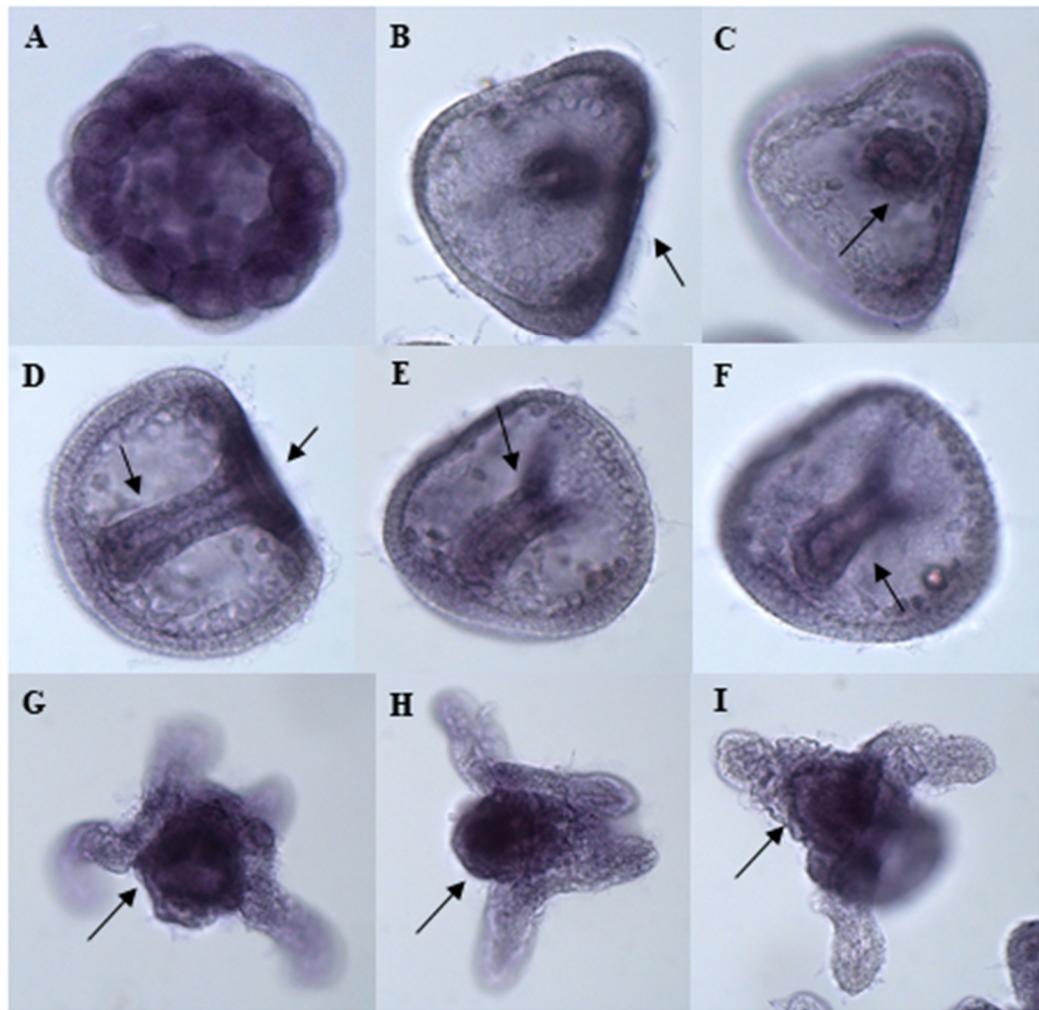
Figure 34 OvoA chromogenic *in situ* hybridisation (CISH) experiments: fixed *P. lividus* embryos hybridised with *OvoA* antisense probe.

A. 64-cell stage; **B-C.** two different focuses of gastrula blastopore view; **D.** Gastrula lateral view; **E-F.** two different focuses of prism stage; **G-I.** three different plutei larvae. Black arrows indicate the antisense probe localisation (for details refer to the text). Pictures were taken at microscope (Zeiss Axio Imager M1) at 20x magnification.
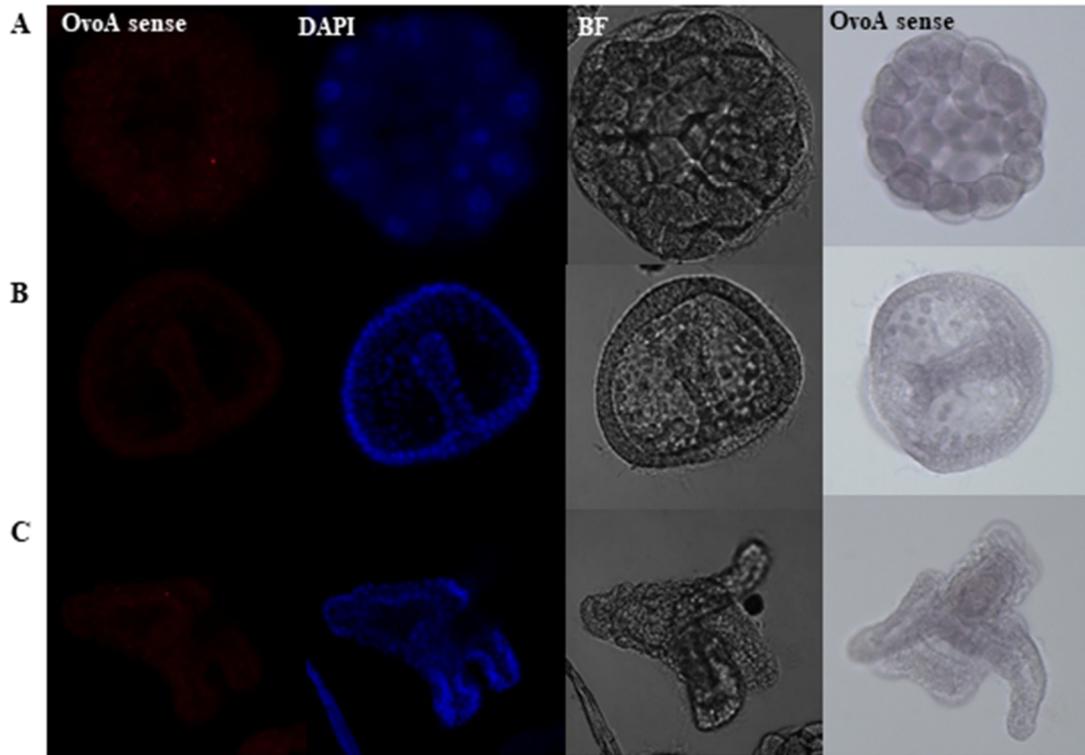
Figure 35 Negative controls for *in situ* hybridization (ISH) experiments: fixed *P. lividus* embryos treated with OvoA sense probe.

Fluorescent and chromogenic detection (FISH and CISH respectively) of OvoA sense probe by ISH is shown: **A.** 64-cell stage; **B.** gastrula; **C.** pluteus larva. For FISH are also shown DAPI staining of nuclei (middle) and images in bright field (BF).

For FISH pictures were taken at confocal microscope (Zeiss LSM 700) at 20x magnification; for CISH embryos were visualised on glass slides under the microscope (Zeiss Axio Imager M1) at 20x magnification.

2.3.2. Temporal expression of OvoA protein from unfertilised eggs to plutei larvae

Different *P. lividus* developmental stages were analysed for OvoA temporal expression through western blot (WB) analyses. The antibody anti-OvoA recognised a band at the apparent molecular weight of 88 kDa, very similar to the theoretical value of the OvoA primary structure (87870.7 Da). The intensity of this band was monitored from unfertilised eggs to plutei larvae. The results showed that OvoA protein is present in the eggs in low quantities, followed by an increase from 64-blastomeres/early blastula stage until the prism stage, with a decrease at the pluteus larva (fig. 36; tab. 2S). The identity of the band at 88 KDa as OvoA was confirmed by mass spectrometry analysis which revealed the presence of 4 peptides belonging to OvoA sequence (tab. 1S; fig. 4S).
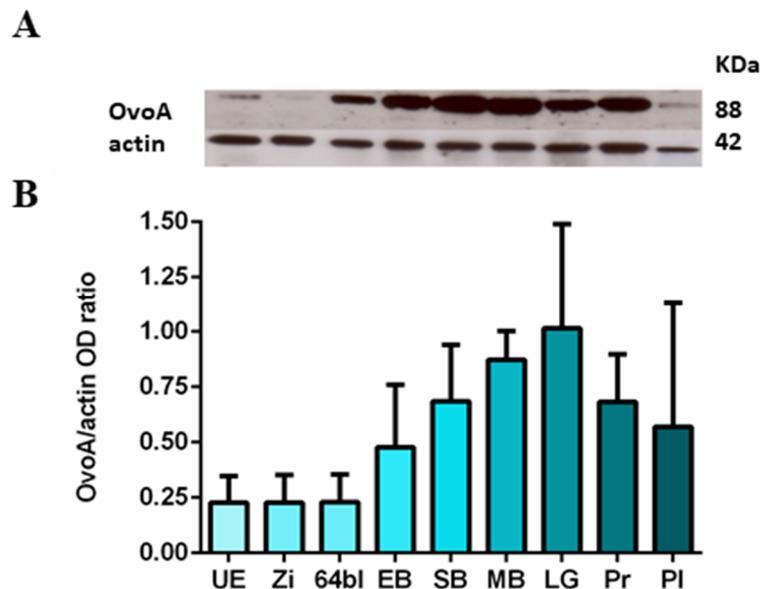
Figure 36 OvoA protein expression during *P. lividus* development.
A. Representative western blot experiment showing the immunopositive bands: OvoA (88 kDa) and actin (42 kDa); **B.** Bar-chart showing the OvoA/actin OD ratio resulting from the densitometry analysis of the immunopositive bands deriving from three biological replicates. Data are presented as means ± standard deviation (see tab. 2S). Abbreviations: UE = unfertilised eggs; Zi = zygote; 64bl

= 64-blastomeres stage; EB = early blastula; SB = swimming blastula; MB = mesenchyme blastula; LG = late gastrula; Pr = prism; Pl = pluteus stage.

2.3.3. Spatial expression of OvoA protein from unfertilised eggs to plutei larvae

Different *P. lividus* developmental stages were analysed for OvoA protein spatial expression through IHC experiments.

Immunolocalisation experiments of the OvoA enzyme performed in unfertilised eggs revealed a faint signal, weakly localised near the plasma membrane (fig. 37A).

In fertilised eggs a stronger signal was detected, compared to unfertilised eggs, dispersal inside the cell and near the nuclear membrane (fig. 37B).

During the first mitotic divisions of the embryo, from zygote to 4-cell stage the OvoA immunopositivity was very faint, however it was weakly localised near the plasma membrane (fig. 37C-E). At 32-cell stage, a differential immunopositivity was detected in relation to the cell cycle phases. Indeed, a stronger signal was detected in S-phase (interphase) blastomeres compared to those ones in M-phase (mitosis) (fig. 38).

The IHC experiments at gastrula stage showed the presence of OvoA in the cytoplasm of all cells without a specific localisation (fig. 39). As development proceeds, the signal became gradually restricted to specific cells and tissues. Indeed, in early echinoplutei there was a strong immunopositivity in the primary mesenchyme cells (PMCs) (fig. 40) and, interestingly, in plutei larvae OvoA was clearly localised, besides in PMCs, in stomach and intestine cells (fig. 41).

Developmental stages probed with pre-immune IgGs, as negative controls, showed absence of staining (fig 42).
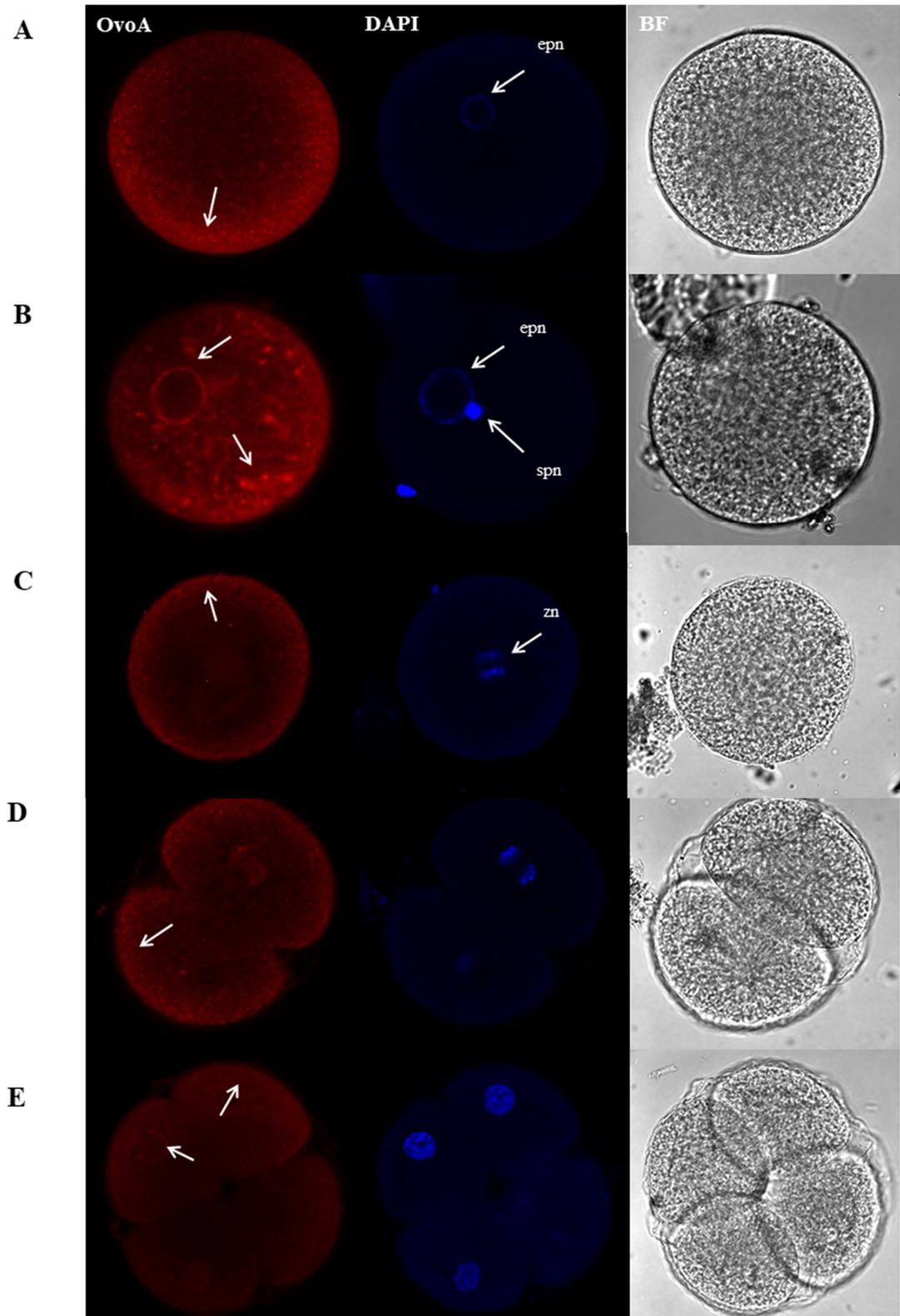
Figure 37 OvoA immunolocalisation in pre-hatching *P. lividus* embryos.

OvoA immunofluorescence (in red, left side), nuclei (labelled in blue with DAPI, middle) and images in bright field (BF) for several pre-hatching embryos are shown: **A.** unfertilised eggs; **B.** fertilised

eggs; **C.** zygote; **D.** 2-cell stage; **E**. 4-cell stage. White arrows indicate OvoA localisation (for details refer to the text).

Abbreviations: epn = egg pronucleus, spn = sperm pronucleus, zn = zygote nucleus. Pictures were taken at confocal microscope (Zeiss LSM 700) at 20x magnification.
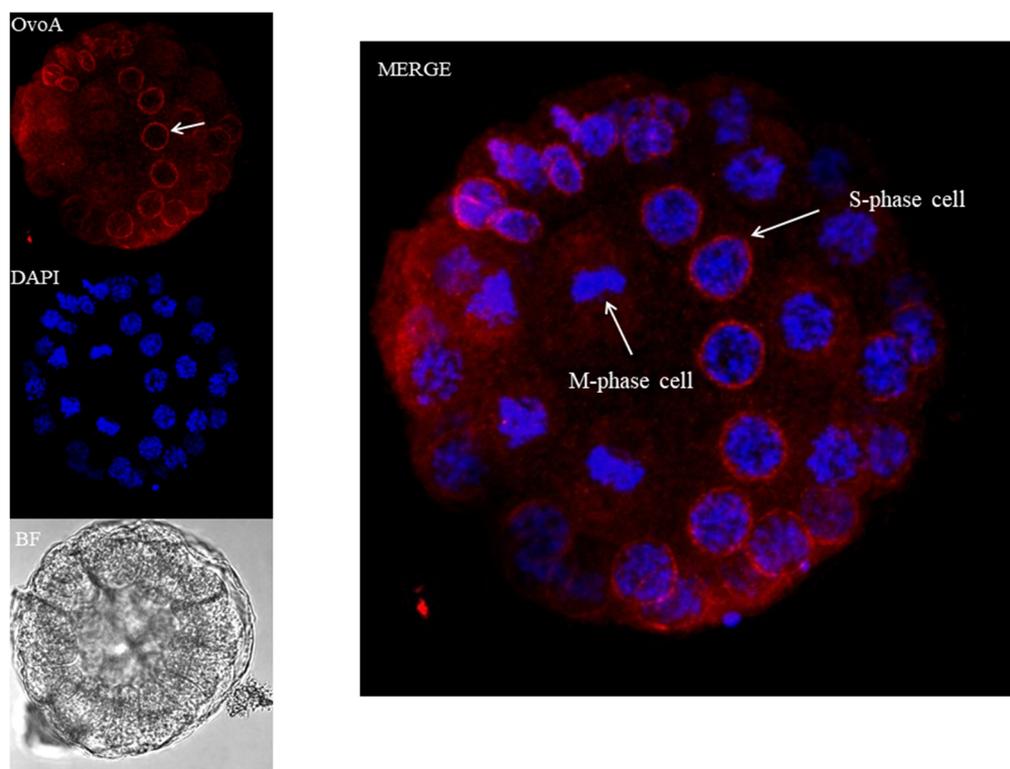
Figure 38 OvoA immunolocalisation in 32-cell stage.

On the left images showing OvoA signal, nuclei staining (DAPI) and bright field (BF) were reported. On the right merge image from OvoA and DAPI signals was reported. Pictures were taken at confocal microscope (Zeiss LSM 700) at 20x magnification and partial maximum intensity Z-projection was obtained through ImageJ software.
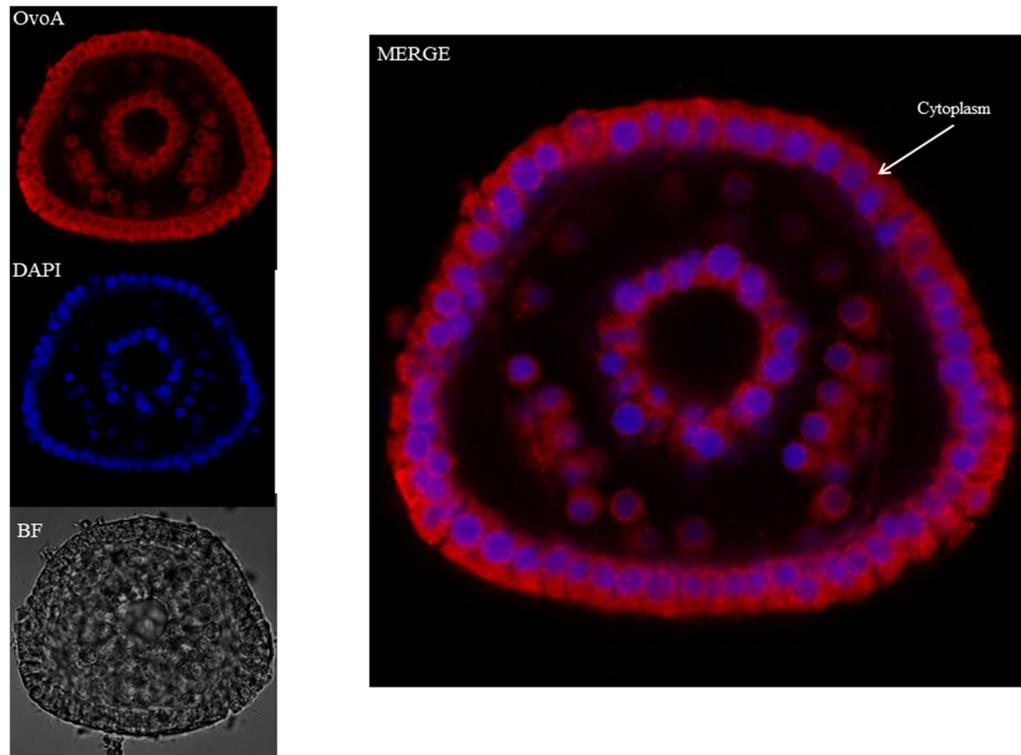
Figure 39 OvoA immunolocalisation in gastrula stage.

On the left images showing OvoA signal, nuclei staining (DAPI) and bright field (BF) were reported. On the right merge image from OvoA and DAPI signals was reported. Pictures were taken at confocal microscope (Zeiss LSM 700) at 20x magnification.
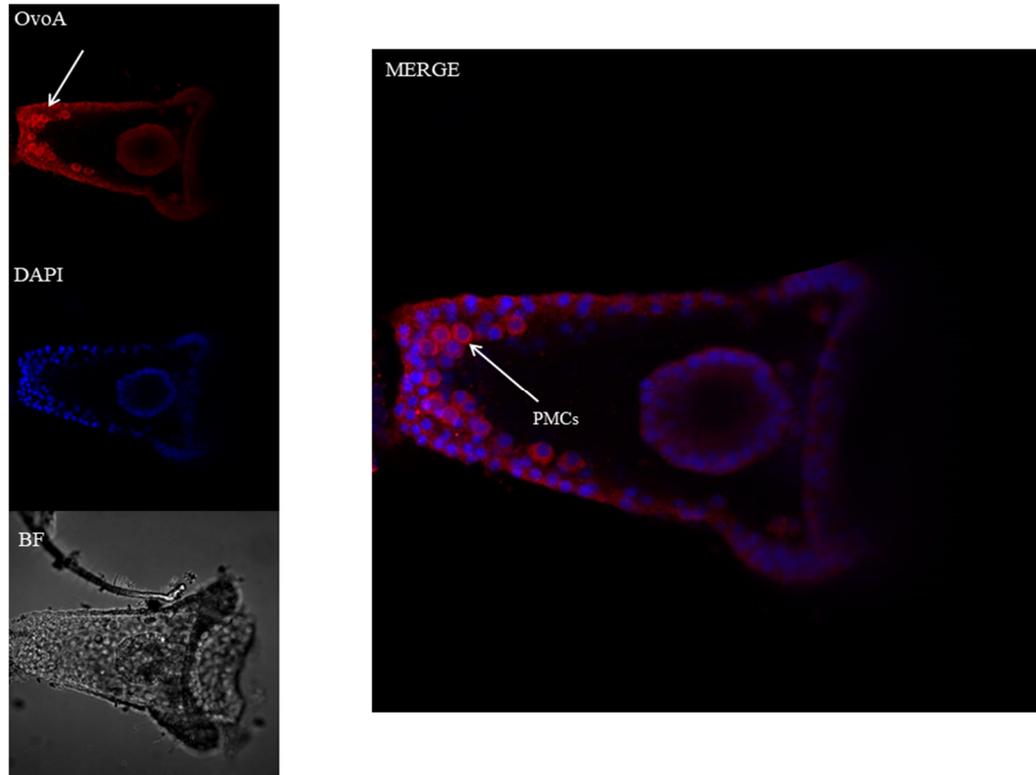
Figure 40 OvoA immunolocalisation in early echinopluteus.

On the left images showing OvoA signal, nuclei staining (DAPI) and bright field (BF) were reported. On the right merge image from OvoA and DAPI signals was reported. Pictures were taken at confocal microscope (Zeiss LSM 700) at 20x magnification and partial maximum intensity Z-projection was obtained through ImageJ software.
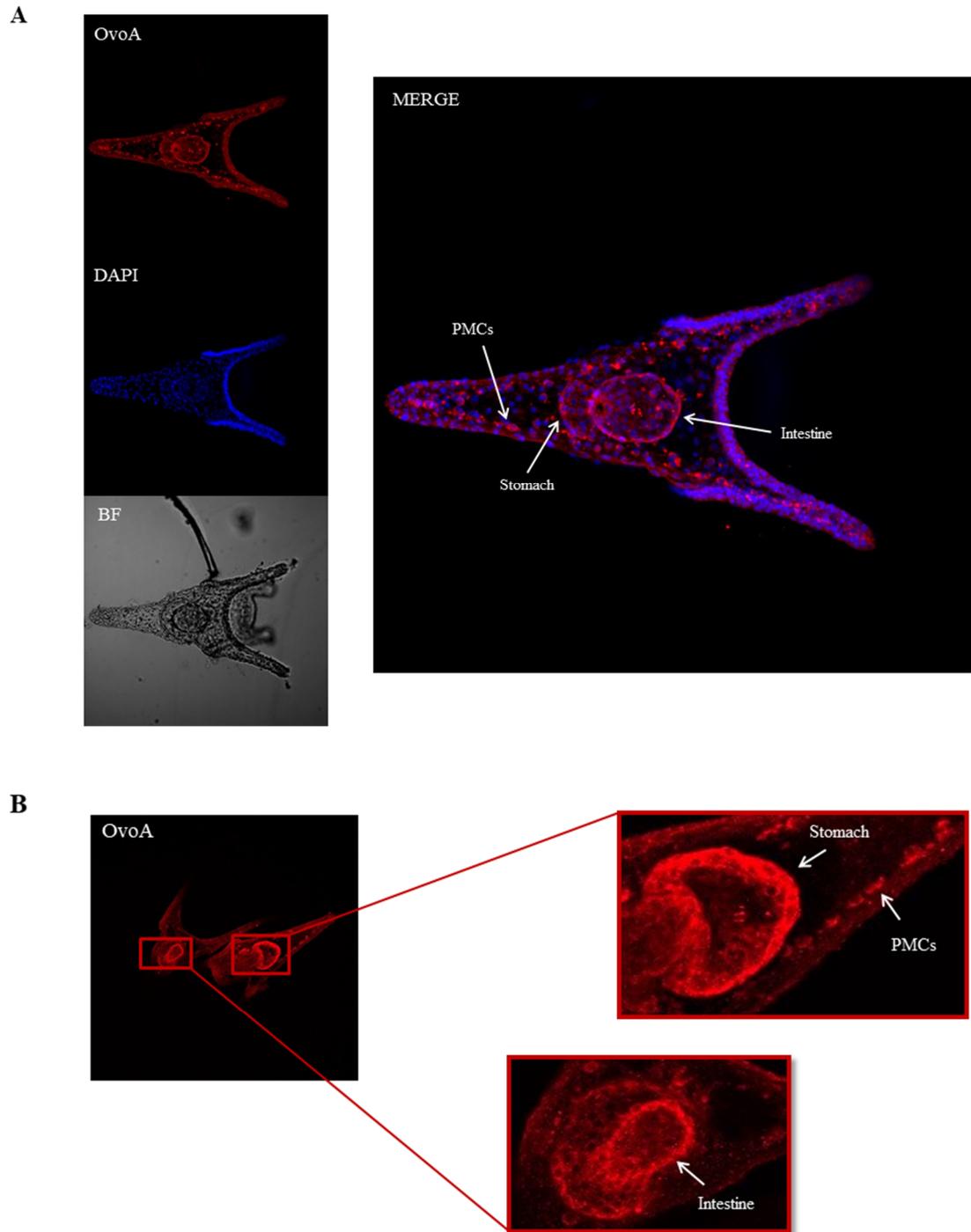
Figure 41 OvoA immunolocalisation in plutei larvae.

A. On the left, images showing OvoA signal, nuclei staining (DAPI) and bright field (BF) were reported. On the right, merge image from OvoA and DAPI signals was reported. **B.** A representative experiment showing zoom images of OvoA signals. Pictures were taken at confocal microscope (Zeiss LSM 700) at 20x magnification and partial maximum intensity Z-projections were obtained through ImageJ software.
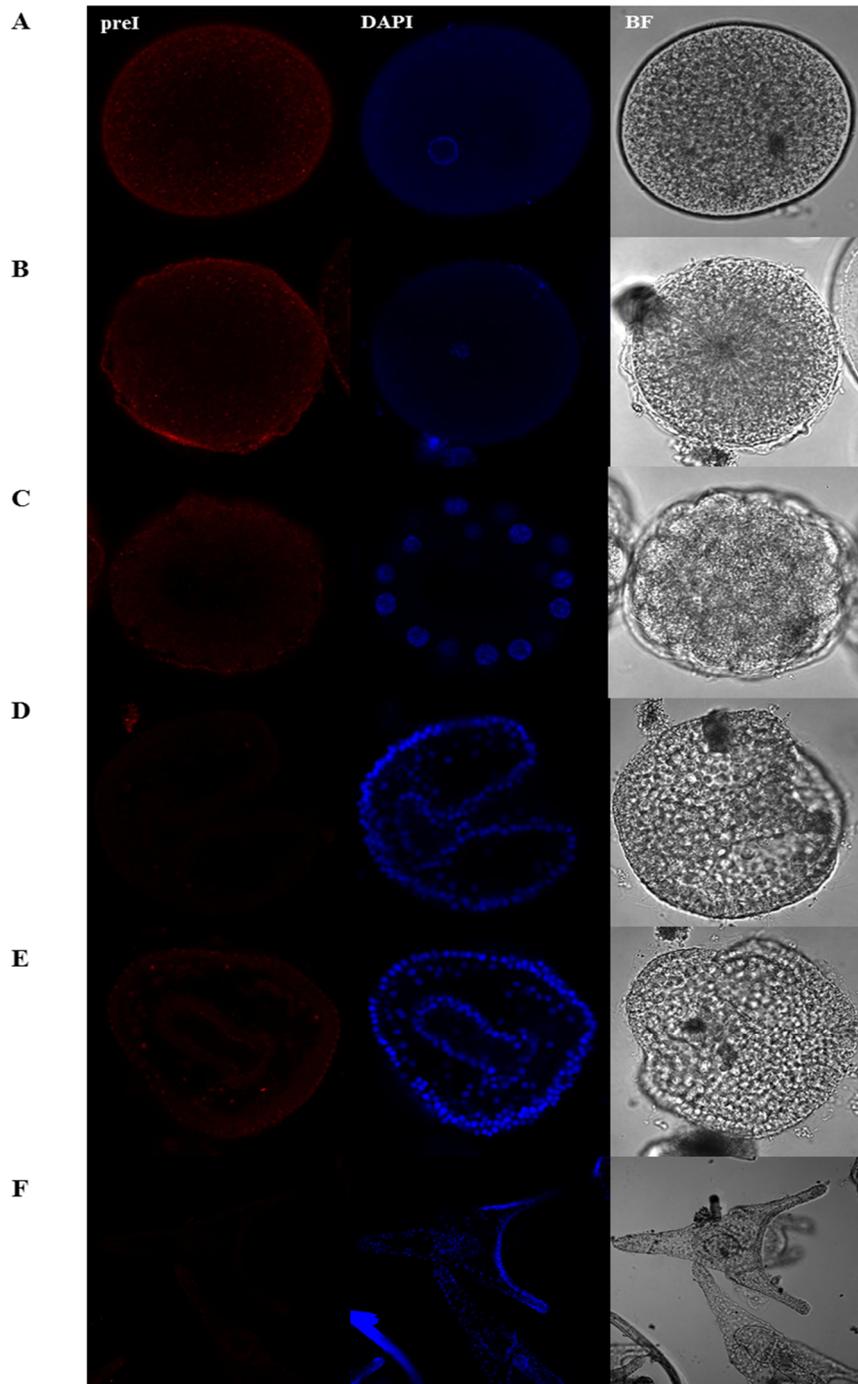
Figure 42 Negative controls for IHC experiments: fixed *P. lividus* embryos treated with pre-immune IgGs.

A. Unfertilised egg; **B.** zygote; **C.** 16-cell stage; **D.** gastrula; **E.** prism; **F.** pluteus. For every stage it is reported the immunoposivitity following pre-immune IgGs (preI) probing (left side), nuclei labelled in blue with DAPI (middle) and image in bright field (BF) (right side).

2.3.4. OvoA perturbation experiments

In order to understand the functional significance of ovothiol during the embryonic development of sea urchin, its formation has been perturbed through morpholino oligonucleotide microinjection, thus blocking the OvoA protein translation and fixed perturbed embryos were analysed for phenotype observation and OvoA protein immunopositivity by IHC experiments. Experiments were performed in triplicate and around 50 embryos were observed under the confocal microscope for each experiment. The perturbed embryos did not have any malformation until gastrula stage at 18/20 hours post fertilisation (fig. 43A-B). The results showed a decrease of the OvoA immunofluorescence in perturbed embryos, revealing a high percentage of malformation (80%) with an extreme phenotype in gastrulae, which were lacking in PMCs ingression and archenteron elongation, resulting in a "ball of cells" with bigger and fragmented nuclei (fig. 43C).

To obtain additional information regarding the relevance of ovothiol formation for *P. lividus* embryos, the phenotype from two different egg batches was compared, before and after the perturbation, and correlated with the OvoA immunofluorescence: one batch was obtained by a female grown up under controlled conditions at SZN (named batch #1) and the other one was obtained by a female taken from the Gulf of Naples (named batch #2). The quality of eggs from batch #2 was lower compared to batch #1 in terms of morphology and success of fertilisation and embryonic development.

The eggs from both batches were analysed through OvoA IHC and the results showed that eggs from batch #2 had less OvoA protein compared to batch #1 (fig. 44A). Moreover, wild type embryos (not microinjected) obtained by batch #2 had a similar phenotype to OvoA perturbed embryos, thus highlithting the importance of OvoA presence for normal embryo development (fig. 44B).
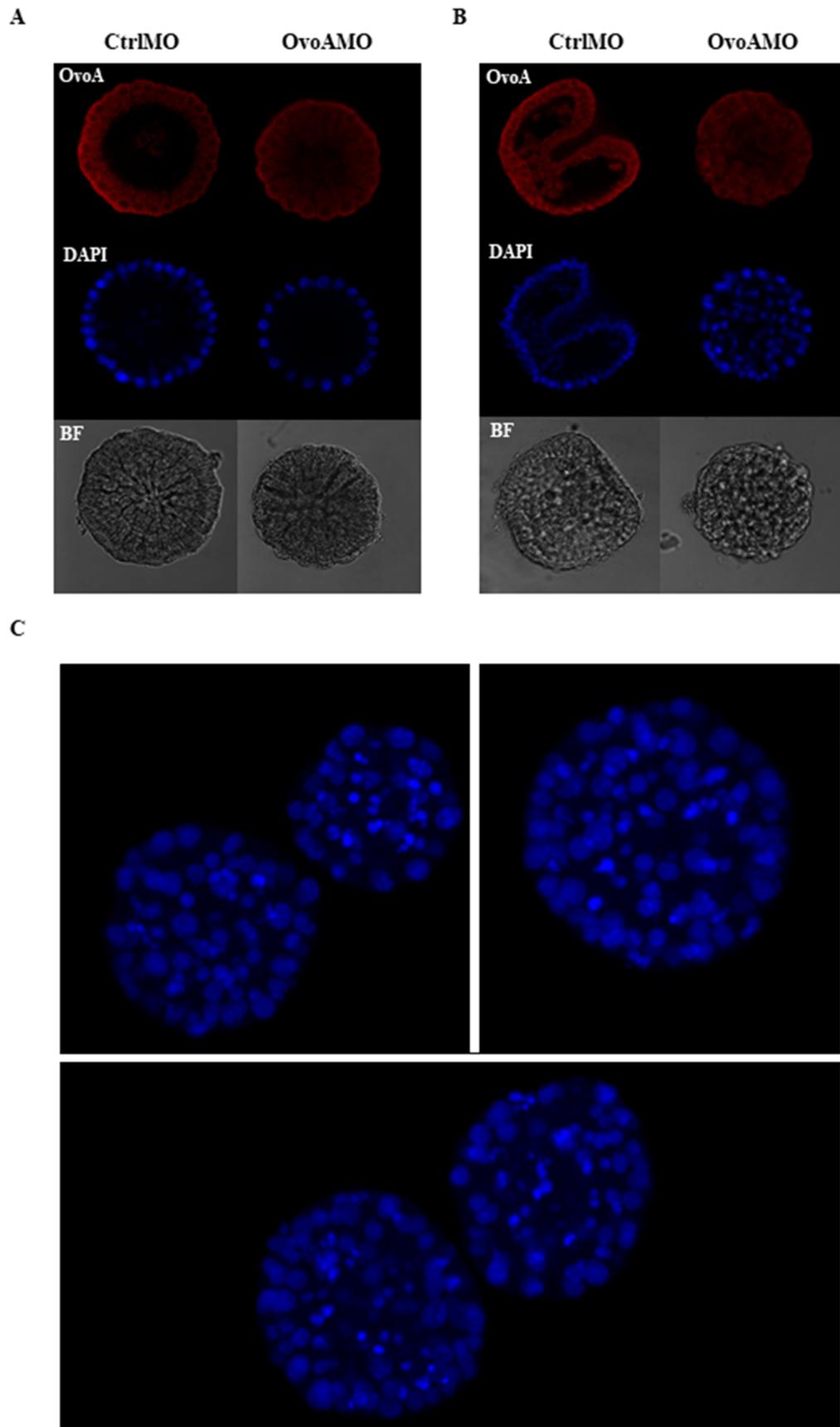
Figure 43 *P. lividus* embryos developed from OvoA morpholino microinjected eggs.
Images showing perturbed embryos are reported. **A.** IHC experiments on 7 hours post-fertilisation
blastulae developed from eggs injected with control morpholino (CtrlMO) and OvoA morpholino

(OvoAMO); **B.** IHC experiments on 20 hours post-fertilisation gastrulae developed from eggs injected with control morpholino (CtrlMO) and OvoA morpholino (OvoAMO). In both A and B panels, OvoA immunopositivity, nuclei staining (DAPI) and images in bright field (BF) are shown. **C.** Nuclei staining of perturbed gastrulae. Pictures were taken at confocal microscope (Zeiss LSM 700) at 20x magnification.
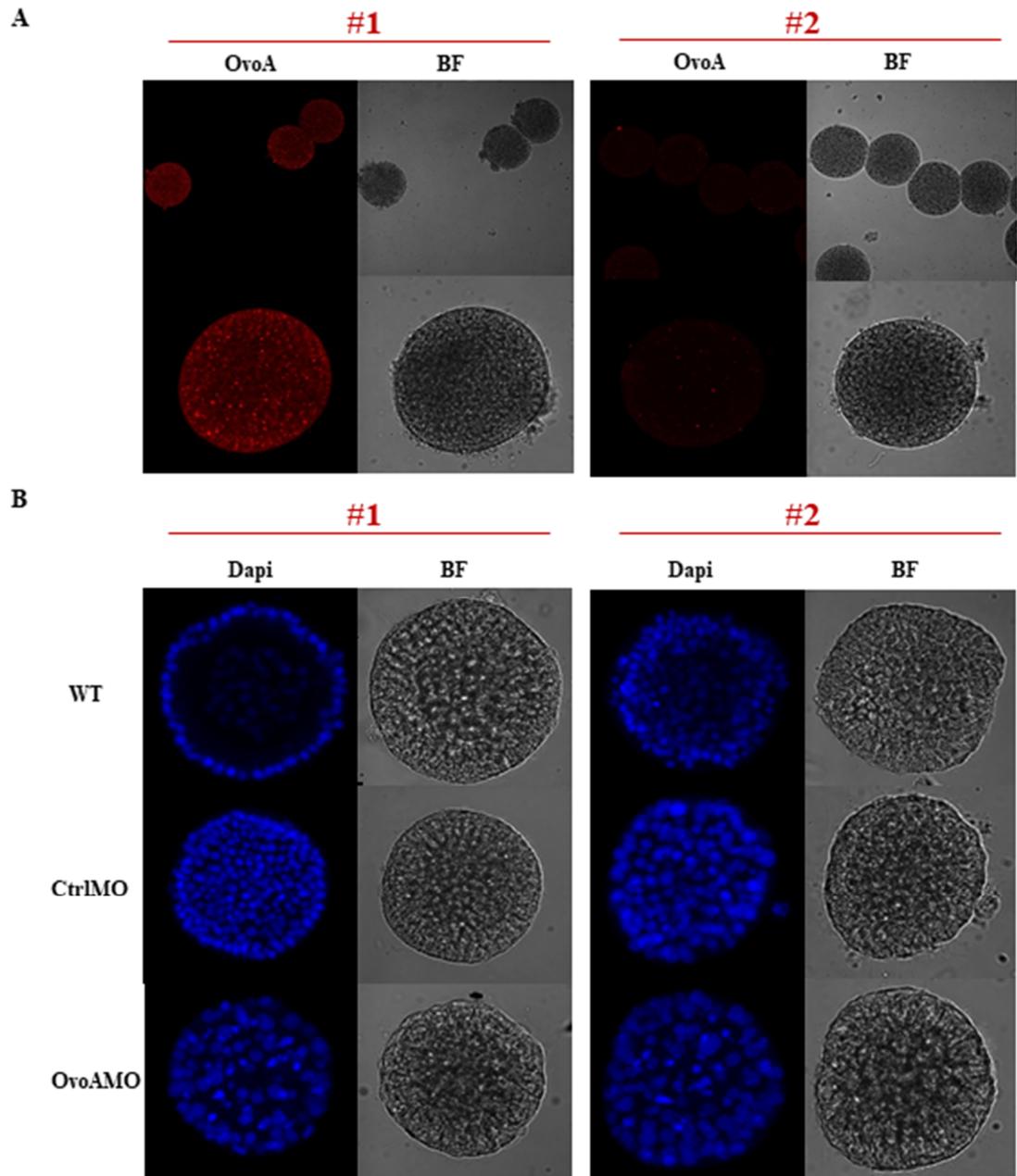
Figure 44 Comparison between OvoA content in unfertilised eggs and embryo phenotype in two *P. lividus* progenies.

A. OvoA immunolocalisation in *P. lividus* unfertilised eggs from two females (batch #1 and #2); **B.** Phenotype observation of wild type (WT, not microinjected), control-morpholino microinjected (CtrlMO) and OvoA perturbated embryos (OvoAMO).

2.4. Discussion

Previous studies suggested that ovothiol plays a key role in sea urchin acting as an antioxidant to protect eggs from the high oxidative burst at fertilisation and developing embryos from environmental cues (Turner *et al.,* 1986 and 1988; Castellano *et al.,* 2016). However, the discovery of ovothiol in other marine organisms with roles different from antioxidant (Selman-Reimer *et al.,* 1991; Röhl *et al.,* 1999) suggests that its physiological role could be wider and not exclusively related to the antioxidant defence.

In this chapter, I investigated the *OvoA* mRNA localisation and the temporal and spatial expression of the enzyme OvoA during the embryonic development of the mediterranean sea urchin *P. lividus*. Moreover, functional studies were performed in order to understand the relevance of ovothiol biosynthesis in this organism.

This work has allowed to give insight into the biological functions of this metabolite during sea urchin development and to obtain interesting information, that in the future may represent a source of inspiration for possible applications of ovothiols for human health and wellness.

Role of ovothiol during early *P. lividus* development

The temporal expression experiments, performed from unfertilised eggs to plutei larvae, allowed to highlight a specular trend of OvoA protein expression levels compared to *OvoA* gene expression data, reported in previous studies, showing high levels in unfertilised eggs, which strongly decrease at early and swimming blastula stages and then increase at pluteus stage (Castellano *et al.,* 2016). The decrease of OvoA protein at the zygotic stage may be probably ascribed to the protein degradation after the exploitation of ovothiol, whose proposed role is to protect the eggs from the oxidative burst at fertilisation (Shapiro *et al.,*

1990). Since unfertilised eggs are rich of OvoA mRNA, it is presumable to hypothesise that the translation of the maternal mRNA is responsible for the protein increase from 64-cell stage/early blastula to prism stage, thus explaining the specular trend between OvoA protein and transcript levels. In sea urchin, fertilisation triggers the entry into S-phase of the eggs blocked at the G1 stage of the cell cycle after the completion of meiosis, and first mitotic division. During the enhanced activation of cell metabolism, protein synthesis is rapidly activated, being dispensable for the S-phase but necessary for the onset of M-phase and subsequent embryonic cell cycles (Wagenaar, 1983; Dubé, 1988; Epel, 1990). In addition, ROS have been proposed to be required for the entry into S-phase (Havens *et al.,* 2006). Therefore, immunohistochemistry data showing a higher expression of OvoA in fertilised eggs may suggest a potential involvement of ovothiol in maintaining a redox balance and preventing the formation of toxic concentrations of free radicals produced during the cell cycle.

This hypothesis is also supported by the finding that OvoA is expressed in all cells of the embryo until prism stage, preferentially in S-phase (interphase) blastomeres compared to those ones in M-phase (mitosis).

The differential OvoA protein localisation found during the cell cycle, mimics, to some extent, the well known periodic expression of cyclins (Evans *et al.,* 1983). This could be a very intriguing point to investigate in the future through some *ad hoc* experiments.

In the gastrula and prism stages, the diffuse localisation of the OvoA protein seems to be in contrast with *in situ* hybridisation experiments, showing that mRNA is more concentrated in the archenteron. However, the accumulation of OvoA transcripts at the archenteron level could be necessary for the following protein accumulation in intestine and stomach, found at the larval stages.

Moreover, the restriction of the protein to few specific cells and larval tissues could be responsible for the overall decrease of the protein levels at the pluteus stage, revealed by

WB analyses, while in early stages the amount of protein is higher because it is expressed in all cells.

Interesting results derived from OvoA perturbation experiments, showing a highly extreme phenotype following blockage of the OvoA protein translation. An impairment of the normal development of the embryo, presumably causing cell death in the blastomeres, was observed. The observation that eggs not in a healthy status had less OvoA inside and, once fertilised, developed in embryos with a phenotype similar to perturbated embryos confirmed that ovothiol plays a key role during early *P. lividus* development.

The results from functional experiments together with the findings on the OvoA protein localisation in relation to the cell cycle phases, suggest that ovothiol could be involved in the mantainment of the correct cell cycle progression, a key step for a normal early development in which the cycle time is extremely short, alternating S and M phases without "Gap" (Tang, 2010; Siefert *et al.,* 2015). Indeed, an impairment of ovothiol biosynthesis may lead to an arrest of the cell cycle causing cell death.

Yet, the peculiar OvoA localisation close to the nuclear membrane could suggest a possible involvement of ovothiol as a protection of the DNA from damaging agents. For instance, among stressfull environmental agents, sea urchin embryos have to face ultraviolet radiation (UVR). These radiations can penetrate up to 7-12 m depth into the sea water column, especially in some areas of the world, thus affecting the fertilisation success, the timing of cleavage and development of sea urchin embryos, due, mainly, to DNA damage, caused both by direct effect of UVR and by the consequent production of reactive oxygen species (Lesser *et al.,* 2003 and bibliography therein). Thus, the OvoA localisation close to nuclear membrane in sea urchin embryos could be responsible for a strictly localised ovothiol production, necessary to protect DNA from several damaging factors, including UVR, thus preserving the genetic information.

Involvement of ovothiol in sea urchin larval skeleton formation

Skeletogenesis is a key morphogenetic event, although transient in sea urchin development (Decker and Lennarz, 1988). The sea urchin larval skeleton is constituted by high magnesium calcite, a soluble form of $CaCO_3$ (Beniash *et al.,* 1997; Raz *et al.,* 2003) and is essential to protect the digestive organs and contributes to the orientation of the arms necessary for an effective swimming and feeding behaviour (Pennington and Strathmann, 1990). Cilias are located along the larval arms, involved in locomotion and orientation, and in the production of currents to direct food to the mouth (Strathmann, 2000, 2007; Strathmann and Grunbaum, 2006).

Since skeletogenic cells (or primary mesenchyme cells, PMCs) and spicules are directly exposed to the external environment, they have to cope with eventual changes in sea water. Indeed, a decrease in environmental pH, like it is predicted in future oceans due to global change, challenges the acid-base regulatory mechanism of PMCs, due to decreased proton gradients. Nevertheless, larvae are able to maintain calcification rates also under acidified conditions due to energy allocation mechanisms and the capability of PMCs to counteract an internal acidified environment, protecting the spicules by dissolution (Martin *et al.,* 2011; Stumpp *et al.,* 2012).

Due to the essential role of skeletogenesis for the fitness of the sea urchin offspring, the ovothiol biosynthesis in this compartment could help the efficient formation of larval skeleton, presumably by helping to maintain a redox/acid-base homeostasis inside skeletogenic cells, considering the redox/acid-base properties of ovothiols (Marjanovic *et al.,* 1995). However, further investigation is necessary in order to clarify this aspect.

Ovothiol formation in sea urchin larval digestive trait

The presence of OvoA in the digestive trait of *P. lividu*s larvae is intruiguing. Interestingly, the analyses of transcriptomic data available in literature, obtained from different developmental stages and adult tissues of *S. purpuratus* revealed that *OvoA* was up-regulated at the pluteus stage and significant levels of OvoA transcript were also found in adult gut (personal communication, Dr. Marco Gerdol, University of Trieste), thus suggesting that ovothiol could play a role not only during embryonic development but also in the adults. Like skeletogenic cells (PMCs), also the larval digestive system is directly exposed to environmental factors, such as changes in pH, due to the inability of sea urchin larvae to regulate the pH in their primary body cavity (Stumpp *et al.,* 2012). In contrast to most vertebrates, whose stomach lumen presents an acidic pH, the larval digestive system of echinoderms operates at an alkaline pH, necessary for an efficient digestion of algal proteins and as a defence mechanism against environmental pathogens (Stumpp *et al.,* 2013, 2015 and bibliography therein). Therefore, the ovothiol biosynthesis along the digestive trait could have a relevant role in maintaining the redox/acid-base homeostasis in this compartment, taking in consideration that gastric pH homeostasis is extremely important to ensure the optimal nutrition of developing larvae.

Moreover, the gut represents an important site of the immune system (Ho *et al.,* 2016; Buckley *et al.,* 2017) and ovothiol could be involved in the gut-associated immune response. Indeed, many immune cell types, especially those ones involved in the first line of defence against pathogens, are known to exert their activity through the generation of reactive oxygen species (ROS), acting as killer agents against foreign microbes (DeVeale *et al.,* 2004; Gomez *et al.,* 2005). In this context, ovothiol could be needed, in this compartment, to counteract ROS in case of infection. However, future studies will be necessary to deepen this aspect.

2.5. Conclusions and perspectives

My work provided interesting results on the role of ovothiol during sea urchin development, highlighting its involvement in processes related to cell cycle, during the early *P. lividus* stages, and to skeletogenesis and digestive system in larvae.

However, some points remain to be clarified. Indeed, further experiments are needed to demonstrate the possible involvement of ovothiol in cell cycle regulation in early sea urchin embryos. In particular, OvoA expression, both at gene and protein level, and/or the formation of ovothiol, measured through HPLC/MS, could be correlated to the expression of cyclins and/or cyclin dependent kinases (cdk).

In this context, it would be interesting to investigate the involvement of ovothiol in cell cycle regulation during sea urchin oogenesis.

Moreover, the effect of perturbating OvoA protein translation in sea urchin embryos remains to be further investigated. The hypothesis is that blocking ovothiol biosynthesis embryonic development is extremely impaired, presumably causing cell cycle arrest and consequent cell death. OvoMO microinjected embryos could be examined by TUNEL (terminal dUTP nick end labeling) assay to demonstrate ongoing apoptotic processes and EdU to detect cell proliferation. Moreover, phenotype rescue experiments could be performed by microinjection of OvoA mRNA (Rizzo *et al.,* 2016).

Furthermore, the effects of OvoA perturbation on genes involved in cell cycle regulation and/or in the sea urchin developmental program, underlying skeleton and gut formation and functionality, could be investigated through different approaches, such as transcriptomic analyses and RT-qPCR of key genes involved in processes under investigation, as well as proteomic/metabolomic investigations to identify the patterns affected.

Yet, an interesting point to investigate could be the correlation of ovothiol formation and the redox gradient occurring during early embryogenesis and determining the oral-aboral axis in the embryos. Although from this study no OvoA gradient was detected in sea urchin eggs

and early developmental stages, *ad hoc* experiments could be performed to address this point. For instance, localisation experiments of OvoA or ovothiol in immobilised embryos (rosettes) in which a respiratory asymmetry is induced (Coffman and Davidson, 2001) could provide further information.

Finally, it could be interesting to investigate the *OvoA* modulation in relation to larval immunity, for instance, by exposing larvae to several pathogens and measuring the *OvoA* gene expression in threatened plutei following the induction of the immune response. In order to detect the *OvoA* modulation in the gut induced to enter in an immune state, gut isolation experiments could be performed and analysed through RT-qPCR and/or RNAseq, providing interesting finding on the potential relation among ovothiol formation and immune response during sea urchin development.

CHAPTER 3

Investigating the light-modulated ovothiol biosynthesis in the diatom *Skeletonema marinoi*

3.1. Aims of the study

The characterisation and identification of the enzyme responsible for the first step of ovothiol biosynthesis, the 5-histidylcysteine sulfoxide synthase (OvoA), allowed to identify OvoAs homologous in a variety of genomes, from proteobacteria to uni- and multicellular eukaryotes revealing an OvoA homologue also in the model diatom *Thalassiosira pseudonana* (Braunshausen and Seebeck, 2011).

The presence of OvoA in diatoms is relevant considering their biotechnological applications (Barra *et al.,* 2014) relied to high growth rate and the ability to adapt to environmental changes (Vardi *et al.,* 2006; Bowler *et al.,* 2008; Brunet *et al.,* 2014). In addition, they represent a rich source of bioactive products, such as carotenoids, vitamins, antioxidants, or polyunsaturated fatty acids (PUFAs) (Barra *et al.,* 2014; Li *et al.,* 2014; Dolch and Marechal, 2015). Since the cost of production of these compounds from microlgae is still elevated, studies aimed to optimise the production of high value products by manipulation of environmental conditions, i.e. light, are greatly encouraged (Smerilli *et al.,* 2017).

From few data scattered from literature, ovothiol biosynthesis in photosynthetic organisms has often been related to light-dependent processes. In the microalga *Dunaliella salina*, for instance, a role as a redox regulator in chloroplasts stimulated by light has been suggested (Selmar-Reimer *et al.,* 1991). Moreover, transcriptomic studies in *Euglena gracilis* revealed the presence of different *OvoA* transcripts in light and dark conditions (O'Neill *et al.,* 2015). The aim of this work is to shed light on ovothiol biosynthesis in the coastal diatom *Skeletonema marinoi*, and to investigate its modulation by light variations and growth phases.

S. marinoi cultures were carried out at a moderate non stressful light condition and then exposed to different stressful light conditions, varying in photon flux density (PFD) and light time evolution (sinusoidal versus square-wave distribution), allowing to investigate the

OvoA gene expression triggered by light stimulus. Samplings were also done from cultures in different growth phases in order to investigate the changes of *OvoA* expression in relationship to the growth capacity and the cell cycle. To highlight the possible action of ovothiol as antioxidant in this system, cellular stress was also monitored in the cultures in all the different experimental conditions. The levels of reactive oxygen species (ROS) and nitric oxide (NO), important messengers of stress response in plants (Crawford and Guo, 2005; Gechev *et al.,* 2006; Grün *et al.,* 2006), were measured with the aim to correlate their formation with *OvoA* expression.

In addition, an insight into the structure and function of nitric oxide synthase (NOS), the enzyme responsible for the arginine-dependent NO production, in *S. marinoi* was provided in this thesis. Taking advantage from the recent identification of NOSs in the green alga *Ostreococcus tauri* (Foresi *et al.,* 2010) and in some diatoms (Di Dato *et al*., 2015), the primary structure of such protein in *S. marinoi* was characterised. Moreover, *NOS* gene expression under stressful light conditions and in different growth phases was examined together with that of *OvoA*, in order to have a broader overview regarding the involvement of NO in the stress response triggered by light and in relation to the cell cycle. The characterisation of NOS in photosynthetic organisms (Correa-Aragunde *et al.,* 2013; Kumar *et al.,* 2015) is a relevant issue considering that the presence of NOS sequences in plant kingdom has long been debated (Guo *et al.,* 2003; Jasid *et al.,* 2006; Moreau *et al.,* 2008).

3.2. Materials and methods

3.2.1. Experimental strategy and sampling

Cultures of the coastal centric diatom *Skeletonema marinoi* (strain CCMP 2092) were carried out in 4.5 L glass flasks with air bubbling at 20 °C, containing seawater previously pre-filtered through a 0.7 mm GF/F glass-fiber filter (WhatmanTM, Whatman International Ltd, Maidstone, UK), autoclaved and enriched with F/2 medium nutrients (Guillard, 1975).

Light was provided by a custom-built LED illumination system which allows to modulate light intensity and spectral composition (Brunet *et al.,* 2014). Light intensity was measured inside each flask by using a laboratory PAR4π sensor (QSL 2101, Biospherical Instruments Inc., San Diego, CA, USA). Preacclimation of cells were performed during a minimum of two weeks at a moderate non stressful sinusoidal light, peaking at 150 µmol photons s^{-1} m^{-2} after 6 h from dawn (LSL150), with a 12:12 light:dark photoperiod. All the experiments were performed in triplicate, lasting 1-2 days depending on the experiment.

Both sinusoidal and square-wave lights were tested at different intensities in order to investigate the effect of different velocities of light increase. Sinusoidal distribution is more similar to natural condition at sea, reaching the midday light intensity peak with a gradual trend that mimics the gradual increase of light intensity during the day. By contrast, the square-wave one constitutes an innatural condition, providing a fast increase of light intensity, kept constant for all the day phase (12h) and then switched off for the night phase (12h), often used in indoor algal cultivation systems.

The stressful experimental conditions were:

-very low sinusoidal light 10

(midday light intensity peak: 10 µmol photons s^{-1} m^{-2}; VLSL10),

-high sinusoidal light 600

(midday light intensity peak: 600 µmol photons s^{-1} m^{-2}; HSL600),

-very low square-wave light 10

(midday light intensity peak: 10 µmol photons s^{-1} m^{-2}; VLSWL10),

-high square-wave light 300

(midday light intensity peak: 300 µmol photons s^{-1} m^{-2}; HSWL300),

-high square-wave light 600

(midday light intensity peak: 600 µmol photons s^{-1} m^{-2}; HSWL600),

-darkness).

The HSWL300 provided the same daily light dose experienced by cells grown under HSL600, allowing to compare square-wave and sinusoidal distributions of light without any influence from different daily light doses.

The spectral composition of the light was kept constant during the pre-acclimation and all the experimental conditions with a ratio of blue:green:red = 50:40:10. Also, in all cultures, cells experienced a 12:12 light:dark photoperiod except during VLSWL10 (very low intensity light was kept constant for the duration of the experiment), and darkness (no "day phase" for the duration of the experiment).

Sampling was done at 2 and 6 h from light switch in the case of high sinusoidal and square-wave light, and additionally at 0.17 h (10 min) in the case of high square-wave conditions to investigate the fast response to the light stress. One sampling at 24 h was also done to evaluate the ability of cells to restore their physiological state after the light stress received the day before. In case of very low sinusoidal and square-wave lights and dark condition, samplings were done every 6h from light switch until 30h.

The experimental setup, research strategy and experiments development for this part of the thesis were done in collaboration with Dr. Arianna Smerilli and Dr. Ida Orefice, from the Department of Integrative Marine Ecology, SZN.

3.2.2. Cell density

2 mL sub-samples from each flask were collected in triplicate and fixed with Lugol's iodine solution (1.5% v/v). One mL of this solution was used to fill a Sedgewick Rafter counting cell chamber and cell counts were performed by using a Zeiss Axioskop 2 Plus light microscope (Carl Zeiss, Göttingen, Germany). Growth curves for control, high, very low light/darkness conditions and growth phases are reported in fig 45, 46, 47 and 48, respectively. In each figure the sampling times are indicated and the relative cell counts are reported in the legend.
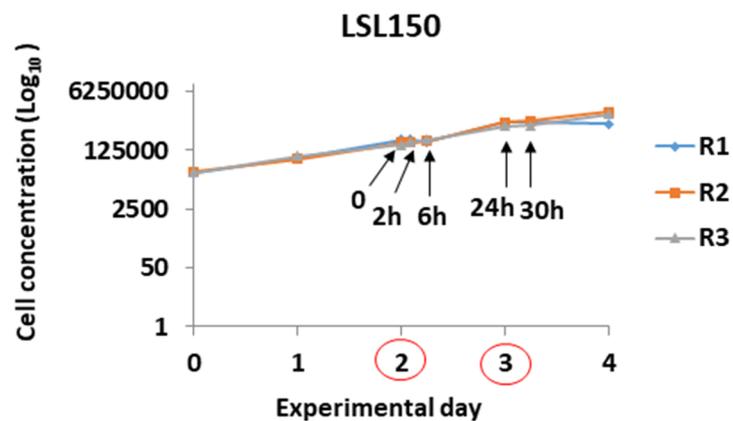
Figure 45 Growth curve of *S. marinoi* cultures under control light condition (low sinusoidal light; midday peak at 150 µmol photons s^{-1} m^{-2}, LSL150).
R1, R2 and R3 represent three biological replicates. Sampling days are highlighted by red circles. Black arrows indicate the experimental times.
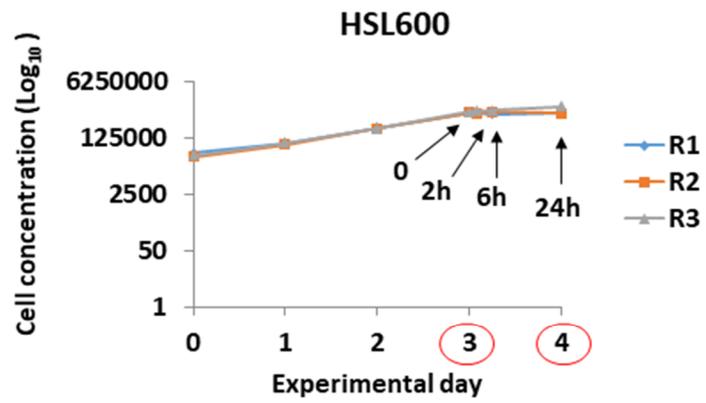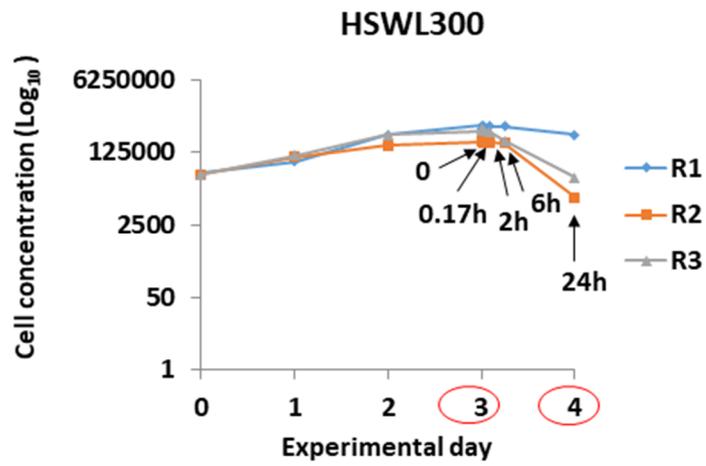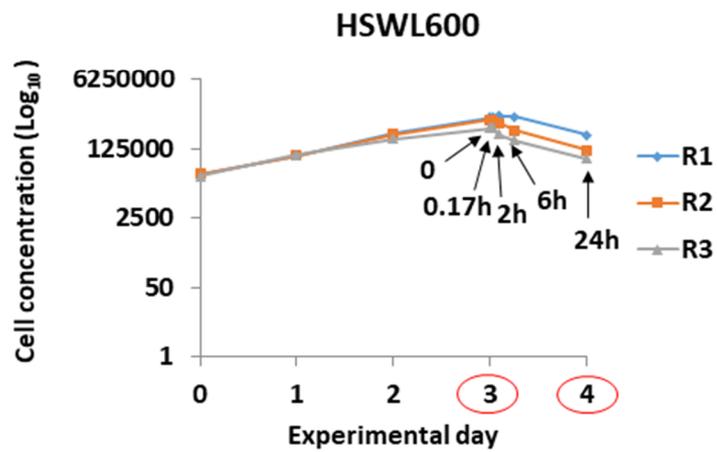
Figure 46 Growth curve of *S. marinoi* cultures under high light conditions.

A. High sinusoidal light; midday peak at 150 µmol photons s^{-1} m^{-2}, HSL600; **B.** High square-wave light; midday peak at 300 µmol photons s^{-1} m^{-2}, HSWL300; **C.** High square-wave light; midday peak at 600 µmol photons s^{-1} m^{-2}, HSWL600. R1, R2 and R3 represent three biological replicates. Sampling days are highlighted by red circles. Black arrows indicate the experimental times.
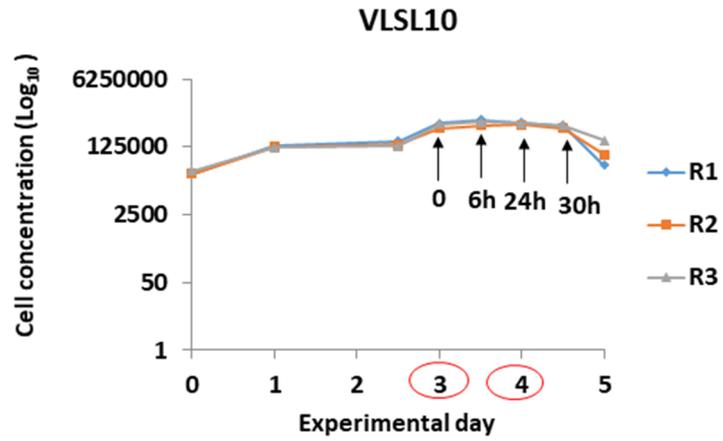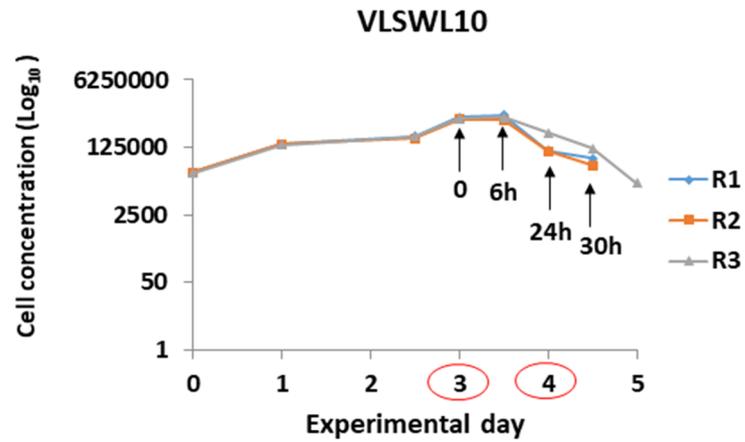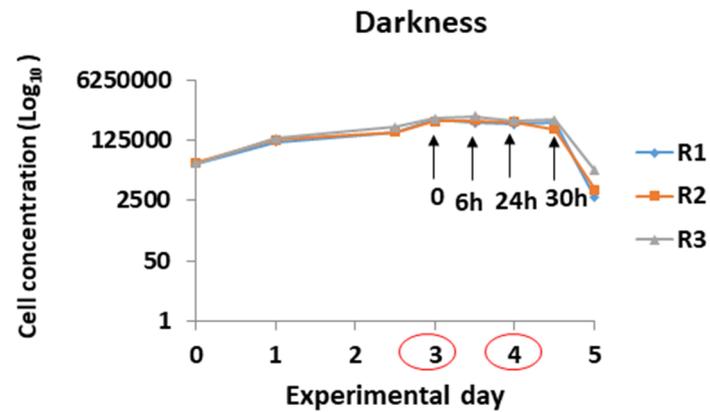
Figure 47 Growth curve of *S. marinoi* cultures under very low light/darkness conditions.
A. Very low sinusoidal light; midday peak at 10 µmol photons s^{-1} m^{-2}, VLSL10; **B.** Very low square-wave light; midday peak at 10 µmol photons s^{-1} m^{-2}, VLSWL10; **C.** Darkness condition. R1, R2 and R3 represent three biological replicates. Sampling days are highlighted by red circles. Black arrows indicate the experimental times.
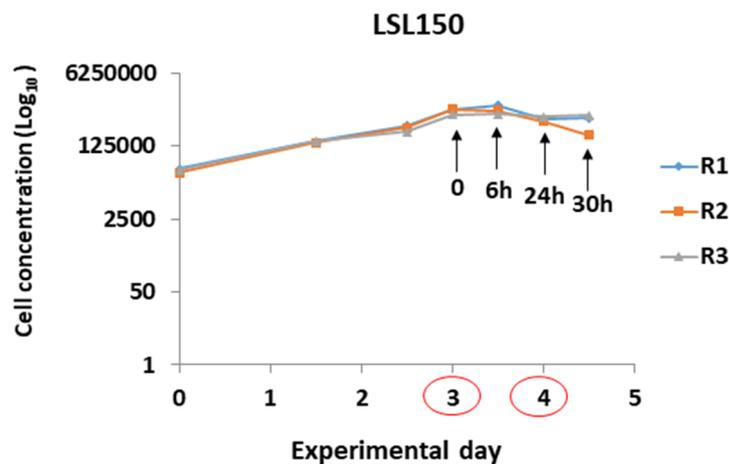
Figure 48 Growth curve of *S. marinoi* cultures along different growth phases.

S. marinoi was grown under control light condition (low sinusoidal light; midday peak at 150 µmol photons s^{-1} m^{-2}, LSL150) and sampled in exponential (day 3) and stationary/senescence (day 4) phase. R1, R2 and R3 represent three biological replicates. Sampling days are highlighted by red circles: day 3 represents the first sampling day, corresponding to t = 0 and t = 6h; day 4 represents the second experimental day, corresponding to t = 24h and t = 30h.

3.2.3. RNA extraction, reverse transcription and best reference genes assessment

The total RNA was extracted from the pellet according to Barra *et al.* 2013 and subjected to DNase treatment using DNase I recombinant, RNase-free (Roche, Basel, Switzerland) according to the manufacturer's protocol.

RNeasy MinElute Cleanup Kit (Qiagen, Venlo, Netherlands) was used to purify and concentrate the total RNA, finally eluted in 20 µL RNase-free water. RNA samples were quantified by assessing the absorbance at 260 nm (ND-1000 Spectrophotometer; NanoDrop Technologies, Wilmington, DE, USA) and then checked for integrity by agarose gel electrophoresis. Eventual gDNA contamination was checked by PCR on RNA samples and agarose gel electrophoresis. 1 µg from each RNA sample was retro-transcribed in

complementary DNA (cDNA) using the iScriptTM cDNA synthesis kit (Bio-Rad Laboratories, Hercules, CA, USA) and the T100 Thermal cycler (Bio-Rad Laboratories, Hercules, CA, USA), following the manufacturer's instructions.

In order to analyse expression levels of specific genes of interest, five putative reference genes were analysed by RT-qPCR to find the most stable genes in our conditions. The selected genes were histone 4 (H4), α- tubulin (TUB A), elongation factor 1α (EF1α), glyceraldehyde-3-phosphate dehydrogenase (GAPDH), and actin (ACT). The best reference gene for each condition was identified using three different algorithms: BestKeeper (Pfaffl *et al.,* 2004); NormFinder (Andersen et al., 2004) and geNorm (Vandesompele *et al.,* 2002). In particular: H4 was used as reference gene in the following conditions: LSL150 (control experiment), HSL600, HSWL300 and darkness; GADPH was used for VLSWL10; ACT for HSWL600 and TUB A for VLSL10 and LSL150 in different growth phases.This part was done in collaboration with Dr. Ida Orefice, Department of Integrative Marine Ecology, SZN.

3.2.4. Reverse transcription-quantitative PCR (RT-qPCR) experiments

The expression levels of *OvoA* and *Nos* genes were analysed. Primers were designed using Primer3 program V. 4.1.0 (primer3.ut.ee) considering the putative sequences reported in the *S. marinoi* transcriptome (MMETSP1039) deposited in the public database iMicrobe (http://data.imicrobe.us/project/view/104). RT-qPCR was performed in MicroAmp Optical 384-Well reaction plate (Applied Biosystems, Foster City, CA, USA) with Optical Adhesive Covers (Applied Biosystems, Foster City, CA, USA) in a Viia7 Real Time PCR System (Applied Biosystem, Foster City, CA, USA). Serial dilutions of cDNA and the obtained cycle threshold (Ct) mean values were used to generate the standard curves in order to calculate primer reaction efficiency (E= $10^{-1/\text{slope}}$) and correlation factor R^2 (tab. 2S). The

qPCR reaction was carried out in 10 µL for each sample, including 5 µL of Fast Start SYBR Green Master Mix with ROX (Roche, Basel, Switzerland), 1 µL of cDNA template (1:25 template dilution) and 0.7 pmol/µL for each primer. The procedure used to obtain the RT-qPCR thermal profile was: 95 °C for 20 s, 40 cycles of 95 °C for 1 s and 60 °C for 20 s. The melting curve of each amplicon was revealed by the program from 60 °C to 95 °C, reading every 0.5 °C. The gene-specific amplification and the absence of primer-dimers was confirmed by the presence of single peaks for all genes. All RT-qPCR reactions were carried out in triplicate and each assay included three no template negative controls for each primer pair. Expression levels were normalised using the most stable reference genes in RT-qPCR and data were analised through the REST tool (Relative Expression Software Tool, Pfaffl *et al.,* 2002). The time 0 before the light switch-on was considered the control condition for each experiment for the evaluation of gene expression.

Data are presented as mean ± standard error and statistical analyses were performed using the Pair Wise Fixed Reallocation Randomisation test by REST. Graphs were builded using GraphPad Prism software V 6.01.

3.2.5. Reactive nitrogen species (RNS) determination

Reactive nitrogen species (RNS) were measured by monitoring nitrite formation through the Griess assay (Green *et al.,* 1982). At different times from dawn, samples were collected by centrifugation at 3600 rpm (2608 rcf) for 15 min at 4°C (Eppendorf 5810 R, rotor A-4-62, Eppendorf AG, model 2231, Hamburg, Germany). The pellets were washed in phosphate buffer (KH_2PO_4 50 mM pH 7.5 + 0.5M NaCl) and centrifuged again in the same conditions. The final pellets were weighed, frozen in liquid nitrogen and then kept at -80°C.

Samples were homogenised by resuspending the pellets in 1 mL of phosphate buffer, vortexing and finally sonicating at 30% amplitude for 1 min (2 cycles with a one-minute-

break between cycles). They were centrifuged at 13000 rpm (13226 rcf) for 15 min at 4°C (Multi speed refrigerated centrifuge, rotor T527, ALC PK121R) and the supernatants were analysed for nitrite content. Aliquots (300 µL) of samples were incubated at room temperature (25°C) with nitrate reductase (1 U/mL) and the enzyme co-factors: FAD (100 µM) and NADPH (0.6 mM). After 2 h, samples were treated for 10 min in the dark with 300 µL of 1% (w/v) sulphanilamide in 5% H_3PO_4 and then with 300 µL of 0.1% (w/v) N-(1-naphthy)-ethylenediaminedihydrochloride for additional 10 min. The absorbance at 540 nm was measured in 1mL cuvettes and the molar concentration of nitrite in the sample was calculated from a standard curve generated using known concentrations of sodium nitrite (0–5 µM). Nitrite content in each sample was determined in triplicate.

Data are presented as means ± SD and analysed by One-way ANOVA ($P < 0.05$) with Tukey's Multiple Comparison Test. Statistics was performed with PAST software package, version 3.14 (Hammer *et al.,* 2001).

3.2.6. Reactive oxygen species (ROS) determination

The reactive oxygen species (ROS) were measured *in vivo* using a fluorescent ROS-sensitive dye, 2',7'-dichlorofluorescein diacetate (H_2DCFDA) (Sigma-Aldrich, Milan, Italy). At different times from dawn, samples were incubated for 30 min in the dark with H_2DCFDA (20 µM). The cells were then collected by centrifugation at 3600 rpm (2608 rcf) for 15 min at 4°C (Eppendorf 5810 R, rotor A-4-62, Eppendorf AG, model 2231, Hamburg, Germany). The pellets were washed in phosphate buffer and centrifuged again in the same conditions. The final pellets were weighed, frozen in liquid N_2 and then kept at -80°C. Samples were homogenised by resuspending the pellets in 0.5 mL of phosphate buffer, vortexing and finally sonicating at 30% amplitude for 1 min (2 cycles with a one-minute-break between cycles). They were centrifuged at 13000 rpm (13226 rcf) for 15 min at 4°C (Multi speed

refrigerated centrifuge, rotor T527, ALC PK121R) and the supernatants were analysed for ROS content. Aliquots (5 µL) of samples were diluted in 100 µL of milliQ water in 96 multiwell plate and the fluorescence was measured using excitation and emission wavelengths of 485 and 530 nm, respectively. The molar concentration of ROS in the sample was calculated from a standard curve generated using known concentrations of 2',7'-dichlorofluorescein (H_2DCF) (0–1 µM). ROS content in each sample was determined in triplicate.

Data are presented as means ± SD and analysed by One-way ANOVA ($P < 0.05$) with Tukey's Multiple Comparison Test. Statistics was performed with PAST software package, version 3.14 (Hammer *et al.,* 2001).

3.2.7. 5-histidylcysteine sulfoxide synthase (OvoA) analysis

MMETSP and NCBI databases were searched for OvoA occurrence in diatoms, resulting in supplementary tables 3S and 4S.

For the alignment, The *Paracentrotus lividus* (AMM72581.1), *Strongylocentrotus purpuratus* (XP_011674521.1), *T. pseudonana* and *Phaeodactylum tricornutum* (XP_002179013.1) OvoA sequences were downloaded from the NCBI protein database. The *S. marinoi* (strain CCMP2092) OvoA sequences were downloaded from the MMETSP website (MMETSP1039: 2388 and 4090). The sequences were aligned with ClustalX and edited with GeneDoc software. The analysis of domains was performed using InterPro database.

Chloroplast transit peptides were searched using ASAFind server (http://rocaplab.ocean.washington.edu/tools/asafind/).

The phylogenetic tree of OvoA homologues from diatoms was inferred using the Neighbor-Joining method (Saitou and Nei, 1987), using sequences from Heterokonta and Chlorophyta

phyla as outgroup. The evolutionary distances were computed using the JTT matrix-based method (Jones *et al.,* 1992) and are in the units of the number of amino acid substitutions per site. The analysis involved 50 amino acid sequences, downloaded from the the NCBI protein database and MMETSP website (all accession numbers are shown in fig. 45 and tab. 3S). All positions containing gaps and missing data were eliminated. There was a total of 239 positions in the final dataset. Evolutionary analyses were conducted in MEGA7 (Kumar *et al.,* 2016).

3.2.8. Nitric Oxide synthase (NOS) analysis

The three *Homo sapiens* NOS sequences (iNOS-inducible NP_000616.3, eNOS-endothelial BAA05652.1 and nNOS-neuronal NP_000611.1) were downloaded from the NCBI protein database. The two *S. marinoi* (strain CCMP2092) NOS sequences (transcript IDs: 3976, 3419) were downloaded from the MMETSP website. The sequences were aligned with ClustalX and edited with GeneDoc software. The analysis of domains was performed using InterPro database. Chloroplast transit peptides were searched using ASAFind server (http://rocaplab.ocean.washington.edu/tools/asafind/).

3.3. Results

3.3.1. Protein Sequence Analysis of *S. marinoi* OvoA

The presence of OvoA homologues in diatoms was disclosed and analysed through comparative sequence analyses, using sequences from other microalgal species as outgroups. OvoA has been found in several diatom transcriptomes (fig. 45) although absent in others, such as *Chaetocerus* genus, *Asterionellopsis glaciasis,* and *Helicotheca tamensis* (tab. 3S). In some diatom transcriptomes two OvoA transcripts were found, as in *Leptocylindrus danicus*, strain B650, and in *Minutocellus polymorphus*, strain NH13 (tab. 3S). Moreover, the analysis allowed to highlight that, in some species, the presence of OvoA transcript depends on the growth condition and, in particular, on nutrients availability (tab. 4S). Thus, for example, in *T. weissflogii,* the *OvoA* transcript is detected under iron and silicate limitation, compared to replete conditions, in which it is not present. In *S. marinoi* (strain Skel A), high concentrations of phosphate and low light conditions are necessary for the expression of *OvoA*. *Skeletonema marinoi* transcriptome, strain CCMP2092, the one used in this study, also revealed the presence of two transcripts, annotated as 2388 and 4090.

OvoA protein sequences from diatoms, representing 28 genera, were used to reconstruct OvoA phylogeny by neighbor-joining (NJ) algorithm. Sequences from heterokonta and chlorophyta phyla were used as outgroups. The results showed that OvoA protein clearly clusters in two different clades reflecting, to some extent, the diatom evolution divergence in centric and pennate species (fig. 49).
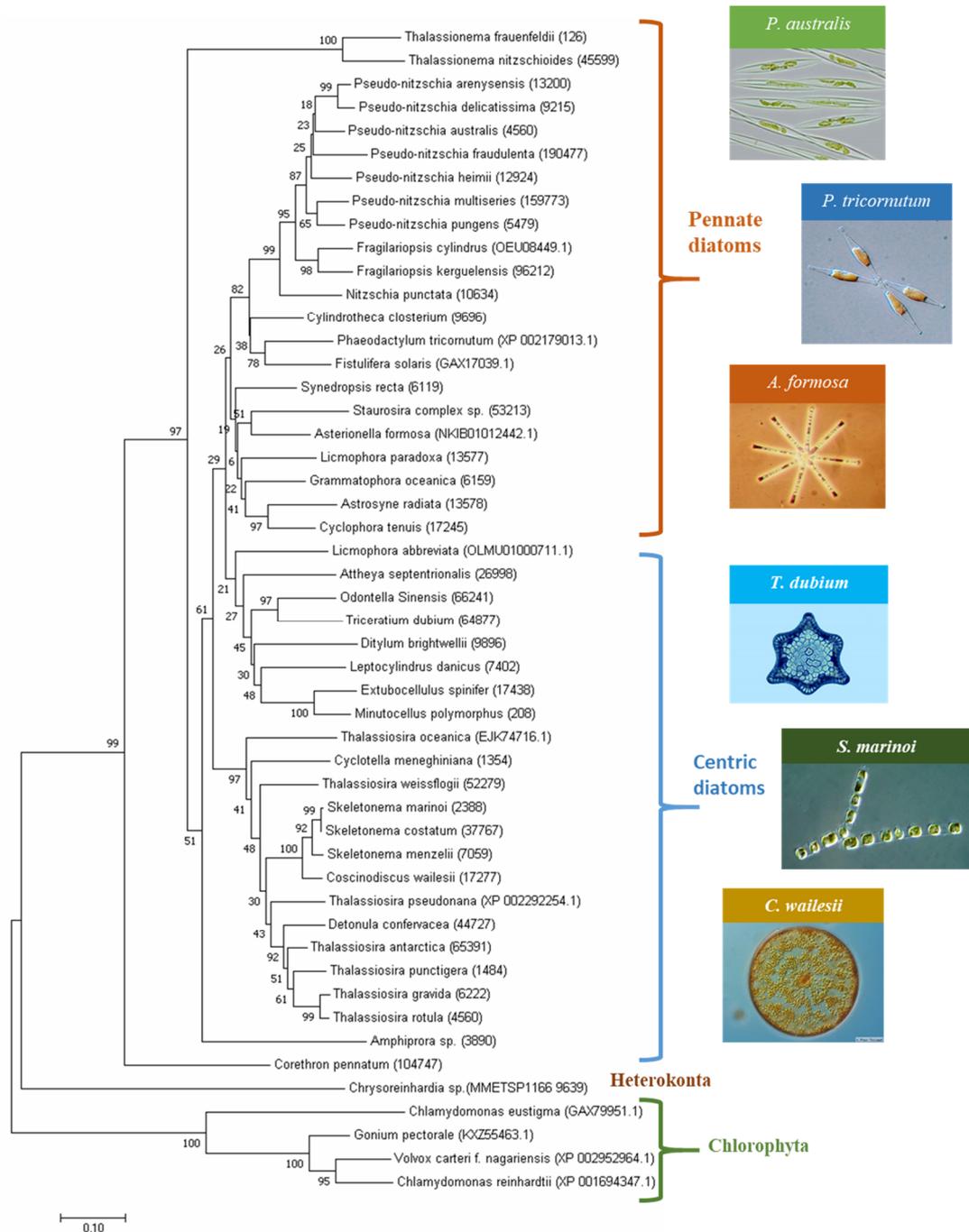
Figure 49 Neighbor joining tree of OvoA homologues in diatoms.

The evolutionary history was inferred using the Neighbor-Joining method (Saitou and Nei, 1987). The optimal tree with the sum of branch length = 6.62215866 is shown. The percentage of replicate trees in which the associated taxa clustered together in the bootstrap test (10000 replicates) are shown next to the branches (Felsenstein, 1985). The tree is drawn to scale, with branch lengths in the same units as those of the evolutionary distances used to infer the phylogenetic tree.

OvoA sequences from diatoms *T. pseudonana, P. tricornutum* and *S. marinoi* (both 2388 and 4090 sequences) were aligned with sequences from sea urchins *P. lividus* and *S. purpuratus* (fig. 50A). Domain analysis revealed that OvoA from diatoms *T. pseudonana, P. tricornutum* contains all the canonical domains of metazoan OvoAs: DinB_2 superfamily, FGE-sulfatase and SAM-transferase. Also the putative binding sites for iron and SAM, key residues important for the enzymatic reactions, and the residues involved in the binding to substrates (cysteine and histidine) were highly conserved (fig. 50B). To investigate the possibility that OvoA protein could be targeted to chloroplasts in diatoms, chloroplast transit peptides were searched in the OvoA protein sequence using the ASAfind software, which gave a negative result. The analysis revealed that, while *S. marinoi* OvoA_2388 (*Sm*OvoA_2388) contains all three domains, including the putative binding sites for iron, SAM and substrates, OvoA_4090 lacks the DinB_2 superfamily domain, the binding site for iron and two of the binding sites for substrates (fig. 50A,B). The two protein sequences from *S. marinoi* share 97% identity on 65% of covering (tab. 3S).

3.3.2. Protein Sequence Analysis of *S. marinoi* Nitric Oxide Synthase (NOS)

NOS has been recently identified in several diatom species, including the pennate *Pseudo-nitzschia multistriata*, which produces a single transcript showing high similarity with cyanobacterial sequences containing all the canonical domains (Di Dato *et al.,* 2015), differently from bacterial NOS-like enzymes, which have only the oxygenase domain and use no-specific cellular reductases to produce NO (Gusarov *et al.,* 2008). In addition, cyanobacteria NOS sequences have an N-terminal globin superfamily domain (fig. 51). Instead, the primary structure of *Ostreococcus tauri* NOS shows the features of a typical iNOS, including the canonical oxygenase and reductase domains, linked by the calmodulin

(CaM) binding site, and lacking the inhibitory loop. Moreover, it contains a partially conserved zinc binding domain which differs from that found in animal NOS enzymes (Alderton *et al.,* 2001), containing a C-(x)3-C motif (where C is Cys and x any residue) instead of the C-(x)4-C sequence (Foresi *et al.,* 2010).

Most of the centric diatoms (*Thalassiosira minuscula*, *Skeletonema costatum, S. marinoi)* showed two different NOS transcripts (Di Dato *et al.,* 2015).

An alignment of the two transcripts of *S. marinoi* (strain CCMP2092) (annotated as 3976 and 3419) with human NOSs is shown in fig. 52A, highlighting the conserved domains with canonical mammalian NOSs. A blastp search in the NCBI database revealed a higher similarity with cyanobacteria sequence for transcript 3976, included the globin superfamily domain, while the transcript 3419 showed higher similarity with *O. tauri* sequence (fig. 52B).

None of the two transcripts of *S. marinoi* contains the inhibitory loop (fig. 52), indicating an inducible feature.

The presence of chloroplast transit peptides in NOS protein sequences was investigated using the ASAfind software, which gave a negative result as for OvoA.
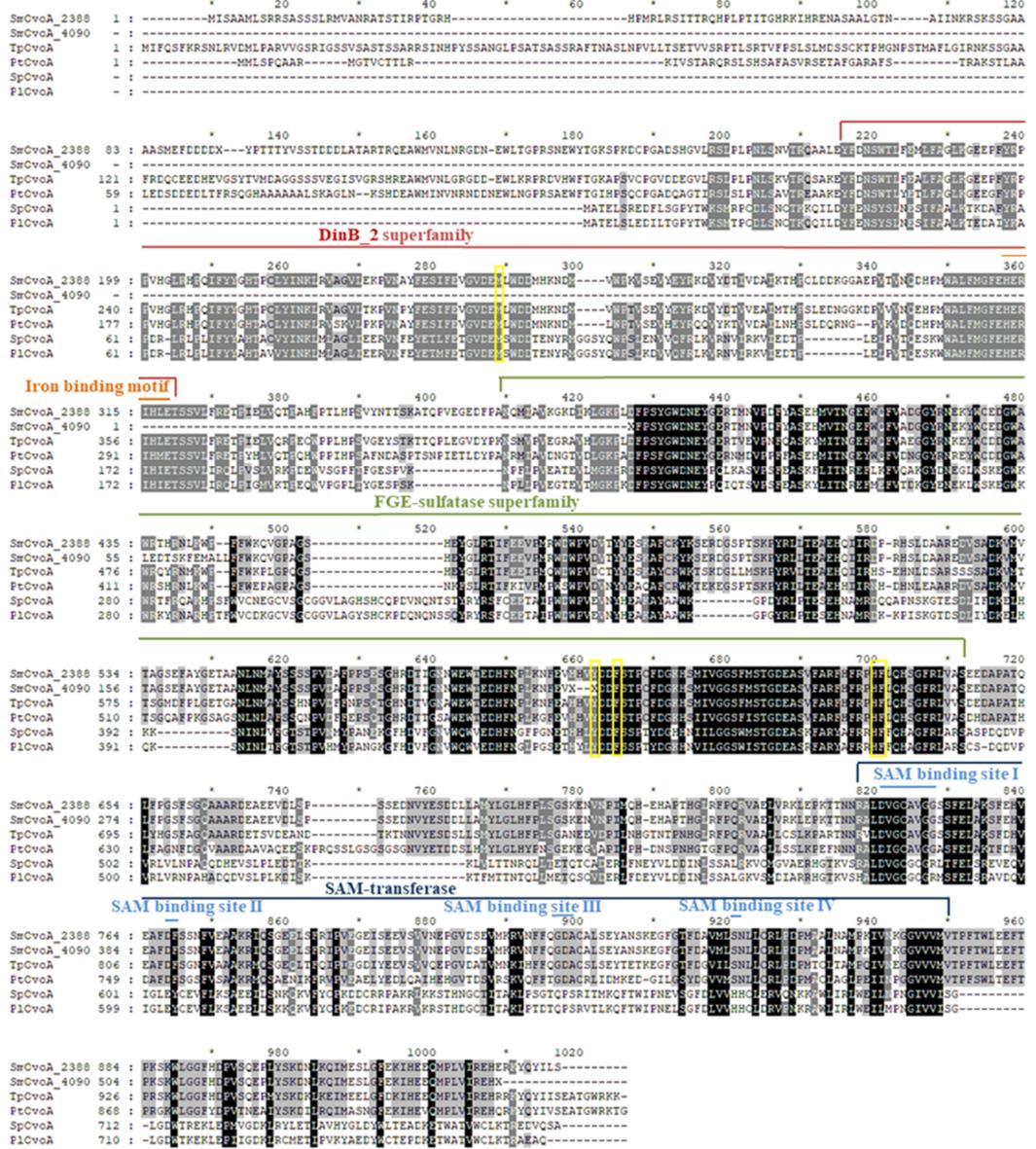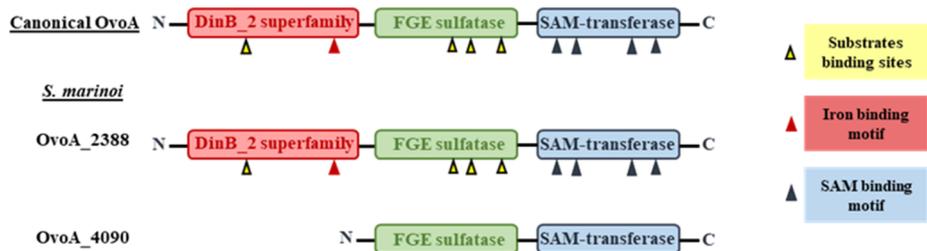
Figure 50 Alignment of diatom and sea urchin OvoA sequences.

A. The OvoA sequences from three species of diatoms (*T. pseudonana*, *P. tricornutum* and *S. marinoi*) and two species of sea urchins (*P. lividus* and *S. purpuratus*) were aligned using ClustalX and Genedoc software. Black, dark-gray and light-gray boxes indicate 100, 80 and 60% residues corservation, respectively. Amino acids that do not share similarity are unshaded. The OvoA canonical domains, DinB superfamily, FGE-sulfatase and SAM-transferase, are indicated as well as

the putative binding sites for iron and SAM. The putative residues accounting for the binding to substrates (cysteine and histidine) are highlighted by yellow boxes. **B.** Scheme of the domain architecture of *S. marinoi* OvoA compared to the canonical metazoan OvoA. Abbreviations: PlOvoA = *Paracentrotus lividus* OvoA; PtOvoA = *Phaeodactylum tricornutum* OvoA; SmOvoA = *Skeletonema marinoi* OvoA; SpOvoA = *Strongylocentrotus purpuratus* OvoA; TpOvoA = *Thalassiosira pseudonana* OvoA.
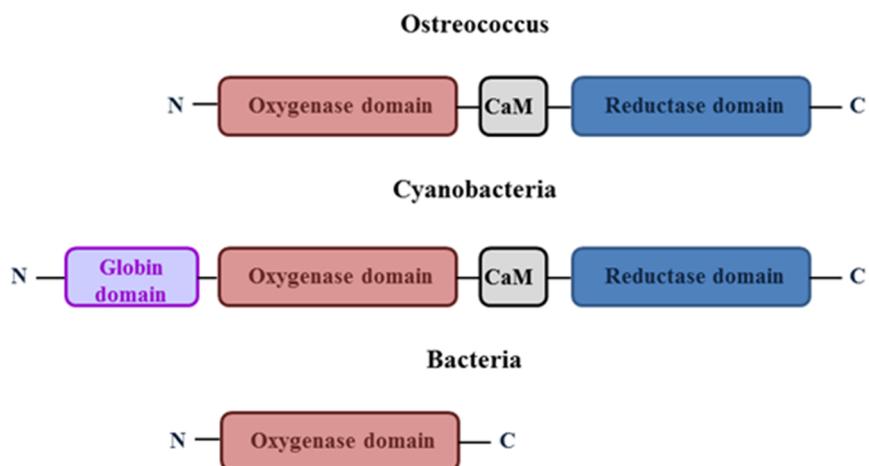
Figure 51 Comparison of domain architecture of NOS from *O. tauri*, cyanobacteria and bacteria.

A

Globin like superfamily

Heme

Oxygenase Domain

BH4 I   BH4 II   BH4 III   BH4 IV

Calmodulin

Inhibitory loop   FMN

FAD pyrophosphate

FAD isoalloxazine

Reductase domain

NADPH ribose   NADPH adenine

NADPH

B

Human

nNOS N — PDZ — Oxygenase — CaM — Reductase — C

Myristoylation and palmitoylation motifs   Inhibitory loop

eNOS N — Oxygenase — CaM — Reductase — C

iNOS N — Oxygenase — CaM — Reductase — C

S. marinoi

Nos_3976 N — Globin — Oxygenase — CaM — Reductase — C

Nos_3419 N — Oxygenase — CaM — Reductase — C

Figure 52 Alignment of *S. marinoi* and Human NOS sequences.
A. The sequences of SmNOS and human eNOS, nNOS, and iNOS were aligned using ClustalX and Genedoc software. Black boxes indicate conserved residues in all five sequences, dark-gray boxes represent conserved residues in four sequences, and light-gray boxes represent conserved residues in three sequences. Amino acids that do not share similarity are unshaded. Putative cofactor binding sites for Heme, BH₄, CaM, FMN, FAD pyrophosphate, FAD isoalloxazine, NADPH ribose, NADPH adenine, and C-terminal domain of NADPH are shown. **B.** Comparison of the domain architecture of human and *S. marinoi* NOSs.

3.3.3. *OvoA* and *NOS* gene expression in *S. marinoi* under different light conditions and growth phases

With the aim to investigate *OvoA* and *Nos* modulation by light and during diatom growth phases, gene expression was assessed in all experimental conditions at different times from the light shift occurring at dawn.

For *OvoA*, specific oligos have been used for the longer identified transcript (2388). For *Nos*, specific oligos have been used for the two inducible transcripts: the first one (cod.3976 named *Nos1*) with a higher similarity with NOS from cyanobacteria and the second one (cod.3419 named *Nos2*) showing higher similarity with *O. tauri* sequence.

The results showed that under control condition (LSL150) *OvoA* gene expression was not significantly affected, whereas a significant down-regulation of *Nos1* and *Nos2* after 6h from dawn was detected, although expression ratio values were relatively close to the threshold value of 2 (fig. 53).

To investigate the modulation by high light, cells were grown under high sinusoidal and square-wave light, following 12:12 light:dark cycle. Interestingly, under HSL600 (high sinusoidal light) a significant up-regulation of *OvoA* gene after 2h was recorded as well as *Nos2* gene up-regulation after 6h from light switch (fig. 54A). At all experimental times, no significant modulation for all genes was observed under HSWL300 (high square-wave light;

fig. 54B), while a significant up-regulation of the three genes was assessed after only 10 min from light switch in the HSWL600 condition, even though the values did not reach the 2 threshold value (fig. 54C).

The opposite light conditions, i.e. very low sinusoidal and square-wave light and total absence of light, were also investigated. Different from the high light experiments, in this case, the light:dark cycle changed among these three conditions. In particular, while light followed a natural 12:12 light:dark cycle in case of very low sinusoidal light, peaking at 10 μmol photons s^{-1} m^{-2} after 6 hours from dawn, the light:dark cycle was 24:0 in case of very low square-wave light and 0:24 in case of darkness condition.

The results showed that under VLSL10 (very low sinusoidal light), *OvoA* and *Nos1* gene expression were not regulated, while *Nos2* was significantly up-regulated after 24h from the light switch (fig. 55A). Under VLSWL10 (very low square-wave light), a down-regulation of all the targeted genes after 24h was observed, with a high significativity at 30h (fig. 55B). Under dark condition, there was a significant decrease of *OvoA* gene expression after 6h from light switch-off, even though not reaching the 2 threshold value, and a significant *Nos2* up-regulation after 24h (fig. 55C).

Gene expression was also assessed under different growth phases. The results showed a significant *Nos1* down-regulation after 6h and 30h (the two midday peaks in exponential and stationary phase, respectively) from dawn, slightly approximating the 2 threshold value (fig. 56). *OvoA* and *Nos1* gene expression were not modulated by stationary growth phase, while *Nos2* was significantly up-regulated in stationary phase, both at 24h (at dawn before the light switch-on) and 30h (the midday peak), although not reaching the threshold value of 2 (fig. 56).
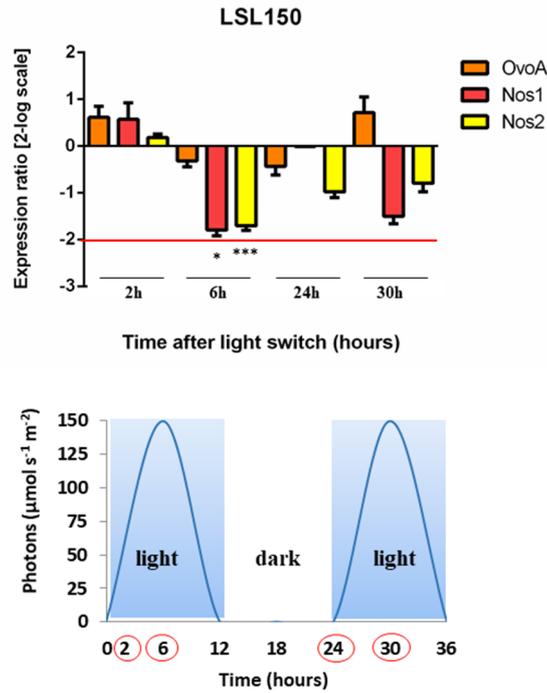
Figure 53 *OvoA* and *Nos* gene expression in *S. marinoi* under control light condition.

OvoA and *Nos* gene expression was assessed at different times from dawn in *S. marinoi* cultures grown under control non stressful light condition (low sinusoidal light, midday peak: 150 µmol photons s^{-1} m^{-2}, LSL150). *OvoA* and *Nos* gene expression levels (on top) and the light:dark cycle (on bottom) are shown. Sampling times are highlighted by red circles on light:dark cycle graphs.

* $p<0.05$ and *** $p<0.001$ represent significance compared to 0 time. Data are presented as means ± Standard error and analysed by REST software.
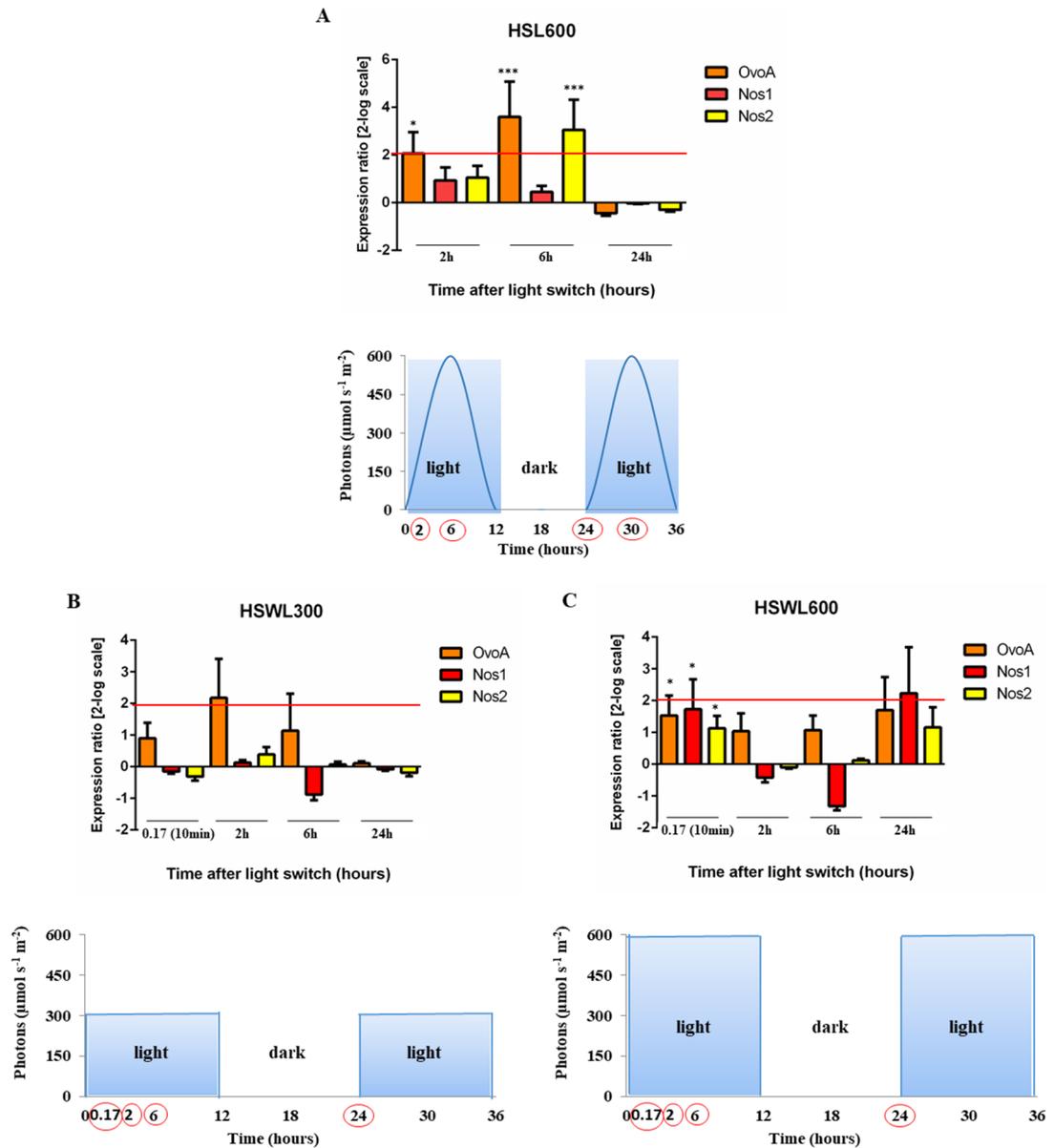
Figure 54 *OvoA* and *Nos* gene expression in *S. marinoi* under high light conditions.

All high light conditions followed a 12:12 light:dark cycle. For each condition/panel, *OvoA* and *Nos* gene expression levels (on top) and the light:dark cycle (on bottom) are shown. Sampling times are highlighted by red circles on light:dark cycle graphs. **A.** High sinusoidal light, midday peak: 600 µmol photons s-1 m^{-2}, HSL600; **B.** High square-wave light, midday peak: 300 µmol photons s^{-1} m^{-2}, HSWL300; **C.** High square-wave light, midday peak: 600 µmol photons s^{-1} m^{-2}, HSWL600. * $p<0.05$ and *** $p<0.001$ represent significance compared to 0 time. Data are presented as means ± Standard error and analysed by REST software.
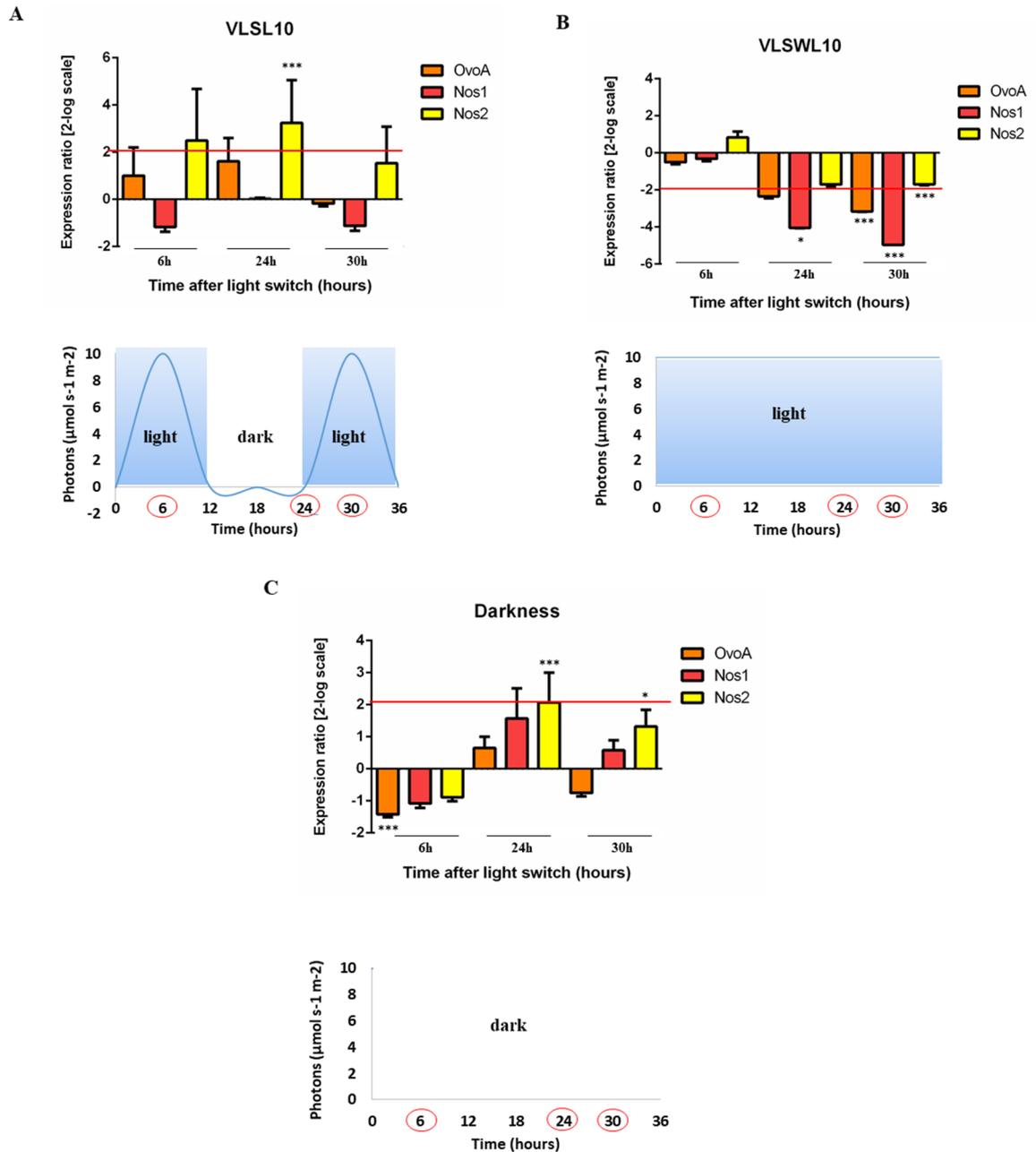
Figure 55 *OvoA* and *Nos* gene expression in *S. marinoi* under very low light conditions and darkness. For each condition/panel, *OvoA* and *Nos* gene expression levels (on top) and the light:dark cycle (on bottom) are shown. Sampling times are highlighted by red circles on light:dark cycle graphs. **A.** Very low sinusoidal light, midday peak: 10 µmol photons s^{-1} m^{-2}, VLSL10; **B.** Very low square-wave light, midday peak: 10 µmol photons s^{-1} m^{-2}, VLSWL10; **C.** darkness. * $p<0.05$ and *** $p<0.001$ represent significance compared to 0 time. Data are presented as means ± Standard error and analysed by REST software.
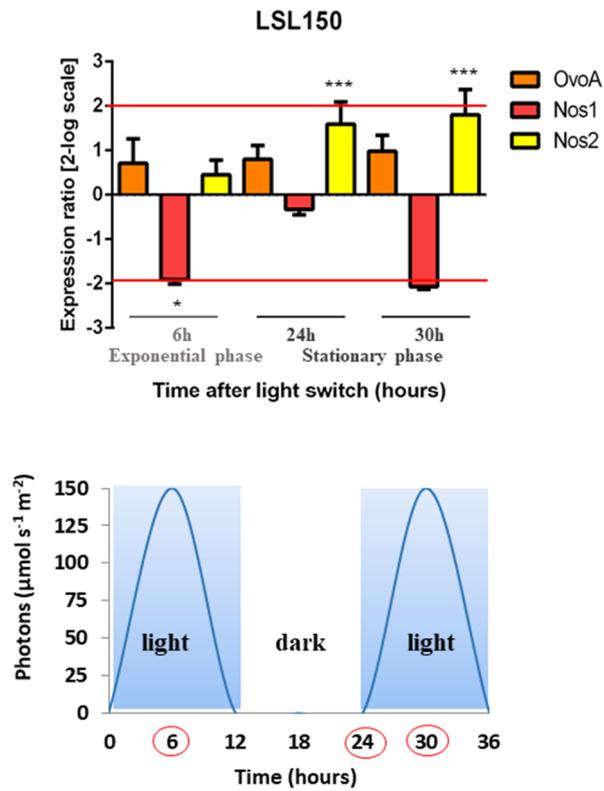
Figure 56 *OvoA* and *Nos* gene expression in *S. marinoi* in different growth phases.

OvoA and *Nos* gene expression was assessed in different growth phases at different times: 6h corresponds to the midday peak in exponential growth phase, 24h and 30h correspond to the 0 time (before the light switch-on) and the midday peak, respectively, in stationary growth phase. *OvoA* and *Nos* gene expression levels (on top) and the light:dark cycle (on bottom) are shown. Sampling times are highlighted by red circles on light:dark cycle graphs. *p<0.05 and ***p<0.001 represent significance compared to 0 time. Data are presented as means ± Standard error and analysed by REST software.

3.3.4. Involvement of nitric oxide (NO) in the light-dependent response and its formation in relation to different growth phases

In marine phytoplankton, nitric oxide (NO) is an important signalling molecule involved in many processes, such as protection from abiotic stress (Li *et al.,* 2013), perception of chemical cues, sensing optimal substrata and regulation of biofueling production (Vardi, 2008). NO can also induce gene expression regulation leading to cell death under light stress (Chung *et al.,* 2008). Indeed, depending on its concentration, NO can be a ROS scavenger, interrupting lipid peroxidation and inducing the expression of antioxidant enzymes, or, at high concentration, it can react with O^{2-} to form peroxynitrite, leading to the damage of biological macromolecules (Neill *et al.,* 2003). Moreover, it has been reported that NO production in marine phytoplankton is stress-type dependent and species specific (Gallina *et al.,* 2014).

In my work, I investigated the involvement of NO in light-dependent stress response in *S. marinoi* by analysing nitrite content in the different experimental light conditions. Under control light condition (LSL150), nitrite content remained almost stable at any experimental time (fig. 57). No significant increase of nitrite levels was observed under HSL600, HSWL300, HSWL600 along the experimental day (fig. 58A-C). However, cells exposed to HSL600 showed an increase of nitrite at 24 h from light switch compared to 0 time (fig. 58A). Same result was found for cells shifted to very low sinusoidal light condition (VLSL10, fig. 59A). Instead, a significant increase in nitrite content was found after 24 and 30 h of continuous VLSWL10 (fig. 59B). No significant increase of nitrite levels was observed under darkness condition (fig. 59C).
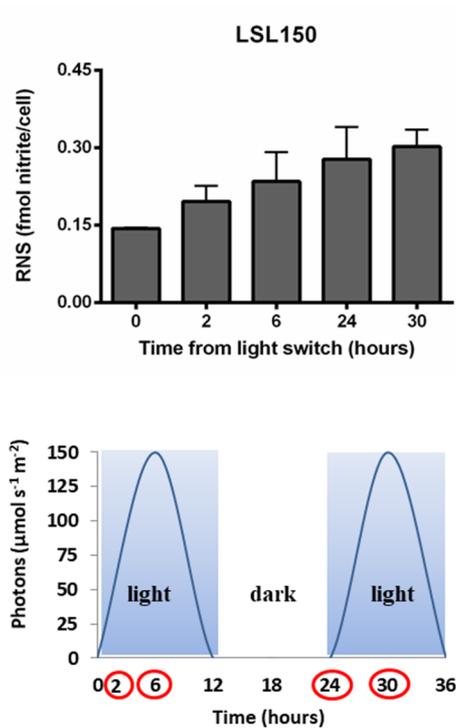
Figure 57 Reactive nitrogen species (RNS) in *S. marinoi* under control light condition.

Nitrite content was measured at different times from dawn in *S. marinoi* cultures acclimated to a control non stressful light condition (low sinusoidal light, midday peak: 150 µmol photons s^{-1} m^{-2}, LSL150). Nitrite content (on top) and the light:dark cycle (on bottom) are shown. Sampling times are highlighted by red circles on light:dark cycle graphs. Data are presented as means ± SD and analysed by One-way ANOVA with Tukey's Multiple Comparison Test.
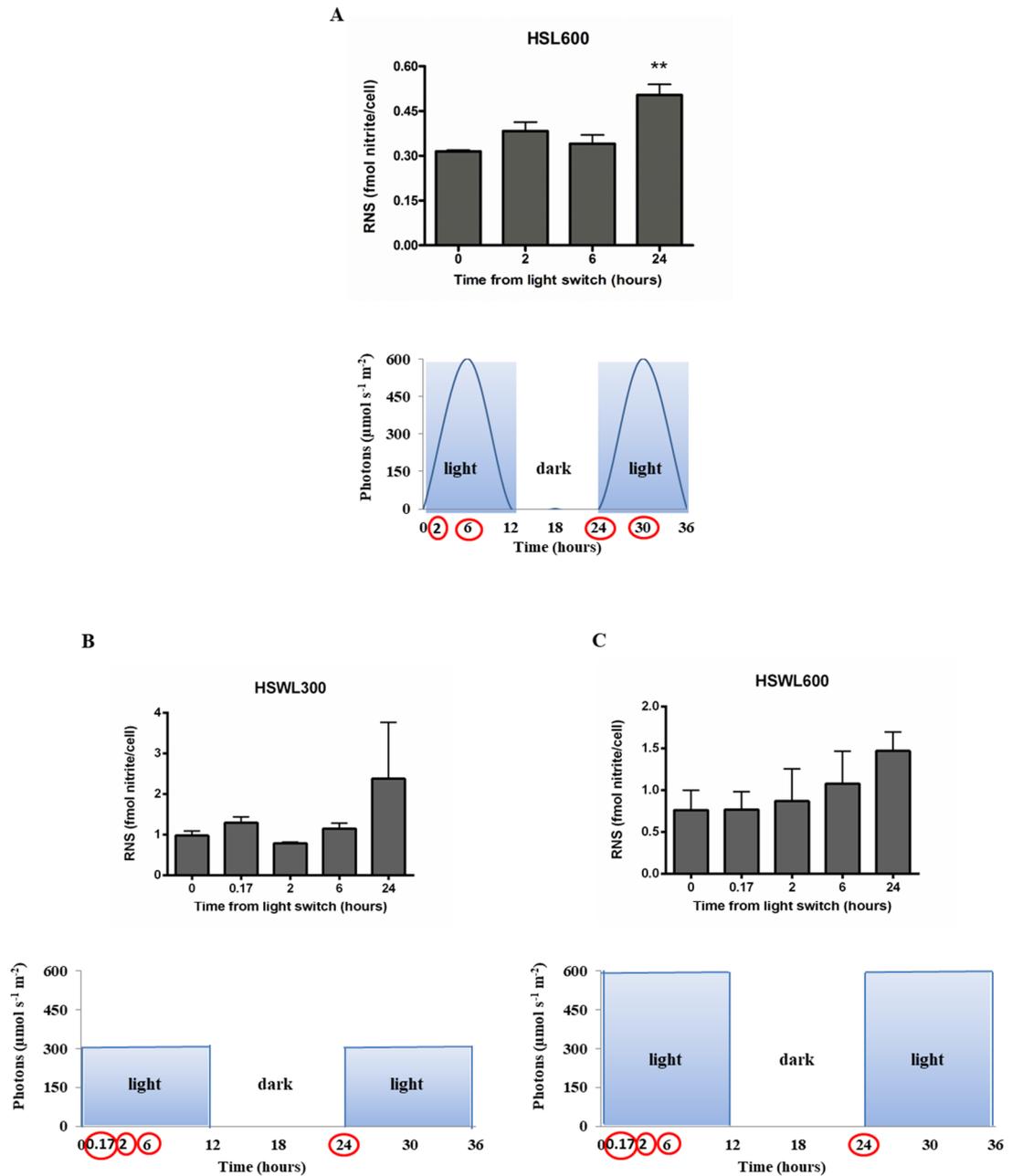
Figure 58 Reactive nitrogen species (RNS) in *S. marinoi* under high light conditions.

Nitrite content was measured at different times from dawn in *S. marinoi* cultures exposed to high light condition. All high light conditions followed a 12:12 light:dark cycle. Nitrite content (on top) and the light:dark cycle (on bottom) are shown. Sampling times are highlighted by red circles on light:dark cycle graphs. **A.** high sinusoidal light, midday peak: 600 µmol photons s^{-1} m^{-2}, HSL600. **p<0.01 represents significance compared to 0 time; **B.** High square-wave light, midday peak: 300 µmol photons s^{-1} m^{-2}, HSWL300; **C.** High square-wave light, midday peak: 600 µmol photons s^{-1} m^{-2}, HSWL600. Data are presented as means ± SD and analysed by One-way ANOVA with Tukey's Multiple Comparison Test.
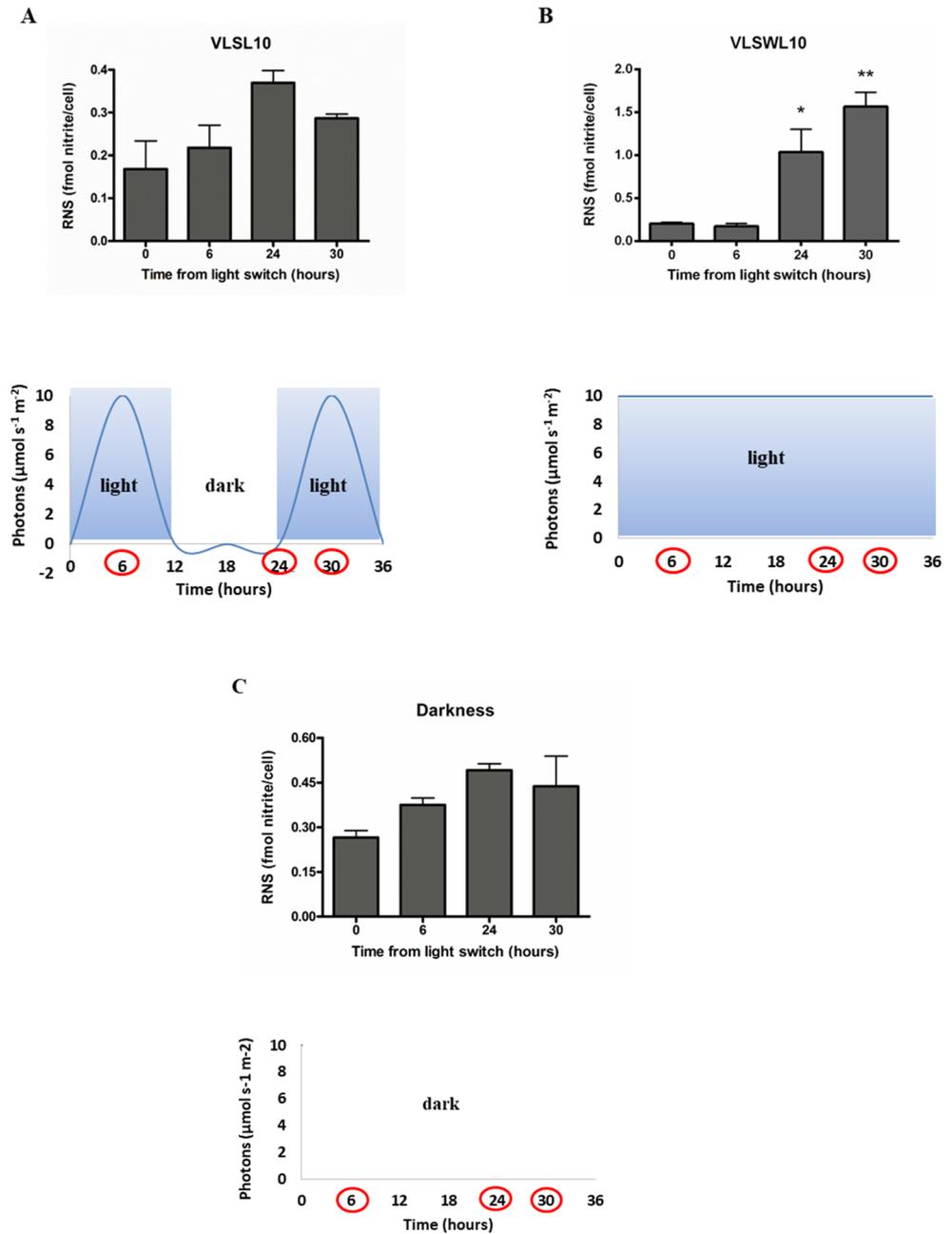
Figure 59 Reactive nitrogen species (RNS) in *S. marinoi* under very low light/darkness conditions. Nitrite content was measured at different times from dawn in *S. marinoi* cultures exposed to very light or darkness condition. **A.** Very low sinusoidal light, midday peak: 10 µmol photons s^{-1} m^{-2}, VLSL10; **B.** Very low square-wave light, midday peak: 10 µmol photons s^{-1} m^{-2}, VLSWL10. *$p<0.05$ and **$p<0.01$ represent significance compared to 0 time and 6h, respectively **C.** Darkness. Nitrite content (on top) and the light:dark cycle (on bottom) are shown. Sampling times are highlighted by red circles on light:dark cycle graphs. Data are presented as means ± SD and analysed by One-way ANOVA with Tukey's Multiple Comparison Test.

Experiments to assess the NO production in different growth phases showed that *S. marinoi* significantly increased nitrite levels in stationary growth phase compared to exponential phase (fig. 60).
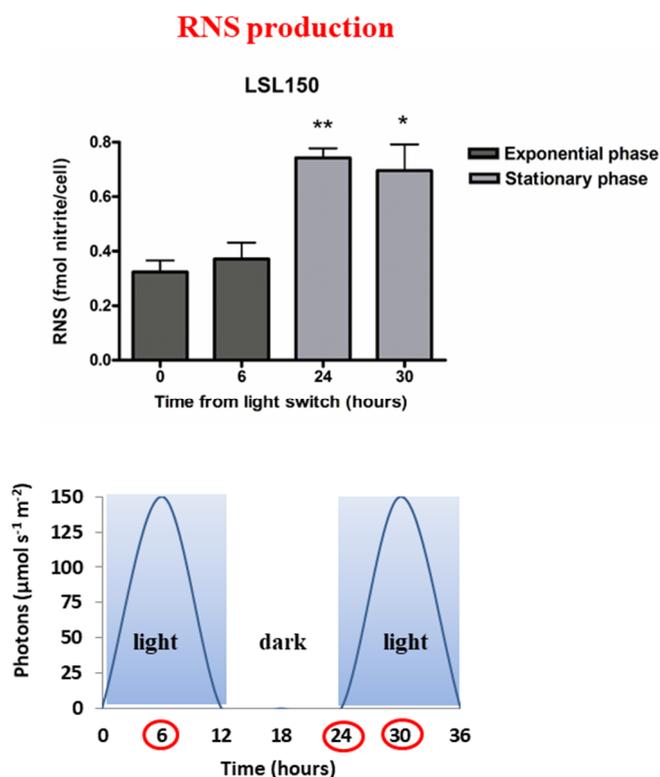
Figure 60 Reactive nitrogen species (ROS) production under different growth phases.
Nitrite content was measured in *S. marinoi* cultures grown under low sinusoidal light (midday peak: 150 µmol photons s^{-1} m^{-2}, LSL150) in different growth phases. Sampling was done at dawn (0 time) and after 6 h from dawn both in exponential and stationary growth phase. * $p<0.05$ represents significance compared to 6h, ** $p<0.01$ represents significance compared to 0 time. Nitrite content (on top) and the light:dark cycle (on bottom) are shown. Sampling times are highlighted by red circles on light:dark cycle graphs. Data are presented as means ± SD and analysed by One-way ANOVA with Tukey's Multiple Comparison Test.

3.3.5. Light- and growth phase- dependent production of ROS

ROS content *in S. marinoi* was analysed at the same light conditions mentioned above. Under control condition (LSL150), ROS content did not increase during the day with the gradual increase of light intensity, whereas a significant decrease was detected at 24 h (sampling time just before dawn) compared to 0 time (fig. 61). Under HSL600, cells enhanced their ROS levels already after 2 h from the light shift remaining high at 24h (fig. 62A), indicating a ROS production triggered by high sinusoidal light. Under HSWL300 and HSWL600, no significant increase of ROS levels was observed, except at 24 h in the HSWL600 condition (fig. 62B,C). Under VLSL10, only at 30 h a significant ROS overproduction was assessed (fig. 63A). Under VLSWL10 condition (fig. 63B) similar results were obtained compared to those under VLSL10, i.e. a significant increase of ROS at 30h.

In dark condition, the cell response was similar to what observed under very low light conditions (VLSL10 or VLSWL10) (fig. 63C), as indicated by a ROS increase after 30h, suggesting that cells accumulated ROS after one day of continuous dark or very low light intensity.

Furthermore, significant increase in ROS levels was detected in stationary phase compared to exponential phase (fig. 64), reflecting the RNS increase (fig. 60).
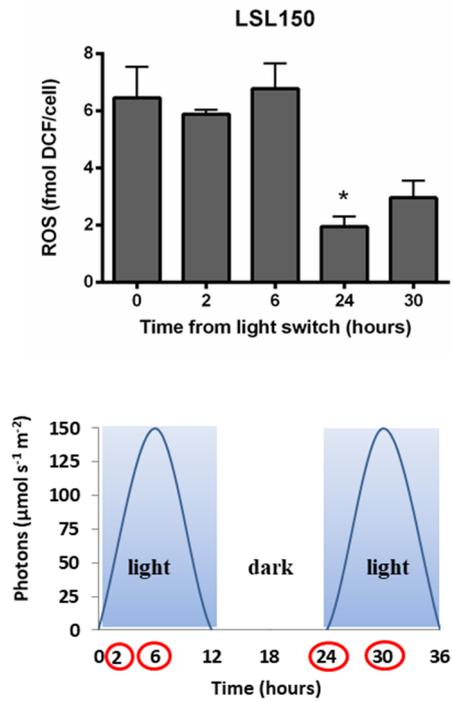
Figure 61 Reactive oxygen species (ROS) in *S. marinoi* under control light condition.

ROS content was measured at different times from dawn in *S. marinoi* cultures acclimated to a control light condition (low sinusoidal light, midday peak: 150 µmol photons s^{-1} m^{-2}, LSL150). ROS content (on top) and the light:dark cycle (on bottom) are shown. Sampling times are highlighted by red circles on light:dark cycle graphs. *$p<0.05$ represents significance compared to 0 time. .Data are presented as means ± SD and analysed by One-way ANOVA with Tukey's Multiple Comparison Test.
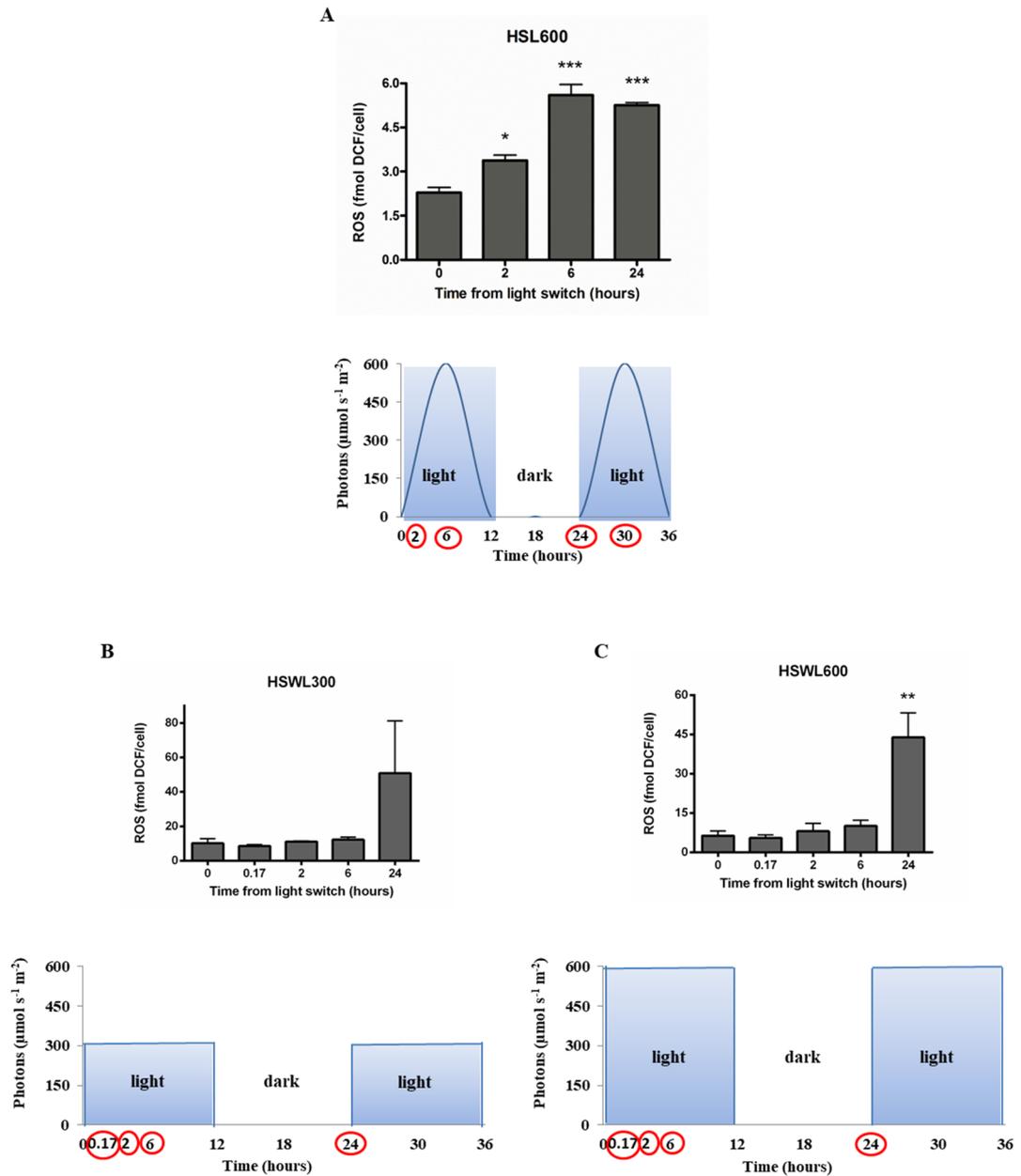
Figure 62 Reactive oxygen species (ROS) in *S. marinoi* under high light conditions.

ROS content was measured at different times from dawn in *S. marinoi* cultures exposed to high light condition. All high light conditions followed a 12:12 light:dark cycle. ROS content (on top) and the light:dark cycle (on bottom) are shown. Sampling times are highlighted by red circles on light:dark cycle graphs. **A.** High sinusoidal light, midday peak: 600 µmol photons s^{-1} m^{-2}, HSL600; **B.** High square-wave light, midday peak: 300 µmol photons s^{-1} m^{-2}, HSWL300; **C.** High square-wave light, midday peak: 600 µmol photons s^{-1} m^{-2}, HSWL600. Data are presented as means ± SD and analysed by One-way ANOVA with Tukey's Multiple Comparison Test. *$p<0.05$, **$p<0.01$, ***$p<0.001$ represent significance compared to 0 time
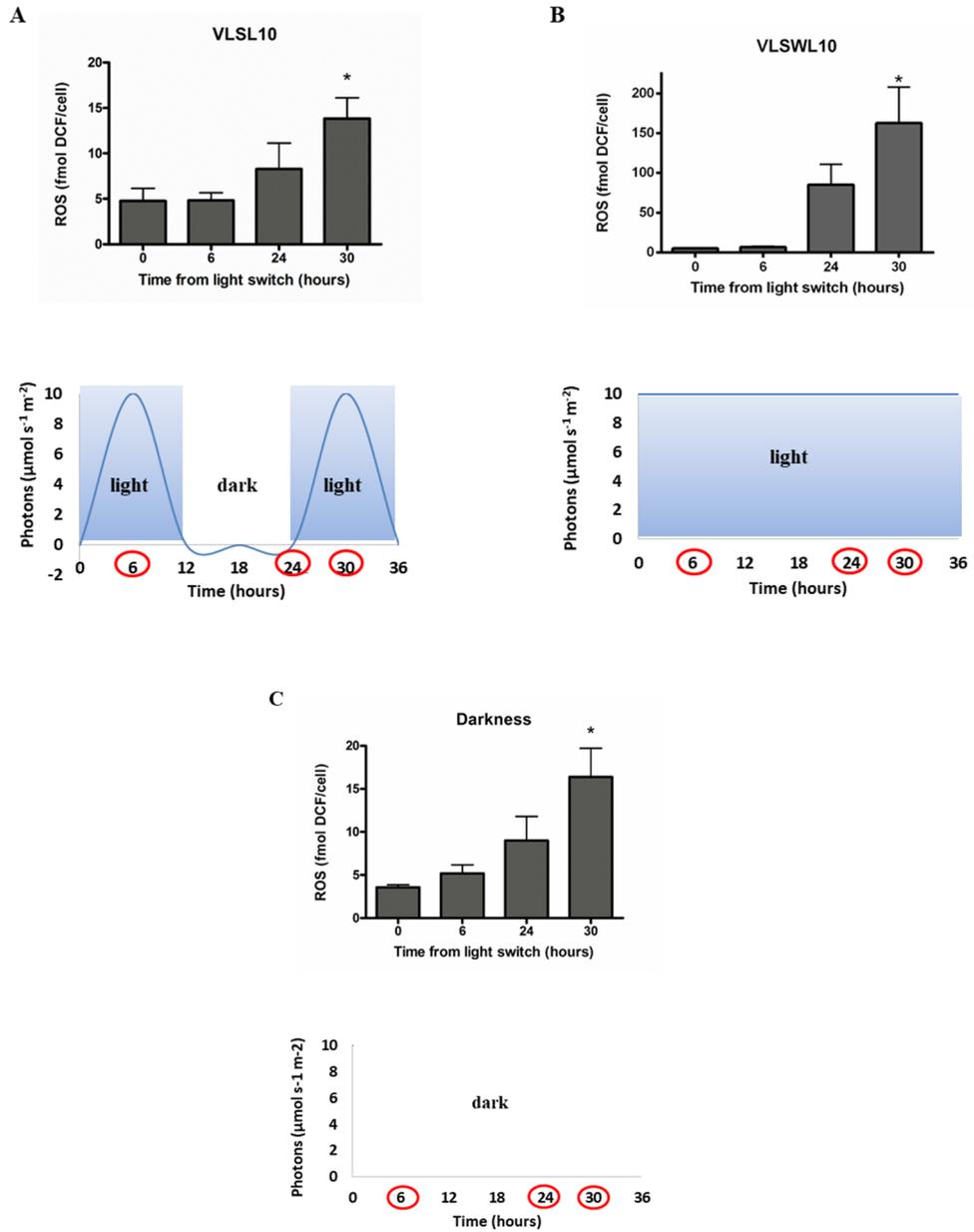
Figure 63 Reactive oxygen species (ROS) in *S. marinoi* under very low light/darkness conditions. ROS content was measured at different times from dawn in *S. marinoi* cultures exposed to very light or darkness condition. **A.** Very low sinusoidal light, midday peak: 10 µmol photons s^{-1} m^{-2}, VLSL10; **B.** Very low square-wave light, midday peak: 10 µmol photons s^{-1} m^{-2}, VLSWL10; **C.** Darkness. ROS content (on top) and the light:dark cycle (on bottom) are shown. Sampling times are highlighted by red circles on light:dark cycle graphs. Data are presented as means ± SD and analysed by One-way ANOVA with Tukey's Multiple Comparison Test. *p<005 represents significance compared to 6h.

ROS production
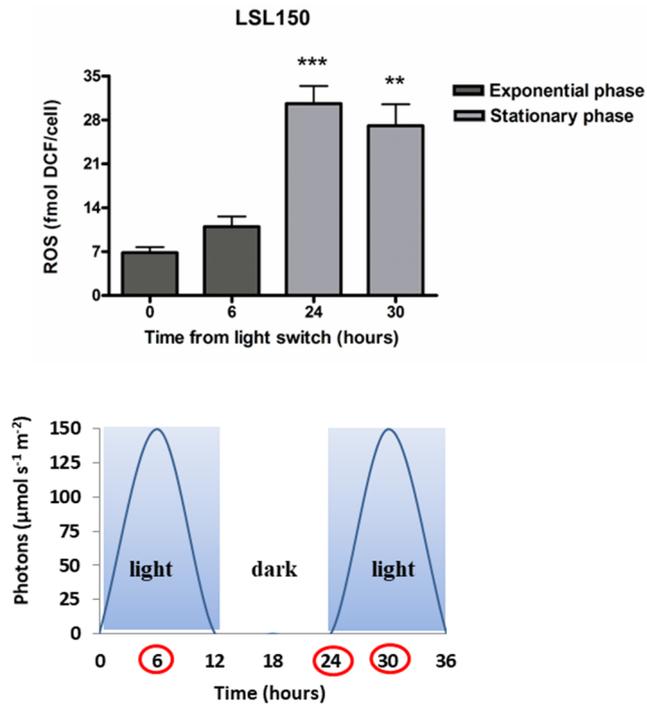
Figure 64 Reactive oxygen species (ROS) production under different growth phases.
ROS content was measured in *S. marinoi* cultures grown under low sinusoidal light (midday peak: 150 µmol photons s^{-1} m^{-2}, LSL150) in different growth phases. Sampling was done at dawn (0 time) and after 6h from dawn both in exponential and stationary growth phase. ROS content (on top) and the light:dark cycle (on bottom) are shown. Sampling times are highlighted by red circles on light:dark cycle graphs. **p<0.01 represents significance compared to 6h, ***p<0.001 represents significance compared to 0 time. .Data are presented as means ± SD and analysed by One-way ANOVA with Tukey's Multiple Comparison Test.

3.4. Discussion

In this chapter, I investigated the light-mediated regulation of the ovothiol biosynthesis in diatoms by studying OvoA, the key enzyme involved in the formation of the metabolite. In particular, I performed different analyses:

- Characterisation of OvoA protein domains in *S. marinoi* including a phylogenetic analysis of OvoA homologues in different diatom species;

- *OvoA* gene expression in relation to growth phases and light, representing this latter parameter one of the key environmental factors influencing diatom growth and physiology (Chandrasekaran *et al.,* 2014).

OvoA from diatoms contains all the canonical metazoan domains, including the key residues important for the enzymatic reaction.

The phylogenetic analysis of OvoA homologues in diatoms reveals that the protein falls in two clades, relative to the two main groups in which they are classified based on their morphology, centric and pennate diatoms, suggesting that, following the acquisition of the gene from the diatom ancestor, it evolved along the two different groups, giving rise to two different proteins. Moreover, the survey revealed that OvoA is not present in all diatom species, presumably following gene loss events, and its expression is presumably modulated by growth conditions, as suggested by the finding that the OvoA transcript finding depends on the nutrient availability, for instance.

In order to investigate the OvoA modulation by light, moderate light acclimated *S. marinoi* cultures were exposed to high light, very low light and darkness.

The *OvoA* gene basal levels and the *Nos1/2* down-regulation at midday under pre-acclimation condition indicates that cells were able to maintain a redox equilibrium along the daily light intensity increase. These results are in accordance with nitrite and ROS levels, which do not increase under control condition, confirming the no-stressful nature of this pre-acclimation condition. This finding is also confirmed by previous studies showing that this

light condition provides the optimal physiological health in *S. marinoi* with enhancement of growth capacity and metabolic state (Chandrasekaran *et al.,* 2014).

The gene expression analyses show that OvoA is up-regulated in *S. marinoi* following light switch to high sinusoidal light (HSL600) after only 2 and 6 hours from dawn. OvoA up-regulation is also observed after only 10 min from light switch to high square-wave light (HSWL600).

These results indicate that OvoA is highly responsive to high light in *S. marinoi* supporting previous evidence that ovothiol biosynthesis is related to light-dependent processes in microalgae (Selman-Reimer *et al.,* 1991; O'Neill *et al.,* 2015). In this context, I analysed for *OvoA* gene expression transcriptomic data available on the pennate diatom *P. tricornutum*, supporting the light-modulated *OvoA* gene expression in diatoms. Indeed, in cultures grown under white light condition (100 $\mu mol\ m^{-2}\ s^{-1}$) and then synchronised by 48 h dark-treatment (Nymark *et al.,* 2013; Valle *et al.,* 2014), *OvoA* gene expression increases after 0.5h re-exposition to white (fig. 65A), blue, green and red monochromatic light (fig. 65B), and then decreases at 6 and 24h from light switch-on (fig. 65).

An important outcome of my study is the analysis of the different behavior of the two *S. marinoi NOSs* to light stimulus. Indeed, under HSL600 an over-expression of *Nos2* (codifying for the enzyme having higher similarity with *O. tauri* Nos) was observed after 6h from light switch, while *Nos1* (codifying for the enzyme having higher similarity with Nos from cyanobacteria) gene expression did not show any variation on dependence from the light intensity.

The *OvoA* and *Nos2* gene expression detected under HSL600 are in line with ROS levels, i.e. increasing after 2 and 6h from light switch, and maintained high at 24h, after the night phase. Nitrite levels, instead, were low until 6h from dawn under HSL600, but they increased after the night phase, indicating a late response in the cells in the NO production and the inability to restore physiological levels of NO after the night period.

Interestingly, *Nos* up-regulation after only 10 min from light switch to HSWL600 is not supported by any increase in nitrite and ROS levels, suggesting that reactive oxygen and nitrogen species are probably scavenged or counteracted by highly fast antioxidant responses and photoprotective mechanisms, likely including also *OvoA* up-regulation.
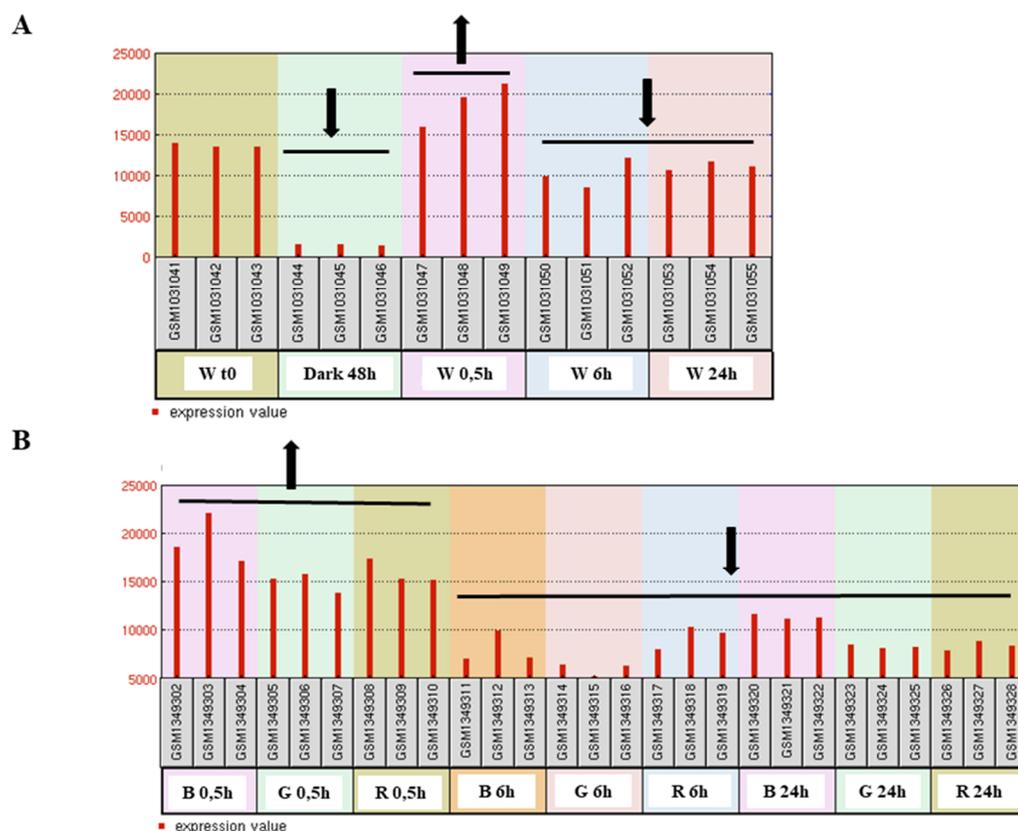
Figure 65 *OvoA* gene modulation by light in *P. tricornutum*

Trascriptomic data obtained from *P. tricornutum* cultures exposed to white (panel A; Accession number: GSE42039), blue, red and green light conditions (panel B; Accession number: GSE55959), following a 48h dark-treatment (Nymark *et al.,* 2013; Valle *et al.,* 2014). Abbreviations: W = white; B = blue; G = green; R = red.

These data, together with the *Nos2* over-expression in stationary phase are in accordance with previous studies showing that *O. tauri Nos* is light and growth phase-dependent (Foresi *et al.,* 2010). *Nos2* gene modulation by growth phase is supported by higher levels of both nitrite and ROS in stationary phase compared to exponential phase cells.

HSL600 also induces important changes in photoprotection mechanisms and photosynthetic acclimation. Indeed, the concentration of the pigment diatoxanthin and its precursor, diadinoxanthin, as well as β-carotene, increased at 2h, in parallel with an increase of the photoprotective mechanism NPQ (non photochemical quenching), peaking at 6h, when NPQ decreased (Brunet, personal communication). Interestingly, the antioxidant molecules increase at 2 and 6h (ascorbic acid and flavonoids) under HSL600 is lower compared to the control condition (LSL150), suggesting their consumption to prevent oxidative stress. Moreover, the high growth rate measured at 24 h suggests that cells are still highly performing under HSL600 revealing that they are able to acclimate to this stressful condition, although the high levels of nitrite and ROS levels revealed at 24h.

From a more general point of view, my data show that exposing cells to HSL600 leads to a time-dependent *OvoA* over-expression along the day. Conversely, HSWL600, whose light course is already known to be more stressful for the cells impairing their "normal" photophysiological regulation (Orefice *et al.,* 2016), leads to a very fast response which is not maintained along the day time maybe because cells can undergo cell death processes. Therefore, from a biotechnological point of view, HSL600 could be the more efficient light condition to be used to enhance ovothiol biosynthesis, since the light increase is able to trigger the *OvoA* gene expression, but, at the same time, the natural light distribution (sinusoidal) typical of HSL600 is not too stressful to impair diatom photophysiology, as in the case of HSWL600.

Cells grown under continuous VLSWL10, a completely unnatural condition, exhibit a down-regulation of the genes *OvoA* and *Nos1/2* at 24h and 30h from light switch, probably due to cell death. Indeed, this light condition strongly impairs the normal cell functioning leading to cell death processes in the population (personal communication, Dr. Arianna Smerilli). Thus, oxidative stress may be produced as consequence of the cell death process, as revealed by the increase of nitrite and ROS levels in this condition.

Finally, another interesting finding is that *OvoA* is down-regulated after 6h of continuous darkness, to reach basal levels after 24h and 30h. These results indicate that a light intensity increase (HSL600) leads to *OvoA* over-expression while the absence of light leads to a downregulation, thus confirming the key role of light in inducing *OvoA* gene expression. However, under darkness condition diatoms stop growing since several cell cycle related genes are light-controlled and darkness induces the arrest in G_1 phase or in both G_1 and G_2+M phases depending on the species (Vaulot *et al.,* 1986; Huysman *et al.,* 2010). Therefore, the *OvoA* modulation by light highlighted in this work could be dependent from the cell cycle light-dependence, and then *OvoA* could be related to mechanisms which regulate cell cycle progression in diatoms.

3.5. Conclusions and perspectives

This study provides an important contribution regarding the ovothiol biosynthesis in diatoms, with the aim to apply light manipulation to enhance amounts of ovothiol for applied research purposes. The relevance of these studies regards the possibility to obtain this promising bioactive compound from an eco-sustainable source, i.e. diatoms. Until now, ovothiol is extracted from sea urchin eggs, which is the most abundant natural source. On the other hand, chemical synthesis is difficult, expensive and not eco-sustainable (Palumbo *et al.,* 2018; Castellano and Seebeck, 2018).

Ongoing experiments are aimed to identify and characterise the form of ovothiol molecules produced by *S. marinoi*. For this purpose, *S. marinoi* will be cultivated under high sinusoidal light (HSL600), which resulted in an *OvoA* over-expression, and the cultures will be collected and analysed through HPLC-MS. This step is crucial for developing research and cultivation strategy regarding the production of the antioxidant ovothiol in diatoms, to enrich the already large potential of microalgae in biotechnological applications, such as cosmetics, pharmaceutics and nutraceutics.

Future prospects are to extract ovothiol from massive cultures of diatoms grown in photobioreactors, under controlled conditions of light, nutrient and temperature in order to maximise its production.

An important finding of this study is also the modulation by growth phases and light of the expression of NOS. The results show a different behavior of the two *S. marinoi* NOS, suggesting a different function of the two enzymes in this species. Further studies are necessary to investigate NOS activity in diatoms, considering the open debate regarding the presence of NOS in photosynthetic organisms. Enzymatic activity studies or perturbation experiments will provide more information regarding the NOS functionality.

CHAPTER 4

4.1. General discussion and conclusions

The aim of my thesis was to get insight into the biological roles of ovothiol in two marine organisms inhabiting coastal areas: sea urchins and diatoms. These two model systems, although evolutionarily distant, have offered the opportunity to obtain a broader view of the biological function of this metabolite in marine environment, considering the pleiotropic activities of this class of molecules (Castellano and Seebeck, 2018).

The results of my work have highlighted some common points regarding the role played by this metabolite in these two systems. Indeed, ovothiol may be involved in the cellular defence system, activated from different types of stressors, which both sea urchin embryos and diatoms are forced to cope with along the water column.

In sea urchins, the embryonic development is an extremely sensitive and key process which allows the successful fitness of the progeny. As broadcast spawners, sea urchins release eggs and sperm in seawater where external fertilisation occurs and embryos develop, entering the plankton community, thus being directly exposed to stressful agents present in the environment. The localisation of OvoA in all blastomeres in the early developmental stages suggests a key role of ovothiol in protecting embryos/larvae from environmental cues. This hypothesis is confirmed by the finding that *OvoA* gene expression increases in developing embryos exposed to different stress agents, such as cadmium and toxic bloom (Castellano *et al.,* 2016). Yet, the *OvoA* spatial expression in the larval digestive trait and in the skeletogenic cells could also be ascribed to the necessity of a strictly localised ovothiol production in two compartments, which are particularly exposed to environmental cues. Indeed, the digestive trait is an important barrier from the external environment, and can be directly in contact with toxins, for examples derived from microalgae, which constitute the larval food, but also with other damaging abiotic factors, like heavy metals, or biotic threats, like larval pathogens. In this connection, the sea urchin larva has been considered a model for gut-associated immune response. When sea urchin larvae are infected with a marine

bacterium, there is an inflammatory response associated to the gut, mediated by the cytokine IL17, which maintains barrier integrity and regulates microbiota composition (Buckley and Rast, 2017). Then, the anti-inflammatory properties exerted from ovothiols in *in vitro* and *in vivo* models (Castellano *et al,* 2018; Brancaccio *et al.,* 2018) may be suggestive of their involvement in the gut-associated immune response in sea urchins.

Moreover, also the skeletogenic cells have to cope with external variables, like for example pH changes. Indeed, when plutei are exposed to elevated seawater pCO_2 to mimic future ocean acidification conditions, the extracellular larval compartment surrounding the PMCs and spicules have the same acidic pH of the external seawater, since the body cavity is not able to compensate external pH (Stumpp *et al.,* 2012). However, measurements of intracellular pH demonstrated that PMCs are able to fully compensate the induced acidosis. Further studies would be necessary to demonstrate the possible involvement of ovothiol in these processes during sea urchin development, i.e. gut immunity and pH compensation mechanisms. _For example, an *OvoA* up-regulation in gut from infected larvae could suggest some relation between ovothiol formation and the immune response, thus representing the starting point for future experiments in this direction. Yet, the acid-base regulation properties of ovothiol could be investigated in sea urchin larvae exposed to different pH conditions, in laboratory controlled or natural conditions, taking advantage from the naturally acidified sites present in Ischia island (Foo *et al.,* 2018).

In the case of diatoms, these microalgae are exposed to continuous variations in light intensity and spectral composition, being uninterruptedly moved by sea currents along the water column. Therefore, they have to rapidly regulate their photophysiology in response to the fast changes in light conditions, ranging from dark or very low intensities and the absence of red in deeper conditions to very high intensities, together with the presence of red and other wavelengths from 400 to 700 nm, near the sea surface. When, in the upper sea water layers, too intense light reaches the cells, they are subjected to oxidative stress, released during the photosynthetic process.

It is known that *S. marinoi* cultures exposed to red and high blue light, miming the light conditions present in the upper sea water layers, up-regulate the expression of antioxidant enzymes like catalase, superoxide dismutase and ascorbate peroxidase (Smerilli *et al.,* 2017). In addition to the activation of these enzymes, the cells may also enhance the formation of antioxidant molecules, i.e. ovothiol, up-regulating *OvoA* gene expression.

Thus, the protection ability of ovothiol is exploited by both systems in two key processes, embryonic development and response to high light, extremely important for survival of sea urchins and diatoms, respectively.

Considering that light is a fundamental factor for the biology and physiology of living organisms, especially for photosynthetic organisms, being the primary source of energy and providing essential information on the surrounding environment (Jaubert *et al.,* 2017 and bibliography therein), ovothiol may act in diatoms not only as an antioxidant but also as a signalling molecule in light-associated processes. Different photoreceptors have been identified in diatoms, including some that are similar to the plant counterpart, and others representing completely new variants (Jaubert *et al.,* 2017). To address this aspect, preliminary experiments could be performed by following the expression of light sensors and *OvoA* in diatom cultures at different light conditions.

However, many aspects remain to be investigated in diatoms. An important issue concerns the identification of the ovothiol produced by diatoms and the detemination of its concentration in relation to other sulphydryl compounds, e.g. glutathione. This could provide an insight about its function as signalling molecule. Ovothiol, possessing a very reactive sulphydryl group, may participate to cellular redox exchange processes, interacting with the sulphydryl groups of other proteins, thus regulating their activity. In the two systems, sea urchins and diatoms, ovothiol can act on different targets depending on the intracellular environment.

Yet, ovothiol can also interact with other intracellular thiols and signalling molecules, such as nitric oxide (Krauth-Siegel and Leroux 2012). Considering the key role of nitric oxide in

various developmental processes, such as life cycle transitions and methamorphosis (Castellano *et al.,* 2014, 2015), ovothiol could indirectly affect these biological processes.

In sea urchin eggs, where ovothiol mainly acts as an antioxidant at fertilisation, the compound is present at millimolar concentration, higher compared to that of glutathione. On this basis, it would be relevant to measure ovothiol and glutathione concentrations in diatoms.

The finding that in diatoms and also in other microalgae, ovothiol production is related to light (Selmar-Reimer *et al.,* 1991; O'Neill *et al.,* 2015) together with the fact that light is an important factor also for non-photosynthetic organisms, regulating circadian rhythms, opens the possibility that a similar relationship may also occur in sea urchins.

Sea urchin larvae, which move, like diatoms, along various layers of the sea water column at different light intensities, have been reported to perceive light (Yoshida, 1966; Millott, 1975; Yerramilli and Johnsen, 2010). The sequencing and the analysis of the *S. purpuratus* genome allowed to identify several classes of opsins, transcription factors and genes involved in photoreceptor cell differentiation and phototransduction cascade (Sodergreen *et al.,* 2006). Moreover, two opsins have been recently characterised in sea urchin larvae (Valero-Gracia *et al.,* 2016). These opsins are involved in non-directional photoreception, which regulates key biological processes, like circadian and seasonal rhythms. Specific experiments will be necessary to demonstrate a possible link between opsins and OvoA. *OvoA* gene expression and/or ovothiol content could be monitored in sea urchin embryos cultured at different light:dark cycles.

Both in sea urchins and diatoms, ovothiol may be involved in maintaining the redox homeostasis in relation to the cell cycle. Indeed, it is relevant the presence of OvoA in interphase cells at early developmental stages in sea urchin and the *OvoA* gene modulation by light in diatoms, which could be indirectly due to the light-dependent regulation of cell cycle in this system. This is an interesting point, eventually to be investigated in future. Indeed, if further experiments would support this finding, it will provide the basis for

potential applications to human health, considering that the cell cycle dis-regulation represents one of the key factors involved in cancer progression.

References

Addis, P., Moccia, D. & Secci, M. (2015) Effect of two different habitats on spine and gonad colour in the purple sea urchin *Paracentrotus lividus*. *Marine Ecology,* **36** (2)**,** 178-184.

Agnello, M. (2017) Introductory Chapter: Sea Urchin - Knowledge and Perspectives. *Sea Urchin - From Environment to Aquaculture and Biomedicine.* InTech.

Alderton, W. K., Cooper, C. E. & Knowles, R. G. (2001) Nitric oxide synthases: structure, function and inhibition. *Biochemical Journal,* **357** (3)**,** 593-615.

Allen, A. E., Dupont, C. L., Oborník, M., Horák, A., Nunes-Nesi, A., McCrow, J. P., Zheng, H., Johnson, D. A., Hu, H., Fernie, A. R. & Bowler, C. (2011) Evolution and metabolic significance of the urea cycle in photosynthetic diatoms. *Nature,* **473,** 203-207.

Amaroli, A., Ferrando, S., Gagliani, M. C., Gallus, L. & Masini, M. A. (2013) Identification of aquaporins in eggs and early embryogenesis of the sea urchin *Paracentrotus lividus. Acta histochemica,* **115** (3)**,** 257-263.

Andersen, C. L., Jensen, J. L. & Ørntoft, T. F. (2004) Normalization of Real-Time Quantitative Reverse Transcription-PCR Data: A Model-Based Variance Estimation Approach to Identify Genes Suited for Normalization, Applied to Bladder and Colon Cancer Data Sets. *Cancer Research,* **64** (15)**,** 5245-5250.

Anderson, J. M. (1986) Photoregulation of the Composition, Function, and Structure of Thylakoid Membranes. *Annual Review of Plant Physiology,* **37** (1)**,** 93-136.

Andreakis, N., D'Aniello, S., Albalat, R., Patti, F. P., Garcia-Fernàndez, J., Procaccini, G.,

Sordino, P. & Palumbo, A. (2011) Evolution of the Nitric Oxide Synthase Family in Metazoans. *Molecular Biology and Evolution,* **28** (1)**,** 163-179.

Andrikou, C., Iovene, E., Rizzo, F., Oliveri, P. & Arnone, M. I. (2013) Myogenesis in the sea urchin embryo: the molecular fingerprint of the myoblast precursors. *EvoDevo,* **4** (1)**,** 33-33.

Annunziata, R., Perillo, M., Andrikou, C., Cole, A. G., Martinez, P. & Arnone, M. I. (2014) Pattern and process during sea urchin gut morphogenesis: The regulatory landscape. *genesis,* **52** (3)**,** 251-268.

Archibald, J. M. (2015) Endosymbiosis and Eukaryotic Cell Evolution. *Current Biology,* **25** (19)**,** R911-R921.

Ariyanayagam, M. R. & Fairlamb, A. H. (2001) Ovothiol and trypanothione as antioxidants in trypanosomatids. *Molecular and Biochemical Parasitology,* **115** (2)**,** 189-198.

Armbrust, E. V. (2009) The life of diatoms in the world's oceans. *Nature,* **459,** 185-192.

Armbrust, E. V., Berges, J. A., Bowler, C., Green, B. R., Martinez, D., Putnam, N. H., Zhou, S., Allen, A. E., Apt, K. E., Bechner, M., Brzezinski, M. A., Chaal, B. K., Chiovitti, A., Davis, A. K., Demarest, M. S., Detter, J. C., Glavina, T., Goodstein, D., Hadi, M. Z., Hellsten, U., Hildebrand, M., Jenkins, B. D., Jurka, J., Kapitonov, V. V., Kröger, N., Lau, W. W. Y., Lane, T. W., Larimer, F. W., Lippmeier, J. C., Lucas, S., Medina, M., Montsant, A., Obornik, M., Parker, M. S., Palenik, B., Pazour, G. J., Richardson, P. M., Rynearson, T. A., Saito, M. A., Schwartz, D. C., Thamatrakoln, K., Valentin, K., Vardi, A., Wilkerson, F. P. & Rokhsar, D. S. (2004) The Genome of the Diatom *Thalassiosira Pseudonana*: Ecology, Evolution, and Metabolism. *Science,* **306** (5693)**,** 79-86.

Bäckström, S. (1957) Content and distribution of ascorbic acid in sea urchin embryos of

different developmental trends. *Experimental Cell Research,* **13** (2)**,** 333-340.

Bailly, F., Azaroual, N. & Bernier, J.-L. (2003) Design, synthesis and glutathione peroxidase-Like properties of ovothiol-Derived diselenides. *Bioorganic & Medicinal Chemistry,* **11** (21)**,** 4623-4630.

Bailly, F., Zoete, V., Vamecq, J., Catteau, J.-P. & Bernier, J.-L. (2000) Antioxidant actions of ovothiol-derived 4-mercaptoimidazoles: glutathione peroxidase activity and protection against peroxynitrite-induced damage. *FEBS Letters,* **486** (1)**,** 19-22.

Barra, L., Chandrasekaran, R., Corato, F. & Brunet, C. (2014) The Challenge of Ecophysiological Biodiversity for Biotechnological Applications of Marine Microalgae. *Marine Drugs,* **12** (3)**,** 1641-1675.

Barra, L., Ruggiero, M. V., Sarno, D., Montresor, M. & Kooistra, W. H. (2013) Strengths and weaknesses of microarray approaches to detect Pseudo-nitzschia species in the field. *Environmental Science and Pollution Research,* **20** (10)**,** 6705-6718.

Beniash, E., Aizenberg, J., Addadi, L. & Weiner, S. (1997) Amorphous calcium carbonate transforms into calcite during sea urchin larval spicule growth. *Proceedings of the Royal Society B: Biological Sciences,* **264** (1380)**,** 461-465.

Benton, M. & Harper, D. A. T. (2009) Protists: Diatoms. *Introduction to Paleobiology and the Fossil Record.* Wiley-Blackwell.

Bodnar, A. G. (2009) Marine invertebrates as models for aging research. *Experimental Gerontology,* **44** (8)**,** 477-484.

Bodnar, A. G. & Coffman, J. A. (2016) Maintenance of somatic tissue regeneration with age in short- and long-lived species of sea urchins. *Aging Cell,* **15** (4)**,** 778-787.

Bottjer, D. J., Davidson, E. H., Peterson, K. J. & Cameron, R. A. (2006) Paleogenomics of

Echinoderms. *Science,* **314** (5801)**,** 956-960.

Boudouresque, C. F. & M., V. (2001) Ecology of *Paracentrotus lividus. Edible Sea Urchins: Biology and Ecology.* Amsterdam, Elsevier.

Bowler, C., Allen, A. E., Badger, J. H., Grimwood, J., Jabbari, K., Kuo, A., Maheswari, U., Martens, C., Maumus, F., Otillar, R. P., Rayko, E., Salamov, A., Vandepoele, K., Beszteri, B., Gruber, A., Heijde, M., Katinka, M., Mock, T., Valentin, K., Verret, F., Berges, J. A., Brownlee, C., Cadoret, J.-P., Chiovitti, A., Choi, C. J., Coesel, S., De Martino, A., Detter, J. C., Durkin, C., Falciatore, A., Fournet, J., Haruta, M., Huysman, M. J. J., Jenkins, B. D., Jiroutova, K., Jorgensen, R. E., Joubert, Y., Kaplan, A., Kroger, N., Kroth, P. G., La Roche, J., Lindquist, E., Lommer, M., Martin-Jezequel, V., Lopez, P. J., Lucas, S., Mangogna, M., McGinnis, K., Medlin, L. K., Montsant, A., Secq, M.-P. O.-L., Napoli, C., Obornik, M., Parker, M. S., Petit, J.-L., Porcel, B. M., Poulsen, N., Robison, M., Rychlewski, L., Rynearson, T. A., Schmutz, J., Shapiro, H., Siaut, M., Stanley, M., Sussman, M. R., Taylor, A. R., Vardi, A., von Dassow, P., Vyverman, W., Willis, A., Wyrwicz, L. S., Rokhsar, D. S., Weissenbach, J., Armbrust, E. V., Green, B. R., Van de Peer, Y. & Grigoriev, I. V. (2008) The Phaeodactylum genome reveals the evolutionary history of diatom genomes. *Nature,* **456** (7219)**,** 239-244.

Bradford, M. M. (1976) A rapid and sensitive method for the quantitation of microgram quantities of protein utilizing the principle of protein-dye binding. *Analytical Biochemistry,* **72** (1)**,** 248-254.

Brancaccio, M., D'Argenio, G., Lembo, V., Palumbo, A. & Castellano, I. (2018) Antifibrotic Effect of Marine Ovothiol in an *In Vivo* Model of Liver Fibrosis. *Oxidative Medicine and Cellular Longevity,* **2018,** 5045734.

Braunshausen, A. & Seebeck, F. P. (2011) Identification and Characterization of the First

Ovothiol Biosynthetic Enzyme. *Journal of the American Chemical Society,* **133** (6)**,** 1757-1759.

Breithaupt, T. & Hardege, J. D. (2012) Pheromones mediating sex and dominance in aquatic animals. *Chemical ecology in aquatic systems.* 1 ed., Oxford University Press.

Brenman, J. E., Chao, D. S., Xia, H., Aldape, K. & Bredt, D. S. (1995) Nitric oxide synthase complexed with dystrophin and absent from skeletal muscle sarcolemma in Duchenne muscular dystrophy. *Cell,* **82** (5)**,** 743-752.

Brown, M. R., Jeffrey, S. W., Volkman, J. K. & Dunstan, G. A. (1997) Nutritional properties of microalgae for mariculture. *Aquaculture,* **151** (1)**,** 315-331.

Brunet, C., Chandrasekaran, R., Barra, L., Giovagnetti, V., Corato, F. & Ruban, A. V. (2014) Spectral radiation dependent photoprotective mechanism in the diatom Pseudo-nitzschia multistriata. *PloS one,* **9** (1)**,** e87015.

Brunet, C. & Lavaud, J. (2010) Can the xanthophyll cycle help extract the essence of the microalgal functional response to a variable light environment? *Journal of Plankton Research,* **32** (12)**,** 1609-1617.

Bryan, N. S. & Grisham, M. B. (2007) Methods to Detect Nitric Oxide and its Metabolites in Biological Samples. *Free radical biology & medicine,* **43** (5)**,** 645-657.

Buckley, K. M. & Rast, J. P. (2017) An Organismal Model for Gene Regulatory Networks in the Gut-Associated Immune Response. *Frontiers in Immunology,* **8,** 1297.

Burgoyne, D. L., Miao, S., Pathirana, C., Andersen, R. J., Ayer, W. A., Singer, P. P., Kokke, W. C. M. C. & Ross, D. M. (1991) The structure and partial synthesis of imbricatine, a benzyltetrahydroisoquinoline alkaloid from the starfish Dermasterias imbricata. *Canadian Journal of Chemistry,* **69** (1)**,** 20-27.

Burke, R. D. (1981) Structure of the digestive tract of the pluteus larva of *Dendraster excentricus* (Echinodermata: Echinoida). *Zoomorphology,* **98** (3)**,** 209-225.

Burke, R. D. & Alvarez, C. M. (1988) Development of the esophageal muscles in embryos of the sea urchin *Strongylocentrotus purpuratus. Cell and Tissue Research,* **252** (2)**,** 411-417.

Castellano, I., Di Tomo, P., Di Pietro, N., Mandatori, D., Pipino, C., Formoso, G., Napolitano, A., Palumbo, A. & A., P. (2018) Anti-Inflammatory Activity of Marine Ovothiol A in an In Vitro Model of Endothelial Dysfunction Induced by Hyperglycemia. *Oxidative Medicine and Cellular Longevity,* **2018** (2087373)**,** 12.

Castellano, I., Ercolesi, E. & Palumbo, A. (2014) Nitric Oxide Affects ERK Signaling through Down-Regulation of MAP Kinase Phosphatase Levels during Larval Development of the Ascidian *Ciona intestinalis. PloS one,* **9** (7)**,** e102907.

Castellano, I., Ercolesi, E., Romano, G., Ianora, A. & Palumbo, A. (2015) The diatom-derived aldehyde decadienal affects life cycle transition in the ascidian *Ciona intestinalis* through nitric oxide/ERK signalling. *Open biology,* **5** (3)**,** 140182.

Castellano, I., Migliaccio, O., D'Aniello, S., Merlino, A., Napolitano, A. & Palumbo, A. (2016) Shedding light on ovothiol biosynthesis in marine metazoans. *Scientific reports,* **6,** 21506.

Castellano, I., Migliaccio, O., Ferraro, G., Maffioli, E., Marasco, D., Merlino, A., Zingone, A., Tedeschi, G. & Palumbo, A. (2018) Biotic and environmental stress induces nitration and changes in structure and function of the sea urchin major yolk protein toposome. *Scientific reports,* **8** (1)**,** 4610-4610.

Castellano, I. & Seebeck, F. P. (2018) On ovothiol biosynthesis and biological roles: from life in the ocean to therapeutic potential. *Natural Product Reports.*

Chandrasekaran, R., Barra, L., Carillo, S., Caruso, T., Corsaro, M. M., Dal Piaz, F., Graziani, G., Corato, F., Pepe, D., Manfredonia, A., Orefice, I., Ruban, A. V. & Brunet, C. (2014) Light modulation of biomass and macromolecular composition of the diatom *Skeletonema marinoi*. *Journal of Biotechnology,* **192,** 114-122.

Cho, K.-O., Hunt, C. A. & Kennedy, M. B. (1992) The rat brain postsynaptic density fraction contains a homolog of the drosophila discs-large tumor suppressor protein. *Neuron,* **9** (5)**,** 929-942.

Chung, C. C., Hwang, S. P. L. & Chang, J. (2008) Nitric Oxide as a Signaling Factor To Upregulate the Death-Specific Protein in a Marine Diatom, *Skeletonema costatum*, during Blockage of Electron Flow in Photosynthesis. *Applied and Environmental Microbiology,* **74** (21)**,** 6521-6527.

Coffman, J. A., Coluccio, A., Planchart, A. & Robertson, A. J. (2009) Oral–aboral axis specification in the sea urchin embryo: III. Role of mitochondrial redox signaling via H_2O_2: III. Role of mitochondrial redox signaling via HO. *Developmental Biology,* **330** (1)**,** 123-130.

Coffman, J. A. & Davidson, E. H. (2001) Oral–Aboral Axis Specification in the Sea Urchin Embryo: I. Axis Entrainment by Respiratory Asymmetry. *Developmental Biology,* **230** (1)**,** 18-28.

Coffman, J. A. & Denegre, J. M. (2007) Mitochondria, redox signaling and axis specification in metazoan embryos. *Developmental Biology,* **308** (2)**,** 266-280.

Coffman, J. A., Wessels, A., Deschiffart, C. & Rydlizky, K. (2014) Oral–aboral axis specification in the sea urchin embryo, IV: Hypoxia radializes embryos by preventing the initial spatialization of nodal activity. *Developmental Biology,* **386** (2)**,** 302-307.

Colasanti, M. & Venturini, G. (1998) Nitric oxide in invertebrates. *Molecular Neurobiology,* **17** (1)**,** 157-174.

Compton, J. C. (2011) *Diatoms: Ecology and Life Cycle.* Nova Science Publishers.

Correa-Aragunde, N., Foresi, N. & Lamattina, L. (2013) Structure diversity of nitric oxide synthases (NOS): the emergence of new forms in photosynthetic organisms. *Frontiers in Plant Science,* **4** (232).

Coutteau, P. & Sorgeloos, P. (1992) The use of algal substitutes and the requirement for live algae in the hatchery and nursery rearing of bivalve molluscs: an international survey. *Journal of Shellfish Research,* **11** (2)**,** 467-476.

Crane, B. R., Arvai, A. S., Ghosh, D. K., Wu, C., Getzoff, E. D., Stuehr, D. J. & Tainer, J. A. (1998) Structure of Nitric Oxide Synthase Oxygenase Dimer with Pterin and Substrate. *Science,* **279** (5359)**,** 2121-2126.

Crawford, N. M. & Guo, F.-Q. (2005) New insights into nitric oxide metabolism and regulatory functions. *Trends in Plant Science,* **10** (4)**,** 195-200.

Crosby, M. E. (2007) The cell cycle: principles of control. *The Yale Journal of Biology and Medicine,* **80** (3)**,** 141-142.

Daff, S., Sagami, I. & Shimizu, T. (1999) The 42-Amino Acid Insert in the FMN Domain of Neuronal Nitric-oxide Synthase Exerts Control over Ca2+/Calmodulin-dependent Electron Transfer. *Journal of Biological Chemistry,* **274** (43)**,** 30589-30595.

Dale, B. (2016) Achieving monospermy or preventing polyspermy? *Research and Reports in Biology,* **7,** 47-57.

Darwin, C. (1859) *On the Origin of Species by Means of Natural Selection.* Murray J, London.

Daunay, S., Lebel, R., Farescour, L., Yadan, J.-C. & Erdelmeier, I. (2016) Short protecting-group-free synthesis of 5-acetylsulfanyl-histidines in water: novel precursors of 5-sulfanyl-histidine and its analogues. *Organic & Biomolecular Chemistry,* **14** (44)**,** 10473-10480.

Davidson, E. H. (2006) The Sea Urchin Genome: Where Will It Lead Us? *Science,* **314** (5801)**,** 939-940.

Davidson, E. H., Hough-Evans, B. R. & Britten, R. J. (1982) Molecular biology of the sea urchin embryo. *Science,* **217** (4554)**,** 17.

Decker, G. L. & Lennarz, W. J. (1988) Skeletogenesis in the sea urchin embryo. *Development,* **103** (2)**,** 231-247.

Deits, T., Farrance, M., Kay, E. S., Medill, L., Turner, E. E., Weidman, P. J. & Shapiro, B. M. (1984) Purification and properties of ovoperoxidase, the enzyme responsible for hardening the fertilization membrane of the sea urchin egg. *Journal of Biological Chemistry,* **259** (21)**,** 13525-13533.

DeVeale, B., Brummel, T. & Seroude, L. (2004) Immunity and aging: the enemy within? *Aging Cell,* **3** (4)**,** 195-208.

Di Dato, V., Musacchia, F., Petrosino, G., Patil, S., Montresor, M., Sanges, R. & Ferrante, M. I. (2015) Transcriptome sequencing of three Pseudo-nitzschia species reveals comparable gene sets and the presence of Nitric Oxide Synthase genes in diatoms. *Scientific reports,* **5,** 12329.

Dolch, L. J. & Marechal, E. (2015) Inventory of fatty acid desaturases in the pennate diatom Phaeodactylum tricornutum. *Marine Drugs,* **13** (3)**,** 1317-1339.

Du, C., Anderson, A., Lortie, M., Parsons, R. & Bodnar, A. G. (2013) Oxidative damage and

cellular defense mechanisms in sea urchin models of aging. *Free Radical Biology and Medicine, 63,* 254-263.

Dubé, F. (1988) Effect of reduced protein synthesis on the cell cycle in sea urchin embryos. *Journal of Cellular Physiology,* **137** (3)**,** 545-552.

Dubinsky, Z. & Stambler, N. (2009) Photoacclimation processes in phytoplankton: mechanisms, consequences, and applications. *Aquatic Microbial Ecology,* **56** (2)**,** 163-176.

Epel, D. (1990) The initiation of development at fertilization. *Cell Differentiation* **29,** 1-12.

Epel, D. (2003) Protection of DNA during early development: adaptations and evolutionary consequences. *Evolution & Development, 5* (1)**,** 83-88.

Evans, T., Rosenthal, E. T., Youngblom, J., Distel, D. & Hunt, T. (1983) Cyclin: a protein specified by maternal mRNA in sea urchin eggs that is destroyed at each cleavage division. *Cell,* **33** (2)**,** 389-396.

Fairlamb, A. H. & A., C. (1992) Metabolism and Functions of Trypanothione in the Kinetoplastida. *Annual review of microbiology,* **46** (1)**,** 695-729.

Fairlamb, A. H., Blackburn, P., Ulrich, P., Chait, B. T. & Cerami, A. (1985) Trypanothione: a novel bis(glutathionyl)spermidine cofactor for glutathione reductase in trypanosomatids. *Science,* **227** (4693)**,** 1485-1487.

Falkowski, P. G. & Raven, J. A. (2007) *Aquatic Photosynthesis.* Princeton University Press.

Filosto, S., Roccheri, M. C., Bonaventura, R. & Matranga, V. (2008) Environmentally relevant cadmium concentrations affect development and induce apoptosis of *Paracentrotus lividus* larvae cultured in vitro. *Cell Biology and Toxicology,* **24** (6)**,** 603-610.

Foerder, C. A. & Shapiro, B. M. (1977) Release of ovoperoxidase from sea urchin eggs hardens the fertilization membrane with tyrosine crosslinks. *Proceedings of the National Academy of Sciences of the United States of America,* **74** (10)**,** 4214-4218.

Foo, S. A., Byrne, M., Ricevuto, E. & Gambi, C. (2018) The carbon dioxide vents of Ischia, Italy, a natural system to assess impacts of ocean acidification on marine ecosystems: An overview of research and comparisons with other vent systems. *Oceanography and Marine Biology: An Annual Review.*

Foresi, N., Correa-Aragunde, N., Parisi, G., Caló, G., Salerno, G. & Lamattina, L. (2010) Characterization of a Nitric Oxide Synthase from the Plant Kingdom: NO Generation from the Green Alga *Ostreococcus tauri* Is Light Irradiance and Growth Phase Dependent. *The Plant Cell.,* **22** (11)**,** 3816-3830.

Foyer, C. H. & Shigeoka, S. (2011) Understanding Oxidative Stress and Antioxidant Functions to Enhance Photosynthesis. *Plant Physiology,* **155** (1)**,** 93-100.

Friedrichs, L., Maier, M. & Hamm, C. (2012) A new method for exact three-dimensional reconstructions of diatom frustules. *Journal of Microscopy,* **248** (2)**,** 208-217.

Gallina, A. A., Brunet, C., Palumbo, A. & Casotti, R. (2014) The effect of polyunsaturated aldehydes on *Skeletonema marinoi* (Bacillariophyceae): the involvement of reactive oxygen species and nitric oxide. *Marine Drugs,* **12** (7)**,** 4165-4187.

Gechev, T. S., Van Breusegem, F., Stone, J. M., Denev, I. & Laloi, C. (2006) Reactive oxygen species as signals that modulate plant stress responses and programmed cell death. *BioEssays,* **28** (11)**,** 1091-1101.

Ghosh, D. K. & Salerno, J. C. (2003) Nitric oxide synthases: domain structure and alignment in enzyme function and control. *Frontiers in bioscience: a journal and virtual library,* **8,** d193-209.

Giudice, G., Sconzo, G. & Roccheri, M. C. (1999) Studies on heat shock proteins in sea urchin development. *Development, Growth & Differentiation,* **41** (4)**,** 375-380.

Godhe, A. (2017) *Skeletonema marinoi. University of Gothenburg, http://cemeb.science.gu.se/research/target-species-imago%20/skeletonema-marinoi.*

Godhe, A., Kremp, A. & Montresor, M. (2014) Genetic and Microscopic Evidence for Sexual Reproduction in the Centric Diatom *Skeletonema marinoi. Protist,* **165** (4)**,** 401-416.

Gomez, C. R., Boehmer, E. D. & Kovacs, E. J. (2005) The aging innate immune system. *Current Opinion in Immunology,* **17** (5)**,** 457-462.

Goncharenko, K. V., Vit, A., Blankenfeldt, W. & Seebeck, F. P. (2015) Structure of the Sulfoxide Synthase EgtB from the Ergothioneine Biosynthetic Pathway. *Angewandte Chemie International Edition,* **54** (9)**,** 2821-2824.

Gould, S. B., Waller, R. F. & McFadden, G. I. (2008) Plastid Evolution. *Annual Review of Plant Biology,* **59** (1)**,** 491-517.

Green, L. C., Wagner, D. A., Glogowski, J., Skipper, P. L., Wishnok, J. S. & Tannenbaum, S. R. (1982) Analysis of nitrate, nitrite, and [15N] nitrate in biological fluids. *Analytical Biochemistry,* **126** (1)**,** 131-138.

Griffith, O. W. & Stuehr, D. J. (1995) Nitric Oxide Synthases: Properties and Catalytic Mechanism. *Annual Review of Physiology,* **57** (1)**,** 707-734.

Griffiths, M. (1966) The carotenoids of the eggs and embryos of the sea urchin *Strongylocentrotus purpuratus. Developmental Biology,* **13** (2)**,** 296-309.

Griffiths, M. & Perrott, P. (1976) Seasonal changes in the carotenoids of sea urchin

Strongylocentrotus droebachiensis. Comparative biochemistry and physiology, **55,** 435-441.

Grouneva, I., Gollan, P. J., Kangasjärvi, S., Suorsa, M., Tikkanen, M. & Aro, E.-M. (2013) Phylogenetic viewpoints on regulation of light harvesting and electron transport in eukaryotic photosynthetic organisms. *Planta,* **237** (2)**,** 399-412.

Gruber, A. & Kroth, P. G. (2017) Intracellular metabolic pathway distribution in diatoms and tools for genome-enabled experimental diatom research. *Philosophical transactions of the Royal Society of London. Series B, Biological Sciences,* **372** (1728).

Grün, S., Lindermayr, C., Sell, S. & Durner, J. (2006) Nitric oxide and gene regulation in plants. *Journal of Experimental Botany,* **57** (3)**,** 507-516.

Guidetti, P., Fraschetti, S., Terlizzi, A. & Boero, F. (2003) Distribution patterns of sea urchins and barrens in shallow Mediterranean rocky reefs impacted by the illegal fishery of the rock-boring mollusc *Lithophaga lithophaga. Marine Biology,* **143,** 1135–1142.

Guillard, R. R. L. (1975) Culture of Phytoplankton for Feeding Marine Invertebrates. *Culture of Marine Invertebrate Animals.* Springer US.

Guo, F. Q., Okamoto, M. & Crawford, N. M. (2003) Identification of a plant nitric oxide synthase gene involved in hormonal signaling. *Science,* **302** (5642)**,** 100-103.

Gusarov, I., Starodubtseva, M., Wang, Z.-Q., McQuade, L., Lippard, S. J., Stuehr, D. J. & Nudler, E. (2008) Bacterial Nitric-oxide Synthases Operate without a Dedicated Redox Partner. *The Journal of biological chemistry,* **283** (19)**,** 13140-13147.

Hamdoun, A. M., Cherr, G. N., Roepke, T. A. & Epel, D. (2004) Activation of multidrug

efflux transporter activity at fertilization in sea urchin embryos (*Strongylocentrotus purpuratus*). *Developmental Biology,* **276,** 452-462.

Hammer, O., Harper, D. A. T. & Ryan, P. D. (2001) PAST: Paleontological Statistics Software Package for Education and Data Analysis. *Palaeontologia Electronica,* **4** (1)**,** 1-9.

Hand, C. E. & Honek, J. F. (2005) Biological chemistry of naturally occurring thiols of microbial and marine origin. *Journal of natural products,* **68** (2)**,** 293-308.

Havens, C. G., Ho, A., Yoshioka, N. & Dowdy, S. F. (2006) Regulation of Late G(1)/S Phase Transition and APC(Cdh1) by Reactive Oxygen Species. *Molecular and Cellular Biology,* **26** (12)**,** 4701-4711.

Heinecke, J. W. & Shapiro, B. M. (1990) Superoxide peroxidase activity of ovoperoxidase, the crosslinking enzyme of fertilization. *Journal of Biological Chemistry,* **265** (9241-9246).

Heyland, A. & Hodin, J. (2014) A detailed staging scheme for late larval development in *Strongylocentrotus purpuratus* focused on readily-visible juvenile structures within the rudiment. *BMC Developmental Biology,* **14** (22).

Higdon, A., Diers, A. R., Oh, J. Y., Landar, A. & Darley-Usmar, V. M. (2012) Cell signalling by reactive lipid species: new concepts and molecular mechanisms. *Biochemical Journal,* **442** (Pt 3)**,** 453-464.

Hinman, V. F. & Burke, R. D. (2018) Embryonic neurogenesis in echinoderms. *Wiley Interdisciplinary Reviews: Developmental Biology,* **7** (4)**,** e316.

Ho, C. H. E., Buckley, K. M., Schrankel, C. S., Schuh, N. W., Hibino, T., Solek, C. M., Bae, K., Wang, G. & Rast, J. P. (2016) Perturbation of gut bacteria induces a coordinated

cellular immune response in the purple sea urchin larva. *Immunology and Cell Biology,* **94** (9)**,** 861-874.

Holler, T. P. & Hopkins, P. B. (1988) Ovothiols as biological antioxidants. The thiol groups of ovothiol and glutathione are chemically distinct. *Journal of the American Chemical Society,* **110** (14)**,** 4837-4838.

Holler, T. P. & Hopkins, P. B. (1990) Ovothiols as free-radical scavengers and the mechanism of ovothiol-promoted NAD(P)H-O$_2$ oxidoreductase activity. *Biochemistry,* **29** (7)**,** 1953-1961.

Holler, T. P., Ruan, F., Spaltenstein, A. & Hopkins, P. B. (1989) Total synthesis of marine mercaptohistidines: ovothiols A, B, and C. *The Journal of Organic Chemistry,* **54** (19)**,** 4570-4575.

Huesgen, P. F., Alami, M., Lange, P. F., Foster, L. J., Schröder, W. P., Overall, C. M. & Green, B. R. (2013) Proteomic Amino-Termini Profiling Reveals Targeting Information for Protein Import into Complex Plastids. *PloS one,* **8** (9)**,** e74483.

Huysman, M. J. J., Martens, C., Vandepoele, K., Gillard, J., Rayko, E., Heijde, M., Bowler, C., Inzé, D., Van De Peer, Y., De Veylder, L. & Vyverman, W. (2010) Genome-wide analysis of the diatom cell cycle unveils a novel type of cyclins involved in environmental signaling. *Genome Biology,* **11** (2)**,** R17.

Ikonomidou, C., Bittigau, P., Koch, C., Genz, K., Hoerster, F., Felderhoff-Mueser, U., Tenkova, T., Dikranian, K. & Olney, J. W. (2001) Neurotransmitters and apoptosis in the developing brain. *Biochemical Pharmacology,* **62** (4)**,** 401-405.

Ito, S., Nardi, G., Palumbo, A. & Prota, G. (1979a) Isolation and characterization of adenochrome, a unique iron(III)-binding peptide from *Octopus vulgaris*. *Journal of the Chemical Society, Perkin Transactions 1,* **0,** 2617-2623.

Ito, S., Nardi, G., Palumbo, A. & Prota, G. (1979b) A possible pathway for the biosynthesis of adenochromines. *Experientia,* **35** (1)**,** 14-15.

Jacob, C. (2006) A scent of therapy: pharmacological implications of natural products containing redox-active sulfur atoms. *Natural Product Reports,* **23** (6)**,** 851-863.

Jasid, S., Simontacchi, M., Bartoli, C. G. & Puntarulo, S. (2006) Chloroplasts as a Nitric Oxide Cellular Source. Effect of Reactive Nitrogen Species on Chloroplastic Lipids and Proteins. *Plant Physiology,* **142** (3)**,** 1246-1255.

Jaubert, M., Bouly, J.-P., Ribera d'Alcalà, M. & Falciatore, A. (2017) Light sensing and responses in marine microalgae. *Current Opinion in Plant Biology,* **37,** 70-77.

Jones, D. T., Taylor, W. R. & Thornton, J. M. (1992) The rapid generation of mutation data matrices from protein sequences. *Bioinformatics,* **8** (3)**,** 275-282.

Juliano, C. E., Swartz, S. Z. & Wessel, G. M. (2010) A conserved germline multipotency program. *Development,* **137** (24)**,** 4113-4126.

Kirk, J. T. O. (1977) Thermal dissociation of fucoxanthin-protein binding in pigment complexes from chloroplasts of Hormosira (phaeophyta). *Plant Science Letters,* **9** (4)**,** 373-380.

Kooistra, W. H. (2008) The Evolution of the Diatoms. *Handbook of Biomineralization: Biological Aspects and Structure Formation.*

Kooistra, W. H., Gersonde, R., Medlin, L. K. & Mann, D. G. (2007) The Origin and Evolution of the Diatoms: Their Adaptation to a Planktonic Existence. In Falkowski, P. G. & Knoll, A. H. (Eds.) *Evolution of Primary Producers in the Sea.* Burlington, Academic Press.

Kooistra, W. H., Sarno, D., Balzano, S., Gu, H., Andersen, R. A. & Zingone, A. (2008)

Global Diversity and Biogeography of Skeletonema Species (Bacillariophyta). *Protist,* **159** (2)**,** 177-193.

Kooistra, W. H. C. F., Gersonde, R., Medlin, L. K. & Mann, D. G. (2007) CHAPTER 11 - The Origin and Evolution of the Diatoms: Their Adaptation to a Planktonic Existence. In Falkowski, P. G. & Knoll, A. H. (Eds.) *Evolution of Primary Producers in the Sea.* Burlington, Academic Press.

Kourtchenko, O., Rajala, T. & Godhe, A. (2018) Growth of a common planktonic diatom quantified using solid medium culturing. *Scientifc Reports,* **8,** 9757.

Krauth-Siegel, R. L. & Leroux, A. E. (2012) Low-molecular-mass antioxidants in parasites. *Antioxidants & Redox Signaling,* **17,** 583-607.

Kroth, P. G. (2002) Protein transport into secondary plastids and the evolution of primary and secondary plastids. *International Review of Cytology.* Academic Press.

Kumar, A., Castellano, I., Patti, F. P., Palumbo, A. & Buia, M. C. (2015) Nitric oxide in marine photosynthetic organisms. *Nitric oxide: biology and chemistry,* **47,** 34-39.

Kumar, S., Stecher, G. & Tamura, K. (2016) MEGA7: Molecular Evolutionary Genetics Analysis Version 7.0 for Bigger Datasets. *Molecular Biology and Evolution,* **33** (7)**,** 1870-1874.

Kyte, J. & Doolittle, R. F. (1982) A simple method for displaying the hydropathic character of a protein. *Journal of Molecular Biology,* **157** (1)**,** 105-132.

Lamas, S., Marsden, P. A., Li, G. K., Tempst, P. & Michel, T. (1992) Endothelial nitric oxide synthase: molecular cloning and characterization of a distinct constitutive enzyme isoform. *Proceedings of the National Academy of Sciences of the United States of America,* **89** (14)**,** 6348-6352.

Larkum, A. W. D. & Vesk, M. (2003) Algal Plastids: Their Fine Structure and Properties. *Photosynthesis in Algae.* Springer Netherlands.

Lavaud, J. (2007) Fast Regulation of Photosynthesis in Diatoms: Mechanisms, Evolution and Ecophysiology. *Functional Plant Science and Biotechonology,* **1,** 267-287.

Lawrence, J. M. (2001) *Edible Sea Urchins: Biology and Ecology.* Elsevier Science, Amsterdam.

Lepetit, B., Volke, D., Szabó, M., Hoffmann, R., Garab, G., Wilhelm, C. & Goss, R. (2007) Spectroscopic and Molecular Characterization of the Oligomeric Antenna of the Diatom *Phaeodactylum tricornutum. Biochemistry,* **46** (34)**,** 9813-9822.

Lesser, M. P., Kruse, V. A. & Barry, T. M. (2003) Exposure to ultraviolet radiation causes apoptosis in developing sea urchin embryos. *The Journal of Experimental Biology,* **206** (Pt 22)**,** 4097-4103.

Lesser, M. P., Kruse, V. A. & Barry, T. M. (2003) Exposure to ultraviolet radiation causes apoptosis in developing sea urchin embryos. *Journal of Experimental Biology,* **206** (22)**,** 4097-4103.

Li, H. & Poulos, T. L. (2005) Structure–function studies on nitric oxide synthases. *Journal of Inorganic Biochemistry,* **99** (1)**,** 293-305.

Li, H. Y., Lu, Y., Zheng, J. W., Yang, W. D. & Liu, J. S. (2014) Biochemical and genetic engineering of diatoms for polyunsaturated fatty acid biosynthesis. *Marine Drugs,* **12** (1)**,** 153-166.

Li, P., Liu, C. Y., Liu, H., Zhang, Q. & Wang, L. (2013) Protective function of nitric oxide on marine phytoplankton under abiotic stresses. *Nitric oxide: biology and chemistry,* **33,** 88-96.

Liao, C. & Seebeck, F. P. (2017) Convergent Evolution of Ergothioneine Biosynthesis in Cyanobacteria. *Chembiochem: a European journal of chemical biology,* **18** (21)**,** 2115-2118.

Liao, I. C., Su, H. M. & Lin, J. H. (1983) Larval foods for Penaeid prawns. *Crustacean Aquaculture,* **1,** 43-68.

Liu, J., García-Cardeña, G. & Sessa, W. C. (1995) Biosynthesis and palmitoylation of endothelial nitric oxide synthase: mutagenesis of palmitoylation sites, cysteines-15 and/or -26, argues against depalmitoylation-induced translocation of the enzyme. *Biochemistry,* **34** (38)**,** 12333-12340.

Liu, J., Hughes, T. E. & Sessa, W. C. (1997) The First 35 Amino Acids and Fatty Acylation Sites Determine the Molecular Targeting of Endothelial Nitric Oxide Synthase into the Golgi Region of Cells: A Green Fluorescent Protein Study. *The Journal of Cell Biology,* **137** (7)**,** 1525-1535.

Lohr, M. & Wilhelm, C. (1999) Algae displaying the diadinoxanthin cycle also possess the violaxanthin cycle. *Proceedings of the National Academy of Sciences,* **96** (15)**,** 8784-8789.

LoPachin, R. M., Gavin, T., Geohagen, B. C. & Das, S. (2007) Neurotoxic Mechanisms of Electrophilic Type-2 Alkenes: Soft–Soft Interactions Described by Quantum Mechanical Parameters. *Toxicological Sciences,* **98** (2)**,** 561-570.

Losic, D., Mitchell, J. G. & Voelcker, N. H. (2009) Diatomaceous Lessons in Nanotechnology and Advanced Materials. *Advanced Materials,* **21** (29)**,** 2947-2958.

Lozy, F. & Karantza, V. (2012) Autophagy and cancer cell metabolism. *Seminars in cell & developmental biology,* **23** (4)**,** 395-401.

Marjanovic, B., Simic, M. G. & Jovanovic, S. V. (1995) Heterocyclic thiols as antioxidants: Why Ovothiol C is a better antioxidant than ergothioneine. *Free Radical Biology and Medicine,* **18** (4)**,** 679-685.

Martin, S., Richier, S., Pedrotti, M.-L., Dupont, S., Castejon, C., Gerakis, Y., Kerros, M.-E., Oberhänsli, F., Teyssié, J.-L., Jeffree, R. & Gattuso, J.-P. (2011) Early development and molecular plasticity in the Mediterranean sea urchin *Paracentrotus lividus* exposed to CO_2 driven acidification. *The Journal of Experimental Biology,* **214** (8)**,** 1357-1368.

Mashabela, G. T. M. & Seebeck, F. P. (2013) Substrate specificity of an oxygen dependent sulfoxide synthase in ovothiol biosynthesis. *Chemical Communications,* **49** (70)**,** 7714-7716.

Matsuda, Y., Nakajima, K. & Tachibana, M. (2011) Recent progresses on the genetic basis of the regulation of CO2 acquisition systems in response to CO2 concentration. *Photosynthesis Research,* **109** (1)**,** 191-203.

McClay, D. R. (2011) Evolutionary crossroads in developmental biology: sea urchins. *Development,* **138** (13)**,** 2639-2648.

McQuoid, M. R., Godhe, A. & Nordberg, K. (2002) Viability of phytoplankton resting stages in the sediments of a coastal Swedish fjord. *European Journal of Phycology,* **37** (2)**,** 191-201.

Migliaccio, O., Castellano, I., Cirino, P., Romano, G. & Palumbo, A. (2015) Maternal Exposure to Cadmium and Manganese Impairs Reproduction and Progeny Fitness in the Sea Urchin *Paracentrotus lividus*. *PloS one,* **10** (6)**,** e0131815.

Migliaccio, O., Castellano, I., Di Cioccio, D., Tedeschi, G., Negri, A., Cirino, P., Romano, G., Zingone, A. & Palumbo, A. (2016) Subtle reproductive impairment through nitric

oxide-mediated mechanisms in sea urchins from an area affected by harmful algal blooms. *Scientific reports,* **6,** 26086.

Migliaccio, O., Castellano, I., Romano, G. & Palumbo, A. (2014) Stress response to cadmium and manganese in *Paracentrotus lividus* developing embryos is mediated by nitric oxide. *Aquatic Toxicology,* **156,** 125-134.

Millott, N. (1975) The Photosensitivity of Echinoids. In Russell, F. & Yonge, M. (Eds.) *Advances in Marine Biology.* New York, Academic Press.

Miralto, A., Barone, G., Romano, G., Poulet, S. A., Ianora, A., Russo, G. L., Buttino, I., Mazzarella, G., Laabir, M., Cabrini, M. & Giacobbe, M. G. (1999) The insidious effect of diatoms on copepod reproduction. *Nature,* **402,** 173-176.

Mirzahosseini, A., Hosztafi, S., Tóth, G. & Noszál, B. (2014) A cost-effective synthesis of enantiopure ovothiol A from L-histidine, its natural precursor. *Arkivoc,* **2014** (6)**,** 1-9.

Mirzahosseini, A., Orgován, G., Hosztafi, S. & Noszál, B. (2014) The complete microspeciation of ovothiol A, the smallest octafarious antioxidant biomolecule. *Analytical and Bioanalytical Chemistry,* **406** (9)**,** 2377-2387.

Montsant, A., Allen, A. E., Coesel, S., Martino, A. D., Falciatore, A., Mangogna, M., Siaut, M., Heijde, M., Jabbari, K., Maheswari, U., Rayko, E., Vardi, A., Apt, K. E., Berges, J. A., Chiovitti, A., Davis, A. K., Thamatrakoln, K., Hadi, M. Z., Lane, T. W., Lippmeier, J. C., Martinez, D., Parker, M. S., Pazour, G. J., Saito, M. A., Rokhsar, D. S., Armbrust, E. V. & Bowler, C. (2007) Identification and comparative genomic analysis of signaling and regulatory components in the diatom *Thalassiosira pseudonana. Journal of Phycology,* **43** (3)**,** 585-604.

Mopper, K. & Kieber, D. J. (2000) Marine photochemistry and its impact on carbon cycling.

The Effects of UV Radiation in the Marine Environment. Cambridge University Press.

Moreau, M., Lee, G. I., Wang, Y., Crane, B. R. & Klessig, D. F. (2008) AtNOS/AtNOA1 is a functional Arabidopsis thaliana cGTPase and not a nitric-oxide synthase. *The Journal of biological chemistry,* **283** (47)**,** 32957-32967.

Müller, P., Li, X.-P. & Niyogi, K. K. (2001) Non-Photochemical Quenching. A Response to Excess Light Energy. *Plant Physiology,* **125** (4)**,** 1558-1566.

Murata, N., Takahashi, S., Nishiyama, Y. & Allakhverdiev, S. I. (2007) Photoinhibition of photosystem II under environmental stress. *Biochimica et Biophysica Acta (BBA) - Bioenergetics,* **1767** (6)**,** 414-421.

Murray, H. W. & Nathan, C. F. (1999) Macrophage Microbicidal Mechanisms In Vivo: Reactive Nitrogen versus Oxygen Intermediates in the Killing of Intracellular Visceral Leishmania donovani. *The Journal of Experimental Medicine,* **189** (4)**,** 741-746.

Nagy, P. (2013) Kinetics and Mechanisms of Thiol–Disulfide Exchange Covering Direct Substitution and Thiol Oxidation-Mediated Pathways. *Antioxidants & Redox Signaling,* **18** (13)**,** 1623-1641.

Naowarojna, N., Huang, P., Cai, Y., Song, H., Wu, L., Cheng, R., Li, Y., Wang, S., Lyu, H., Zhang, L., Zhou, J. & Liu, P. (2018) In Vitro Reconstitution of the Remaining Steps in Ovothiol A Biosynthesis: C–S Lyase and Methyltransferase Reactions. *Organic letters,* **20** (17)**,** 5427-5430.

Nardi, G. & Cipollaro, M. (1988) 1-Methyl-4-thiohistidine and Glutathione in the Developing Embryo of the Sea Urchin, *Paracentrotus lividus*. *Development, Growth & Differentiation,* **30** (4)**,** 383-389.

Neill, S. J., Desikan, R. & Hancock, J. T. (2003) Nitric Oxide Signalling in Plants. *The New Phytologist,* **159** (1)**,** 11-35.

Nelson, D. M., Treguer, P., Brzezinski, M. A., Leynaert, A. & Queguiner, B. (1995) Production and dissolution of biogenic silica in the ocean: Revised global estimates, comparison with regional data and relationship to biogenic sedimentation. *Global Biogeochemical Cycles,* **9** (3)**,** 359-372.

Newton, G. L., Arnold, K., Price, M. S., Sherrill, C., Delcardayre, S. B., Aharonowitz, Y., Cohen, G., Davies, J., Fahey, R. C. & Davis, C. (1996) Distribution of thiols in microorganisms: mycothiol is a major thiol in most actinomycetes. *Journal of bacteriology,* **178** (7)**,** 1990-1995.

Nichols, D. (1972) The water-vascular system in living and fossil echinoderms. *Paleontology,* **15,** 519–538.

Nymark, M., Valle, K. C., Hancke, K., Winge, P., Andresen, K., Johnsen, G., Bones, A. M. & Brembu, T. (2013) Molecular and Photosynthetic Responses to Prolonged Darkness and Subsequent Acclimation to Re-Illumination in the Diatom *Phaeodactylum tricornutum. PloS one,* **8** (3)**,** e58722.

Okazaki, K. (1975) Spicule Formation by Isolated Micromeres of the Sea-Urchin Embryo. *American Zoologist,* **15** (3)**,** 567-581.

Olney, J. W. (2002) New Insights and New Issues in Developmental Neurotoxicology. *NeuroToxicology,* **23** (6)**,** 659-668.

O'Neill, E. C., Trick, M., Hill, L., Rejzek, M., Dusi, R. G., Hamilton, C. J., Zimba, P. V., Henrissat, B. & Field, R. A. (2015) The transcriptome of *Euglena gracilis* reveals unexpected metabolic capabilities for carbohydrate and natural product biochemistry. *Molecular BioSystems,* **11** (10)**,** 2808-2820.

Orefice, I., Chandrasekaran, R., Smerilli, A., Corato, F., Caruso, T., Casillo, A., Corsaro, M. M., Dal Piaz, F., Ruban, A. V. & Brunet, C. (2016) Light-induced changes in the photosynthetic physiology and biochemistry in the diatom *Skeletonema marinoi*. *Algal Research,* **17,** 1-13.

Orefice, I., Musella, M., Smerilli, A., Sansone, C., Chandrasekaran, R., Corato, F. & Brunet, C. (2019) Role of nutrient concentrations and water movement on diatom's productivity in culture. *Scientific reports,* **9** (1)**,** 1479.

Palumbo, A. (2005) Nitric oxide in marine invertebrates: A comparative perspective. *Comparative Biochemistry and Physiology Part A: Molecular & Integrative Physiology,* **142** (2)**,** 241-248.

Palumbo, A., Castellano, I. & Napolitano, A. (2018) Ovothiol: a potent natural antioxidant from marine organisms. *Blue Biotechnology. Production and Use of Marine Molecules. Part 2: Marine Molecules for Disease Treatment/Prevention and for Biological Research.* La Barre and S. S. Bates, Eds. ed., Wiley VCH, Weinheim, Germany.

Palumbo, A., D'Ischia, M., Misuraca, G. & Prota, G. (1982) Isolation and structure of a new sulphur-containing aminoacid from sea urchin eggs. *Tetrahedron Letters,* **23** (31)**,** 3207-3208.

Palumbo, A., Misuraca, G., D'Ischia, M., Donaudy, F. & Prota, G. (1984) Isolation and distribution of 1-methyl-5-thiol-l-histidine disulphide and a related metabolite in eggs from echinoderms. *Comparative Biochemistry and Physiology Part B: Comparative Biochemistry,* **78** (1)**,** 81-83.

Parker, M. S., Mock, T. & Armbrust, E. V. (2008) Genomic Insights into Marine Microalgae. *Annual Review of Genetics,* **42** (1)**,** 619-645.

Parks, A. L., Parr, B. A., Chin, J. E., Leaf, D. S. & Raff, R. A. (1988) Molecular Analysis of Heterochronic Changes in the Evolution of Direct Developing Sea-Urchins. *Journal of Evolutionary Biology,* **1,** 27-44.

Pathirana, C. & Andersen, R. J. (1986) Imbricatine, an unusual benzyltetrahydroisoquinoline alkaloid isolated from the starfish *Dermasterias imbricata. Journal of the American Chemical Society,* **108** (26)**,** 8288-8289.

Patron, N. J. & Waller, R. F. (2007) Transit peptide diversity and divergence: A global analysis of plastid targeting signals. *BioEssays,* **29** (10)**,** 1048-1058.

Pearse, J. & Cameron, R. (1991) Echinodermata: Echinoidea. *Reproduction of Marine Invertebrate.*

Pennington, J. T. & Strathmann, R. R. (1990) Consequences of the Calcite Skeletons of Planktonic Echinoderm Larvae for Orientation, Swimming, and Shape. *The Biological Bulletin,* **179** (1)**,** 121-133.

Pfaffl, M. W., Horgan, G. W. & Dempfle, L. (2002) Relative expression software tool (REST©) for group-wise comparison and statistical analysis of relative expression results in real-time PCR. *Nucleic Acids Research,* **30** (9)**,** e36-e36.

Pfaffl, M. W., Tichopad, A., Prgomet, C. & Neuvians, T. P. (2004) Determination of stable housekeeping genes, differentially regulated target genes and sample integrity: BestKeeper – Excel-based tool using pair-wise correlations. *Biotechnology Letters,* **26** (6)**,** 509-515.

Pinsino, A., Matranga, V., Trinchella, F. & Roccheri, M. C. (2010) Sea urchin embryos as an in vivo model for the assessment of manganese toxicity: developmental and stress response effects. *Ecotoxicology,* **19** (3)**,** 555-562.

Pyszniak, A. M. & Gibbs, S. P. (1992) Immunocytochemical localization of photosystem I and the fucoxanthin-chlorophylla/c light-harvesting complex in the diatom *Phaeodactylum tricornutum*. *Protoplasma,* **166** (3)**,** 208-217.

Ragni, R., Cicco, S., Vona, D., Leone, G. & Farinola, G. M. (2016) Biosilica from diatoms microalgae: smart materials from bio-medicine to photonics. *Journal of Materials Research,* **32** (2)**,** 279-291.

Raven, P. H. (1970) A Multiple Origin for Plastids and Mitochondria. *Science,* **169** (3946)**,** 641-646.

Raz, S., Hamilton, P. C., Wilt, F. H., Weiner, S. & Addadi, L. (2003) The Transient Phase of Amorphous Calcium Carbonate in Sea Urchin Larval Spicules: The Involvement of Proteins and Magnesium Ions in Its Formation and Stabilization. *Advanced Functional Materials,* **13** (6)**,** 480-486.

Reece, J. B., Urry, L. A., Cain, M. L., Wasserman, S. A., Minorsky, P. A. & Jackson, R. B. (2013) Animal Development. *Campbel Biology.* 10 ed., Pearson.

Reinfelder, J. R. (2011) Carbon Concentrating Mechanisms in Eukaryotic Marine Phytoplankton. *Annual Review of Marine Science,* **3** (1)**,** 291-315.

Rhee, S. G., Yang, K.-S., Kang, S. W., Woo, H. A. & Chang, T.-S. (2005) Controlled Elimination of Intracellular H_2O_2: Regulation of Peroxiredoxin, Catalase, and Glutathione Peroxidase via Post-translational Modification. *Antioxidants & Redox Signaling,* **7** (5-6)**,** 619-626.

Rivero, A. (2006) Nitric oxide: an antiparasitic molecule of invertebrates. *Trends in Parasitology,* **22** (5)**,** 219-225.

Rizzo, F., Coffman, J. A. & Arnone, M. I. (2016) An Elk transcription factor is required for

Runx-dependent survival signaling in the sea urchin embryo. *Developmental Biology,* **416** (1)**,** 173-186.

Rohl, I., Schneider, B., Schmidt, B. & Zeeck, E. (1999) L-ovothiol A: the egg release pheromone of the marine polychaete *Platynereis Dumerilii:* Anellida: Polychaeta. *Zeitschrift für Naturforschung C,* **54c,** 1145–1147.

Romano, G., Costantini, M., Buttino, I., Ianora, A. & Palumbo, A. (2011) Nitric Oxide Mediates the Stress Response Induced by Diatom Aldehydes in the Sea Urchin *Paracentrotus lividus*. *PloS one,* **6** (10)**,** e25980.

Romano, G., Costantini, M., Buttino, I., Ianora, A. & Palumbo, A. (2011) Nitric oxide mediates the stress response induced by diatom aldehydes in the sea urchin *Paracentrotus lividus*. *PloS one,* **6** (10)**,** e25980-e25980.

Rossi, F., Nardi, G., Palumbo, A. & Prota, G. (1985) 5-thiolhistidine, a new amino acid from eggs of *Octopus vulgaris. Comparative Biochemistry and Physiology Part B: Comparative Biochemistry,* **80** (4)**,** 843-845.

Roth, M. S. (2014) The engine of the reef: photobiology of the coral–algal symbiosis. *Frontiers in Microbiology,* **5,** 422.

Round, F. E., Crawford, R. M. & Mann, D. G. (1990) *The Diatoms. Biology and Morphology of the Genera*. Cambridge University Press.

Ruppert, E. E., Fox, R. & Barnes, R. D. (2004) *Invertebrate Zoology: A Functional Evolutionary Approach.* Thomson-Brooks/Cole, United States.

Russo, G. L., Russo, M., Castellano, I., Napolitano, A. & Palumbo, A. (2014) Ovothiol isolated from sea urchin oocytes induces autophagy in the Hep-G2 cell line. *Marine Drugs,* **12** (7)**,** 4069-4085.

Saitou, N. & Nei, M. (1987) The neighbor-joining method: a new method for reconstructing phylogenetic trees. *Molecular Biology and Evolution,* **4** (4)**,** 406-425.

Sakai, H. (1962) Studies on Sulfhydryl Groups during Cell Division of Sea Urchin Egg: V. Change in contractility of the thread model in relation to cell division. *The Journal of General Physiology,* **45** (3)**,** 427-438.

Sala, E., Ribes, M., Hereu, B., Zabala, M., Alva, V., Coma, R. & J., G. (1998) Temporal variability in abundance of the sea urchins *Paracentrotus lividus* and *Arbacia lixula* in the northwestern Mediterranean: comparison between a marine reserve and an unprotected area. *Marine Ecology Progress Series,* **168,** 135–145.

Salerno, J. C., Harris, D. E., Irizarry, K., Patel, B., Morales, A. J., Smith, S. M. E., Martasek, P., Roman, L. J., Masters, B. S. S., Jones, C. L., Weissman, B. A., Lane, P., Liu, Q. & Gross, S. S. (1997) An Autoinhibitory Control Element Defines Calcium-regulated Isoforms of Nitric Oxide Synthase. *Journal of Biological Chemistry,* **272** (47)**,** 29769-29777.

Santella, L., Limatola, N. & Chun, J. T. (2015) Calcium and actin in the saga of awakening oocytes. *Biochemical and biophysical research communications,* **460** (1)**,** 104-113.

Saravanan, V. & Godhe, A. (2010) Genetic heterogeneity and physiological variation among seasonally separated clones of *Skeletonema marinoi* (Bacillariophyceae) in the Gullmar Fjord, Sweden. *European Journal of Phycology,* **45** (2)**,** 177-190.

Sarno, D., Kooistra, W. H., Medlin, L. K., Percopo, I. & Zingone, A. (2005) Diversity in the genus skeletonema (bacillariophyceae). II. An assessment of the taxonomy of *S. Costatum*-like species with the description of four new species *Journal of Phycology,* **41** (1)**,** 151-176.

Schomer, B. & Epel, D. (1998) Redox Changes during Fertilization and Maturation of

Marine Invertebrate Eggs. *Developmental Biology,* **203** (1)**,** 1-11.

Schreiber, V., Dersch, J., Puzik, K., Bäcker, O., Liu, X., Stork, S., Schulz, J., Heimerl, T., Klingl, A., Zauner, S. & Maier, U. G. (2017) The Central Vacuole of the Diatom *Phaeodactylum tricornutum*: Identification of New Vacuolar Membrane Proteins and of a Functional Di-leucine-based Targeting Motif. *Protist,* **168** (3)**,** 271-282.

Seebeck, F. P. (2010) In Vitro Reconstitution of Mycobacterial Ergothioneine Biosynthesis. *Journal of the American Chemical Society,* **132** (19)**,** 6632-6633.

Seebeck, F. P. (2013) Thiohistidine Biosynthesis. *CHIMIA International Journal for Chemistry,* **67** (5)**,** 333-336.

Selman-Reimer, S., Duhe, R. J., Stockman, B. J. & Selman, B. R. (1991) L-1-N-methyl-4-mercaptohistidine disulfide, a potential endogenous regulator in the redox control of chloroplast coupling factor 1 in Dunaliella. *Journal of Biological Chemistry,* **266** (1)**,** 182-188.

Sessa, W. C., Harrison, J. K., Barber, C. M., Zeng, D., Durieux, M. E., D'Angelo, D. D., Lynch, K. R. & Peach, M. J. (1992) Molecular cloning and expression of a cDNA encoding endothelial cell nitric oxide synthase. *Journal of Biological Chemistry,* **267** (22)**,** 15274-15276.

Shapiro, B. M. & Hopkins, P. B. (1991) Ovothiols-biological and chemical perspectives. *Advances in Enzymology and Related Areas of Molecular Biology,* **64,** 291-316.

Shapiro, B. M. & Turner, E. (1988) Oxidative stress and the role of novel thiol compounds at fertilization. *Biofactors,* **1,** 85-88.

Shapiro, B. M., Turner, E. E., Hopkins, P. B., Klevit, R. E., Holler, T. P. & Spaltenstein, A. (1990) Antioxidant thiohistidine compounds.

Siefert, J. C., Clowdus, E. A. & Sansam, C. L. (2015) Cell cycle control in the early embryonic development of aquatic animal species. *Comparative Biochemistry and Physiology Part C: Toxicology & Pharmacology,* **178,** 8-15.

Sly, B. J., Hazel, J. C., Popodi, E. M. & Raff, R. A. (2002) Patterns of gene expression in the developing adult sea urchin central nervous system reveal multiple domains and deep-seated neural pentamery. *Evolution & Development,* **4** (3)**,** 189-204.

Smerilli, A., Orefice, I., Corato, F., Gavalas Olea, A., Ruban, A. V. & Brunet, C. (2017) Photoprotective and antioxidant responses to light spectrum and intensity variations in the coastal diatom *Skeletonema marinoi. Environmental microbiology,* **19** (2)**,** 611-627.

Smetacek, V. (1999) Diatoms and the Ocean Carbon Cycle. *Protist,* **150** (1)**,** 25-32.

Smith, A. B. & Kroh, A. (2013) Chapter 1 - Phylogeny of Sea Urchins. *Developments in Aquaculture and Fisheries Science.* Elsevier.

Smith, V. J. (1981) Invertebrate blood cells. *The Echinoderms.* Academic Press, New York.

Sodergren, E., Weinstock, G. M., Davidson, E. H., Cameron, R. A., Gibbs, R. A., Angerer, R. C., Angerer, L. M., Arnone, M. I., Burgess, D. R., Burke, R. D., Coffman, J. A., Dean, M. & Elphick, M. R. E., Charles A ; Foltz, Kathy R ; Hamdoun, Amro ; Hynes, Richard O ; Klein, William H ; Marzluff, William ; Mcclay, David R ; Morris, Robert L ; Mushegian, Arcady ; Rast, Jonathan P ; Smith, L Courtney ; Thorndyke, Michael C ; Vacquier, Victor D ; Wessel, Gary M ; Wray, Greg ; Zhang, Lan ; Elsik, Christine G ; Ermolaeva, Olga ; Hlavina, Wratko ; Hofmann, Gretchen ; Kitts, Paul ; Landrum, Melissa J ; Mackey, Aaron J ; Maglott, Donna ; Panopoulou, Georgia ; Poustka, Albert J ; Pruitt, Kim ; Sapojnikov, Victor ; Song, Xingzhi ; Souvorov, Alexandre ; Solovyev, Victor ; Wei, Zheng ; Whittaker, Charles A ; Worley, Kim ; Durbin, K

James ; Shen, Yufeng ; Fedrigo, Olivier ; Garfield, David ; Haygood, Ralph ; Primus, Alexander ; Satija, Rahul ; Severson, Tonya ; Gonzalez-Garay, Manuel L ; Jackson, Andrew R ; Milosavljevic, Aleksandar ; Tong, Mark ; Killian, Christopher E ; Livingston, Brian T ; Wilt, Fred H ; Adams, Nikki ; Bellé, Robert ; Carbonneau, Seth ; Cheung, Rocky ; Cormier, Patrick ; Cosson, Bertrand ; Croce, Jenifer ; Fernandez-Guerra, Antonio ; Genevière, Anne-Marie ; Goel, Manisha ; Kelkar, Hemant ; Morales, Julia ; Mulner-Lorillon, Odile ; Robertson, Anthony J ; Goldstone, Jared V ; Cole, Bryan ; Epel, David ; Gold, Bert ; Hahn, Mark E ; Howard-Ashby, Meredith ; Scally, Mark ; Stegeman, John J ; Allgood, Erin L ; Cool, Jonah ; Judkins, Kyle M ; Mccafferty, Shawn S ; Musante, Ashlan M ; Obar, Robert A ; Rawson, Amanda P ; Rossetti, Blair J ; Gibbons, Ian R ; Hoffman, Matthew P ; Leone, Andrew ; Istrail, Sorin ; Materna, Stefan C ; Samanta, Manoj P ; Stolc, Viktor ; Tongprasit, Waraporn ; Tu, Qiang ; Bergeron, Karl-Frederik ; Brandhorst, Bruce P ; Whittle, James ; Berney, Kevin ; Bottjer, David J ; Calestani, Cristina ; Peterson, Kevin ; Chow, Elly ; Yuan, Qiu Autumn ; Elhaik, Eran ; Graur, Dan ; Reese, Justin T ; Bosdet, Ian ; Heesun, Shin ; Marra, Marco A ; Schein, Jacqueline ; Anderson, Michele K ; Brockton, Virginia ; Buckley, Katherine M ; Cohen, Avis H ; Fugmann, Sebastian D ; Hibino, Taku ; Loza-Coll, Mariano ; Majeske, Audrey J ; Messier, Cynthia ; Nair, Sham V ; Pancer, Zeev ; Terwilliger, David P ; Agca, Cavit ; Arboleda, Enrique ; Chen, Nansheng ; Churcher, Allison M ; Hallböök, F ; Humphrey, Glen W ; Idris, Mohammed M ; Kiyama, Takae ; Liang, Shuguang ; Mellott, Dan ; Mu, Xiuqian ; Murray, Greg ; Olinski, Robert P ; Raible, Florian ; Rowe, Matthew ; Taylor, John S ; Tessmar-Raible, Kristin ; Wang, D ; Wilson, Karen H ; Yaguchi, Shunsuke ; Gaasterland, Terry ; Galindo, Blanca E ; Gunaratne, Herath J ; Juliano, Celina ; Kinukawa, Masashi ; Moy, Gary W ; Neill, Anna T ; Nomura, Mamoru ; Raisch, Michael ; Reade, Anna ; Roux, Michelle M ; Song, Jia L ; Su, Yi-Hsien ; Townley, Ian K ; Voronina, Ekaterina ; Wong, Julian L ; Amore, Gabriele ; Branno, Margherita

; Brown, Euan R ; Cavalieri, Vincenzo ; Duboc, Véronique ; Duloquin, Louise ; Flytzanis, Constantin ; Gache, Christian ; Lapraz, François ; Lepage, Thierry ; Locascio, Annamaria ; Martinez, Pedro ; Matassi, Giorgio ; Matranga, Valeria ; Range, Ryan ; Rizzo, Francesca ; Röttinger, Eric ; Beane, Wendy ; Bradham, Cynthia ; Byrum, Christine ; Glenn, Tom ; Hussain, Sofia ; Manning, Gerard ; Miranda, Esther ; Thomason, Rebecca ; Walton, Katherine ; Wikramanayke, Athula ; Wu, Shu-Yu ; Xu, Ronghui ; Brown, C Titus ; Chen, Lili ; Gray, Rachel F ; Lee, Pei Yun ; Nam, Jongmin ; Oliveri, Paola ; Smith, Joel ; Muzny, Donna ; Bell, Stephanie ; Chacko, Joseph ; Cree, Andrew ; Curry, Stacey ; Davis, Clay ; Dinh, Huyen ; Dugan-Rocha, Shannon ; Fowler, Jerry ; Gill, Rachel ; Hamilton, Cerrissa ; Hernandez, Judith ; Hines, Sandra ; Hume, Jennifer ; Jackson, Laronda ; Jolivet, Angela ; Kovar, Christie ; Lee, Sandra ; Lewis, Lora ; Miner, George ; Morgan, Margaret ; Nazareth, Lynne V ; Okwuonu, Geoffrey ; Parker, David ; Pu, Ling-Ling ; Thorn, Rachel ; Wright, Rita (2006) The Genome of the Sea Urchin *Strongylocentrotus purpuratus*. *Science,* **314** (5801)**,** 941-952.

Song, H., Her, A. S., Raso, F., Zhen, Z., Huo, Y. & Liu, P. (2014) Cysteine Oxidation Reactions Catalyzed by a Mononuclear Non-heme Iron Enzyme (OvoA) in Ovothiol Biosynthesis. *Organic letters,* **16** (8)**,** 2122-2125.

Song, H., Leninger, M., Lee, N. & Liu, P. (2013) Regio-selectivity of the Oxidative C-S Bond Formation in Ergothioneine and Ovothiol Biosyntheses. *Organic letters,* **15** (18)**,** 4854-4857.

Spies, H. S. & Steenkamp, D. J. (1994) Thiols of intracellular pathogens. Identification of ovothiolA in *Leishmania donovani* and structural analysis of a novel thiol from *Mycobacterium bovis*. *European Journal of Biochemistry,* **224,** 203-213.

Steenkamp, D. J., Weldrick, D. & Spies, H. S. C. (1996) Studies on the Biosynthesis of

Ovothiol A. *European Journal of Biochemistry,* **242** (3)**,** 557-566.

Strathmann, R. R. (2000) Functional design in the evolution of embryos and larvae. *Seminars in cell & developmental biology,* **11** (6)**,** 395-402.

Strathmann, R. R. (2007) Time and Extent of Ciliary Response to Particles in a Non-Filtering Feeding Mechanism. *The Biological Bulletin,* **212** (2)**,** 93-103.

Strathmann, R. R. & Grünbaum, D. (2006) Good eaters, poor swimmers: compromises in larval form. *Integrative and Comparative Biology,* **46** (3)**,** 312-322.

Stumpp, M., Hu, M., Casties, I., Saborowski, R., Bleich, M., Melzner, F. & Dupont, S. (2013) Digestion in sea urchin larvae impaired under ocean acidification. *Nature Climate Change,* **3,** 1044-1049.

Stumpp, M., Hu, M. Y., Melzner, F., Gutowska, M. A., Dorey, N., Himmerkus, N., Holtmann, W. C., Dupont, S. T., Thorndyke, M. C. & Bleich, M. (2012) Acidified seawater impacts sea urchin larvae pH regulatory systems relevant for calcification. *Proceedings of the National Academy of Sciences,* **109** (44)**,** 18192-18197.

Stumpp, M., Hu, M. Y., Tseng, Y.-C., Guh, Y.-J., Chen, Y.-C., Yu, J.-K., Su, Y.-H. & Hwang, P.-P. (2015) Evolution of extreme stomach pH in bilateria inferred from gastric alkalization mechanisms in basal deuterostomes. *Scientific reports,* **5,** 10421.

Su, H. M., Lei, C. H. & Liao, I. C. (1990) Effect of temperature, illumination and salinity on the growth rates of *Skeletonema costatum. Journal of fisheries Society Taiwan,* **17,** 213- 222.

Tang, Z. I. (2010) The Domino and Clock Models of Cell Cycle Regulation. *Nature Education,* **3** (9).

Tapley, D. W., Buettner, G. R. & Shick, J. M. (1999) Free radicals and chemiluminescence

as products of the spontaneous oxidation of sulfide in seawater, and their biological implications. *Biology Bulletin,* **196,** 52-56.

Telford, M. J., Lowe, C. J., Cameron, C. B., Ortega-Martinez, O., Aronowicz, J., Oliveri, P. & Copley, R. R. (2014) Phylogenomic analysis of echinoderm class relationships supports Asterozoa. *Proceedings of the Royal Society B: Biological Sciences,* **281** (1786)**,** 20140479.

Turner, E., Hager, L. J. & Shapiro, B. M. (1988) Ovothiol replaces glutathione peroxidase as a hydrogen peroxide scavenger in sea urchin eggs. *Science,* **242** (4880)**,** 939-941.

Turner, E., Klevit, R., Hager, L. J. & Shapiro, B. M. (1987) Ovothiols, a family of redox-active mercaptohistidine compounds from marine invertebrate eggs. *Biochemistry,* **26** (13)**,** 4028-4036.

Turner, E., Klevitj, R., Hopkinsj, P. B. & Shapiro, B. M. (1986) Ovothiol: A Novel Thiohistidine Compound from Sea Urchin Eggs That Confers NAD(P)H-0_2 Oxidoreductase Activity on Ovoperoxidase. *The Journal of biological chemistry,* **261,** 13056-13063.

Valero-Gracia, A., Petrone, L., Oliveri, P., Nilsson, D.-E. & Arnone, M. I. (2016) Non-directional Photoreceptors in the Pluteus of *Strongylocentrotus purpuratus*. *Frontiers in Ecology and Evolution,* **4** (127).

Valle, K. C., Nymark, M., Aamot, I., Hancke, K., Winge, P., Andresen, K., Johnsen, G., Brembu, T. & Bones, A. M. (2014) System Responses to Equal Doses of Photosynthetically Usable Radiation of Blue, Green, and Red Light in the Marine Diatom *Phaeodactylum tricornutum*. *PloS one,* **9** (12)**,** e114211.

Vamecq, J., Maurois, P., Bac, P., Bailly, F., Bernier, J. L., Stables, J. P., Husson, I. & Gressens, P. (2003) Potent mammalian cerebroprotection and neuronal cell death

inhibition are afforded by a synthetic antioxidant analogue of marine invertebrate cell protectant ovothiols. *The European journal of neuroscience,* **18** (5)**,** 1110-1120.

Vandesompele, J., De Preter, K., Pattyn, F., Poppe, B., Van Roy, N., De Paepe, A. & Speleman, F. (2002) Accurate normalization of real-time quantitative RT-PCR data by geometric averaging of multiple internal control genes. *Genome Biology,* **3** (7)**,** research0034.0031-research0034.0011.

Vardi, A. (2008) Cell signaling in marine diatoms. *Communicative & integrative biology,* **1** (2)**,** 134-136.

Vardi, A., Formiggini, F., Casotti, R., De Martino, A., Ribalet, F., Miralto, A. & Bowler, C. (2006) A Stress Surveillance System Based on Calcium and Nitric Oxide in Marine Diatoms. *PLoS Biology,* **4** (3)**,** 411-419.

Vaulot, D., Olson, R. J. & Chisholm, S. W. (1986) Light and dark control of the cell cycle in two marine phytoplankton species. *Experimental Cell Research,* **167** (1)**,** 38-52.

Villareal, T. A. (1992) Buoyancy properties of the giant diatom Ethmodiscus. *Journal of Plankton Research,* **14** (3)**,** 459-463.

Vogt, R. N., Spies, H. S. C. & Steenkamp, D., J. (2001) The biosynthesis of ovothiol A (N1-methyl-4-mercaptohistidine). *European Journal of Biochemistry,* **268** (20)**,** 5229-5241.

Vogt, R. N. & Steenkamp, D. J. (2003) The metabolism of S-nitrosothiols in the trypanosomatids: the role of ovothiol A and trypanothione. *Biochemical Journal,* **371** (Pt 1)**,** 49-59.

Wagenaar, E. B. (1983) The timing of synthesis of proteins required for mitosis in the cell cycle of the sea urchin embryo. *Experimental Cell Research,* **144** (2)**,** 393-403.

Wall, S., B., Oh, J.-Y., Diers, A. R. & Landar, A. (2012) Oxidative Modification of Proteins: An Emerging Mechanism of Cell Signaling. *Frontiers in Physiology,* **3,** 369.

Wang, L., Qu, X., Xie, Y. & Lv, S. (2017) Study of 8 Types of Glutathione Peroxidase Mimics Based on β-Cyclodextrin. *Catalysts,* **7** (10)**,** 289.

Weaver, K. H. & Rabenstein, D. L. (1995) Thiol/Disulfide Exchange Reactions of Ovothiol A with Glutathione. *The Journal of Organic Chemistry,* **60** (6)**,** 1904-1907.

Whitaker, M. & Patel, R. (1990) Calcium and cell cycle control. *Development,* **108** (4)**,** 525.

Wilhelm, C., Jungandreas, A., Jakob, T. & Goss, R. (2014) Light acclimation in diatoms: From phenomenology to mechanisms. *Marine Genomics,* **16,** 5-15.

Winterbourn, C. C. & Hampton, M. B. (2008) Thiol chemistry and specificity in redox signaling. *Free Radical Biology and Medicine,* **45** (5)**,** 549-561.

Wolf, F., Sigl, R. & Geley, S. (2007) '... The end of the beginning': cdk1 thresholds and exit from mitosis. *Cell cycle (Georgetown, Tex.),* **6** (12)**,** 1408-1411.

Wood, N. J., Mattiello, T., Rowe, M. L., Ward, L., Perillo, M., Arnone, M. I., Elphick, M. R. & Oliveri, P. (2018) Neuropeptidergic Systems in Pluteus Larvae of the Sea Urchin *Strongylocentrotus purpuratus*: Neurochemical Complexity in a "Simple" Nervous System. *Frontiers in Endocrinology,* **9** (628).

Wray, G. A. & Raff, R. A. (1989) Evolutionary modification of cell lineage in the direct-developing sea urchin *Heliocidaris erythrogramma. Developmental Biology,* **132** (2)**,** 458-470.

Yajima, M. & Wessel, G. M. (2011) Small micromeres contribute to the germline in the sea urchin. *Development,* **138** (2)**,** 237-243.

Yerramilli, D. & Johnsen, S. (2010) Spatial vision in the purple sea urchin *Strongylocentrotus purpuratus* (Echinoidea). *The Journal of Experimental Biology,* **213,** 249-255.

Yoshida, M. (1966) Photosensitivity. In RA, B. (Ed.) *Physiology of Echinodermata.* New York, Wiley Interscience.

Zoete, V., Bailly, F., Catteau, J.-P. & Bernier, J.-L. (1997) Design, synthesis and antioxidant properties of ovothiol-derived 4-mercaptoimidazoles. *Journal of the Chemical Society, Perkin Transactions 1,* **0** (20)**,** 2983-2988.

Zoete, V., Bailly, F., Vezin, H., Teissier, E., Duriez, P., Fruchart, J.-C., Catteau, J.-P. & Bernier, J.-L. (2000) 4-Mercaptoimidazoles derived from the naturally occurring antioxidant ovothiols 1. Antioxidant properties. *Free Radical Research,* **32** (6)**,** 515-524.

Supplementary material

Polyclonal Ab against a mix of synthetic peptides
"201507-00019 " "201507-00020" "201507-00021"

Code "FCA/15"

SERUM DILUTION	Preimmune serum RABBIT 1	Immune serum RABBIT 1	Preimmune serum RABBIT 2	Immune serum RABBIT 2
1/100	0,598	3,500	0,667	3,500
1/300	0,169	3,500	0,254	3,500
1/900	0,075	3,500	0,030	3,500
1/2700	0,005	1,979	0,023	2,143
1/8100	0,000	1,662	0,000	1,000
1/24300	0,000	0,687	0,000	0,321
1/72900	0,000	0,254	0,000	0,124

ELISA test against peptide "201507-00019" conjugated to KLH

Polyclonal Ab against a mix of synthetic peptides
"201507-00019 " "201507-00020" "201507-00021"

Code "FCA/15"

SERUM DILUTION	Preimmune serum RABBIT 1	Immune serum RABBIT 1	Preimmune serum RABBIT 2	Immune serum RABBIT 2
1/100	0,598	3,500	0,667	3,500
1/300	0,169	3,500	0,254	3,500
1/900	0,075	3,500	0,030	2,272
1/2700	0,005	1,928	0,023	1,254
1/8100	0,000	1,154	0,000	0,762
1/24300	0,000	0,567	0,000	0,299
1/72900	0,000	0,325	0,000	0,023
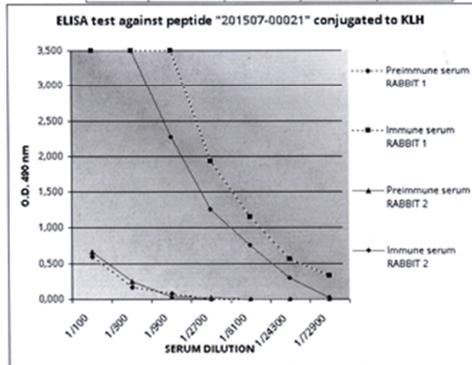
ELISA test against peptide "201507-00021" conjugated to KLH

Polyclonal Ab against a mix of synthetic peptides
"201507-00019 " "201507-00020" "201507-00021"

Code "FCA/15"

SERUM DILUTION	Preimmune serum RABBIT 1	Immune serum RABBIT 1	Preimmune serum RABBIT 2	Immune serum RABBIT 2
1/100	0,598	3,500	0,667	3,500
1/300	0,169	3,500	0,254	2,528
1/900	0,075	1,301	0,030	0,964
1/2700	0,005	0,499	0,023	0,652
1/8100	0,000	0,215	0,000	0,451
1/24300	0,000	0,146	0,000	0,254
1/72900	0,000	0,051	0,000	0,150

ELISA test against peptide "201507-00020" conjugated to KLH
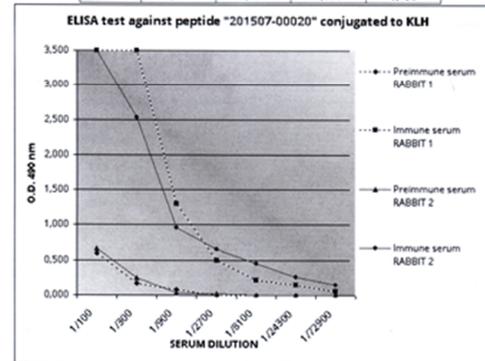
Figure 1S Elisa test of immune and pre-immune serum against a mix of synthetic peptides.
Elisa test showing the presence of reactive anti-OvoA IgGs in the immune sera from both rabbits using preimmune sera as negative controls.
201507-00019 = peptide 1 (P1); 201507-00020 = peptide 2 (P2); 201507-00021 = peptide 4 (P4)

Purified Polyclonal Ab against a mix of synthetic peptides "201507-00019 " "201507-00020" "201507-00021"

Code "FCA/15"

ABs concentration (µg/mL)	Purified Ab RABBIT 1	Purified Ab RABBIT 2
N.D.	3,500	3,500
5	3,500	3,500
1,67	3,500	3,500
0,53	3,500	3,500
0,18	3,109	3,500
0,06	1,807	2,385
0,02	0,757	2,214
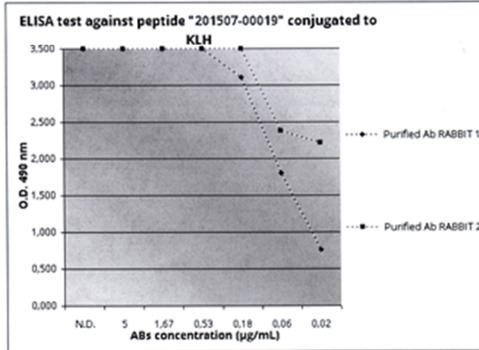
ELISA test against peptide "201507-00019" conjugated to KLH

Purified Polyclonal Ab against a mix of synthetic peptides "201507-00019 " "201507-00020" "201507-00021"

Code "FCA/15"

ABs concentration (µg/mL)	Purified Ab RABBIT 1	Purified Ab RABBIT 2
N.D.	3,500	3,500
5	3,500	3,500
1,67	3,163	3,500
0,53	2,020	3,500
0,18	0,930	3,312
0,06	0,415	2,985
0,02	0,162	1,662
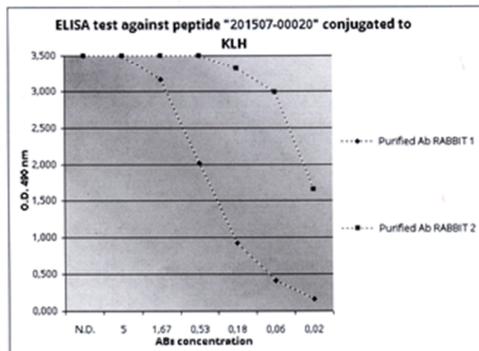
ELISA test against peptide "201507-00020" conjugated to KLH

Purified Polyclonal Ab against a mix of synthetic peptides "201507-00019 " "201507-00020" "201507-00021"

Code "FCA/15"

ABs concentration (µg/mL)	Purified Ab RABBIT 1	Purified Ab RABBIT 2
N.D.	3,500	3,500
5	3,500	3,500
1,67	3,500	3,500
0,53	3,172	3,500
0,18	1,986	3,500
0,06	1,343	3,500
0,02	0,581	1,951

ELISA test against peptide "201507-00021" conjugated to KLH
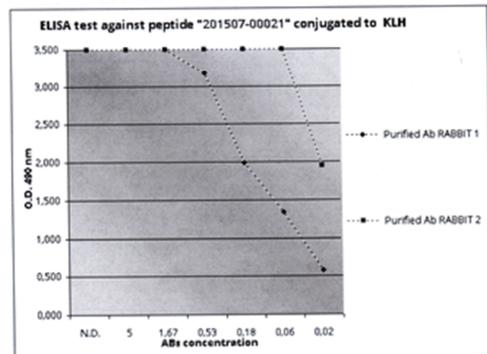
Figure 2S Elisa test of purified polyclonal Abs against a mix of synthetic peptides.

Elisa test showing the specificity of anti-OvoA IgGs purified from immune sera of both rabbits.

201507-00019 = peptide 1 (P1); 201507-00020 = peptide 2 (P2); 201507-00021 = peptide 4 (P4)
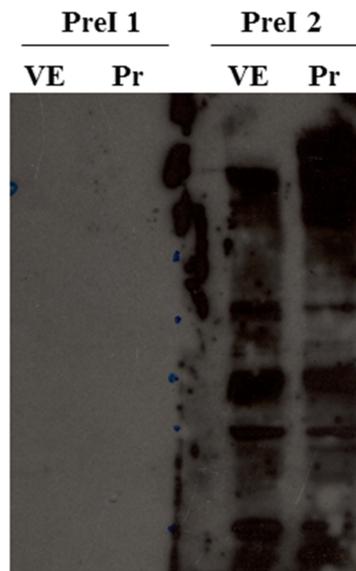
Figure 3S Immunoreactivity of pre-immune IgGs in WB experiment.

Abbreviations: Pre-immune IgGs from rabbit 1 (PreI 1); Pre-immune IgGs from rabbit 2 (PreI 2); virgin eggs (VE); Prism stage (Pr).

Table 1S OvoA identification

Peptides identified by mass spectrometry analysis in the protein band (88 kDa) extracted by the electrophoresis gel and recognised, in SDS-PAGE, by the antibody against OvoA. In the table, peptide sequence, X correlation (XCorr), charge, molecular weight (MH+) and number of missed cleavages are indicated. Modified aminoacids are shown in lowercase letters.

Peptide sequence	XCorr	Charge	MH+ [Da]	# Missed Cleavages
LWEILmPNGIVVISGLGDwTKEK	1.76	3	2659.3753	1
SninltfgtstpvhmypangK	1.66	3	2291.1300	0
AyAAWKGPGYRLPTESEHnAMR	1.52	3	2551.1777	2
IHIETSSVLIRqLPIGmVKTPEQWV PGPLTYGESPSK	1.51	4	4105.1515	2

5-histidylcysteine sulfoxide synthase [Paracentrotus lividus]

MATELSLEDILTGPYTWKSMTPCDLSNCTKQQILDYFENSYSLNESIFAALKTEDAIYKAPD
RLRLPLIFYYAHTAVVYINKLMLAGLIEERVNFEYETMFETGVDEMSWDDTENYRMGGS
YQWPSLKDVVQFRLKVRNVIRKVIEDTPLELPVTQESKWWAMFMGFEHER**IHIETSSVLI
RQLPIGMVKTPEQWVPGPLTYGESPSK**NPLLPVEGTEVTMGKPKDFPSYGWDNEYPQI
QTSVPSFEASKYLITNREFMEFVTDKGYENEKLWSKEGWKWRKYRNARHPTFWVCDKG
CVSGCGGVLAGYSHCKPDQNQNSSQYRYRSFCEETAIPWDWPVEVNYHEAK**AYAAWKG
PGYRLPTESEHNAMR**DKKPISKGTDSDLIYDKELHQK**SNINLTFGTSTPVHMYPANGK**G
FHDVFGNVWQWVEDHFNGLPGSETHYLYDDFSSPTYDGKHNVILGGSWISTGDEASRFA
RYAFRRHFFQHAGFRLARSCSDQDVPVRLVRNPAHADQDVSLPLKDISKKTFMTTNTQLL
METQSCVDERLFDEYVLDDINLSSALGKVSMDIARRHGTKVSHALDVGCGCGRMSFELSR
AVDQVIGLEYCEVFLKSAEELLSKKQKVFYCPKEDCRIPAKRVKRSTHDGCTITAKLPTDT
QPSRVTLKQFTWIPNELSGFDLVVHHCLDRVPNKRAWLIR**LWEILMPNGIVVISGLGDW
TKEK**LEPIIGDKLRCMETIPVKYAEDYWCTEPDKETWATVWCLKTRAEAQ

Figure 4S OvoA protein sequence

Position of the antigenic peptides (highlited in red) identified by mass spectrometry analysis in the

OvoA protein sequence.

Table 2S Western blot analysis of OvoA in *P.lividus* developmental stages.

Western blot analysis has been performed on three biological triplicates (batches #1, #2 and #3) and the densitometry ratio values of OvoA/actin immunopositive bands are reported in table as OvoA/actin optical densitometry (OD). Abbreviations: UE = unfertilised eggs; Zi = zygote; 64bl = 64-blastomeres stage; EB = early blastula; SB = swimming blastula; MB = mesenchyme blastula; LG = late gastrula; Pr = prism; Pl = pluteus stage.

Developmental stage	OvoA/actin OD				
	#1	#2	#3	average	st-dev
UE	0,147815	0,1700856	0,3659475	0,2279494	0,120027
Zi	0,142746	0,1661682	0,3714835	0,2267991	0,125846
64bl	0,150942	0,1635677	0,3754143	0,2299748	0,126112
EB	0,245019	0,3970721	0,7913947	0,4778288	0,281998
SB	0,416655	0,7147103	0,9224745	0,6846132	0,254249
MB	0,985213	0,732052	0,902723	0,8733294	0,129115
LG	1,558071	0,8019882	0,6864876	1,0155156	0,473402
Pr	0,763896	0,845168	0,4418754	0,6836466	0,213287
Pl	0,511878	0,0427947	1,1563409	0,5703377	0,55907

Table 2S Genes analysed for RT-qPCR: primer sequences, PCR amplicon sizes, temperature of annealing (Ta), primer efficiencies (E) and correlation factor (R^2).

Gene	Forward primer (5′⇒3′)	Reverse primer (5′⇒3′)	Amplicon size (bp)	Ta (°C)	E	R^2
OvoA	AAAGAGATGGCTCGCCTACA	GATTTGCAGCAGTCTCACCA	171	60	1.96	0.998
Nos1	AAAGCCAGCCACAGATTCGA	ACTAAAGCCAAGACCAGCCC	228	60	1.97	0.989
Nos2	TGGGTTTCGGTAGTTCTGCC	ACAACGTCGCTGTCCAGATT	159	60	1.97	0.998

Table 3S OvoA presence/absence in diatom transcriptomes and genomes.

The presence of OvoA transcript in diatom transcriptomes and genomes is shown. The sequence covering, E value and identity values using OvoA from *Skeletonema marinoi*, strain CCMP2092 (the one used in this study), as query was reported.

Species	Strain	Sample ID	OvoA ID	Query cover (%)	E value	Identity (%)
Amphiprora paludosa	CCMP125	MMETSP1065	-			
Amphiprora sp.	CCMP467	MMETSP0724	15031	89	0.0	47
Amphiprora sp	CCMP467	MMETSP0725	3890	86	0.0	48
			17467	68	0.0	50
Amphiprora sp.	CCMP467	MMETSP0726	129	86	0.0	48
			9618	69	0.0	46
Amphiprora sp.	CCMP467	MMETSP0727	5310	86	0.0	47
Amphora coffeaeformis	CCMP127	MMETSP0316	-			
Amphora coffeaeformis	CCMP127	MMETSP0317	-			
Amphora coffeaeformis	CCMP127	MMETSP0318	-			
Asterionella formosa	BG1	SAMN07280877	NKIB01012442.1	54	0.0	70
Asterionellopsis glacialis	CCMP134	MMETSP0705	-			
Asterionellopsis glacialis	CCMP134	MMETSP0706	-			
Asterionellopsis glacialis	CCMP134	MMETSP0707	-			
Asterionellopsis glacialis	CCMP134	MMETSP0708	-			
Asterionellopsis glacialis	-	MMETSP0713	-			
Asterionellopsis glacialis	CCMP1581	MMETSP1394	-			
Astrosyne radiata	13vi08-1A	MMETSP0418	13578	86	0.0	67
Attheya septentrionalis	CCMP2084	MMETSP1449	26998	95	0.0	69
Aulacoseira subarctica	CCAP 1002/5	MMETSP1064	-			

Chaetoceros affinis	CCMP159	MMETSP0088	-			
Chaetoceros affinis	CCMP159	MMETSP0090	-			
Chaetoceros affinis	CCMP159	MMETSP0091	-			
Chaetoceros affinis	CCMP159	MMETSP0092	-			
Chaetocerus brevis	CCMP164	MMETSP1435	-			
Chaetoceros curvisetus	-	MMETSP0716	-			
Chaetoceros curvisetus	-	MMETSP0717	-			
Chaetoceros curvisetus	-	MMETSP0718	-			
Chaetoceros curvisetus	-	MMETSP0719	-			
Chaetoceros debilis	MM31A-1	MMETSP0149	-			
Chaetoceros debilis	MM31A-1	MMETSP0150	-			
Chaetocerus dichaeta	CCMP1751	MMETSP1447	-			
Chaetoceros neogracile	CCMP1317	MMETSP0751	-			
Chaetoceros neogracile	CCMP1317	MMETSP0752	-			
Chaetoceros neogracile	CCMP1317	MMETSP0753	-			
Chaetoceros neogracile	CCMP1317	MMETSP0754	-			
Chaetoceros neogracile	RCC1993	MMETSP1336	-			
Chaetoceros sp.	UNC1202	MMETSP1429	-			
Chaetoceros sp.	GSL56	MMETSP0200	-			
Corethron hystrix	308	MMETSP0010	-			
Corethron pennatum	L29A3	MMETSP0169	6655	88	0.0	58
Corethron pennatum	L29A3	MMETSP0171	104747	89	0.0	57
Coscinodiscus wailesii	CCMP2513	MMETSP1066	17277	100	0.0	86
Craspedostauros australis	CCMP3328	MMETSP1442	-			
Cyclophora tenuis	ECT3854	MMETSP0397	17245	73	0.0	67
Cyclotella meneghiniana	CCMP 338	MMETSP1057	1354	100	0.0	70
Cylindrotheca closterium	KMMCC:B-181	MMETSP0017	9696	90	0.0	69

Dactyliosolen fragilissimus	-	MMETSP0580	-			
Detonula confervacea	CCMP 353	MMETSP1058	-			
Detonula confervacea	CCMP 353	MMETSP1058	44727	99	0.0	71
Ditylum brightwellii	GSO103	MMETSP1002	6770	84	0.0	65
Ditylum brightwellii	GSO103	MMETSP1005	4075	88	0.0	72
Ditylum brightwellii	GSO104	MMETSP1010	635	99	0.0	65
Ditylum brightwellii	GSO104	MMETSP1012	9896	99	0.0	60
Ditylum brightwellii	GSO104	MMETSP1013	7584	99	0.0	65
Ditylum brightwellii	GSO105	MMETSP0998	6118	98	0.0	65
Ditylum brightwellii	GSO105	MMETSP1001	742	99	0.0	65
Ditylum brightwellii	Pop1 (SS4)	MMETSP1062	8035	99	0.0	65
Ditylum brightwellii	Pop2 (SS10)	MMETSP1063	10788	99	0.0	65
Entomoneis sp.	CCMP2396	MMETSP1443	-			
Eucampia antarctica	CCMP1452	MMETSP1437	-			
Extubocellulus spinifer	CCMP396	MMETSP0696	-			
Extubocellulus spinifer	CCMP396	MMETSP0698	-			
Extubocellulus spinifer	CCMP396	MMETSP0699	17438	92	0.0	68
Fistulifera solaris	JPCC DA0580	SAMD00018578	GAX17039.1	90	0.0	68
Fragilariopsis cylindrus	CCMP1102	SAMN02744060	OEU08449.1	88	0.0	65
Fragilariopsis kerguelensis	L26-C5	MMETSP0735	2597	97	0.0	65
Fragilariopsis kerguelensis	L26-C5	MMETSP0734	12340	97	0.0	65
Fragilariopsis kerguelensis	L2-C3	MMETSP0908	96212	97	0.0	65
Fragilariopsis kerguelensis	L2-C3	MMETSP0906	23693	97	0.0	65
Fragilariopsis kerguelensis	L2-C3	MMETSP0907	738	97	0.0	65
Fragilariopsis kerguelensis	L2-C3	MMETSP0909	151201	90	0.0	68
Grammatophora oceanica	CCMP 410	MMETSP0009	6159	93	0.0	68
Helicotheca tamensis	CCMP826	MMETSP1171	-			

Leptocylindrus danicus	CCMP1856	MMETSP1362	7402	99	0.0	64
Leptocylindrus danicus	B650	MMETSP0321	25627	100	0.0	65
			765	85	0.0	69
Leptocylindrus danicus	B651	MMETSP0322	997	89	0.0	66
Licmophora abbreviata	-	SAMEA104638370	OLMU01000711.1	59	0.0	67
Licmophora paradoxa	CCMP2313	MMETSP1360	13577	82	0.0	71
Minutocellus polymorphus	NH13	MMETSP1070	5030	95	0.0	65
			20311	61	0.0	67
Minutocellus polymorphus	RCC2270	MMETSP1322	208	93	0.0	67
Minutocellus polymorphus	CCMP3303	MMETSP1434	-			
Nitzschia punctata	CCMP561	MMETSP0744	4981	92	0.0	68
Nitzschia punctata	CCMP561	MMETSP0745	6642	92	0.0	68
Nitzschia punctata	CCMP561	MMETSP0746	10634	92	0.0	69
Nitzschia punctata	CCMP561	MMETSP0747	13427	92	0.0	69
Odontella Sinensis	Grunow 1884	MMETSP0160	66241	81	0.0	72
Phaeodactylum tricornutum	CCAP 1055/1	SAMN02953727	XP_002179013.1	96	0.0	66
Proboscia alata	PI-D3	MMETSP0174	-			
Proboscia alata	PI-D3	MMETSP0176	-			
Proboscia inermis	CCAP1064/1	MMETSP0816	-			
Pseudo-nitzschia arenysensis	B593	MMETSP0329	13200	97	0.0	65
Pseudo-nitzschia australis	10249 10 AB	MMETSP0139	4483	90	0.0	68
			14011	67	0.0	65
Pseudo-nitzschia australis	10249 10 AB	MMETSP0140	4560	90	0.0	68
			24110	75	0.0	66
Pseudo-nitzschia australis	10249 10 AB	MMETSP0141	3565	90	0.0	68
			5443	56	0.0	65
Pseudo-nitzschia australis	10249 10 AB	MMETSP0142	22598	90	0.0	68

Species	Strain	ID	Value			
Pseudo-nitzschia delicatissima	UNC1205	MMETSP1432	19423	63	0.0	66
Pseudo-nitzschia delicatissima	B596	MMETSP0327	9215	99	0.0	64
Pseudo-nitzschia fraudulenta	WWA7	MMETSP0850	-			
Pseudo-nitzschia fraudulenta	WWA7	MMETSP0851	190477	51	0.0	62
Pseudo-nitzschia fraudulenta	WWA7	MMETSP0852	-			
Pseudo-nitzschia fraudulenta	WWA7	MMETSP0853	-			
Pseudo-nitzschia heimii	UNC1101	MMETSP1423	12924	92	0.0	67
Pseudo-nitzschia multiseries	CLN-47	jgi|Psemu1	159773	93	0.0	67
Pseudo-nitzschia pungens	cingulata	MMETSP1060	25962	93	0.0	67
Pseudo-nitzschia pungens	pungens	MMETSP1061	5479	90	0.0	69
Rhizosolenia setigera	CCMP 1694	MMETSP0789	-			
Skeletonema costatum	1716	MMETSP0013	37767	100	0.0	99
			15016	93	0.0	99
Skeletonema dohrnii	SkelB	MMETSP0562	3445	84	0.0	99
Skeletonema dohrnii	SkelB	MMETSP0563	-			
Skeletonema grethea	CCMP 1804	MMETSP0578	58658	97	0.0	90
Skeletonema marinoi	skelA	MMETSP0918	4419	100	0.0	99
Skeletonema marinoi	skelA	MMETSP0920	-			
Skeletonema marinoi	FE60	MMETSP1040	-			
Skeletonema marinoi	SM1012Hels-07	MMETSP0319	-			
Skeletonema marinoi	CCMP2092	MMETSP1039	2388	100	0.0	100
			4090	65	0.0	97
Skeletonema marinoi	UNC1201	MMETSP1428	-			
Skeletonema marinoi	SM1012Den-03	MMETSP0320	-			
Skeletonema menzelii	CCMP793	MMETSP0603	-			
Skeletonema menzelii	CCMP793	MMETSP0604	7059	100	0.0	90
Skeletonema japonicum	CCMP2506	MMETSP0593	-			

Stauroneis constricta	CCMP1120	MMETSP1352	-			
Staurosira complex	CCMP2646	MMETSP1361	53213	96	0.0	66
Stephanopyxis turris	CCMP815	MMETSP0794	-			
Synedropsis recta	CCMP1620	MMETSP1176	6119	88	0.0	69
Striatella unipunctata	CCMP2910	MMETSP0800	-			
Thalassionema frauenfeldii	CCMP 1798	MMETSP0786	126	89	0.0	60
Thalassionema nitzschioides	L26-B	MMETSP0156	24508	100	0.0	56
Thalassionema nitzschioides	L26-B	MMETSP0158	45599	100	0.0	56
Thalassionema nitzschioides	Unknown	MMETSP0693	-			
Thalassiosira antarctica	CCMP982	MMETSP0902	56055	83	0.0	77
Thalassiosira antarctica	CCMP982	MMETSP0903	55218	74	0.0	78
Thalassiosira antarctica	CCMP982	MMETSP0904	55219	72	0.0	79
Thalassiosira antarctica	CCMP982	MMETSP0905	65391	84	0.0	79
Thalassiosira gravida	GMp14c1	MMETSP0492	-			
Thalassiosira gravida	GMp14c1	MMETSP0493	-			
Thalassiosira gravida	GMp14c1	MMETSP0494	-			
Thalassiosira miniscula	CCMP1093	MMETSP0737	-			
Thalassiosira miniscula	CCMP1093	MMETSP0738	-			
Thalassiosira miniscula	CCMP1093	MMETSP0739	-			
Thalassiosira miniscula	CCMP1093	MMETSP0740	-			
Thalassiosira oceanica	CCMP1005	MMETSP0973	4316	92	0.0	72
Thalassiosira oceanica	CCMP1005	MMETSP0970	17342	99	0.0	68
Thalassiosira oceanica	CCMP1005	MMETSP0971	4915	93	0.0	71
Thalassiosira oceanica	CCMP1005	MMETSP0972	90	92	0.0	72
Thalassiosira oceanica	CCMP1005	SAMN02981384	EJK74716.1	92	0.0	72
Thalassiosira pseudonana	CCMP1335	SAMN02744045	XP_002292254.1	92	0.0	75
Thalassiosira punctigera	Tpunct2005C2	MMETSP1067	1484	97	0.0	77

Thalassiosira rotula	CCMP3096	MMETSP0403	9901	98	0.0	76
Thalassiosira rotula	CCMP3096	MMETSP0404	4560	98	0.0	72
Thalassiosira rotula	GSO102	MMETSP0910	46892	98	0.0	70
Thalassiosira rotula	GSO102	MMETSP0911	48884	50	0.0	75
Thalassiosira rotula	GSO102	MMETSP0912	-			
Thalassiosira rotula	GSO102	MMETSP0913	-			
Thalassiosira sp.	FW	MMETSP1059	76803	92	0.0	75
Thalassiosira sp.	NH16	MMETSP1071	15147	66	0.0	75
Thalassiosira weissflogii	CCMP1010	MMETSP1405	-			
Thalassiosira weissflogii	CCMP1010	MMETSP1406	-			
Thalassiosira weissflogii	CCMP1010	MMETSP1407	-			
Thalassiosira weissflogii	CCMP1010	MMETSP1408	8185	92	0.0	76
Thalassiosira weissflogii	CCMP1010	MMETSP1409	39534	92	0.0	76
Thalassiosira weissflogii	CCMP1010	MMETSP1410	41744	66	0.0	74
Thalassiosira weissflogii	CCMP1010	MMETSP1411	47991	65	0.0	76
Thalassiosira weissflogii	CCMP1010	MMETSP1412	9266	73	0.0	78
Thalassiosira weissflogii	CCMP1010	MMETSP1413	-			
Thalassiosira weissflogii	CCMP1010	MMETSP1414	55494	90	0.0	78
Thalassiosira weissflogii	CCMP1010	MMETSP1415	52279	92	0.0	75
Thalassiosira weissflogii	CCMP1010	MMETSP1416	5892	92	0.0	77
Thalassiosira weissflogii	CCMP1010	MMETSP1417	5541	92	0.0	77
Thalassiosira weissflogii	CCMP1010	MMETSP1418	7953	92	0.0	76
Thalassiosira weissflogii	CCMP1010	MMETSP1419	4507	92	0.0	77
Thalassiosira weissflogii	CCMP1010	MMETSP1420	59130	88	0.0	76
Thalassiosira weissflogii	CCMP1010	MMETSP1421	38302	49	0.0	79
Thalassiosira weissflogii	CCMP1010	MMETSP1422	39961	92	0.0	75
Thalassiosira weissflogii	CCMP1010	MMETSP0898	-			

Thalassiosira weissflogii	CCMP1010	MMETSP0899	51206	49	0.0	77
Thalassiosira weissflogii	CCMP1010	MMETSP0900	43433	84	0.0	77
Thalassiosira weissflogii	CCMP1010	MMETSP0901	8423	92	0.0	77
Thalassiosira weissflogii	CCMP1336	MMETSP0878	45067	89	0.0	76
Thalassiosira weissflogii	CCMP1336	MMETSP0879	38866	92	0.0	76
Thalassiosira weissflogii	CCMP1336	MMETSP0880	41024	75	0.0	78
Thalassiosira weissflogii	CCMP1336	MMETSP0881	40943	68	0.0	76
Thalassiosira weissflogii	CCMP1336	MMETSP0881	-			
Thalassiothrix antarctica	L6-D1	MMETSP0152	-			
Thalassiothrix antarctica	L6-D1	MMETSP0154	-			
Triceratium dubium	CCMP147	MMETSP1175	64877	87	0.0	72

Table 4S *OvoA* expression in diatoms in different growth conditions.

Presence of OvoA transcript in transcriptomes from diatoms grown in different conditions is highlighted in blue.

Species	Strain	Sample ID	OvoA	Growth conditions	
E. spinifer	CCMP396	MMETSP0696		nitrate 2.97 µmol/L	light 649 umol photons/m²/s
		MMETSP0698		no nitrate	light 643 umol photons/m²/s
		MMETSP0699	▓	nitrate 2.97 µmol/L; 2.5 mg L-1 nocodazole	light 204 umol photons/m²/s
P. fraudulenta	WWA7	MMETSP0850		silicate 106.1 µmol/kg; CO_2 390 ppm	light 90 µmol photons/m²/s
		MMETSP0851	▓	silicate 10.6 µmol/kg; CO_2 390 ppm	light 92 µmol photons/m²/s
		MMETSP0852		silicate 106.1 µmol/kg; CO_2 750 ppm	light 403 µmol photons/m²/s
		MMETSP0853		silicate 10.6 µmol/kg; CO_2 750 ppm	light 441 µmol photons/m²/s
S. dohrnii	skelB	MMETSP0562	▓	nitrate 882 µmol/L	light 165 µmol photons/m²/s
		MMETSP0563		nitrate 10 µmol/L	light 149 µmol photons/m²/s
S. marinoi	skelA	MMETSP0918	▓	phosphate 36.2 µmol/kg	light 164 µmol photons/m²/s
		MMETSP0920		phosphate 0.6 µmol/kg	light 414 µmol photons/m²/s
S. menzelii	CCMP793	MMETSP0603		nitrate 882 µmol/L	light 153 µmol photons/m²/s
		MMETSP0604	▓	nitrate 10 µmol/L	light 154 µmol photons/m²/s
T. rotula	GSO102	MMETSP0910	▓	phosphate 0.4 µmol/kg	light 383 µmol photons/m²/s
		MMETSP0911	▓	iron 4 nmol/L	light 390 µmol photons/m²/s
		MMETSP0912		iron 4 nmol/L Fe; phosphate 0.4 µmol/kg	light 398 µmol photons/m²/s
		MMETSP0913		phosphate 38.6 µmol/kg	light 406 µmol photons/m²/s
T. weissflogii	CCMP1010	MMETSP1405		iron 400 nmol/L; silicate 106 µmol/kg	light 633 µmol photons/m²/s
		MMETSP1406		iron 400 nmol/L; silicate 106 µmol/kg	light 639 µmol photons/m²/s

		MMETSP1407		iron 400 nmol/L; silicate 106 µmol/kg	light 644 µmol photons/m²/s
		MMETSP1408		iron 400 nmol/L; silicate 10.6 µmol/kg	light 650 µmol photons/m²/s
		MMETSP1409		iron 400 nmol/L; silicate 10.6 µmol/kg	light 656 µmol photons/m²/s
		MMETSP1410		iron 400 nmol/L; silicate 10.6 µmol/kg	light 594 µmol photons/m²/s
		MMETSP1411		iron 4 nmol/L; silicate 10.6 µmol/kg	light 406 µmol photons/m²/s
		MMETSP1412		iron 4 nmol/L; silicate 10.6 µmol/kg	light 598 µmol photons/m²/s
		MMETSP1413		iron 4 nmol/L; silicate 10.6 µmol/kg	light 603 µmol photons/m²/s
		MMETSP1414		2h after 10 nmol/L iron addition to iron Lim (4nM Fe)	light 606 µmol photons/m²/s
		MMETSP1415		2h after 10 nmol/L iron addition to iron Lim (4nM Fe)	light 610 µmol photons/m²/s
		MMETSP1416		2h after 10 nmol/L iron addition to iron Lim (4nM Fe)	light 614 µmol photons/m²/s
		MMETSP1417		8h after 10 nmol/L iron addition to iron Lim (4nM Fe)	light 618 µmol photons/m²/s
		MMETSP1418		8h after 10 nmol/L iron addition to iron Lim (4nM Fe)	light 623 µmol photons/m²/s
		MMETSP1419		8h after 10 nmol/L iron addition to iron Lim (4nM Fe)	light 630 µmol photons/m²/s
		MMETSP1420		24h after 10 nmol/L iron addition to iron Lim (4nM Fe)	light 635 µmol photons/m²/s
		MMETSP1421		24h after 10 nmol/L iron addition to iron Lim (4nM Fe)	light 640 µmol photons/m²/s
		MMETSP1422		24h after 10 nmol/L iron addition to Fe Lim (4nM Fe)	light 646 µmol photons/m²/s
		MMETSP0898		iron 400 nmol/L; silicate 106 µmol/Kg	light 399 µmol photons/m²/s
		MMETSP0899		iron 4 nmol/L; silicate 10.6 µmol/Kg	light 139 µmol photons/m²/s

		MMETSP0900		iron 400 nmol/L; silicate 10.6 µmol/Kg	light 138 µmol photons/m²/s
		MMETSP0901		iron 400nM; silicate 106 µmol/Kg; nitrite not added to the media (but was probably between 0 and 88.2 µM as the culture was started with a 1:10 dilution of a replete culture)	light 444 µmol photons/m²/s